Spring 2015

The effect of maximum aggregate size on the shear strength of geometrically scaled reinforced concrete beams

Derek Robert Daluga
Purdue University

Graduate School Form 30
Updated 1/15/2015

PURDUE UNIVERSITY
GRADUATE SCHOOL
Thesis/Dissertation Acceptance

This is to certify that the thesis/dissertation prepared

By Derek Robert Daluga

Entitled

The Effect of Maximum Aggregate Size on the Shear Strength of Geometrically Scaled Reinforced Concrete Beams

For the degree of Master of Science in Civil Engineering

Is approved by the final examining committee:

Santiago Pujol
Chair

Mete A. Sozen

Ayhan Irfanoglu

To the best of my knowledge and as understood by the student in the Thesis/Dissertation Agreement, Publication Delay, and Certification Disclaimer (Graduate School Form 32), this thesis/dissertation adheres to the provisions of Purdue University's "Policy of Integrity in Research" and the use of copyright material.

Approved by Major Professor(s): Santiago Pujol

Approved by: Dulcy Abraham 4/28/2015

Head of the Departmental Graduate Program Date

THE EFFECT OF MAXIMUM AGGREGATE SIZE ON THE SHEAR STRENGTH OF GEOMETRICALLY SCALED REINFORCED CONCRETE BEAMS

A Thesis

Submitted to the Faculty

of

Purdue University

by

Derek Robert Daluga

In Partial Fulfillment of the

Requirements for the Degree

of

Master of Science in Civil Engineering

May 2015

Purdue University

West Lafayette, Indiana

To my parents, Daniel & Susan Daluga

ACKNOWLEDGEMENTS

I would like to thank

- Dr. Santiago Pujol for his support and mentorship during my graduate education.
- the other members of my committee, Dr. Ayhan Irfanoglu and Dr. Mete Sozen, for their assistance and involvement in this thesis.
- the John E. Goldberg family for the fellowship, which allowed me to complete this research.
- Dr. Karl Reineck and ACI-ASCE Committee 445 for sharing their shear database collection.
- the staff of Bowen Laboratory at Purdue University who taught me so much and were always willing to help.
- Kaylor McCain for building the formwork for two of the specimens tested.
- BASF, Dayton Superior, IMI, and MMFX for their generous donations to the project.
- my family and friends who provided support to me throughout my education at Purdue University. You have made this a very worthwhile experience. Thank you.

TABLE OF CONTENTS

Page

LIST OF TABLES

Table Page

LIST OF FIGURES

Figure Page

Figure Page

Figure Page

Figure Page

Figure Page

LIST OF SYMBOLS

Symbol	Description	Page Introduced
a	shear span	xviii
a_g	maximum aggregate size	xviii
a_{g50}	size of sieve opening catching 50% of particles	22
A_s	cross-sectional area of reinforcing bars	43
b	cross-sectional width	3
b_r	average width of flexure beam at fracture location	30
d	effective depth	xviii
d_c	diameter of cylinder	30
d_r	average depth of flexure beam at fracture location	30
f'_c	compressive strength of a standard 6 x 12 in. cylinder	xviii
f_c	shear stress at comparable loading stage	7
f_r	modulus of rupture	18
f_t	tensile strength of concrete	29
f_y	unit yield stress of reinforcement	43
E_c	Young's modulus of concrete	3

Symbol	Description	Page Introduced
E_s	Young's modulus of steel	3
h	cross-sectional depth	xviii
I_g	moment of inertia of gross cross-section	18
j	ratio of the internal lever arm to the effective depth	3
k	ratio of the depth to the neutral axis to the effective depth	3
l_c	length of cylinder	29
L	span length	18
M_{cr}	moment at cracking	18
n	modular ratio	3
P	applied concentrated load	14
P_c	concentrated load at comparable loading stage	7
P_{cr}	load at first observed crack	18
P_{eq}	concentrated load from weight of loading apparatus	13
P_t	total concentrated load	13
P_{sw}	load from self-weight	13
S_1	stress corresponding to a longitudinal strain of 50 millionths	30
S_2	stress corresponding to 40% of the ultimate load	30
v	unit shear stress	13

Symbol	Description	Page Introduced
V	shear force	3
v_c	nominal shear stress	3
ε_2	longitudinal strain produced by stress S_2	30
ρ	longitudinal reinforcement ratio	xviii

ABSTRACT

Daluga, Derek R. M.S.C.E., Purdue University, May 2015. The Effect of Maximum Aggregate Size on the Shear Strength of Geometrically Scaled Reinforced Concrete Beams. Major Professor: Santiago Pujol.

Shear strength of reinforced concrete beams without web reinforcement has been reported to decrease with increases in depth. This is often referred to as a size effect. This reduction in shear strength has been reported to decrease with the use of web reinforcement and increases in maximum aggregate size.

The purpose of this study was to test two hypotheses 1) shear strength increases with increases in maximum aggregate size and 2) aggregate gradation affects this increase in shear strength. Maximum aggregate size is defined here as the size of the smallest sieve opening through which all aggregate particles pass.

The proposed hypotheses were tested against results from ten simply-supported 12 in. deep beams, two simply-supported 48 in. deep beams, described in Appendix E, and previous test results (Taylor 1972, Chana 1981, Murray 2010, McCain 2012). All beams tested in this study had the same length, effective depth, width, concrete cover, and longitudinal reinforcement size and spacing. The variables controlled in the experiments and described in this report were maximum aggregate size and gradation. Maximum aggregate size varied from 3/8 to 1 in.

A database was compiled using results presented here and previous results (Taylor 1972, Chana 1981, Murray 2010, McCain 2012) to evaluate the proposed hypotheses. This database had test beams with dimensions and parameters within the following ranges:

$$2.3 \le a/d \le 3.0$$

$$2700 \text{ psi} \le f_c' \le 5700 \text{ psi}$$

$$8 \text{ in.} \le h \le 48 \text{ in.}$$

$$3/8 \text{ in.} \le a_g \le 2 \text{ in.}$$

$$0.63\% \le \rho \le 1.7\%$$

where:

a = shear span

d = effective depth

f'_c = compressive strength of a standard 6 x 12 in. cylinder

h = cross-sectional depth

a_g = maximum aggregate size

ρ = longitudinal reinforcement ratio

The test results studied supported the first hypothesis. In two out of two groups of tests of comparable beams in which the only nominal difference was maximum aggregate size, an increase in maximum aggregate size led to an increase in shear strength.

The second hypothesis was not supported by the test results studied. For the same maximum aggregate size, the unit shear strength was not observed to change within the range of tested aggregate gradations.

CHAPTER 1. INTRODUCTION

Shear failures in reinforced concrete beams have been studied since the early 1900's (ACI-ASCE Committee 326 1962a). Understanding shear has been difficult though because it is affected by many parameters. Kani (1966) stated "only by reducing the number of variables to a minimum are we able to attribute the results of our investigation to the individual parameters inherent in a reinforced concrete beam."

Current design methods for shear are based predominantly on the test results of 194 beams, with depths smaller than 24 in. (ACI-ASCE Committee 326 1962b). 88% of these beams had depths smaller than 16 in. (Murray 2010). Shear strength of beams has been reported to decrease with increases in depth (Chapter 2). This is often termed a size effect and is more noticeable in beams without transverse reinforcement (Frosch 2000).

Taylor (1972) noted this decrease in unit shear strength with increasing depth could be reduced by scaling geometrically all beam dimensions. He tested beams in which the ratios of cover, maximum aggregate size, width, and longitudinal reinforcement size and spacing to depth were the same. His focus on scaling yielded a 20% decrease in unit shear strength between beams with depths of 9.8 to 39.4 in.

Murray (2010) and McCain (2012) reported results similar to Taylor's (1972). Murray and McCain tested beams ranging from 12 to 30 in. in depth. Experimental results reported by Taylor, Murray, and McCain showed reduction in shear strength attributed to size could be less than 20% if width, cover, maximum aggregate size, and longitudinal reinforcement size and spacing were scaled in proportion to depth.

CHAPTER 2. LITERATURE REVIEW

Table 2.1 provides a summary of research on shear strength of reinforced concrete beams without transverse reinforcement. Table 2.2 provides a summary of data from a shear database collected by Reineck et al. (2003) and test results from Murray (2010) and McCain (2012). Data are plotted in Figure 2.1 depth (Leonhardt 1962, Kani 1967, Bhal 1968, Walraven 1978, Sneed 2007). The data in this figure come from tests of beams in which concrete cover, maximum aggregate size, and longitudinal size and spacing were not always scaled in proportion to depth. Only shear span-to-effective depth ratios between 2.3 and 4.0 are shown in Figure 2.1.

2.1 Reinforced Concrete Beams without Shear Reinforcement

Ritter, as early as 1899, realized that the basic cause of shear failures in reinforced concrete beams was diagonal tension (ACI-ASCE Committee 326 1962a).

Mörsch understood shear failures were controlled by tension around the same time as Ritter. Mörsch developed the following expression, Equation 2-1, for nominal shear stress (ACI-ASCE Committee 326 1962a).

$$v_c = \frac{V}{bjd} \tag{2-1}$$

where:

v_c = nominal shear stress
V = shear force
b = cross-sectional width
j = $1 - k/3$
$k = \sqrt{\rho^2 n^2 + 2\rho n} - \rho n$
ρ = longitudinal reinforcement ratio
$n = E_s / E_c$
E_s = Young's modulus of steel
E_c = Young's modulus of concrete
d = effective depth

Mörsch believed shear strength of reinforced concrete was dependent upon concrete compressive strength. Consequently, it was recommended shear strength, *v*, be limited to $0.02f'_c$ for beams without web reinforcement to resist sudden failure. This recommendation implied concrete compressive strength was the main variable affecting shear strength (ACI-ASCE Committee 326 1962b). Although the limit on shear strength has changed, it is still expressed exclusively in terms of the compressive strength of concrete.

Talbot (1909) noted shear strength of beams was influenced by longitudinal reinforcement ratio, length to depth ratio, and concrete compressive strength. His conclusions were based on 106 test beams with a depth of 11 in. and without transverse reinforcement. Talbot's experiments went mostly unnoticed until the mid-20th century, when Clark introduced the term shear span-to-effective depth ratio, *a*/*d*, where *a* is shear span length and *d* is effective depth (ACI-ASCE Committee 326 1962b).

Leonhardt and Walther (1962) questioned the extrapolation of data from small to large test beams without web reinforcement. They tested 28 beams ranging in depth from 7.1 to 26.4 in., where cover, maximum aggregate size, and longitudinal spacing of the beam were not

scaled in proportion to depth. Cross-sectional width and longitudinal reinforcement size were increased in the same proportions as depth. Leonhardt and Walther tested two series: Series D had one layer of reinforcement and Series C had one to three layers of reinforcement. Beams in both series failed in shear. In Series D, the mean shear strength of beams with a depth of 6.3 in. ($3.4\sqrt{f'_c}$) was approximately 22% larger than the strength of beams with a depth of 12.6 in. ($2.7\sqrt{f'_c}$). In Series C, the beam with a depth of 7.1 in. ($3.0\sqrt{f'_c}$) was 24% stronger than the beam with a depth of 26.4 in. ($2.3\sqrt{f'_c}$). Leonhardt and Walther concluded the difference between unit shear strengths in the series was related to bond. They stated bond was dependent upon the total surface area of the longitudinal reinforcement and as bond decreased, shear cracks propagated further.

Acharya and Kemp (1965) tested reinforced concrete beams without web reinforcement to understand the effects of dowel force. Before their work, it had been assumed dowel force did not contribute to shear strength of the beam at failure. They noted compressive stresses in test beams were not within the range of concrete if dowel force effects were not considered. Acharya and Kemp concluded dowel force must attribute towards 60% of the shear transfer.

Kani (1966) tested beams focusing on individual variables to understand shear in concrete. The studied variables were compressive strength, shear span-to-effective depth ratio, reinforcement ratio, and beam width. His conclusions were based on 133 test beams. Kani concluded unit shear strength was affected by shear span-to-effective depth ratio and longitudinal reinforcement ratio. He stated results from test beams with shear span-to-effective depth ratios smaller than approximately 2.5 were not comparable to results from test beams with larger ratios because of arch action. He also concluded concrete strength and width does not affect unit shear strength, normalized with respect to $\sqrt{f'_c}$, (where f'c is in units of psi).

Fenwick and Paulay (1968) investigated the influence of dowel force and aggregate interlock. They concluded shear resistance in beams was attributed to interactions within the inclined crack, not the compression zone. Fenwick and Paulay concluded dowel force

and aggregate interlock contributed towards approximately 20% and 60% of the shear resistance of a beam.

Fenwick and Paulay (1968) stated load deformation characteristics were dependent upon the air and water content of the cement paste. Larger aggregate collected more water and cementitious buildup. The accumulation caused a "spongy layer" in the concrete, resulting in an increased deflection.

Fenwick and Paulay (1968) believed concrete cover, width, longitudinal reinforcement size and spacing, shear span-to-effective depth ratio, and tensile strength of concrete played key roles in shear strength of beams without web reinforcement.

Sneed (2007) designed and tested eight beams with different ratios of width and bar size to depth. Her intent was to understand the influence of depth on shear strength of reinforced concrete beams without transverse reinforcement and to estimate a lower-bound value for shear strength. Sneed tested beams with depths ranging from 12 to 36 in. and a shear span-to-effective depth ratio of 3.0. Concrete compressive strength was 10,000 psi. She limited the maximum aggregate size to 3/8 in. for all specimens.

Sneed's (2007) results showed a 66% decrease in unit shear strength between beams with depths of 12 and 36 in. and the same width. A decrease of 44% in unit shear strength was observed between beams with depths of 12 and 36 in. and scaled widths. Sneed concluded, unless steps were taken to avoid a reduction in shear strength when increasing depth, a reduction as low as one-half could be expected in the unit shear strength value given in ACI 318-05.

2.2 Mechanisms of Shear Resistance

Factors influencing shear strength include: shear transfer in the uncracked concrete, aggregate interlock, dowel force, arch action, and shear reinforcement (ACI-ASCE Committee 426 1973). Figure 2.2 illustrates the contribution of these methods of shear transfer in a cracked beam.

Aggregate interlock is the interaction among aggregate particles between opposite sides of inclined cracks. Walraven (1981) noted the "microroughness of the crack, caused by the aggregate particles projecting from the crack plane, dominates the macroroughness, due to overall undulations of the crack faces." The idea is that the same size crack with increases in aggregate size will yield an increase in shear strength because of the influence of aggregate interlock.

Aggregate interlock can be idealized using a two-phase construct made up of fully cured cement paste and a collection of aggregate particles represented by spheres (Figure 2.3). The bond zone, the contact area between the aggregate and cement paste, is the weakest part of the system, therefore cracks tend to run along the perimeter of the aggregate (Walraven 1981). For high strength concrete (f'_c > ~10,000 psi) the crack may pass through the aggregate. Otherwise, the shear force is initially resisted by the interaction of the aggregate and cavity in the mortar left by the particle (Figure 2.4). As the crack width increases, the contact area between the aggregate particle and mortar decreases. This decrease in contact area causes an increase in strain. The idea is that smaller crack widths provide more interaction between aggregate particles and mortar, and therefore less strain in the mortar.

Dowel force is the shear force in the longitudinal steel. Parameters affecting dowel force include: longitudinal reinforcement size and spacing and stiffness and strength of concrete around the longitudinal reinforcement. Dowel force causes splitting cracks, which cause a decrease in dowel force (Fenwick and Paulay 1968).

2.3 Effect of Scaling

Researchers have reported unit shear strength to decrease with increases in beam depth (ACI-ASCE Committee 445 1998). A plausible cause for this decrease is wider cracks form in beams with larger depths. Wider cracks have less interaction between protruding aggregate particles and therefore transfer less shear.

Figure 2.5 shows a comparison of test results from beams in which concrete cover, maximum aggregate size, and longitudinal reinforcement size and spacing were within a narrower range than test beams in Figure 2.1. Only results from beams with shear span-to-effective depth ratios between 2.3 and 3.0 are shown in Figure 2.5. The observed decrease in unit shear strength in Figure 2.5 is less defined than beams with a wider range of parameters (Figure 2.1). Section 5.4 provides further discussion on this reduced decrease in shear strength by focusing on beams with comparable nondimensional properties such as shear span-to-effective depth ratio and relative aggregate size. Relative aggregate size will be defined here as the ratio of maximum aggregate size to effective depth.

The effects of scaling were visible in crack widths and patterns. Sneed (2007) tested beams where concrete cover, maximum aggregate size, and reinforcement size and spacing were not scaled in proportion to depth. Figure 2.6 shows a comparison of the crack patterns from her tests for beams with different depths, but at similar loading stages. Comparable loading stages are defined here as a stage with a similar shear stress, f_c, in beams with different longitudinal reinforcement ratios (Equation 2-2)

$$f_c = \frac{P_c}{bh} \tag{2-2}$$

where:

P_c = concentrated load at a comparable loading stage
b = cross-sectional width
h = cross-sectional depth

In Figure 2.6, two crack patterns are superimposed. They were scaled using different geometric factors to allow this superposition. Two supports are shown because concrete cover in the test beams was not scaled in proportion to depth. The beam with a depth of 36 in. had eleven flexural cracks, while the beam with a 12 in. depth had two cracks. Figure 2.7 shows the increase in the number of cracks when increasing depth for all beams tested by Sneed (2007). Test beams with dimensions including, concrete cover, width, and longitudinal reinforcement size and spacing scaled proportional to depth, had similar crack

patterns (Figure 2.8, McCain 2012). The 12 in. deep beam had six flexural cracks and the 30 in. deep beams had seven flexural cracks. Crack patterns were drawn at similar loading stages (Equation 2-2). Beams with all dimensions increased in proportion to depth had a similar number of cracks. Table 2.3 shows the number of cracks observed at similar loading stresses (Sneed 2007, McCain 2012). Data from Sneed's (2007) tests show an increase in the number of cracks with increases in depth (Figure 2.7). Data from McCain's (2012) test show negligible change in the number of cracks with increases in depth (Figure 2.9).

Crack spacing, in addition to crack patterns, is dependent upon concrete cover (Broms 1965). Similar relative crack spacing was observed in beams where concrete cover was scaled proportionally with increases in depth (Table 2.3). Table 2.3 also shows that similar relative crack spacing was not observed in test beams where concrete cover was not scaled in proportion to depth. The data from Sneed's (2007) tests from Table 2.3, plotted in Figure 2.10, show a 50% decrease in mean relative crack spacing between beams with depths of 12 and 36 in. The data from McCain's (2012) test from Table 2.3, plotted in Figure 2.11, show a 2% decrease in mean relative crack spacing between beams with depths of 12 and 30 in.

Taylor (1972) focused on scaling all dimensions in a beam with respect to depth. These dimensions included concrete cover, maximum aggregate size, and longitudinal reinforcement size and spacing. The largest beam was defined by Taylor as his prototype beam with a depth of 39.4 in. and a maximum aggregate size of 1-1/2 in. Other beams had dimensions equal to 1/2 and 1/4 times the dimension of the prototype. A constant shear span-to effective depth ratio of 3.0 was used. Taylor observed a 20% decrease in unit shear strength between depths of 9.8 and 39.4 in. He reported as aggregate size increased, the mechanism of aggregate interlock, which he said accounts for 40% of the shear resistance, increased. He concluded shear strength was a function of the maximum aggregate size. Taylor also concluded properly scaled beams will have a similar number of cracks.

Murray (2010) designed and tested eight beams with dimensions and parameters including cover, longitudinal reinforcement size and spacing, and width geometrically scaled with

respect to depth to reproduce similar results to Taylor (1972). Aggregate size was isolated as a variable to focus on the effects of maximum aggregate size. Depth of the beams ranged from 12 to 30 in. The shear span-to-effective depth ratio was 2.3. Murray (2010) observed when all dimensions and parameters were scaled in proportion to depth, including concrete cover, maximum aggregate size, and reinforcement size and spacing, test specimens reached unit shear strengths similar to the beams tested by Taylor (1972).

McCain (2012) tested the same hypothesis as Murray (2010) with beams ranging between a depth of 12 and 30 in. McCain tested ten beams scaling concrete cover, maximum aggregate size, longitudinal reinforcement size and spacing, and width in proportion to depth. McCain tested beams with a shear span-to-effective depth ratio of 2.3 and 2.9. His test results showed a 5% decrease in mean unit shear strength between 12 and 30 in. deep beams with a shear span-to-effective depth of 2.3 (Murray 2010, McCain 2012). A 13% decrease in mean unit shear strength was observed between 12 and 30 in. deep beams with a shear span-to-effective depth of 2.9 (McCain 2012). McCain concluded if all dimensions and parameters including the concrete cover, and maximum aggregate size, longitudinal reinforcement size and spacing, and width were scaled in proportion to the depth, size effect appeared to be nearly eliminated.

CHAPTER 3. EXPERIMENTAL PROGRAM

The hypotheses tested in this study were 1) shear strength increases with increases in maximum aggregate size and 2) aggregate gradation affects this increase in shear strength.

3.1 Test Specimens

To test the proposed hypotheses ten 12 in. deep reinforced concrete beams without transverse reinforcement were loaded to failure. The beams were nominally identical except for aggregate size and gradation. Maximum aggregate sizes of 3/8, 1/2, and 1 in. were used. Maximum aggregate size is defined here as the size of the smallest sieve opening through which all aggregate particles pass. Beam dimensions and parameters are shown in Table 3.1. The specimens were designed to resemble the small beams tested by Murray (2010) and McCain (2012). Depth and effective depth were 12 and 10.5 in. Test beams had a shear span length of 30 in. providing a shear span-to-effective depth ratio of 2.9.

The test beams were designed to fail in shear, not in flexure or bond. The longitudinal reinforcement was composed of three grade 100 # 4 bars spaced at 3 in. on center, providing a reinforcement ratio of 0.63%. Web reinforcement was provided outside of the shear span to improve bond conditions and prevent pull out failures. This web reinforcement was composed of eight grade 60 # 3 closed stirrups spaced at 1-7/8 in. on center on each end. The cross section and elevation of the test beams are shown in Figure 3.1 and Figure 3.2.

3.2 Test Procedure

Testing was conducted at Purdue University's Robert L. and Terry L. Bowen Laboratory for Large-Scale Civil Engineering Research. The test setup is shown in Figure 3.3. The

specimens were tested in three-point loading, where the applied load was centered between roller supports. Load was applied to the specimen using two 30 ton center-holed hydraulic cylinders located above the beam. The hydraulic cylinders were controlled with a hand pump. Threaded rods, which passed through the hydraulic cylinders, were placed in tension as the pistons in the cylinders extended. Load from the hydraulic cylinders was applied to the test beam through a steel tube placed on a steel plate above the test beam. Load was monitored using two 20 kip capacity load cells placed on top of the hydraulic cylinders. See Appendix C for a detailed description of the test setup.

Deflection was measured using six linear variable differential transformers (LVDT). The LVDTs were attached to the beam with aluminum brackets. The LVDTs were located at support points, quarter points, and 3 in. north and south from midspan. Midspan deflection was approximated as the average of the north and south midspan LVDTs because the loading rig prevented access to the midspan. Vertical deflection at the supports was measured using LVDTs with a range of ± 1/2 in. while the quarter and midspan deflections were measured using LVDTs with a range of ± 1 in. Accuracies of LVDTs are provided in Table C.3

Load was increased in increments of 3 kip. Cracks were marked and measured after each increment. This process continued until the unit shear stress reached 1.0 to 1.6$\sqrt{f'_c}$, where f'_c is in units of psi, after which, the beam was loaded continuously until failure.

After shear failure, external reinforcement was used to test the side that did not fail (Figure 3.4). External reinforcement was located on the side of the beam where shear failure occurred. It was composed of five external stirrups, spaced at 5 in. on center. After the installation of the external reinforcement, the beam was loaded to 9 kip, 18 kip, and then to failure. Cracks were marked and measured at each additional load step. See Appendix C for a detailed description of equipment used during each test.

Bolts were placed between support plates to prevent the test beam from rolling during placement. These bolts were removed before testing in all beams except Specimen H-1. (Figure 3.5). The reported mean unit shear strength of Specimen H-2 was 1.9 $\sqrt{f'_c}$. The

reported mean unit shear strength of Specimen H-1 was 1.9 $\sqrt{f'_c}$. The test data were comparable, therefore, data from Specimen H-1 were not discarded.

CHAPTER 4. EXPERIMENTAL RESULTS

A summary of test results, including those previously reported by Murray (2010) and McCain (2012), is provided in Table 4.1. In this study, results from beams of different sizes were compared in terms of unit shear strength. Unit shear strength, *v*, is defined as peak shear per unit area, (Equation 4-1).

$$v = \frac{P_t / 2}{bd} \tag{4-1}$$

where:

$P_t = P + P_{eq} + P_{sw}$

$P =$ applied concentrated load

$P_{eq} =$ concentrated load from weight of loading apparatus

$P_{sw} =$ load from self-weight

$b =$ cross-section width

$d =$ effective depth

The unit weight of the beam was assumed to be 150 lb/ft^3. Weight of the loading apparatus, P_{eq}, used in tests done by Murray (2010), McCain (2012), and specimens described in Section 3.1 and Appendix E are listed in Table 4.2.

4.1 Load-Deflection Curves

Load-deflection curves for the ten test beams are shown in Figure 4.1 through Figure 4.10. Decreases in applied load observed after load increments were likely to have been caused by creep and relaxation. For beams tested twice (once per side), load-deflection curves are reported for the initial failure only. LVDTs were removed because they were in the way of the external reinforcement and the deflection of the strengthened beam was deemed to

be of little relevance. Deflection was measured with LVDTs calibrated with an accuracy of 0.004 in. and reported to the nearest 0.01 in. Midspan deflection was recorded as the average of the two LVDTs placed 3 in. north and south of the load point (Figure D.1). Midspan deflection was corrected for rigid-body motion using the displacements measured at supports. Load was measured with two load cells, calibrated with an accuracy of 80 lb, and reported to the nearest 100 lb. Reported load is the sum of the east and west load cell. All recorded data are available at datacenterhub (https://datacenterhub.org).

4.2 Cracking

Cracks were marked and measured at each load increment. Cracks were measured using a crack comparator in 0.005 in. increments. The first flexural crack formed near the midspan in all of the beams. Additional flexural cracks formed as load increased. Table 4.3 lists the load at which the first flexural cracks were observed in addition to the number of flexural cracks marked on the beams at comparable loading stages, including results from Murray (2010) and McCain (2012). Comparable loading stages are defined here as a stage with similar shear stresses, f_c, in beams with different longitudinal reinforcement ratios (Equation 4-2)

$$f_c = \frac{P}{bh}$$

where:

P = applied concentrated load
b = cross-sectional width
h = cross-sectional depth

All beams failed because of the formation of an inclined crack, causing shear failure. The inclined crack extended between the load and support points. The propagation of the critical inclined crack was recorded using a high speed camera in all tests except Specimens F-3-S, F-3-N, and I-1-N. The propagation, in 17 of the 20 test beams, is shown in Figure 4.11 through Figure 4.27.

4.3 Failure

The critical inclined crack observed in each test is observed illustrated in Figure 4.28 through Figure 4.47. The mode of failure of all specimens was shear.

Horizontal cracks caused by shear forces in the reinforcement (dowel force) formed in all specimens during failure causing partial loss of bond with the longitudinal reinforcement. The splitting cracks propagated towards the beam ends. None of the beams failed because of bond.

At failure, Specimens F-3-S, F-3-N, H-1-N, H-2-N, I-2-S, I-2-N, J-1-N, and K-2-N had nearly vertical cracks form near the compression face of the beam (Figure D.12e). Size and orientation of these cracks varied among specimens. The origin of the crack varied. The crack in Specimen F-3-S, I-2-S, I-2-N, and J-1-N started at the critical inclined (shear) crack and in Specimen F-3-N, H-1-N, H-2-N, and K-2-N started at the top face. The crack formed in the compression zone after the critical inclined crack was fully developed.

High-speed video of 17 out of the 20 tests are available at datacenterhub (https://datacenterhub.org). The failures were recorded using a high speed camera in all tests except Specimens F-3-S, F-3-N, and I-1-N.

CHAPTER 5. ANALYSIS OF THE RESULTS

The average unit shear strengths of the specimens described in Section 3.1 and Appendix E and the 12 in. deep beams tested by Murray (2010) and McCain (2012) are listed in Table 5.1. This chapter discusses trends revealed by these results.

5.1 Load-Deflection Curves

A way to judge the quality of the tests described in Chapter 4 is to compare results from specimens with the same nominal properties. Load-deflection curves from specimens with the same nominal properties are compared in Figure 5.1 through Figure 5.5. Midspan deflection was corrected for rigid-body motion using the displacements measured at the supports.

Figure 5.6 shows a comparison of all measured load-deflection curves. All beams had a similar initial stiffnesses and cracked at flexural stresses ranging between $9\sqrt{f'_c}$ and $13\sqrt{f'_c}$, where f'_c is in units of psi. The largest difference between specimens with the same nominal properties, except for maximum aggregate size, was 40%.

5.2 Crack Patterns

One reason to expect a difference in shear strength between beams with different cover-to-depth ratios is that they have different crack patterns. This study concentrated on comparing beams with similar cover-to-depth ratios. Cover is defined here as distance from the nearest concrete face to the centroid of the longitudinal reinforcement.

Two crack patterns superimposed in Figure 2.6 had different cover-to-depth ratios. The cover-to-depth ratio for the 36 in. deep beam (0.11) was 63% smaller than the cover-to-depth ratio in the 12 in. deep beam (0.30). At comparable loading stages, the 36 in. beam

had eleven cracks and the 12 in. deep beam had two cracks. Comparable loading stages are defined here as states with similar steel stresses for beams with equal longitudinal reinforcement ratios or similar shear stresses from beams with different reinforcement ratios. This same comparison is shown in Figure 2.7 for all beams tested by Sneed (2007). This figure shows a positive correlation between number of cracks and effective depth. The plot could be interpreted to suggest that number of cracks is a function of depth. In reality, the driving variable is the cover-to-depth ratio. If beams have the same cover-to-depth ratio, then crack patterns are similar. Specimen G-1 (h = 48 in.) and Specimen F-4 (h = 12) in. had the same cover-to depth ratio. Specimen G-1 had ten flexure cracks and Specimen F-4 had nine flexure cracks at comparable loading stages (Figure 5.7). The number of flexural cracks was not always the same in tests done by McCain (2012) and tests described in Section 3.1 and Appendix E, but on average, the number of cracks did not change with depth (Table 4.3 and Figure 5.8). On average, the 12 in. deep beams had seven flexural cracks while the 30 and 48 in. deep beam had eight and nine.

Beams of different sizes, but similar cover-to-depth ratios develop comparable crack patterns that lead to similar inclined cracks. A comparison of the critical inclined cracks in Specimen F-3 and G-1 with a depth of 12 and 48 in. is illustrated in Figure 5.9. In this figure, two crack patterns are superimposed. They were scaled using different geometric factors to allow this superposition. There is no clear difference between the inclined crack in the small and large beam. This correlation was also observed in Figure 5.10 through Figure 5.19 which show the superposition of inclined cracks observed in the north and south sides of the same specimen. When comparing Figure 5.9 and Figure 5.10 through Figure 5.19, it was observed if all beam dimensions are scaled in proportion to depth, the geometry of the critical inclined crack is similar in beams of different size.

Crack spacing has also been observed to be influenced by cover, and was an indicator that proper scaling was achieved. A list of the average flexural crack spacing-to-effective depth ratio is shown in Table 5.2. The data in this table are plotted in Figure 5.20 and show an 8% decrease in mean relative crack spacing between beams with depths of 12 and 48 in.

The number of cracks and relative crack spacing indicated proper scaling was achieved among beams described in Section 3.1 and Appendix E and tests done by McCain (2012).

5.3 Concrete Tensile Strength

Shear strength is related to concrete tensile strength, and tensile strength is sensitive to aggregate size and surface properties. This section examines to what extent the results were influenced by the concrete tensile strength. The tensile strength of concrete, summarized in Table 5.3, was estimated using three methods. The first method is approximated by Equation 5-1.

$$f_r = \frac{M_{cr} \cdot h/2}{I_g} = \frac{\frac{P_{cr}L}{4} \cdot h/2}{\frac{bh^3}{12}} = \frac{3}{2}\frac{P_{cr}L}{bh^2} \tag{5-1}$$

where:

f_r = modulus of rupture
M_{cr} = moment at cracking
h = cross-sectional depth
I_g = moment of inertia of gross cross section
P_{cr} = load at first observed crack
L = span

The second and third methods of estimating the tensile strength of concrete were the ASTM 496 “Standard Test Method for Splitting Tensile Strength of Cylindrical Concrete Specimens” and the ASTM C78 “Standard Test Method for Flexural Strength of Concrete (Using Simple Beam with Third-Point Loading)”. The ASTM test methods are described in Appendix A.

Figure 5.21 shows a comparison between unit shear strength and concrete tensile strength computed using the three methods described. There is no clear trend in this figure, indicating that concrete tensile strength did not influence the shear strength within the range tested.

The largest difference in estimated tensile strength occurred in Series K. In this series, the modulus of rupture obtained from Equation 5-1 was approximately 800 psi. The tensile strength obtained from the split cylinder test was 50 % smaller (~400 psi). It was difficult to observe the development of the first flexural crack in small beams. The start of the first crack may have been unnoticed resulting in a skewed tensile strength estimated by Equation 5-1.

Figure 5.22 shows a comparison between tensile strength of concrete computed using the three methods described and maximum aggregate size. There appears to be no clear trend in this figure indicating that scaling did not affect concrete tensile strength.

5.4 Effect of Geometric Scaling

It has been observed that the decrease in unit shear strength with increases in depth is lower than 20% if dimensions and parameters in beam tests including aggregate size, concrete cover, and longitudinal size and spacing increase in proportion to depth (Taylor 1972, Murray 2012, McCain 2012). To reproduce this same trend, unit shear strength was plotted against effective depth (Figure 5.23). Data in this figure are listed in Table 4.1. Test beams included had similar ratios of concrete cover, maximum aggregate size, and reinforcement size and spacing to depth. Figure 5.23 shows a 13% decrease in unit shear strength between test beams with depths of 12 and 48 in. In test beams where concrete cover and reinforcement size and spacing were not scaled in proportion to depth, a 65% decrease was observed in unit shear strength between test beams with depths of 12 and 36 in. (Figure 2.1, Sneed 2007). It can be concluded that size effect in beams can be reduced by scaling concrete cover, maximum aggregate size, and longitudinal reinforcement size and spacing in proportion to depth.

Direct comparisons of unit shear strength are simpler to make among beams with similar relative aggregate size. Relative aggregate size is defined here as the ratio of maximum aggregate size to effective depth. In Figure 5.24, beams with similar relative aggregate size are grouped. Series F, I, J and G had a similar relative aggregate size (0.048) and Series E and H had the same relative aggregate size (0.036). Series K had a relative

aggregate size of 0.10, and was not compared with the other test beam results. In Figure 5.25 the beam results are organized according to depth. A decrease of 16% in the unit shear strength was observed between Series F, I, and J (h = 12 in.) and Series G (h = 48 in.) (Figure 5.25). A 3% decrease in unit shear strength was observed between Series H (h = 12 in.) and Series E (h = 30 in.) (Figure 5.25).

5.5 Aggregate Interlock

Figure 5.26 shows the unit shear strength of beams with the same depth (12 in.) plotted against maximum aggregate size. This figure shows a 23% increase in mean shear strength between test results of beams with maximum aggregate size of 3/8 and 1 in. An increase of 30% was observed in shorter beams tested by Murray (2010) (Figure 5.27). Figure 5.28 and Figure 5.29 illustrate additional comparisons between shear strength and maximum aggregate size for beams tested by Taylor (1972) and Chana (1981). In these beams, all dimensions and parameters other than maximum aggregate size were scaled in proportion to depth. The figures show that although not every increase in aggregate size resulted in an increase in shear strength, mean shear strength tended to increase with increases in relative aggregate size. This was observed in all but one series tested by Taylor with a depth of 9.2 in. (Figure 5.30). It is plausible that the observed decrease in unit shear strength is due to a lack of results. Tests done by Chana and Taylor used cube sizes ranging from 70 mm to 200 mm to estimate concrete compressive strength. For this reason, these test results were not comparable to those done by Murray and beams described in Section 3.1 and Appendix E.

The effect of aggregate size was also illustrated by two comparisons made using the data in Table 2.2 and Table 5.1. The first comparison is among results of test beams with the same depth and different maximum aggregate sizes (Figure 5.31, Taylor 1972, Murray 2010, McCain 2012). Figure 5.31 shows as maximum aggregate size increases, and all other dimensions and parameters remain the same, unit shear strength increases. This same comparison can be made with data from beams tested by McCain and beams described in Section 3.1 (Figure 5.32).

The second comparison shows the increase in unit shear strength with constant aggregate size and a decrease in depth (Figure 5.33, Taylor 1972, Murray 2010). This same comparison can be made with data from beams tested by McCain (2012) and beams described in Section 3.1 (Figure 5.34). This increase in unit shear strength with a decrease in depth can also be explained by the increase in relative aggregate size. Based on the two comparisons, assuming all other dimensions and parameters are the same, it is plausible that increases in maximum aggregate size improved aggregate interlock which led to increases in unit shear strength.

5.5.1 Shear Database

The inferred effect of aggregate interlock is also evaluated in the shear database collected by Reineck et al. (2003). An increase in unit shear strength with an increase in relative aggregate size is illustrated in beams with wide ranges of nondimensional properties in Figure 5.35. Unit shear strength of beams without transverse reinforcement appears to be influenced by aggregate interlock. This supports the idea that increases in maximum aggregate size lead to increases in unit shear strength.

5.6 Aggregate Gradation

The second hypothesis tested in this study was that aggregate gradation affects the increase in unit shear strength associated with increases in maximum aggregate size.

Aggregate gradation was studied by comparing results from Series F, I, and J. Table 5.4 summarizes the properties of the mixes used for each series. Each mix had aggregate with different gradations. Particle distributions of the mixes used are shown in Figure 5.36. Mix I had high portions of fine particles and low of large particles. Mix J had the opposite gradation, it had high portions of large particles and low of small particles. Mix F had an intermediate gradation. All three mixes had the same maximum aggregate size. The only difference among them was the gradation. It was difficult to quantify gradation using a single parameter. The size of the sieve opening catching 50% of the particles is used here to differentiate between mixes with different gradations. This parameter is referred to as

a_{g50} (Table 5.4). It was observed that aggregate gradation did not affect unit shear strength within the range tested (Figure 5.37).

CHAPTER 6. CONCLUSION

This study was done to test two hypotheses: 1) unit shear strength increases with increases in maximum aggregate size and 2) aggregate gradation affects this increase in unit shear strength.

The variables controlled in the experiments described in this report were maximum aggregate size and aggregate gradation.

Test results studied supported the first hypothesis. A 20% increase in mean shear strength was observed between beams with a maximum aggregate size of 3/8 and 1 in. The second hypothesis was not supported within the range tested.

LIST OF REFERENCES

LIST OF REFERENCES

Acharya, D. N., and Kemp, K. O., "Significance of Dowel Forces on the Shear Failure of Rectangular Reinforced Concrete Beams Without Web Reinforcement." *Journal of the American Concrete Institute,* V. 62, No. 10, 1965, pp. 1265-1278

ACI-ASCE Committee 326. 1962a. "Shear and Diagonal Tension." *Journal of the American Concrete Institute* 59 (1): 3–30.

ACI-ASCE Committee 326. 1962b. "Shear and Diagonal Tension." *Journal of the American Concrete Institute* 59 (2): 277–333.

ACI-ASCE Committee 426. 1973. "The Shear Strength of Reinforced Concrete Members." *ASCE, Journal of Structural Engineering* 99 (6): 1091–1187.

ACI-ASCE Committee 445 on Shear and Torsion. 1998. "Recent Approaches to Shear Design of Structural Concrete." *Journal of Structural Engineering* 124 (12): 1375–1417.

ASTM Standard A370. 2013. "Standard Test Methods and Definitions for Mechanical Testing of Steel Products." West Conshohocken, PA: ASTM International. doi:10.1520/A0370-13.2.

ASTM Standard C143. 2012. "Standard Test Method for Slump of Hydraulic-Cement Concrete." West Conshohocken, PA: ASTM International. doi:10.1520/C0143.

ASTM Standard C39. 2012. "Standard Test Method for Compressive Strength of Cylindrical Concrete Specimens." West Conshohocken, PA: ASTM International. doi:10.1520/C0039.

ASTM Standard C469. 2014. “Standard Test Method for Static Modulus of Elasticity and Poisson’s Ratio of Concrete in Compression.” West Conshohocken, PA: ASTM International. doi:10.1520/C0469.

ASTM Standard C496. 2011. “Standard Test Method for Splitting Tensile Strength of Cylindrical Concrete Specimens.” West Conshohocken, PA: ASTM International. doi:10.1520/C0496.

ASTM Standard C78. 2010. “Standard Test Method for Flexural Strength of Concrete (Using Simple Beam with Third-Point Loading).” West Conshohocken, PA: ASTM International.

Bažant, Zdenek P, and Kazemi, Mohammad T. 1991. “Size Effect on Diagonal Shear Failure of Beams without Stirrups.” *ACI Structural Journal* 88 (3): 268–76.

Broms, Bengt B. 1965. “Crack Width and Crack Spacing in Reinforced Concrete Members.” *Journal of the American Concrete Institute* 62 (10): 1237–55.

Chana, P. S. 1981. “Some Aspects of Modelling the Behaviour of Reinforced Concrete under Shear Loading.” *Cement and Concrete Association*

Fenwick, R. C., and Paulay, Thomas. 1968. “Mechanisms of Shear Resistance of Concrete Beams.” *ASCE, Journal of Structural Engineering* 94 (No. ST 10, October): 2325–50.

Frosch, Robert J. 2000. “Behavior of Large-Scale Reinforced Concrete Beams with Minimum Shear Reinforcement.” *ACI Structural Journal* 97 (97): 814–20. doi:10.14359/9626.

Kani, G. N. J. 1966. “Basic Facts Concerning Shear Failure.” *Journal of the American Concrete Institute* 63 (6): 675–92.

Kani, G. N. J. 1967. “How Safe Are Our Large Reinforced Concrete Beams?” *ACI Journal* 64 (3): 128–41.

Leonhardt, F., and Walther, R. 1962. “Contribution to the Treatment of Shear in Reinforced Concrete: Influence of the Absolute Beam Height on the Carrying Capacity under Shear.” *National Research Council of Canada: Technical Translation 1172*, No. 3: 53–62.

McCain, Kaylor. 2012. “The Effect of Scale on the Resistance of Reinforced Concrete Beams to Shear.” Purdue University, West Lafayette, IN, 2012.

Murray, Matthew R. 2010. “An Investigation of the Unit Shear Strength of Geometrically Scaled Reinforced Concrete Beams.” Purdue University, West Lafayette, IN, 2010.

Reineck, Karl-Heinz, Kuchma, Daniel A., Kim, Kang Su, and Marx, Sina. 2003. “Shear Database for Reinforced Concrete Members without Shear Reinforcement.” *ACI Structural Journal* 100 (2): 240–49.

Shioya, T, Iguro, M., Nojiri, Y., Akiyama, H., and Okada, T. 1990. “Shear Strength of Large Reinforced Concrete Beams.” *ACI Structural Journal* 118 (Special Publication): 259–80. doi:10.1617/s11527-007-9223-3.

Sozen, Mete A., Ichinose, Toshikats, and Pujol, Santiago. 2014. *Principles of Reinforced Concrete Construction*. Boca Raton, FL: CRC Press.

Sneed, Lesley. 2007. “Influence of Member Depth on the Shear Strength of Concrete Beams.” Purdue University, West Lafayette, IN, 2007.

Talbot, A. N. 1909. “Tests of Reinforced Concrete Beams Resistance to Web Stresses.” *University If Illinois Bulletin, Engineering Experiment Station* 6 (16): 84.

Taylor, Howard P. J. 1972. “Shear Strength of Large Beams.” *Journal of the Structural Division* 98 (11): 2473–90.

Taylor, Howard P. J. 1974. “The Fundamental Behavior of Reinforced Concrete Beams in Bending and Shear By.” *ACI Journal* 42 (Special Publication): 43–78.

Tompos, Eric J, and Frosch, Robert J. 2003. “Influence of Beam Size, Longitudinal Reinforcement, and Stirrup Effectiveness on Concrete Shear Strength.” *ACI Structural Journal* 99 (5): 559–67.

Walraven, Joost C. 1981. “Fundamental Analysis of Aggregate Interlock.” *ASCE, Journal of Structural Engineering* 107 (ST 11): 219–31

APPENDICES

Appendix A Materials

A.1 Concrete

Ten specimens were cast from five different batches of concrete, with a nominal compressive strength of 4000 psi. The concrete supplier was Irving Materials, Inc. in West Lafayette, Indiana. The maximum aggregate size ranged from 3/8 to 1 in. The maximum aggregate size is defined here as the size of the smallest sieve opening through which all particles passed. The design mix proportions are summarized in Table A.1. Particle distributions for mixes used in Series F, I, and J are illustrated in Figure 5.36 and summarized in Table A.2. Particle distributions for each aggregate type are shown in Figure A.1 and listed in Table A.3.

The batched concrete mixture proportions are summarized in Table A.4. At the arrival of the concrete mixer, slump was measured and recorded following the ASTM C143 Standard Test Method for Slump of Hydraulic-Cement Concrete.

The concrete was placed in cylinder molds and formwork in two equal lifts. A vibrator was used to consolidate the concrete after each lift. The top surface of concrete was finished with a hand float and was refinished with a trowel.

After the concrete set, a layer of wet burlap and plastic were placed over the concrete. The burlap and plastic remained on the specimen for the entire duration of the curing process. The total curing time is shown in Table A.5. Batches were cured for different time durations to influence concrete compressive strength. Formwork was stripped after three days for each specimen, except specimens in Series F, which were stripped after one day. Specimens were allowed to dry for at least two weeks before testing.

For each batch, cylinders measuring 6 in. in diameter and 12 in. in length were tested in a Forney machine with a capacity of 60,000 lb (Model Number: F-60C-DFM/I). The cylinders were tested in compression according to the ASTM C39 Standard Test Method for Compressive Strength of Cylindrical Concrete Specimens. Cylinders were capped at

both ends with pad caps (2500 to 7000 psi range) and placed in steel retainer rings (Figure A.2). The cylinders were loaded at a rate of 60,000 ± 12,000 psi/min until failure. A summary of test-day compressive cylinder strengths is listed in Table A.6.

The tensile strength of concrete was calculated in accordance with ASTM C496 Standard Test Method for Splitting Tensile Strength of Cylindrical Concrete Specimens. Casted cylinders, measuring 6 in. in diameter and 12 in. in length, were tested in a Forney machine with a capacity of 60,000 lb (Model Number: F-60-DFM/I) Tensile strength was calculated by applying a diametral force along the length of the cylinder with 1/8 in. plywood strips placed between the bottom bearing plate and top bearing strip (Figure A.3). The applied diametral force increased at a rate of approximately 16,900 ± 5700 psi/min. Splitting tensile strength, f_t, was computed using Equation A-1.

$$f_t = \frac{2P}{\pi l_c d_c} \tag{A-1}$$

where:

P = applied concentrated load
l_c = length of cylinder
d_c = diameter of cylinder

Tensile strength for each specimen at test day is listed in Table A.6.

The modulus of elasticity was determined using the ASTM C469 Standard Test Method for Static Modulus of Elasticity and Poisson's Ratio of Concrete in Compression. Casted cylinders measuring 6 in. in diameter and 12 in. in length were tested in a Forney machine with a capacity of 60,000 lb (Model Number: F-60C-DFM/I). The cylinders were loaded in three cycles. The cylinders were loaded to half the measured compressive strength, according to ASTM C39. Cylinders were capped with pad caps and placed in steel retainer rings. A compressometer was attached to each cylinder and measurements were read from a dial gage while loading (Figure A.4). Modulus of elasticity, E, was calculated using Equation A-2.

$$E_c = \frac{S_2 - S_1}{\varepsilon_2 - 0.000050} \quad \text{(A-2)}$$

where:

S_2 = stress corresponding to 40% of the ultimate load

S_1 = stress corresponding to a longitudinal strain of 50 millionths

ε_2 = longitudinal strain produced by stress S_2

Modulus of elasticity for each specimen on test day is listed in Table A.6.

Modulus of rupture was measured in accordance with the ASTM C78 Standard Test Method for Flexural Strength of Concrete (Using Simple Beam with Third-Point Loading). Prismatic beams with a 6 by 6 in. section and a span length of 18 in. were tested in a Forney machine with a capacity of 60,000 lb (Model Number: F-60C-DFM/I, Figure A.5). Specimens were loaded using a third-point method at a rate of 1800 ± 300 psi/min until rupture. Modulus of rupture, f_r, was calculated using Equation A-3.

$$f_r = \frac{PL}{b_r d_r^2} \quad \text{(A-3)}$$

where:

L = span length

b_r = average width at fracture

d_r = average depth at fracture

Modulus of rupture for each specimen on test day is listed in Table A.6.

A.2 Steel

Each beam contained three longitudinal bars along the bottom of the entire beam and transverse reinforcement outside the shear span. The bars came from five different heats (Table A.7). All specimens were built using #4 Grade 100 bars for longitudinal reinforcement and #3 Grade 60 bars for web reinforcement. MMFX Steel Corporation of America provided the # 4 Grade 100 reinforcing bars. J & K Supply Inc. provided the #3 Grade 60 reinforcing bars.

Steel reinforcing bars were tested in accordance with the ASTM A370 Standard Test Methods and Definitions for Mechanical Testing of Steel Products. Three 36 in. long coupons were cut from bars from each heat. The coupon was loaded in tension in a Baldwin Testing Machine (Model Number: 120BTE) with an Instron controller. The loading rate was 0.15 in./min up to a strain of 0.0065 in./in. and then 1.2 in./min until fracture. The strain was measured using an 8 in. Epsilon extensometer (Model Number: 634.25E-54). The elongation at rupture, modulus of elasticity, tensile strength, ultimate strain, and yield strength were recorded. The elongation at rupture was calculated by measuring the change in length of the failed section of the coupon, notched in 8 in. increments. Yield stress was calculated using a 2% offset in accordance with ASTM A370. Results of these tests are summarized in Table A.8.

Appendix B Specimen Fabrication

Formwork for each beam was constructed using high density overlay plywood and construction lumber connected by screws (Figure B.1). Joints, seams, and notches in the plywood were sealed with caulk. Form oil was sprayed evenly on the formwork prior to placement of the reinforcement.

Stirrups were bent using a portable rebar bender. Web reinforcement consisted of eight closed stirrups, spaced at 1-7/8in., placed outside the shear span on both sides of the beam. The layout and dimensions of the web reinforcement are shown in Figure 3.2. Two longitudinal bars, from the same heat as the web reinforcement bars, were tied to the top of the stirrups. Top longitudinal reinforcement terminated outside of the shear span (Figure B.2). Bottom longitudinal bars were cut to have the same length as the beam to monitor bar slip during the test. Web and longitudinal reinforcement were tied together with steel ties. Chairs, with a 1-1/4 in. height, were placed within the shear span (Figure B.3). Dayton Superior Aztec 1-1/4 in. Spacer Wheels were placed outside of the shear span. Lifting inserts were used outside of the shear span.

After specimens were allowed to dry for at least two weeks, as built dimensions were recorded (Table B.1). Bottom longitudinal reinforcement location was measured at the ends of the specimen. The bottom bars were exposed in all series, except I and J. For this reason, Series I and J did not have all dimensions recorded.

Appendix C Experimental Setup

The experimental setup was the same for all beams tested. An elevation view for the test setup is displayed in Figure C.1. Steel plates, centered on rollers, were attached to the bottom of the specimen. The rollers were supported by steel plates attached to reaction blocks. Hydro-Stone gypsum cement was used to attach the plates to the concrete and level the reaction blocks to the floor. The dimensions of the plates and reaction block are summarized in Table C.1.

After shear failure, external reinforcement was used to strengthen the side of the beam that failed and test the side that did not fail. LVDTs were removed for the second test because 1) they were in the way of the external reinforcement and 2) the deflection of the strengthened beam was deemed to be of little relevance. The LVDTs were removed to protect them in the second part of the test. Five external stirrups, made with ½ in. threaded rod and C3x5 steel channels, were spaced at 5 in. on center. The external reinforcement was located between center load plate and support (Figure C.2).

Load was applied to the beam by placing two 1 in. diameter 125 ksi threaded rods in tension using two 30 ton capacity hydraulic hollow plunger cylinders (Model Number: RCH306). The hydraulic cylinders applied the load to the test beam through a steel tube, HSS 10 x 4 x 5/8. The transfer tube was resting on a 3/4 in. plate, which was attached to the beam using Hydro-Stone gypsum cement.

Load was measured using two 20 kip load cells (Model Number: 3174-20K). The load cells were calibrated using a 120 kip capacity Baldwin Testing Machine (Model Number 120BTE) with an Instron controller. Calibrations, which were done by loading the cells in compression and using a 2 V excitation, are listed in Table C.2. The loading apparatus setup of each test is displayed in Figure C.3

Vertical deflection was measured using six Schaevitz linear variable differential transformers (LVDT). The LVDTs were located at supports, quarter spans, and 3 in. south and north of midspan (Figure D.1). LVDTs were calibrated using a Trimos Height Gage

(Model Number: V-1004). LVDT calibration results, which were obtained using a 30 V excitation, are listed in Table C.3. LVDT steel housing was clamped to a support frame. Threaded rods connected to LVDT cores were fastened to aluminum brackets epoxied to the concrete surface using Loctite Heavy Duty Epoxy (Figure C.4). Midspan deflection was approximated as the mean of the two LVDTs near midspan. This midspan deflection was compared to a Federal Full Jeweled Dial Gages (Model Number: D81S, Figure C.5). The dial gage had an accuracy of 0.001 in. It was placed 3 in. north of midspan for Series F, H, and K and at the midspan for Series I and J. The readings from the dial gage were within 0.1 in. of the LVDT results.

A Vishay Measurements Group Data Acquisition System 5000 was used to monitor and convert the voltage signals from the load cells and LVDTs. Vishay Measurement Group StrainSmart (Version 3.10) displayed and recorded the loads and displacements.

Bar slip was measured using Federal Full Jeweled Dial Gages with a precision of 0.001 in. (Model Number: D81S). The dial gages were attached to steel brackets epoxied to the end of the beam using Loctite Heavy Duty Epoxy (Figure C.6). Each dial gage was placed with the spindle in contact with the exposed center longitudinal bar. Since the longitudinal bars were not visible in Series I and J, a chisel was used to expose the end of the bars.

Cracks were marked with permanent marker and labeled with the corresponding load during increments specified in Section 3.2. Cracks were measured using a crack comparator in 0.005 in. increments. A 4 by 4 in. grid was marked on the beam with chalk to aid in documenting cracking. A Nikon Digital Camera D3200 mounted on an EpicPro GigaPan stand was used to collect the panorama pictures after each load increment. The panorama pictures were stitched together using GigaPan Stitch software.

Failures of beams were recorded in 17 of 20 tests using a high speed camera at a frame rate of 5000 frames per second. Three failures could not be captured. An Ultima FASTCAM (Model Number: APX RS) was used as a recording device. The high-speed video was recorded with Photron FASTCAM Viewer (PFV) software.

Appendix D Additional Test Results

D.1 Deflection

Deflections were measured using linear variable deflection transducers (LVDT). Deflections were corrected for rigid-body motion using the displacements measured at supports. Deflection profiles for each beam are shown in Figure D.2 through Figure D.11. The horizontal axis corresponds to the location of each LVDT as shown in Figure D.1.

Deflection at failure was measured within 0.1 seconds of the recorded failure load. Each beam, except for Specimen H-1 and K-1, failed on the south side first.

D.2 Bar Slip

Federal Full Jeweled Dial Gages (Model Number: D81S) were used to measure bar slip in the center longitudinal reinforcement bar on the north and south sides of the specimen. Slip measured after failure is shown in Table D.1. The dial gages did not read bar slip before failure, indicating anchorage condition was not observed to have influenced the strength of the beam.

D.3 Crack Widths and Patterns

At each load increment, cracks were marked with permanent marker and measured. Crack maps are illustrated in Figure D.12 through Figure D.21. Measured crack widths are summarized in Table D.2 through Table D.11. Each crack number in the tables corresponds to a crack labeled in the figures. Flexural cracks, located near the midspan of the beam, were the first observed cracks to form in each specimen. Cracks formed nearer the supports as load increased. Observed flexural cracks were vertical near the tension face of the beam, but propagated towards the load plate as load increased.

.

Appendix E Series G

Series G beams were built and tested with the help of Kaylor McCain. Table E.1 and Table E.2 summarize tables and figures used to describe Series G.

Appendix F Tables

Table 2.1 Summary of Existing Literature

Year	Author(s)	Summary of Research
1909	Talbot	Tested 106 beams to find the effects of shear reinforcement in reinforced concrete beams. He concluded 1) beams without shear reinforcement depend on the quality and strength of the concrete, 2) short deep beams yield a larger unit shear strength than beams with longer spans, and 3) higher percentages of reinforcement yield larger unit shear strengths.
1962	Joint ACI-ASCE Committee 326	Gathered current test results of beams tested without shear reinforcement. All beams had depths less than 24 in. 88% had depths smaller than 16 in. Current design codes are based on this collection of beams.
1962	Leonhardt and Walther	Tested 12 beams altering the beam depth. Concrete cover was increased in proportion to depth. Aggregate size was kept the same. They concluded that 1) unit shear strength was dependent upon effective depth and 2) bond of longitudinal reinforcement was dependent upon surface area.
1965	Acharya and Kemp	Tested 20 beams to find the effects of dowel force. They noted, if dowel force was not considered as a mechanism of shear transfer, stresses in the concrete would be outside of a feasible range. They concluded dowel force contributed toward 60% of the shear force transfer.

Table 2.1 Continued

Year	Author(s)	Summary of Research
1965	Broms	Tested beams altering the effective depth. He estimated that crack size increased with increasing crack spacing. He concluded cracking spacing was proportional to the concrete cover.
1966	Kani	Tested 133 beams to find the influence of concrete compressive strength, reinforcement ratio, and shear span-to-effective depth ratio in unit shear strength. He concluded 1) unit shear strength, normalized with respect to $\sqrt{f'_c}$, (where f'_c is in units of psi) did not depend on concrete strength and 2) unit shear strength was dependent upon reinforcement ratio and shear span-to-effective depth ratio.
1967	Kani	Tested beams to find the influence of beam depth and width. Concrete cover and maximum aggregate size were not scaled in proportion to depth. He observed a 40% decrease in unit shear strength between beams with depths of 6 and 48 in. He concluded width did not influence unit shear strength.
1968	Fenwick and Paulay	Tested beams to research the mechanisms through which shear was transferred through cracks in reinforced concrete. They concluded 1) aggregate interlock contributed up to 60% of shear strength, 2) dowel force was affected by concrete cover and bar spacing and 3) arch action in beams could allow beams to retain strength after the development of a diagonal crack.

Table 2.1 Continued

Year	Author(s)	Summary of Research
1968	Bhal	Tested beams keeping concrete compressive strength, shear span-to-effective depth ratio, and reinforcement ratio the same. Concrete cover and maximum aggregate size were not scaled in proportion to depth. He tested beams with depths ranging between 13.8 and 49.2 in. He concluded unit shear strength decreased as effective depth increased.
1972	Taylor	Tested 15 beams with depths ranging from 9.8 to 39.4 in. He is noted as one of the first to scale all dimensions and parameters, including concrete cover, maximum aggregate size, reinforcement spacing in proportion to depth. He concluded 1) there was a decrease in unit shear strength with increases in effective depth and 2) this decrease could be mitigated if all dimensions and parameters were scaled geometrically in proportion to depth.
1973	Joint ACI-ASCE Committee 426	Reviewed recent test results to understand shear transfer in reinforced concrete beams. They stated the five basic methods of shear transfer were concrete shear stress, aggregate interlock, dowel force, arch action, and shear reinforcement.

Table 2.1 Continued

Year	Author(s)	Summary of Research
1981	Chana	Tested beams scaling all dimensions and parameters including: concrete cover, maximum aggregate size, width, and reinforcement size and spacing. He tested small beams ranging between depths of 4.8 and 16 in. He concluded even if aggregate size was scaled, there was a significant size effect.
1990	Shioya, Iguro, Nojiri, and Akiyama	Reviewed experimental and theoretical studies of shear strength of reinforced concrete beams. They concluded maximum aggregate size only affects unit shear strength in beams with depths smaller than 24 in.
1991	Bažant and Kazemi	Tested beams with depths ranging between 1 to 16 in. and without scaling the dimensions and parameters in proportion to depth. A decrease of over 50% was observed in the unit shear strength. They concluded size effect would govern larger beams.
1998	Joint ACI-ASCE Committee 445	Described recent approaches to shear design and the concrete contribution to shear strength. It was stated that wider crack widths developed in beams with large effective depths. They concluded 1) larger crack widths corresponded to smaller shear strengths, 2) a shear span-to-effective depth ratio less than 2.5 would transmit shear directly to the support through arch action, and 3) tensile strain increased with less longitudinal reinforcement because of reductions in the compression zone.

Table 2.1 Continued

Year	Author(s)	Summary of Research
2000	Frosch	Tested two duplicate beams, with a depth of 36 in. and minimum reinforcement, to investigate the contribution of concrete and longitudinal reinforcement towards size effect. He concluded that since the shear stress was within the lower bound of scatter for shear, size effect did not significantly influence the shear stress.
2003	Reineck and Kuchma	Created a database of 398 beams without shear reinforcement. This database was collected to aid further development of the understanding of the shear strength in structural concrete members.
2003	Tompos and Frosch	Tested beams with low levels of reinforcement. The beam depths tested were 18 and 36 in. They concluded 1) unit shear strength decreased with increases in depth and 2) considering the scatter in results, that longitudinal reinforcement had a greater influence in shear strength than beam size.

Table 2.1 Continued

Year	Author(s)	Summary of Research
2007	Sneed	Tested eight simply-supported beams varying the effective depth while keeping other dimensions and parameters the same. Concrete cover, maximum aggregate size, and reinforcement spacing were not geometrically scaled. She concluded there was a reduction as low as half the value given in ACI 318-05 in unit shear strength with increasing depth.
2010	Murray	Tested eight beams with depths of 12 and 30 in. All dimensions and parameters including concrete cover, maximum aggregate size, width, and reinforcement ratio and layout were geometrically scaled. The shear span-to-effective depth ratio was 2.3. He observed a 16% decrease in unit shear strength when depth increased from 12 to 30 in.
2012	McCain	Tested four beams with a depth of 30 in. and six beams with a depth of 12 in. The shear span-to-effective depth ratio ranged between 2.3 and 2.9. All dimensions and parameters including concrete cover, maximum aggregate size, width, and reinforcement ratio and layout were geometrically scaled. He observed a 13% decrease in unit shear strength between beams with the same shear span-to-effective depth ratio.

Table 2.2 Previous Tests Focusing on Effective Depth and Unit Shear Strength

Researcher	Specimen ID	Beam Geometry				a/d	Concrete		Reinforcement			Peak Load, P (kip)	$v_T / \sqrt{f'_c}$
		Depth, h (in.)	Width, b (in.)	Effective Depth, d (in.)	Concrete Cover** (in.)		Compressive Strength, f'_c (psi)	Max Agg. Size, a_g (in.)	A_s (in^2)	Ratio, ρ (%)	Yield Stess, f_y (ksi)		
Leonhardt and Walther (1962)	D2/1	6.3	3.9	5.5	0.8	3.0	4540	0.59	0.36	1.68	60	4.8	3.3
	D2/2	6.3	3.9	5.5	0.8	3.0	4540	0.59	0.36	1.68	60	5.2	3.6
	D3/1	9.4	5.9	8.3	1.1	3.0	4900	0.59	0.79	1.62	60	10.4	3.0
	D3/2	9.4	5.9	8.3	1.1	3.0	4900	0.59	0.79	1.61	60	9.7	2.8
	D4/1	12.6	7.9	11.0	1.6	3.0	5010	0.59	1.45	1.67	64	16.6	2.7
	D4/2	12.6	7.9	11.0	1.6	3.0	5010	0.59	1.45	1.67	64	16.3	2.7
	C-1	7.1	3.9	5.9	1.2	3.0	5560	1.18	0.31	1.35	62	4.9	2.8
	C-2	13	5.9	11.8	1.2	3.0	5560	1.18	0.93	1.34	62	14.6	2.8
	C-3	19.7	7.9	17.7	2.0	3.0	5560	1.18	1.87	1.34	62	22.8	2.2
	C-4	26.4	8.9	23.9	2.5	3.0	5560	1.18	2.80	1.32	62	34.2	2.2
Kani (1967)	41	6	6.0	5.6	0.4	2.4	3950	0.75	0.87	2.61	55	11.6	5.5
	52	6	6.0	5.5	0.6	3.9	3600	0.75	0.88	2.69	57	6.5	3.3
	55	6	5.9	5.3	0.7	3.0	3640	0.75	0.88	2.80	57	7.3	3.9
	56	6	6.0	5.4	0.6	3.5	3950	0.75	0.87	2.67	58	6.3	3.1
	58	6	6.0	5.5	0.6	3.4	3950	0.75	0.87	2.66	60	6.5	3.2
	59	6	6.1	5.5	0.5	2.7	3860	0.75	0.88	2.63	57	11.3	5.4
	60	6	6.1	5.5	0.6	2.9	3880	0.75	0.88	2.65	57	8.8	4.3
	83	12	6.1	10.7	1.3	3.0	3980	0.75	1.80	2.74	50	14.6	3.5
	84	12	6.0	10.7	1.3	4.0	3980	0.75	1.80	2.84	50	12.5	3.1
	95	12	6.0	10.8	1.2	2.5	3670	0.75	1.80	2.75	49	16.4	4.1
	96	12	6.0	10.8	1.2	3.9	3670	0.75	1.80	2.76	49	12.7	3.2
	97	12	6.0	10.9	1.1	3.0	3950	0.75	1.75	2.68	53	14.1	3.4
	98	12	6.0	10.8	1.2	2.5	3800	0.75	1.75	2.68	53	17.2	4.3
	99	12	6.0	10.7	1.3	2.5	3800	0.75	1.75	2.73	53	17.4	4.4
	63	24	6.1	21.4	2.6	4.0	3800	0.75	3.60	2.77	51	21.0	2.6
	65	24	5.9	21.8	2.3	2.5	3910	0.75	3.61	2.82	54	25.3	3.2
	71	24	6.1	21.4	2.6	3.0	3970	0.75	3.48	2.66	54	23.0	2.8
	74	24	6.0	20.6	3.4	3.1	3950	0.75	3.51	2.84	53	24.2	3.1
	75	24	6.0	20.6	3.4	3.1	3960	0.75	3.51	2.84	53	24.3	3.1
	76	24	6.0	20.4	3.6	2.6	4460	0.75	3.51	2.87	54	25.8	3.2
	3042	48	6.1	43.0	5.0	2.5	3830	0.75	7.06	2.71	54	53.3	3.3
	3043	48	6.1	43.1	4.9	3.0	3910	0.75	7.06	2.71	55	37.1	2.3
	3044	48	6.0	43.2	4.8	4.0	4280	0.75	7.06	2.72	55	35.8	2.1
	273	12	24.1	10.7	1.3	4.0	3940	0.75	6.99	2.72	55	46.4	2.9
	274	12	24.1	10.6	1.4	3.0	3940	0.75	6.99	2.73	55	56.2	3.5
Bhal (1968)*	B1	13.8	9.5	11.8	2.0	3.0	3360	1.18	1.43	1.28	63	16.0	2.5
	B2	25.6	9.5	23.6	2.0	3.0	4290	1.18	2.86	1.28	63	26.9	1.8
	B3	37.4	9.5	35.4	2.0	3.0	3990	1.18	4.29	1.28	63	37.4	1.8
	B4	49.2	9.5	47.2	2.0	3.0	3660	1.18	5.72	1.28	63	42.1	1.6
	B5	25.6	9.5	23.6	2.0	3.0	3860	1.18	1.43	0.64	63	24.0	1.7
	B6	25.6	9.5	23.6	2.0	3.0	3590	1.18	1.35	0.60	63	25.9	1.9
	B7	37.4	9.5	35.4	2.0	3.0	3950	1.18	2.15	0.64	63	31.5	1.5
	B8	37.4	9.5	36.0	1.4	3.0	4020	1.18	2.02	0.59	62	28.7	1.3
Taylor (1972)*	A-1	39.4	15.8	36.6	2.8	3.0	4170	1.50	7.79	1.35	63	80.7	2.2
	A-2	39.4	15.8	36.6	2.8	3.0	3280	0.75	7.79	1.35	63	73.9	2.2
	B-1	19.7	7.9	18.3	1.4	3.0	3890	1.50	1.95	1.35	63	23.4	2.6
	B-2	19.7	7.9	18.3	1.4	3.0	3190	0.75	1.95	1.35	63	19.6	2.4
	B-3	19.7	7.9	18.3	1.4	3.0	4120	0.375	1.95	1.35	63	19.2	2.1
	C-1	9.8	3.9	9.2	0.7	3.0	3300	0.75	0.49	1.35	63	5.1	2.4
	C-2	9.8	3.9	9.2	0.7	3.0	3300	0.375	0.49	1.35	63	5.4	2.6
	C-3	9.8	3.9	9.2	0.7	3.0	3550	0.375	0.49	1.35	63	6.2	2.9
	C-4	9.8	3.9	9.2	0.7	3.0	2680	0.375	0.49	1.35	63	5.1	2.7
	C-5	9.8	3.9	9.2	0.7	3.0	2890	0.375	0.49	1.35	63	6.1	3.1

* Cubes used for concrete compressive strength. Converted to 6 by 12 in. cylinder strength using factors suggested by Reineck et al.(2003): 0.72 (100 mm cube), 0.75 (120 mm cube), 0.79 (150 mm cube), 0.83 (200 mm cube)

** Concrete cover is defined as distance from the nearest concrete face to the centroid of longitudinal reinforcement

Table 2.2 Continued

Researcher	Specimen ID	Beam Geometry				a/d	Concrete		Reinforcement			Peak Load, P (kip)	$v_T / \sqrt{f'_c}$
		Depth, h (in.)	Width, b (in.)	Effective Depth, d (in.)	Concrete Cover** (in.)		Compressive Strength, f'_c (psi)	Max Agg. Size, a_g (in.)	A_s (in^2)	Ratio, ρ (%)	Yield Stess, f_y (ksi)		
Walraven (1978)*	A1	5.9	7.9	4.9	1.0	3.0	3500	0.63	0.32	0.83	64	6.7	2.9
	A2	17.7	7.9	16.5	1.2	3.0	3500	0.63	0.97	0.74	64	15.9	2.1
	A3	29.5	7.9	28.3	1.2	3.0	3500	0.63	1.77	0.79	64	22.7	1.7
Chana (1981)*	2.1a	16	8.0	14.0	2.0	3.0	5650	0.79	1.89	1.69	69	21.6	2.6
	2.1b	16	8.0	14.0	2.0	3.0	5650	0.79	1.89	1.69	69	21.8	2.6
	2.2a	16	8.0	14.0	2.0	3.0	4760	0.79	1.89	1.69	69	19.6	2.5
	2.2b	16	8.0	14.0	2.0	3.0	4760	0.79	1.89	1.69	69	21.2	2.7
	2.3a	16	8.0	14.0	2.0	3.0	5180	0.79	1.89	1.69	69	22.3	2.8
	2.3b	16	8.0	14.0	2.0	3.0	5180	0.79	1.89	1.69	69	21.7	2.7
	3.1a	8	3.9	7.0	1.0	3.0	3560	0.39	0.48	1.74	61	5.4	3.3
	3.1b	8	3.9	7.0	1.0	3.0	3560	0.39	0.48	1.74	61	5.4	3.3
	3.2a	8	3.9	7.0	1.0	3.0	3790	0.39	0.48	1.74	61	5.5	3.3
	3.2b	8	3.9	7.0	1.0	3.0	3790	0.39	0.48	1.74	61	5.7	3.4
	3.3a	8	3.9	7.0	1.0	3.0	4130	0.39	0.48	1.74	61	6.0	3.4
	3.3b	8	3.9	7.0	1.0	3.0	4130	0.39	0.48	1.74	61	5.2	3.0
	D1	8	3.9	7.0	1.0	3.0	3260	0.39	0.48	1.74	61	5.0	3.2
	D2	8	3.9	7.0	1.0	3.0	3340	0.39	0.48	1.74	61	5.3	3.3
	D3	8	3.9	7.0	1.0	3.0	4610	0.39	0.48	1.74	61	4.8	2.6
Sneed (2007)	1-1	12	12	9.1	2.9	3.0	9580	3/8	1.32	1.21	63	29.5	2.8
	1-2	24	12	20.9	3.1	3.0	9580	3/8	3.16	1.26	66	31.4	1.3
	1-3	30	12	26.8	3.2	3.0	9430	3/8	4.00	1.24	69	33.2	1.1
	1-4	36	12	32.4	3.6	3.0	10840	3/8	5.08	1.31	69	37.7	0.9
	2-1	12	8	9.2	2.8	3.0	9940	3/8	0.93	1.26	70	12.9	1.8
	2-2	24	16	20.8	3.2	3.0	9400	3/8	4.00	1.20	69	35	1.1
	2-3	30	20	26.9	3.1	3.0	9880	3/8	7.00	1.30	69	58.8	1.1
	2-4	36	24	32.4	3.6	3.0	10570	3/8	10.16	1.31	69	79.3	1.0
Murray (2010)	A-1	30	22.5	26.25	3.8	2.3	3600	1	4.68	0.79	66	146	2.2
	A-2	30	22.5	26.25	3.8	2.3	4700	1	4.68	0.79	69	132	1.7
	B-1	12	9.0	10.5	1.5	2.3	3600	1	0.93	0.98	62	34	3.0
	B-2	12	9.0	10.5	1.5	2.3	3600	1	0.93	0.98	62	40	3.6
	C-1	12	9.0	10.5	1.5	2.3	4900	1	0.60	0.63	128	44	3.4
	C-2	12	9.0	10.5	1.5	2.3	4700	1	0.60	0.63	128	39	3.1
	D-1	12	9.0	10.5	1.5	2.3	2700	1/2	0.60	0.63	128	22	2.3
	D-2	12	9.0	10.5	1.5	2.3	2800	1/2	0.60	0.63	128	23	2.4
McCain (2012)	A-3	30	22.5	26.25	3.8	2.3	4000	1	4.68	0.79	67	190	2.6
	A-4	30	22.5	26.25	3.8	2.3	4500	1	4.68	0.79	67	183	2.4
	D-3	12	9.0	10.5	1.5	2.3	4400	1/2	0.60	0.63	130	27	2.2
	D-4	12	9.0	10.5	1.5	2.3	4500	1/2	0.60	0.63	130	31	2.5
	D-5	12	9.0	10.5	1.5	2.3	4500	1/2	0.60	0.63	130	31	2.5
	D-6	12	9.0	10.5	1.5	2.3	4600	1/2	0.60	0.63	130	29	2.3
	E-1	30	22.5	26.25	3.8	2.9	4300	1	4.68	0.79	75	130	1.8
	E-2	30	22.5	26.25	3.8	2.9	4300	1	4.68	0.79	75	136	1.9
	E-2-S	30	22.5	26.25	3.8	2.9	4400	1	4.68	0.79	75	142	1.9
	F-1	12	9.0	10.5	1.5	2.9	4900	1/2	0.93	0.98	84	27	2.1
	F-2	12	9.0	10.5	1.5	2.9	5000	1/2	0.93	0.98	84	29	2.2

* Cubes used for concrete compressive strength. Converted to 6 by 12 in. cylinder strength using factors suggested by Reineck et al.(2003): 0.72 (100 mm cube), 0.75 (120 mm cube), 0.79 (150 mm cube), 0.83 (200 mm cube)

** Concrete cover is defined as distance from the nearest concrete face to the centroid of longitudinal reinforcement

Table 2.3 Crack Information

Researcher	Specimen	Effective Depth (in.)	Stress in Concrete*, f_c (ksi)	Number of Cracks	Average Flexural Crack Spacing (in.)	Spacing-to-Effective Depth Ratio
Sneed (2007)	1-1	9.1	0.14	3	6	0.66
	1-2	20.9	0.14	8	10	0.48
	1-3	26.8	0.14	9	8	0.30
	1-4	32.4	0.14	14	11	0.34
	2-1	9.2	0.13	2	5	0.54
	2-2	20.8	0.14	7	10	0.48
	2-3	26.9	0.14	11	7	0.26
	2-4	32.4	0.14	11	9	0.28
McCain (2012)	E-1	26.25	0.13	8	11	0.42
	E-2	26.25	0.13	7	11	0.42
	F-1	10.5	0.14	5	4	0.38
	F-2	10.5	0.14	6	5	0.48
* Estimated stress at the load at which flexure cracks were counted (Equation 2-2)						

Table 3.1 Beam Properties

Specimen	Depth, h (in.)	Width, b (in.)	Effective Depth, d (in.)	Shear Span, a (in.)	Compressive Strength, f'_c (psi)	Max Agg. Size, a_g (in.)	Reinforcement Bar Diamer (in.)	Reinforcement Ratio, ρ (%)	Yield Stress, f_y (ksi)
B-1*	12	9	10.5	24	3600	1	0.625	0.98	62
B-2*	12	9	10.5	24	3600	1	0.625	0.98	62
C-1*	12	9	10.5	24	4900	1	0.5	0.63	128
C-2*	12	9	10.5	24	4700	1	0.5	0.63	128
D-1*	12	9	10.5	24	2700	1/2	0.5	0.63	128
D-2*	12	9	10.5	24	2800	1/2	0.5	0.63	128
D-3**	12	9	10.5	24	4400	1/2	0.5	0.63	130
D-4**	12	9	10.5	24	4500	1/2	0.5	0.63	130
D-5**	12	9	10.5	24	4500	1/2	0.5	0.63	130
D-6**	12	9	10.5	24	4600	1/2	0.5	0.63	130
F-1**	12	9	10.5	30	4900	1/2	0.625	0.98	84
F-2**	12	9	10.5	30	5000	1/2	0.625	0.98	84
F-3-S	12	9	10.5	30	4900	1/2	0.5	0.63	134
F-3-N	12	9	10.5	30	4900	1/2	0.5	0.63	134
F-4-S	12	9	10.5	30	4900	1/2	0.5	0.63	134
F-4-N	12	9	10.5	30	4900	1/2	0.5	0.63	134
H-1-N	12	9	10.5	30	4100	3/8	0.5	0.63	134
H-1-S	12	9	10.5	30	4100	3/8	0.5	0.63	134
H-2-S	12	9	10.5	30	4100	3/8	0.5	0.63	134
H-2-N	12	9	10.5	30	4100	3/8	0.5	0.63	134
I-1-S	12	9	10.5	30	4400	1/2	0.5	0.63	137
I-1-N	12	9	10.5	30	4400	1/2	0.5	0.63	137
I-2-S	12	9	10.5	30	4200	1/2	0.5	0.63	137
I-2-N	12	9	10.5	30	4200	1/2	0.5	0.63	137
J-1-S	12	9	10.5	30	3300	1/2	0.5	0.63	137
J-1-N	12	9	10.5	30	3300	1/2	0.5	0.63	137
J-2-S	12	9	10.5	30	3300	1/2	0.5	0.63	137
J-2-N	12	9	10.5	30	3300	1/2	0.5	0.63	137
K-1-N	12	9	10.5	30	4000	1	0.5	0.63	137
K-1-S	12	9	10.5	30	4000	1	0.5	0.63	137
K-2-S	12	9	10.5	30	4300	1	0.5	0.63	137
K-2-N	12	9	10.5	30	4300	1	0.5	0.63	137
G-1-N***	12	9	10.5	30	4500	2	2.257	0.79	76
G-1-S***	12	9	10.5	30	4500	2	2.257	0.79	76
G-2-N***	12	9	10.5	30	3400	2	2.257	0.79	76
G-2-S***	12	9	10.5	30	3400	2	2.257	0.79	76
* Murray (2010)									
** McCain (2012)									
*** Details on Series G are found in Appendix E									

Table 4.1 Summary of Test Results

Specimen	Depth, h (in.)	Width, b (in.)	Effective Depth, d (in.)	Shear Span , a (in)	Compressive Strength, f'_c (psi)	Max Agg. Size, a_g (in.)	A_s (in^2)	Reinforcement Ratio, ρ (%)	a/d	Peak Load, P (kip)	$v/\sqrt{f'_c}$	$v_T/\sqrt{f'_c}$ ***
B-1*	12	9	10.5	24	3600	1	0.93	0.98	2.3	34	3.0	3.0
B-2*	12	9	10.5	24	3600	1	0.93	0.98	2.3	40	3.5	3.6
C-1*	12	9	10.5	24	4900	1	0.6	0.63	2.3	44	3.3	3.4
C-2*	12	9	10.5	24	4700	1	0.6	0.63	2.3	39	3.0	3.1
D-1*	12	9	10.5	24	2700	1/2	0.6	0.63	2.3	22	2.3	2.3
D-2*	12	9	10.5	24	2800	1/2	0.6	0.63	2.3	23	2.3	2.4
D-3**	12	9	10.5	24	4400	1/2	0.6	0.63	2.3	27	2.2	2.2
D-4**	12	9	10.5	24	4500	1/2	0.6	0.63	2.3	31	2.5	2.5
D-5**	12	9	10.5	24	4500	1/2	0.6	0.63	2.3	31	2.4	2.5
D-6**	12	9	10.5	24	4600	1/2	0.6	0.63	2.3	29	2.3	2.3
F-1**	12	9	10.5	30	4900	1/2	0.93	0.98	2.9	27	2.0	2.1
F-2**	12	9	10.5	30	5000	1/2	0.93	0.98	2.9	29	2.2	2.2
F-3-S	12	9	10.5	30	4900	1/2	0.6	0.63	2.9	27.0	2.0	2.1
F-3-N	12	9	10.5	30	4900	1/2	0.6	0.63	2.9	27.0	2.0	2.1
F-4-S	12	9	10.5	30	4900	1/2	0.6	0.63	2.9	26.6	2.0	2.1
F-4-N	12	9	10.5	30	4900	1/2	0.6	0.63	2.9	31.2	2.4	2.4
H-1-N	12	9	10.5	30	4100	3/8	0.6	0.63	2.9	19.9	1.6	1.7
H-1-S	12	9	10.5	30	4100	3/8	0.6	0.63	2.9	24.9	2.1	2.1
H-2-S	12	9	10.5	30	4100	3/8	0.6	0.63	2.9	21.6	1.8	1.9
H-2-N	12	9	10.5	30	4100	3/8	0.6	0.63	2.9	23.3	1.9	2.0
I-1-S	12	9	10.5	30	4400	1/2	0.6	0.63	2.9	24.8	2.0	2.0
I-1-N	12	9	10.5	30	4400	1/2	0.6	0.63	2.9	30.0	2.4	2.5
I-2-S	12	9	10.5	30	4200	1/2	0.6	0.63	2.9	23.8	1.9	2.0
I-2-N	12	9	10.5	30	4200	1/2	0.6	0.63	2.9	27.2	2.2	2.3
J-1-S	12	9	10.5	30	3300	1/2	0.6	0.63	2.9	22.9	2.1	2.2
J-1-N	12	9	10.5	30	3300	1/2	0.6	0.63	2.9	23.8	2.2	2.3
J-2-S	12	9	10.5	30	3300	1/2	0.6	0.63	2.9	22.7	2.1	2.2
J-2-N	12	9	10.5	30	3300	1/2	0.6	0.63	2.9	26.9	2.5	2.6
K-1-N	12	9	10.5	30	4000	1	0.6	0.63	2.9	27.5	2.3	2.4
K-1-S	12	9	10.5	30	4000	1	0.6	0.63	2.9	28.9	2.4	2.5
K-2-S	12	9	10.5	30	4300	1	0.6	0.63	2.9	29.7	2.4	2.5
K-2-N	12	9	10.5	30	4300	1	0.6	0.63	2.9	32.0	2.6	2.6
G-1-N****	48	24	42.0	120	4500	2	8	0.79	2.9	204.4	1.5	1.7
G-1-S****	48	24	42.0	120	4500	2	8	0.79	2.9	233.4	1.7	1.9
G-2-N****	48	24	42.0	120	3400	2	8	0.79	2.9	205.7	1.7	2.0
G-2-S****	48	24	42.0	120	3400	2	8	0.79	2.9	190.2	1.6	1.8

* Murray (2010)

** McCain (2012)

*** Includes self-weight of beam and weight of loading equipment

**** Details on Series G are found in Appendix E

Table 4.2 Weight of Testing Apparatus

Series	Weight (lb)
A*	500
B, C, D*	100
D, F **	100
E**	500
F, H, I, J, K	270
G	1700
* Murray (2010)	
** McCain (2012)	

Table 4.3 Summary of Cracking Results

Specimen	Depth (in.)	First Observed Crack		Number of Flexural Cracks	Stress in Concrete**, f_c (ksi)	Average First Observed Crack Load (kip)	Average Number of Flexural Cracks
		Load, P_{cr} (kip)	$\sqrt{f'_c}$ (units of psi)				
E-1*	30	27	4.6	8	0.13	29	8
E-2*	30	30	5.1	7	0.13		
F-1*	12	11	10.9	5	0.14	12	6
F-2*	12	12	11.8	6	0.14		
F-3	12	9	8.9	8	0.14	9	9
F-4	12	9	8.9	9	0.14		
H-1	12	9	8.9	6	0.11	9	7
H-2	12	9	8.9	8	0.14		
I-1	12	9	9.8	4	0.14	9	5
I-2	12	9	9.8	6	0.14		
J-1	12	9	9.8	8	0.14	9	7
J-2	12	9	9.8	6	0.14		
K-1	12	12	9.4	5	0.14	12	5
K-2	12	12	9.4	5	0.14		
G-1***	48	40	3.9	10	0.14	45	9
G-2***	48	50	5.6	7	0.10		
* McCain (2012)							
** Estimated stress at the load at which flexure cracks were counted (Equation 2-2)							
*** Details on Series G are found in Appendix E							

Table 5.1 Average Unit Shear Strength at Failure

Specimen	Effective Depth, d (in.)	Max Agg. Size, a_g (in.)	a/d	$v_T / \sqrt{f'_c}$ ***	Average
B-1*	10.5	1	2.3	3.0	3.3
B-2*	10.5	1	2.3	3.6	
C-1*	10.5	1	2.3	3.4	3.2
C-2*	10.5	1	2.3	3.1	
D-1*	10.5	1/2	2.3	2.3	2.3
D-2*	10.5	1/2	2.3	2.4	
D-3**	10.5	1/2	2.3	2.2	2.4
D-4**	10.5	1/2	2.3	2.5	
D-5**	10.5	1/2	2.3	2.5	
D-6**	10.5	1/2	2.3	2.3	
F-1**	10.5	1/2	2.9	2.1	2.2
F-2**	10.5	1/2	2.9	2.2	
F-3-S	10.5	1/2	2.9	2.1	
F-3-N	10.5	1/2	2.9	2.1	
F-4-S	10.5	1/2	2.9	2.1	
F-4-N	10.5	1/2	2.9	2.4	
H-1-N	10.5	3/8	2.9	1.7	1.9
H-1-S	10.5	3/8	2.9	2.1	
H-2-S	10.5	3/8	2.9	1.9	
H-2-N	10.5	3/8	2.9	2.0	
I-1-S	10.5	1/2	2.9	2.0	2.2
I-1-N	10.5	1/2	2.9	2.5	
I-2-S	10.5	1/2	2.9	2.0	
I-2-N	10.5	1/2	2.9	2.3	
J-1-S	10.5	1/2	2.9	2.2	2.3
J-1-N	10.5	1/2	2.9	2.3	
J-2-S	10.5	1/2	2.9	2.2	
J-2-N	10.5	1/2	2.9	2.6	
K-1-N	10.5	1	2.9	2.4	2.5
K-1-S	10.5	1	2.9	2.5	
K-2-S	10.5	1	2.9	2.5	
K-2-N	10.5	1	2.9	2.6	
G-1-N****	42	2	2.9	1.7	1.9
G-1-S****	42	2	2.9	1.9	
G-2-N****	42	2	2.9	2.0	
G-2-S****	42	2	2.9	1.8	

* Murray (2010)

** McCain (2012)

*** Includes self-weight of beam and weight of loading equipment

**** Details on Series G are found in Appendix E

Table 5.2 Average Flexural Crack Spacing Comparison

Specimen	Effective Depth (in.)	Stress in Concrete**, f_c (ksi)	Average Flexural Crack Spacing (in.)	Spacing-to-Effective Depth Ratio
E-1*	26.25	0.13	11	0.4
E-2*	26.25	0.13	11	0.4
F-1*	10.5	0.14	4	0.4
F-2*	10.5	0.14	5	0.5
F-3	10.5	0.14	4	0.4
F-4	10.5	0.14	4	0.4
H-1	10.5	0.11	6	0.6
H-2	10.5	0.14	5	0.5
I-1	10.5	0.14	6	0.6
I-2	10.5	0.14	5	0.5
J-1	10.5	0.14	5	0.5
J-2	10.5	0.14	5	0.5
K-1	10.5	0.14	6	0.6
K-2	10.5	0.14	5	0.5
G-1***	42	0.14	16	0.4
G-2***	42	0.10	17	0.4
* McCain (2012)				
** Estimated stress at which flexure cracks were counted (Equation 2-2)				
*** Details on Series G are found in Appendix E				

Table 5.3 Concrete Tensile Strength

Specimen	Compressive Strength, f'_c (psi)	First Observed Crack			Flexure Test		Split Cylinder Test	
		Load, P_{cr} (kip)	Calculated Modulus from P_{cr} (psi)	$\sqrt{f'_c}$ (units of psi)	Modulus of Rupture (psi)	$\sqrt{f'_c}$ (units of psi)	Tensile Strength, f_t (psi)	$\sqrt{f'_c}$ (units of psi)
B-1*	3600	15.9	883	14.7	880	14.7	520	8.7
B-2*	3600	20.7	1150	19.2	1150	19.2	520	8.7
C-1*	4900	18.4	1022	14.6	1020	14.6	560	8.0
C-2*	4700	18.3	1017	14.8	1020	14.9	560	8.2
D-1*	2700	15	833	16.0	850	16.4	400	7.7
D-2*	2800	15	833	15.7	850	16.1	400	7.6
D-3**	4400	15	833	12.6	570	8.6	440	6.6
D-4**	4500	12	667	9.9	500	7.5	480	7.2
D-5**	4500	12	667	9.9	540	8.0	480	7.2
D-6**	4600	12	667	9.8	740	10.9	470	6.9
F-1**	4900	11	764	10.9	640	9.1	490	7.0
F-2**	5000	12	833	11.8	650	9.2	450	6.4
F-3	4900	9	625	8.9	750	10.7	510	7.3
F-4	4900	9	625	8.9	750	10.7	510	7.3
H-1	4100	9	625	9.8	370	5.8	310	4.8
H-2	4100	9	625	9.8	370	5.8	310	4.8
I-1	4400	9	625	9.4	470	7.1	440	6.6
I-2	4200	9	625	9.6	470	7.3	440	6.8
J-1	3300	9	625	10.9	480	8.4	330	5.7
J-2	3300	9	625	10.9	480	8.4	330	5.7
K-1	4000	12	833	13.2	530	8.4	360	5.7
K-2	4300	12	833	12.7	530	8.1	360	5.5
G-1***	4500	40	260	3.9	N/A	N/A	450	6.7
G-2***	3400	50	326	5.6	N/A	N/A	410	7.0
* Murray (2010)								
** McCain (2012)								
*** Details on Series G are found in Appendix E								

Table 5.4 Aggregate Properties for Mixes in Series F, I, and J

Series	Sand Design Weight (lb/yd^3)	Pea Gravel Design Weight (lb/yd^3)	a_{g50}
F	1540	1800	0.16
I	2359	610	0.06
J	0	3103	0.21

Table A.1 Design Mixture Proportions

Materials	Mixture						
	F	H**	I	J	K	G-1	G-2
#2 Stone	N/A	N/A	N/A	N/A	N/A	1836 lb/yd^3	1939 lb/yd^3
# 8 Gravel	N/A	N/A	N/A	N/A	1822 lb/yd^3	N/A	N/A
Pea Gravel	1785 lb/yd^3	N/A	597 lb/yd^3	3086 lb/yd^3	N/A	N/A	N/A
#23 Sand	1525 lb/yd^3	2973 lb/yd^3	2343 lb/yd^3	N/A	1379 lb/yd^3	1471 lb/yd^3	1548 lb/yd^3
Cement	435 lb/yd^3	655 lb/yd^3	530 lb/yd^3	480 lb/yd^3	275 lb/yd^3	275 lb/yd^3	288 lb/yd^3
Fly Ash	N/A	N/A	N/A	N/A	87.5 lb/yd^3	100 lb/yd^3	103 lb/yd^3
Water*	412 lb/yd^3	451 lb/yd^3	367lb/yd^3	331 lb/yd^3	210 lb/yd^3	202 lb/yd^3	208 lb/yd^3
Air Entrainment	N/A	N/A	N/A	N/A	4.75 oz/yd^3	1.5 oz/yd^3	1.7oz/yd^4
Water Reducer	30 oz/yd^3	N/A	N/A	N/A	7.5 oz/yd^3	26 oz/yd^3	28 oz/yd^3
Slump	1.5"	8.75"	4"	8.75"	4"	3.5"	3.5"
W/C Ratio	0.47	0.69	0.69	0.69	0.58	0.54	0.53
* Water weight includes moisture in aggregate							
** Four gallons of water added to truck. Table accounts for the addition.							

Table A.2 Gradation of Mixes

Sieve	Size	Series F	Series I	Series J
	in	Percent Passing		
1/2	0.50	100	100	100
3/8	0.375	99.9	100.0	99.9
1/4	0.25	81.7	92.0	71.2
#4	0.187	59.0	81.5	36.1
#8	0.094	31.9	61.5	1.5
#30	0.023	19.0	37.2	0.3
#50	0.012	8.3	16.1	0.2
#100	0.006	1.1	2.1	0.2
#200	0.003	0.3	0.5	0.1
Pan		0	0	0

Table A.3 Gradation of Aggregate

Sieve	Size	#23 Sand	Pea Gravel	#8 Gravel*	#2 Stone*
	in	Percent Passing			
2	2	100	100	100	100
1	1	100	100	100	9
3/4	0.75	100	100	88.4	4.8
1/2	0.50	100	100	54.6	2.7
3/8	0.375	100	99.9	40.8	N/A
1/4	0.25	100	71.2	N/A	N/A
#4	0.187	98.9	36.1	1.1	N/A
#8	0.094	84.6	1.5	0.1	N/A
#30	0.023	51.4	0.3	N/A	N/A
#50	0.012	22.2	0.2	N/A	N/A
#100	0.006	2.8	0.2	N/A	N/A
#200	0.003	0.6	0.1	N/A	N/A
Pan	0.00	0	0	0	0
* Gradation from supplier quality test report					

Table A.4 Batched Concrete Mixture Proportions

Materials	Mixture						
	F	H**	I	J	K	G-1	G-2
#2 Stone	N/A	N/A	N/A	N/A	N/A	1836 lb/yd^3	1939 lb/yd^3
# 8 Gravel	N/A	N/A	N/A	N/A	1822 lb/yd^3	N/A	N/A
Pea Gravel	1785 lb/yd^3	N/A	597 lb/yd^3	3086 lb/yd^3	N/A	N/A	N/A
#23 Sand	1525 lb/yd^3	2973 lb/yd^3	2343 lb/yd^3	N/A	1379 lb/yd^3	1471 lb/yd^3	1548 lb/yd^3
Cement	435 lb/yd^3	655 lb/yd^3	530 lb/yd^3	480 lb/yd^3	275 lb/yd^3	275 lb/yd^3	288 lb/yd^3
Fly Ash	N/A	N/A	N/A	N/A	87.5 lb/yd^3	100 lb/yd^3	103 lb/yd^3
Water*	412 lb/yd^3	451 lb/yd^3	367lb/yd^3	331 lb/yd^3	210 lb/yd^3	202 lb/yd^3	208 lb/yd^3
Air Entrainment	N/A	N/A	N/A	N/A	4.75 oz/yd^3	1.5 oz/yd^3	1.7oz/yd^4
Water Reducer	30 oz/yd^3	N/A	N/A	N/A	7.5 oz/yd^3	26 oz/yd^3	28 oz/yd^3
Slump	1.5"	8.75"	4"	8.75"	4"	3.5"	3.5"
W/C Ratio	0.47	0.69	0.69	0.69	0.58	0.54	0.53
* Water weight includes moisture in aggregate							
** Four gallons of water added to truck (table accounts for the addition)							

Table A.5 Curing Time for Each Mixture

Mixture	Curing Time (day)
F	1
H	35
I	7
J	35
K	14
G-1	9
G-2	56

Table A.6 Test Day Concrete Strengths

Mixture	Specimen	Compressive Strength, f'_c (psi)	Split Cylinder Tensile Strength (psi)	Modulus of Rupture (psi)	Modulus of Elasticity (ksi)
F	F-3	4900	510	750	3700
	F-4	4900			
H	H-1	4100	310	370	2400
	H-2	4100			
I	I-1	4300	440	470	3100
	I-2	4300			
J	J-1	3300	330	480	2800
	J-2	3300			
K	K-1	4000	360	530	4000
	K-2	4300	380		
G	G-1	4500	450	N/A	N/A
	G-2	3400	410		

Table A.7 Specimen Reinforcement Heats

Series	Heat	
	Longitudinal Steel	Transverse Steel
F	1	3
H	1	3
I	2	4
J	2	4
K	2	5
G	6	7

Table A.8 Steel Reinforcement Properties

Heat	**Bar Size**	**Specification**	**Elongation at Rupture (%)**	**Ultimate Strength (ksi)**	**Yield Stress, f_y (ksi)**
1	#4	ASTM A1035-11, Gr. 100	7.6	173	134
2	#4		7.9	174	137
3	#3	ASTM A615-12, Gr. 60	11.6	112	74
4	#3	ASTM A615-11, Gr. 60	10	108	71
5	#3	ASTM A615-12, Gr. 60	15	111	76
6*	#18	ASTM A615-12, Gr. 60	13	111	76
7*	#5	ASTM A615-12, Gr. 60	14.9	102	67
* Properties from Mill Cert					

Table B.1 As-Built Dimensions

Specimen	Length (in.)	b (in.)	h (in.)	d (in.)	A (in.)	B (in.)	C (in.)	D (in.)
F-3	90	9	12	10 9/16	1 9/16	3	2 7/8	1 5/8
F-4	90	9	12 1/16	11 9/16	1 7/16	3	3	1 5/8
H-1	90	9	12 1/16	10 5/8	1 9/16	2 15/16	3	1 1/2
H-2	90	9	12 1/16	10 5/8	1 9/16	2 15/16	3	1 1/2
I-1*	90	9	12 1/16	10 9/16	N/A	4 1/2	N/A	N/A
I-2*	90	9	12 1/16	10 9/16	N/A	4 1/2	N/A	N/A
J-1*	89 15/16	9	12 1/16	10 9/16	N/A	4 1/2	N/A	N/A
J-2*	90	9	12 1/16	10 9/16	N/A	4 1/4	N/A	N/A
K-1	90	9	12 1/16	10 9/16	1 1/2	3	3	1 1/2
K-2	90	9	12	10 1/2	1 7/16	3	3	1 1/2
G-1	360 1/16	24	48 1/8	42 3/16	6	12	6	N/A
G-2	360 1/16	24 1/16	48 1/8	42 3/16	6 1/16	12	6	N/A
* B dimension is measured from left face of beam to reinforcement (A+B in figure below)								

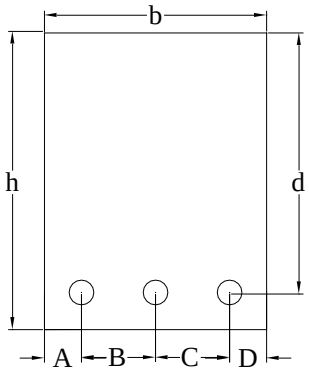

Series F, H, I, J, and K

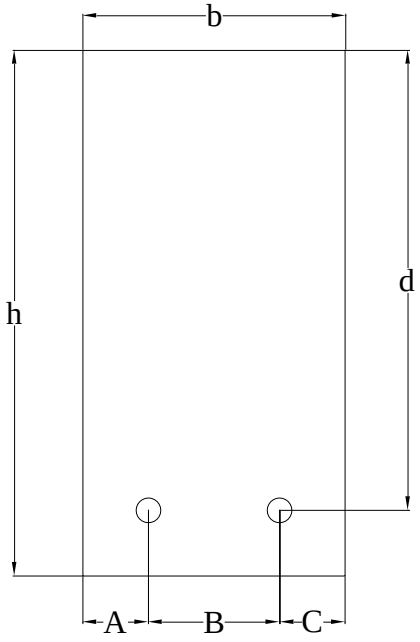

Series G

Table C.1 Hardware Dimensions

Series	Plate A	Plate B	Plate C	Reaction Block	Roller (Length x Diameter)
F, H, I, J, K	9" x 4" x 3/4"	10-1/2" x 5" x 3/4"	N/A	36" x 12" x 11-1/2"	10-1/2" x 1"
G	24" x 10" x 2"	36" x 8" x 3"	36" x 12" x 3"	48" x 18" x 18"	36" x 3"

Table C.2 Load Cells and Pressure Transducer Calibrations

Series	Name	Model Number	Serial Number	Range	Sensitivity (mV/V/lb)	Accuracy (lb)
F, H, I, J, K	East Load Cell	3174 - 20K	4448	20000 lb	-4.93E-05	80
	West Load Cell	3174 - 20K	4451	20000 lb	-5.02E-05	60
G	Pressure Transducer: West Hydraulic Cylinder	PX302-10KGV	71008	100,000 psi	4.97E-05	570
	Pressure Transducer: East Hydraulic Cylinder				4.98E-05	670

Table C.3 LVDT Calibrations

Series	Name	Model Number	Serial Number	Range (± in.)	Sensitivity (mV/V/in.)	Accuracy (in.)
F, H, I, J, K	South Support	DC - E250	12971	0.25	-1349	0.001
	South Quarter	DC - E1000	X0135	1	-327	0.003
	South Midspan	DC - E1000	J7562	1	-339	0.002
	North Midspan	DC - E1000	J7434	1	-340	0.002
	North Quarter	DC - E1000	J7557	1	-334	0.002
	North Support	DC - E250	7943	0.25	-1289	0.001
G	South Support	DC - E250	12838	0.25	-1287	0.001
	South Quarter	DC - E1000	X0135	1	-341	0.009
	Midspan	DC - E1000	J7434	1	-340	0.003
	North Quarter	DC - E1000	J7557	1	-340	0.004
	North Support	DC - E250	7943	0.25	-1221	0.004

Table D.1 Measure Bar Slip

Specimen	Bar Slip (in.)	
	South/East End	North/West End
B-1*	0.000	0.002
B-2*	0.000	0.003
C-1*	0.000	0.000
C-2*	0.000	0.000
D-1*	0.000	0.000
D-2*	0.000	0.000
D-3**	0.003	0.000
D-4**	0.000	N/A***
D-5**	0.000	0.000
D-6**	0.000	0.000
F-1**	0.000	0.000
F-2**	0.000	0.001
F-3	0.000	0.001
F-4	0.000	0.001
H-1	0.000	0.001
H-2	0.002	0.002
I-1	0.000	0.000
I-2	0.000	0.000
J-1	0.000	0.000
J-2	0.000	0.001
K-1	N/A***	0.000
K-2	0.000	0.001
G-1	0.000	0.000
G-2	0.003	0.000
* Murray (2010)		
**McCain (2012)		
*** Dial gage fell off at failure		

Table D.2 Specimen F-3 Crack Widths

Crack Number	Crack Width (in.)			
	9 kip	12 kip	15 kip	18 kip
1	<0.005	<0.005	<0.005	<0.005
2	<0.005	<0.005	0.005	0.005
3	<0.005	<0.005	<0.005	0.005
4		<0.005	0.005	0.005
5		<0.005	<0.005	<0.005
6			<0.005	0.005
7			<0.005	<0.005
8			0.005	0.005
9				<0.005
10				<0.005

Table D.3 Specimen F-4 Crack Widths

Crack Number	Crack Width (in.)				
	9 kip	12 kip	15 kip	18 kip	21 kip
1	<0.005	0.005	0.005	0.010	0.010
2	<0.005	0.010	0.010	0.010	0.010
3	<0.005	0.010	0.010	0.010	0.015
4	<0.005	0.005	0.005	0.005	0.005
5	<0.005	<0.005	0.005	0.005	0.010
6			<0.005	0.005	0.005
7			<0.005	0.010	0.010
8			0.005	0.005	0.005
9			0.005	0.010	0.010
10				<0.005	<0.005
11				<0.005	0.005

Table D.4 Specimen H-1 Crack Widths

Crack Number	**Crack Width (in.)**	
	9 kip	**12 kip**
1	<0.005	<0.005
2	<0.005	0.005
3	<0.005	0.005
4	<0.005	0.005
5	<0.005	0.005
6		<0.005

Table D.5 Specimen H-2 Crack Widths

Crack Number	**Crack Width (in.)**		
	9 kips	**12 kips**	**15 kips**
1	<0.005	0.005	0.005
2	<0.005	0.005	0.015
3	<0.005	0.005	0.005
4	<0.005	<0.005	0.005
5	<0.005	0.005	0.010
6	<0.005	<0.005	0.005
7			<0.005
8			<0.005

Table D.6 Specimen I-1 Crack Widths

Crack Number	Crack Width (in.)			
	9 kip	**12 kip**	**15 kip**	**18 kip**
1	0.005	0.005	0.010	0.010
2		<0.005	0.005	0.005
3		<0.005	0.005	0.010
4			<0.005	0.005
5				<0.005
6				<0.005
7				0.005

Table D.7 Specimen I-2 Crack Widths

Crack Number	Crack Width (in.)			
	9 kip	**12 kip**	**15 kip**	**18 kip**
1	<0.005	0.005	0.005	0.010
2	<0.005	0.005	0.005	0.005
3	<0.005	0.005	0.010	0.010
4		<0.005	0.005	0.010
5		0.005	0.005	0.015
6			<0.005	<0.005
7				<0.005

Table D.8 Specimen J-1 Crack Widths

Crack Number	Crack Width (in.)			
	9 kip	12 kip	15 kip	18 kip
1	<0.005	<0.005	<0.005	<0.005
2	<0.005	<0.005	0.005	0.010
3	<0.005	<0.005	0.005	0.005
4	<0.005	<0.005	0.005	0.005
5	<0.005	<0.005	<0.005	<0.005
6		<0.005	<0.005	0.005
7			<0.005	0.005
8			<0.005	<0.005
9				<0.005

Table D.9 Specimen J-2 Crack Widths

Crack Number	Crack Width (in.)			
	9 kip	12 kip	15 kip	18 kip
1	<0.005	<0.005	0.005	0.005
2		<0.005	<0.005	<0.005
3		<0.005	0.005	0.005
4		<0.005	<0.005	<0.005
5			<0.005	<0.005
6			0.005	0.010
7				<0.005
8				<0.005

Table D.10 Specimen K-1 Crack Widths

Crack Number	Crack Width (in.)		
	12 kip	15 kip	18 kip
1	<0.005	<0.005	0.005
2	<0.005	<0.005	<0.005
3	<0.005	<0.005	<0.005
4		<0.005	0.005
5		<0.005	0.005
6			<0.005

Table D.11 Specimen K-2 Crack Widths

Crack Number	Crack Width (in.)		
	12 kip	15 kip	18 kip
1	<0.005	0.005	0.010
2	<0.005	0.005	0.005
3		<0.005	<0.005
4		<0.005	<0.005
5		<0.005	<0.005
6			<0.005
7			<0.005
8			<0.005

Table E.1 Series G Table Descriptions

Table Number	Description
Table 3.1	Beam Properties
Table 4.1	Summary of Test Results
Table 4.3	Summary of Cracking Results
Table 5.1	Average Unit Shear Strength at Failure
Table 5.2	Average Flexural Crack Spacing Comparison
Table 5.3	Concrete Tensile Strength
Table A.1	Design Mixture Proportions
Table A.4	Batched Concrete Mixture Proportions
Table A.5	Curing Time for Each
Table A.6	Test Day Concrete Strengths
Table A.7	Specimen Reinforcement Heats
Table A.8	Steel Reinforcement Properties
Table B.1	As-Built Dimensions
Table C.1	Hardware Dimensions
Table C.2	Load Cells and Pressure Transducer Calibrations
Table C.3	LVDT Calibrations
Table E.3	Specimen G-1 Crack Widths
Table E.4	Specimen G-2 Crack Widths

Table E.2 Series G Figure Descriptions

Figure Number	Description
Figure E.1	Series G Elevation View of Beam
Figure E.2	Series G Cross Section View of 48 in. Deep Beam
Figure E.3	Series G Experimental Test Setup
Figure E.4	Series G Experimental Test Setup with External Stirrups
Figure E.5	Specimen G-1 Load-Deflection Curve
Figure E.6	Specimen G-2 Load-Deflection Curve
Figure E.7	Specimen G-2: South Side Failure Inclined Crack
Figure E.8	Elevation View of Series G Test Setup
Figure E.9	Series G Loading Setup
Figure E.10	Series G LVDT Experimental Setup
Figure E.11	Series G LVDT Locations
Figure E.12	Specimen G-1 Deflection Profile
Figure E.13	Specimen G-2 Deflection Profile
Figure E.14	Specimen G-1 Crack Maps
Figure E.15	Specimen G-2 Crack Map

Table E.3 Specimen G-1 Crack Widths

Crack Number	Crack Width (in.)			
	40 kip	**80 kip**	**120 kip**	**160 kip**
1	<0.005	<0.005	<0.005	N/A
2		<0.005	0.010	
3		<0.005	0.015	
4		0.005	0.015	
5		<0.005	0.005	
6			<0.005	
7			0.015	
8			0.005	
9			<0.005	

Table E.4 Specimen G-2 Crack Widths

Crack Number	Crack Width (in.)	
	80 kip	**120 kip**
1	<0.005	0.010
2	0.010	0.015
3	0.005	0.005
4	0.005	0.010
5		0.005
6		<0.005
7		0.015

Appendix G Figures

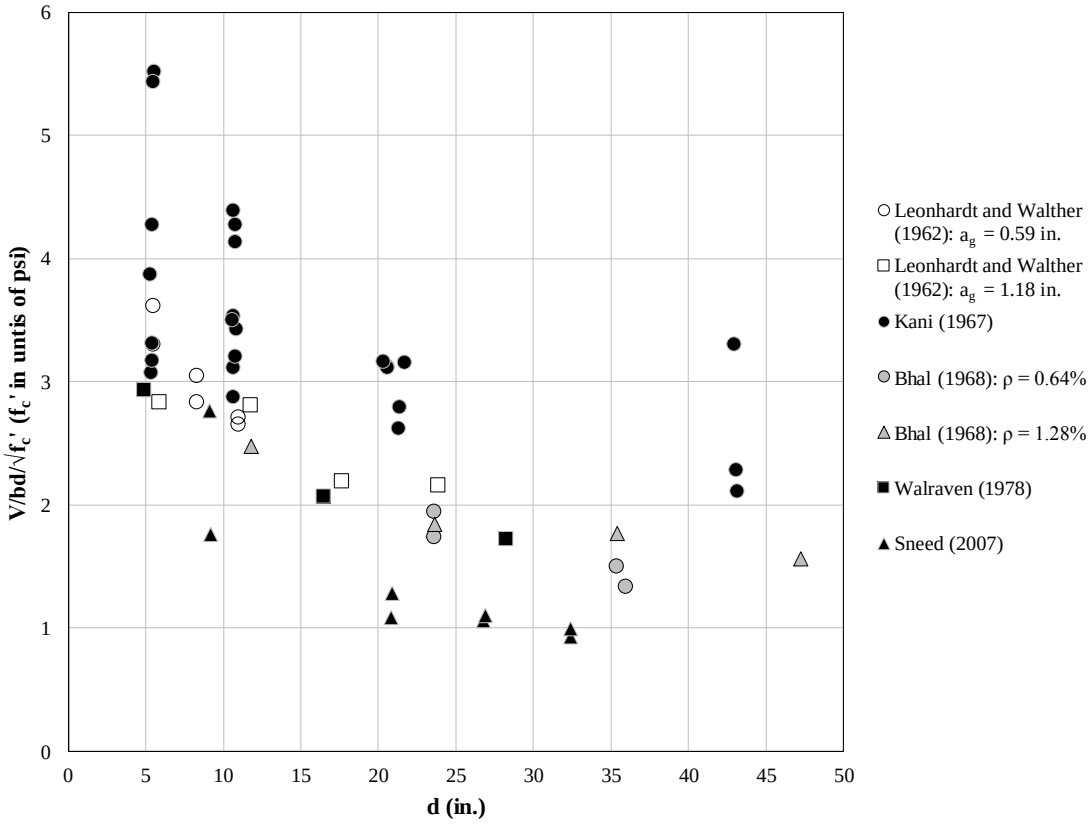

Figure 2.1 Shear Test Results: One

Note: In these tests concrete cover, maximum aggregate size and longitudinal reinforcement size and spacing were not all scaled in proportion to beam depth.

$$2.3 \le a/d \le 4.0$$

$$3/8 \text{ in.} \le a_g \le 1.2 \text{ in.}$$

$$0.01 \le a_g/d \le 0.2$$

$$3400 \text{ psi} \le f_c^{'} \le 10{,}800 \text{ psi}$$

$$6 \text{ in.} \le h \le 49 \text{ in.}$$

$$0.6\% \le \rho \le 2.9\%$$

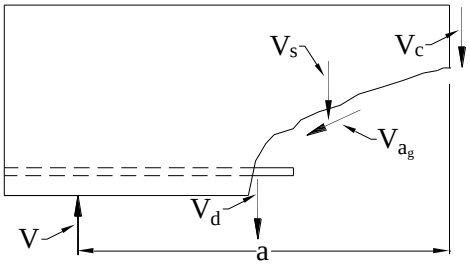

a = Shear Span
V = Shear Force
V_{a_g} = Shear Force Carried by Aggregate Interlock
V_c = Shear Force in Compression Zone
V_d = Shear Force in Dowel
V_s = Shear Reinforcement Force

Figure 2.2 Types of Shear Transfer

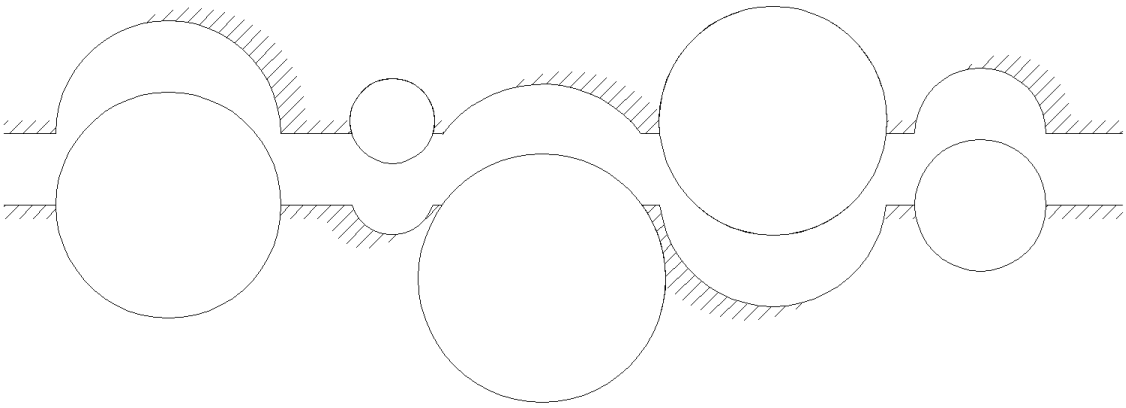

Figure 2.3 Structure of Crack Plane

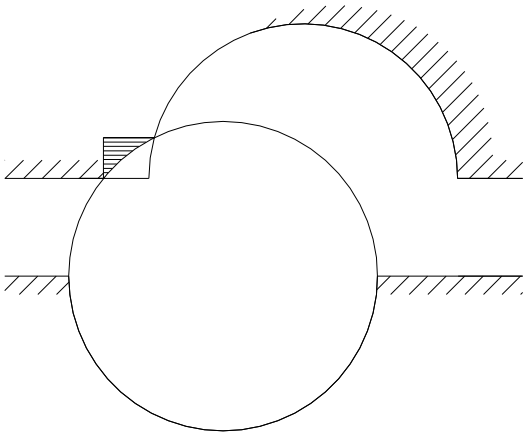

Figure 2.4 Contact Area between Matrix and Aggregate

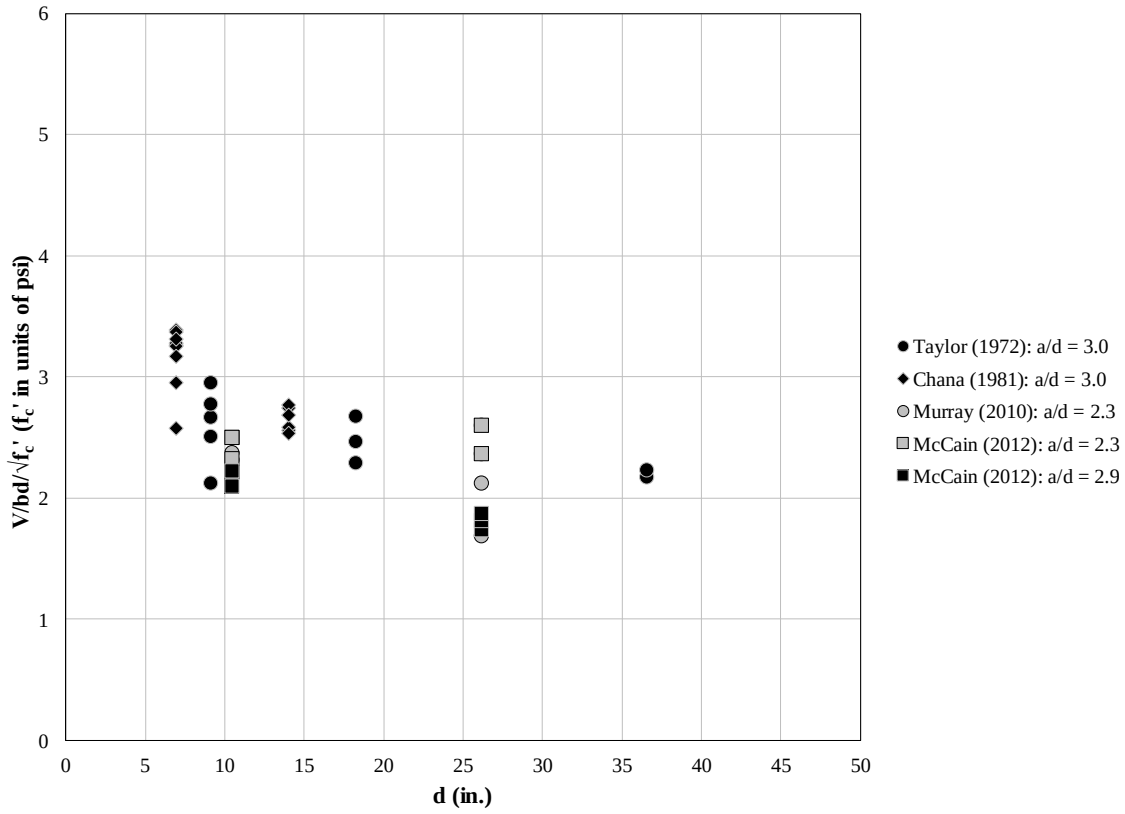

Figure 2.5 Shear Test Results: Two

Note: In these tests, among beams tested by the same researcher, concrete cover, and longitudinal reinforcement size and spacing were scaled in proportion to beam depth.

$$2.3 \le a/d \le 3.0$$

$$3/8 \text{ in.} \le a_g \le 1\text{-}1/2 \ \textit{in.}$$

$$0.02 \le a_g/d \le 0.1$$

$$2600 \text{ psi} \le f_c^{'} \le 5700 \text{ psi}$$

$$7.9 \text{ in.} \le h \le 39.4 \text{ in.}$$

$$0.63\% \le \rho \le 1.74\%$$

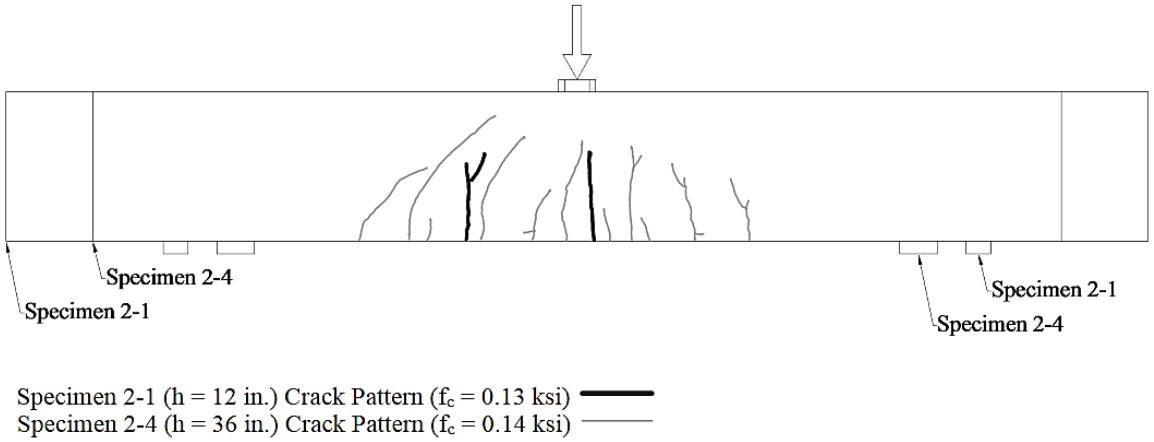

Figure 2.6 Crack Patterns (Sneed 2007)

Note: Concrete cover, width, and longitudinal reinforcement size and spacing were not all scaled in proportion to beam depth. Crack comparisons were made at comparable loading stages (*P/bh*). Test beams in this figure had the following dimensions and parameters:

$$a/d = 3.0$$
$$a_g = 3/8 \text{ in.}$$
$$0.012 \le a_g/d \le 0.041$$
$$9400 \text{ psi} \le f_c' \le 10,600 \text{ psi}$$
$$12 \text{ in.} \le h \le 36 \text{ in.}$$
$$0.13 \le P/bh \le 0.14$$
$$1.26\% \le \rho \le 1.31\%$$

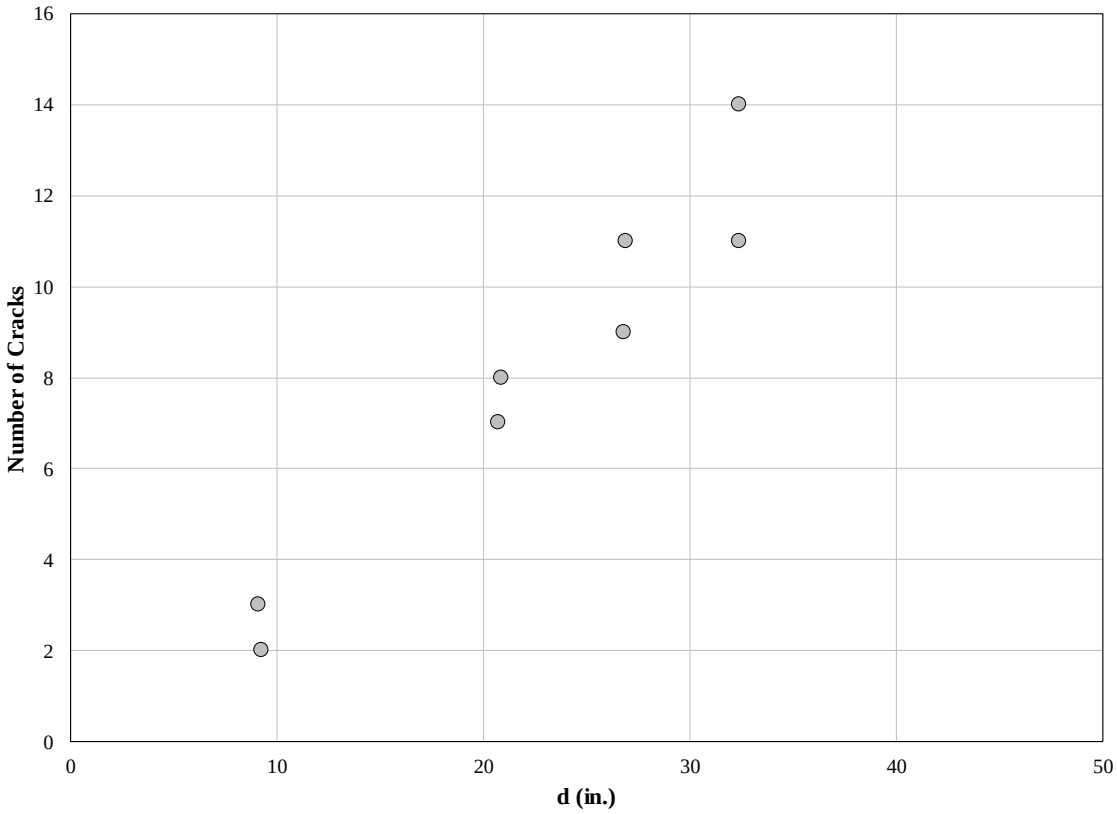

Figure 2.7 Number of Flexural Cracks (Sneed 2007)

Note: Concrete cover, width, and longitudinal reinforcement size and spacing not were scaled in proportion to beam depth. Crack comparisons were made at comparable loading stages (*P/bh*). Test beams in this figure had the following dimensions and parameters:

$$a/d = 3.0$$
$$a_g = 3/8 \text{ in.}$$
$$0.012 \le a_g/d \le 0.041$$
$$9400 \text{ psi} \le f_c^{'} \le 10{,}800 \text{ psi}$$
$$12 \text{ in.} \le h \le 36 \text{ in.}$$
$$0.13 \le P/bh \le 0.14$$
$$1.26\% \le \rho \le 1.31\%$$

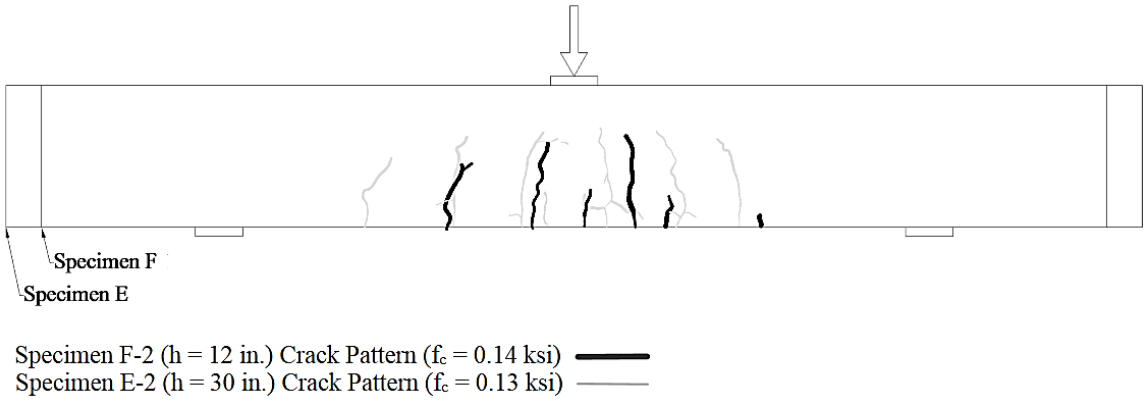

Figure 2.8 Crack Patterns (McCain 2012)

Note: Concrete cover, width, and longitudinal reinforcement size and spacing were scaled in proportion to beam depth. Crack comparisons were made at comparable loading stages (*P/bh*). Test beams in this figure had the following dimensions and parameters:

$$a/d = 2.9$$

$$1/2 \text{ in.} \le a_g \le 1 \text{ in.}$$

$$0.04 \le a_g/d \le 0.05$$

$$4300 \text{ psi} \le f_c' \le 5000 \text{ psi}$$

$$12 \text{ in.} \le h \le 30 \text{ in.}$$

$$0.13 \le P/bh \le 0.14$$

$$0.79\% \le \rho \le 0.98\%$$

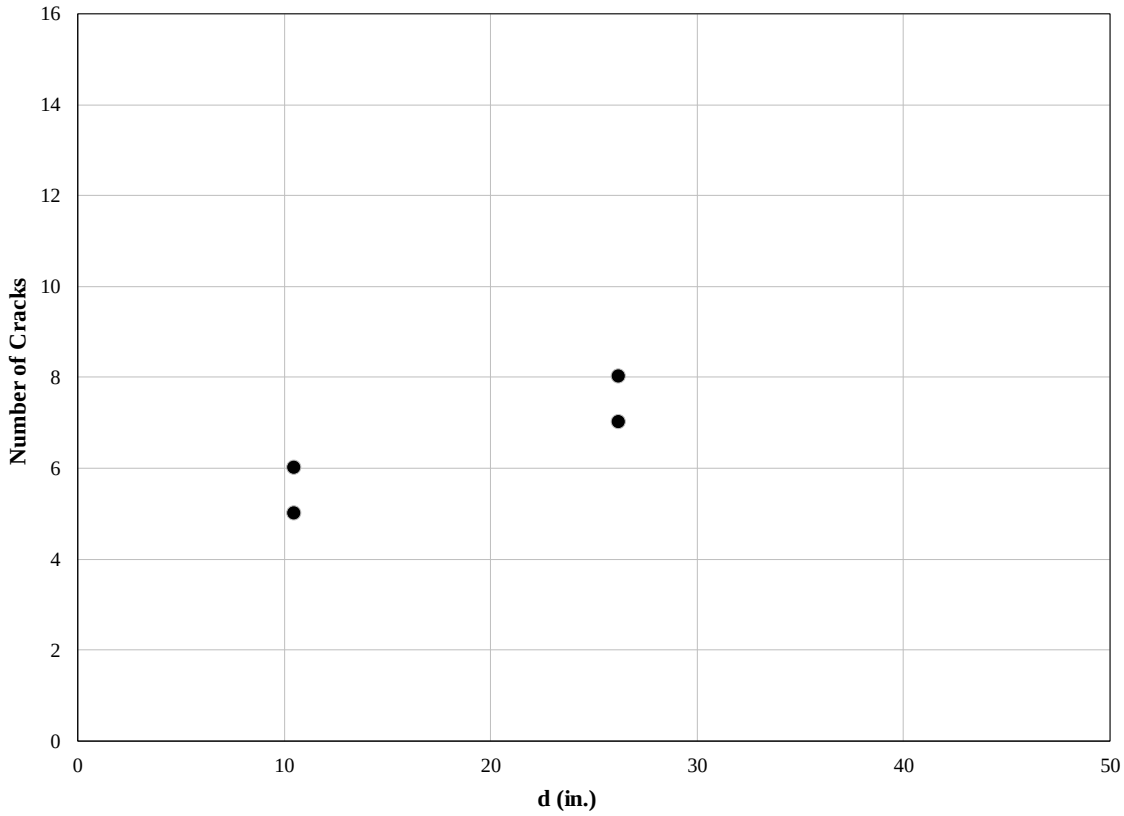

Figure 2.9 Number of Flexural Cracks (McCain 2012)

Note: Concrete cover, width, and longitudinal reinforcement size and spacing were scaled in proportion to beam depth. Crack comparisons were made at comparable loading stages (*P/bh*). Test beams in this figure had the following dimensions and parameters:

$$a/d = 2.9$$
$$1/2 \text{ in.} \le a_g \le 1 \text{ in.}$$
$$0.038 \le a_g/d \le 0.048$$
$$4300 \text{ psi} \le f_c^{'} \le 5000 \text{ psi}$$
$$12 \text{ in.} \le h \le 30 \text{ in.}$$
$$0.13 \le P/bh \le 0.14$$
$$0.79\% \le \rho \le 0.98\%$$

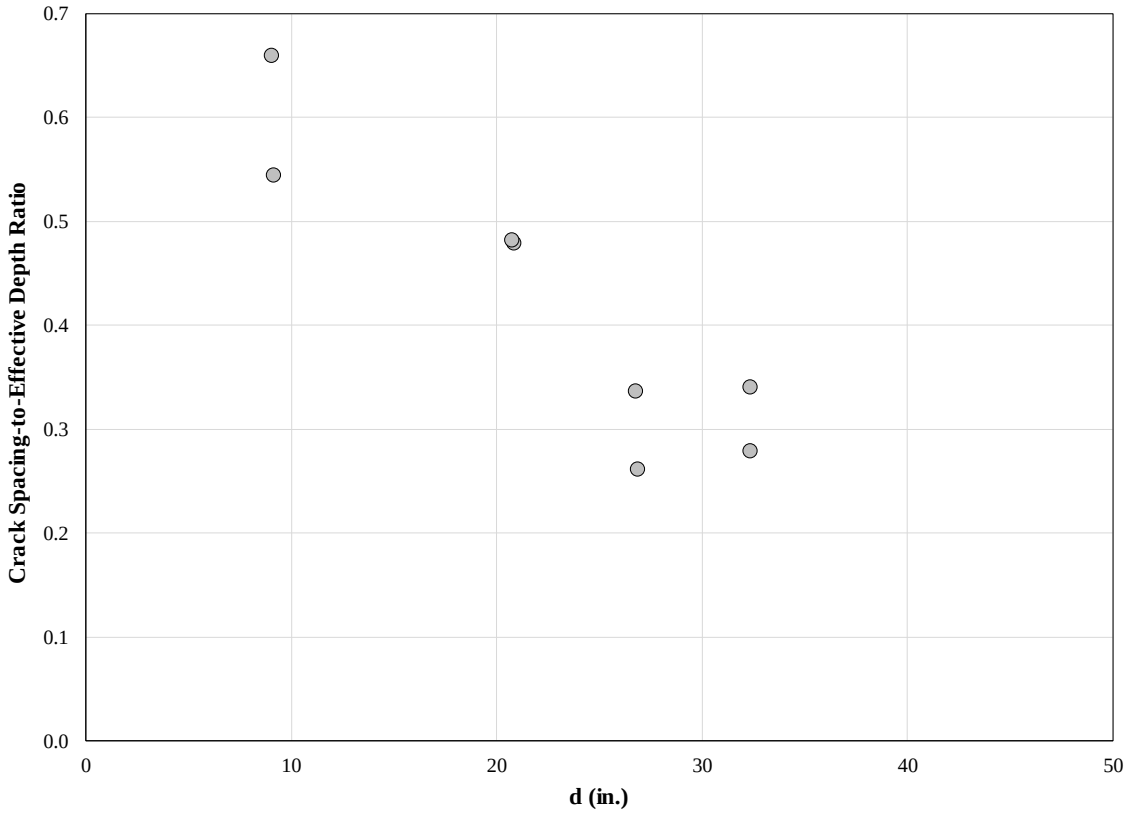

Figure 2.10 Relative Crack Spacing (Sneed 2007)

Note: Concrete cover, width, and longitudinal reinforcement size and spacing were not scaled in proportion to beam depth. Crack comparisons were made at comparable loading stages (*P/bh*). Test beams in this figure had the following dimensions and parameters:

$$a/d = 3.0$$
$$a_g = 3/8 \text{ in.}$$
$$0.01 \le a_g/d \le 0.04$$
$$9400 \text{ psi} \le f_c^{'} \le 10{,}800 \text{ psi}$$
$$12 \text{ in.} \le h \le 36 \text{ in.}$$
$$0.13 \le P/bh \le 0.14$$
$$1.20\% \le \rho \le 1.31\%$$

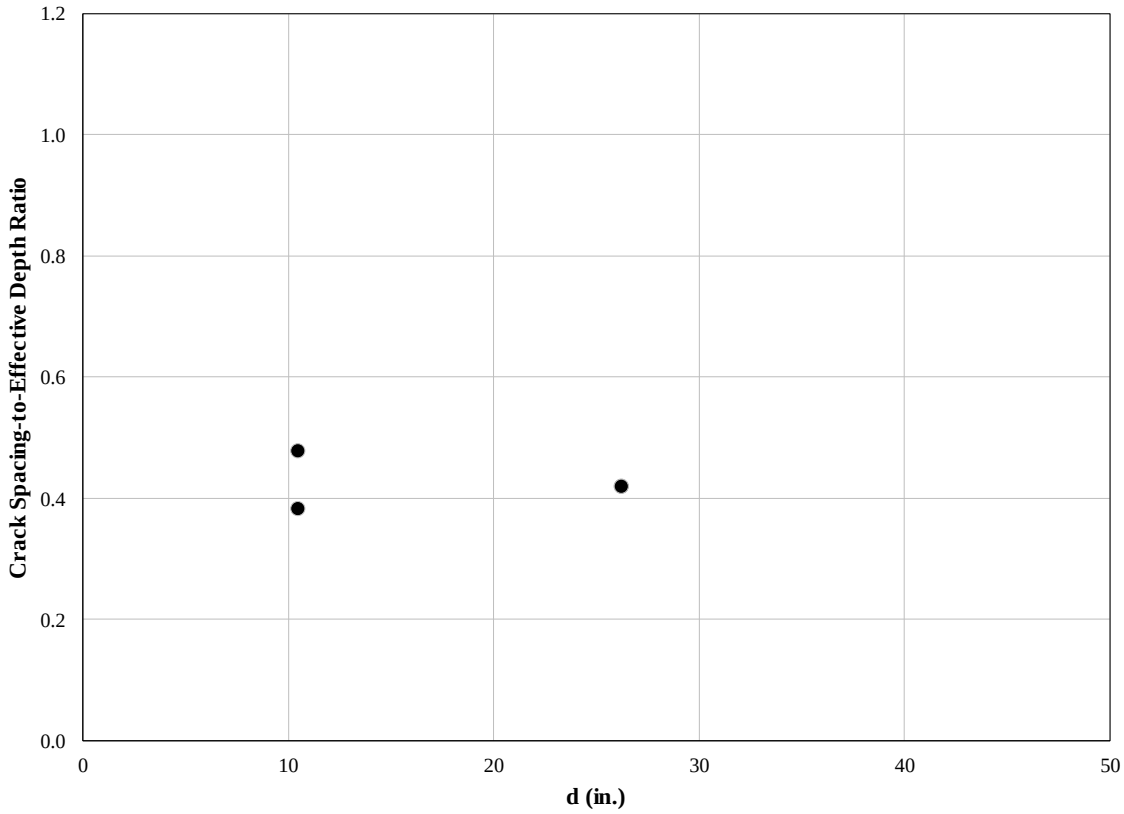

Figure 2.11 Relative Crack Spacing (McCain 2012)

Note: Concrete cover, width, and longitudinal reinforcement size and spacing were scaled in proportion to beam depth. Crack comparisons were made at comparable loading stages (*P/bh*). Test beams in this figure had the following dimensions and parameters:

$$a/d = 2.9$$
$$1/2 \text{ in.} \le a_g \le 1 \text{ in.}$$
$$0.04 \le a_g/d \le 0.05$$
$$4300 \text{ psi} \le f_c^{'} \le 5000 \text{ psi}$$
$$12 \text{ in.} \le h \le 30 \text{ in.}$$
$$0.13 \le P/bh \le 0.14$$
$$0.79\% \le \rho \le 0.98\%$$

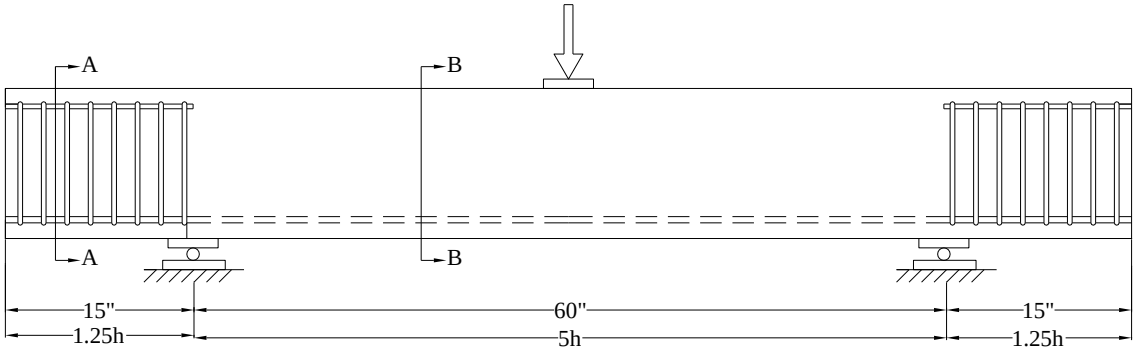

Figure 3.1 Elevation View of Beam

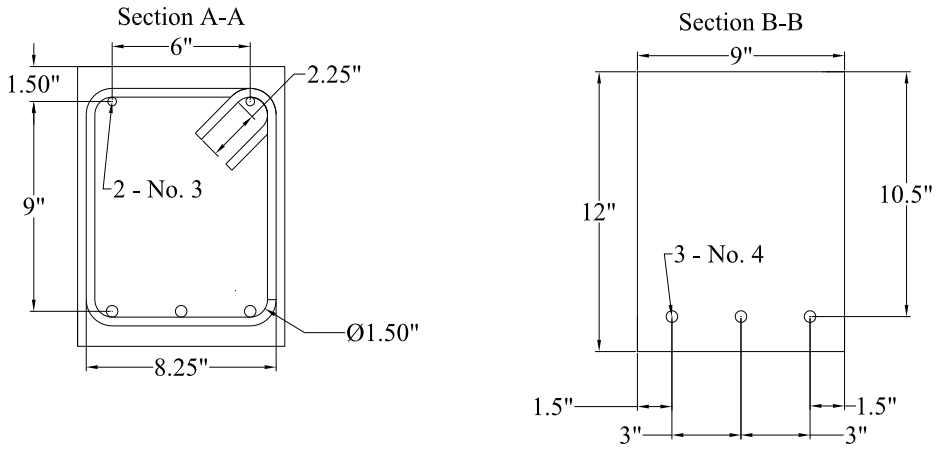

Figure 3.2 Cross Section View of 12 in. Deep Beam

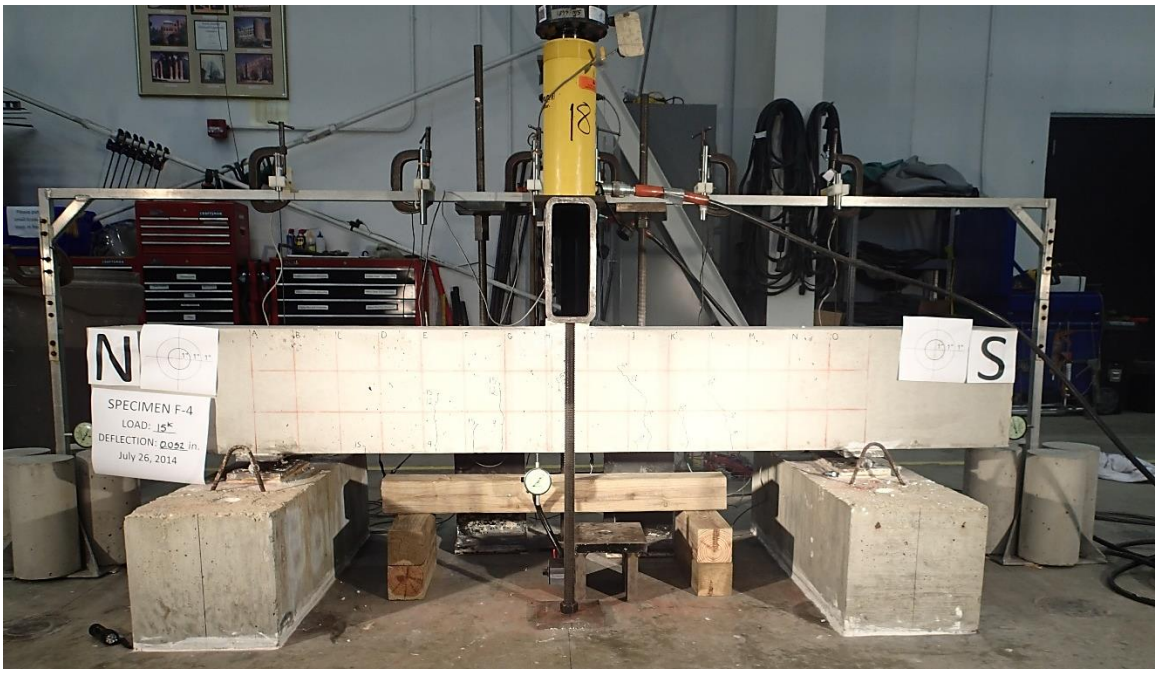

Figure 3.3 Experimental Test Setup

Figure 3.4 Experimental Test Setup with External Stirrups

Figure 3.5 Bolt under Support Plate

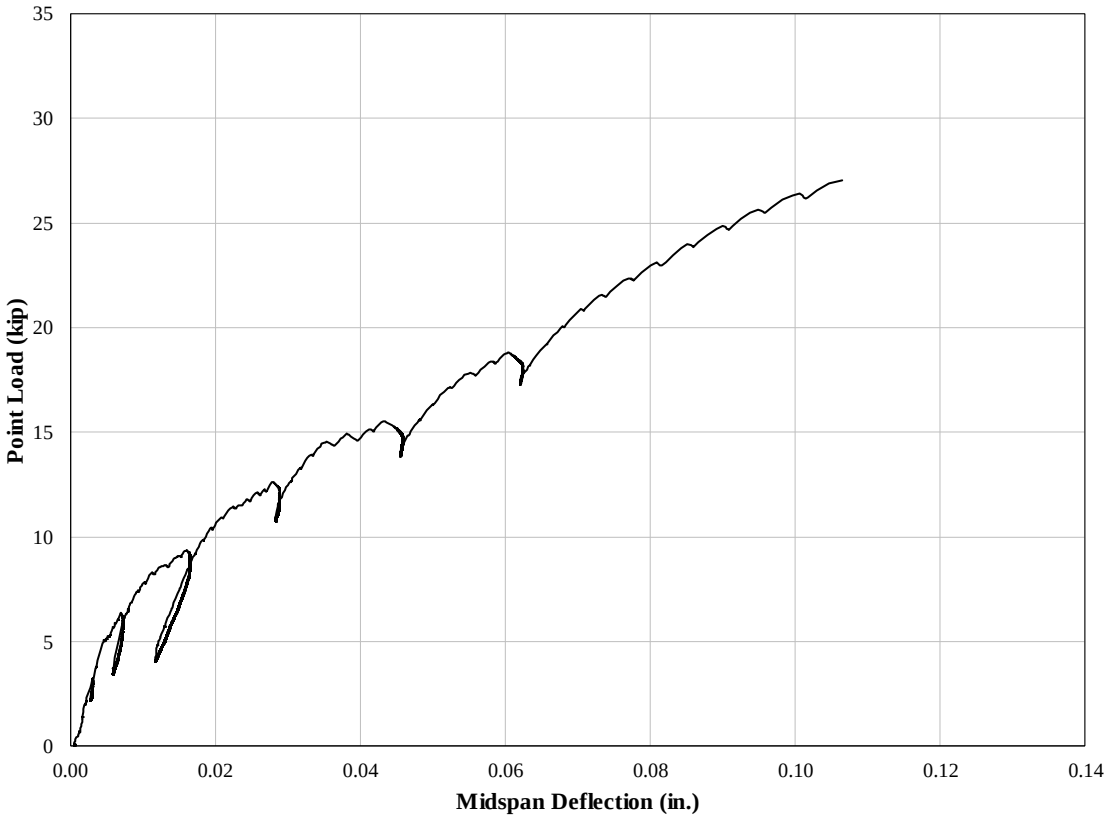

Figure 4.1 Specimen F-3 Load-Deflection Curve

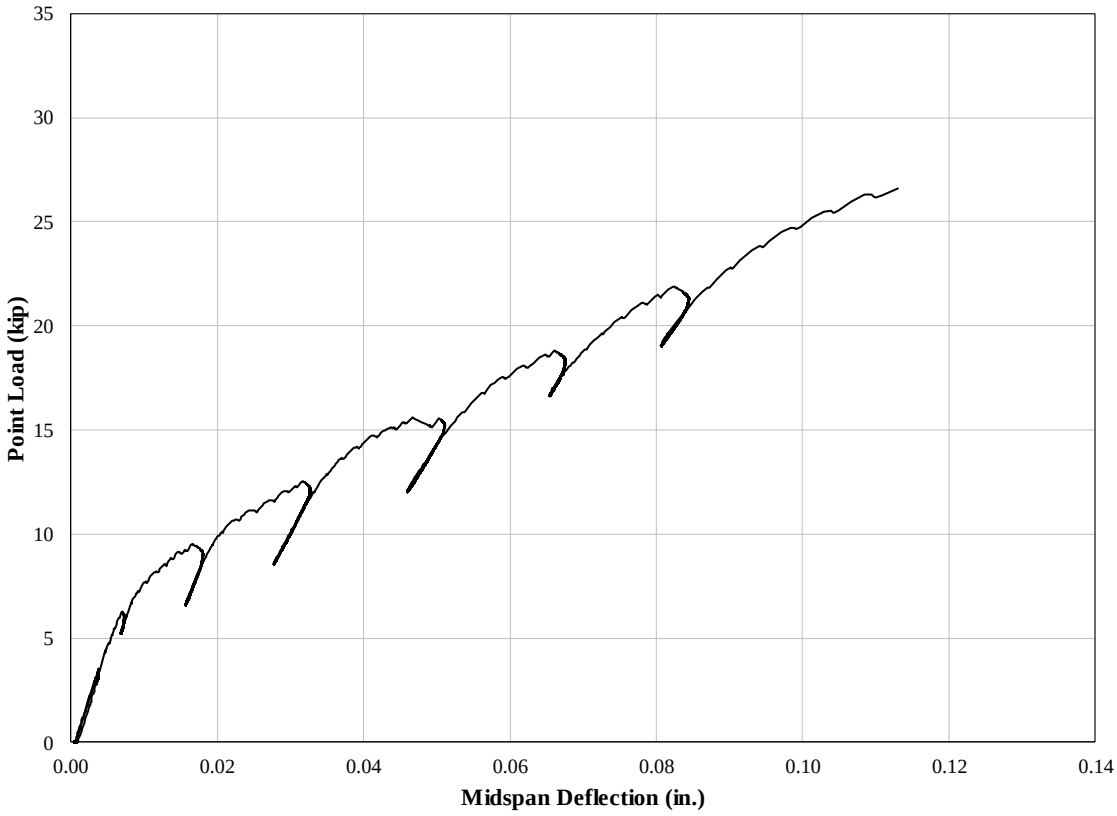

Figure 4.2 Specimen F-4 Load-Deflection Curve

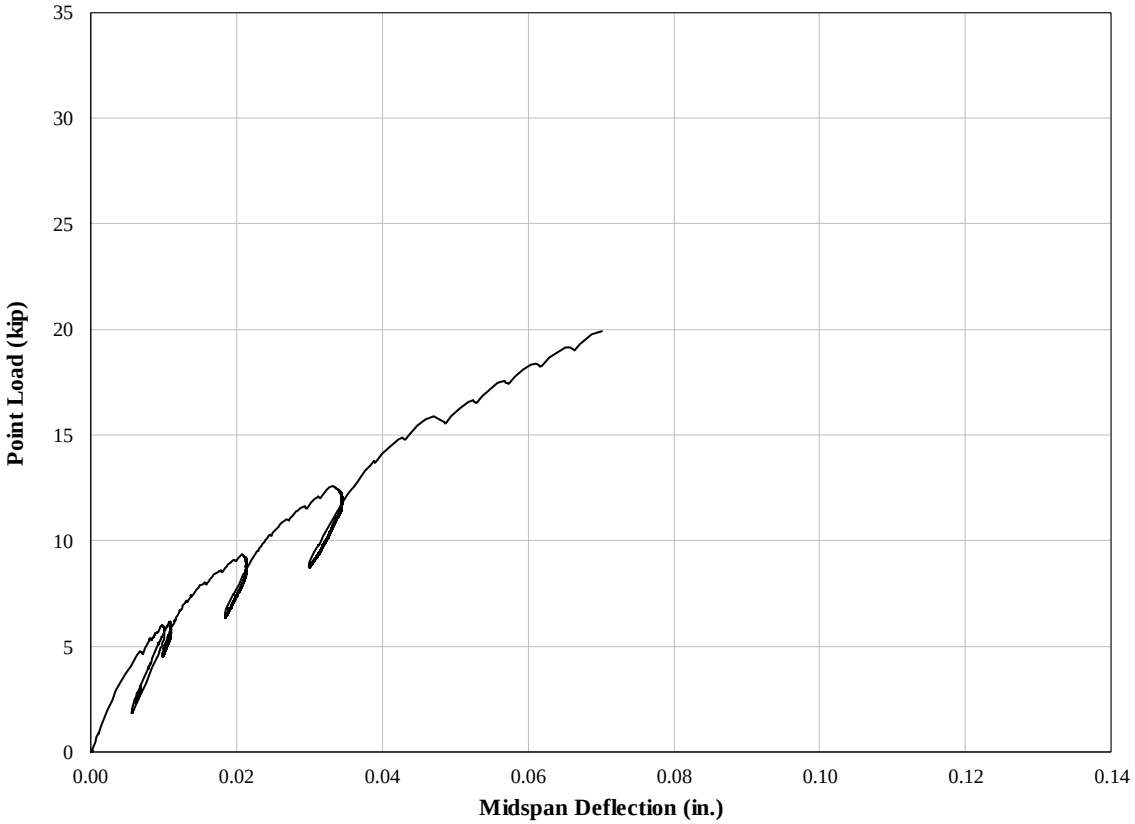

Figure 4.3 Specimen H-1 Load-Deflection Curve

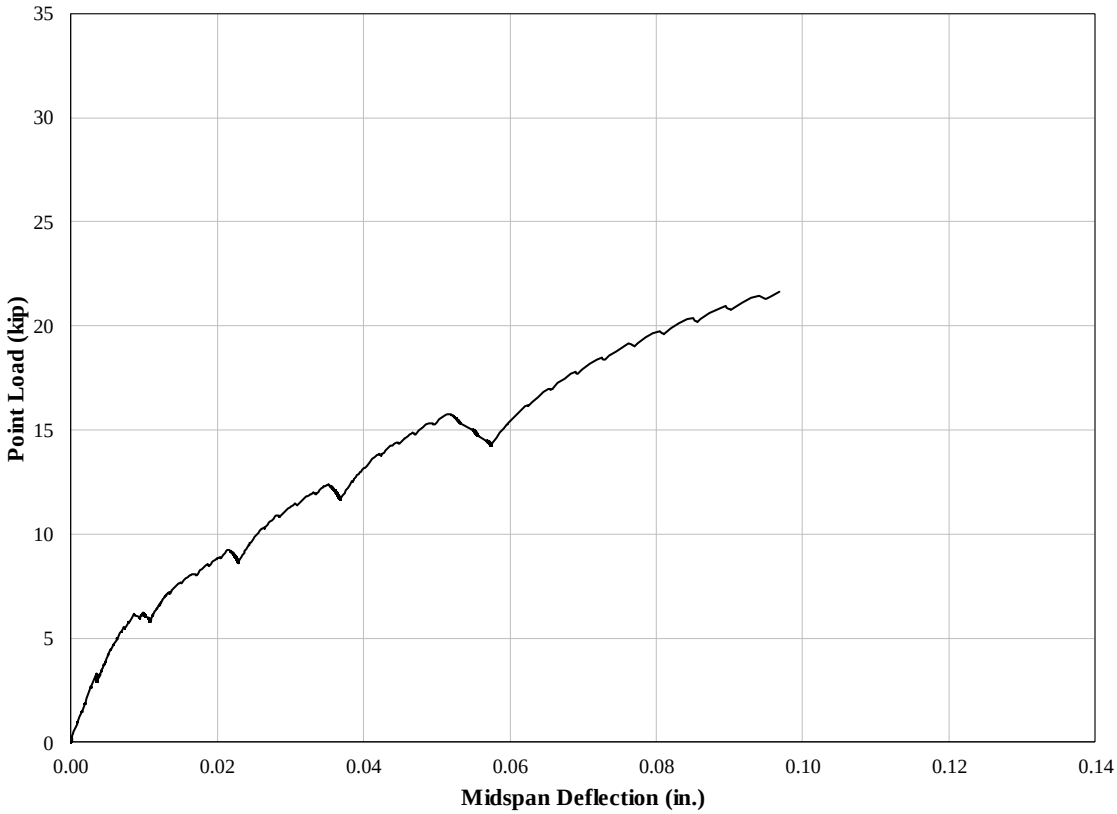

Figure 4.4 Specimen H-2 Load-Deflection Curve

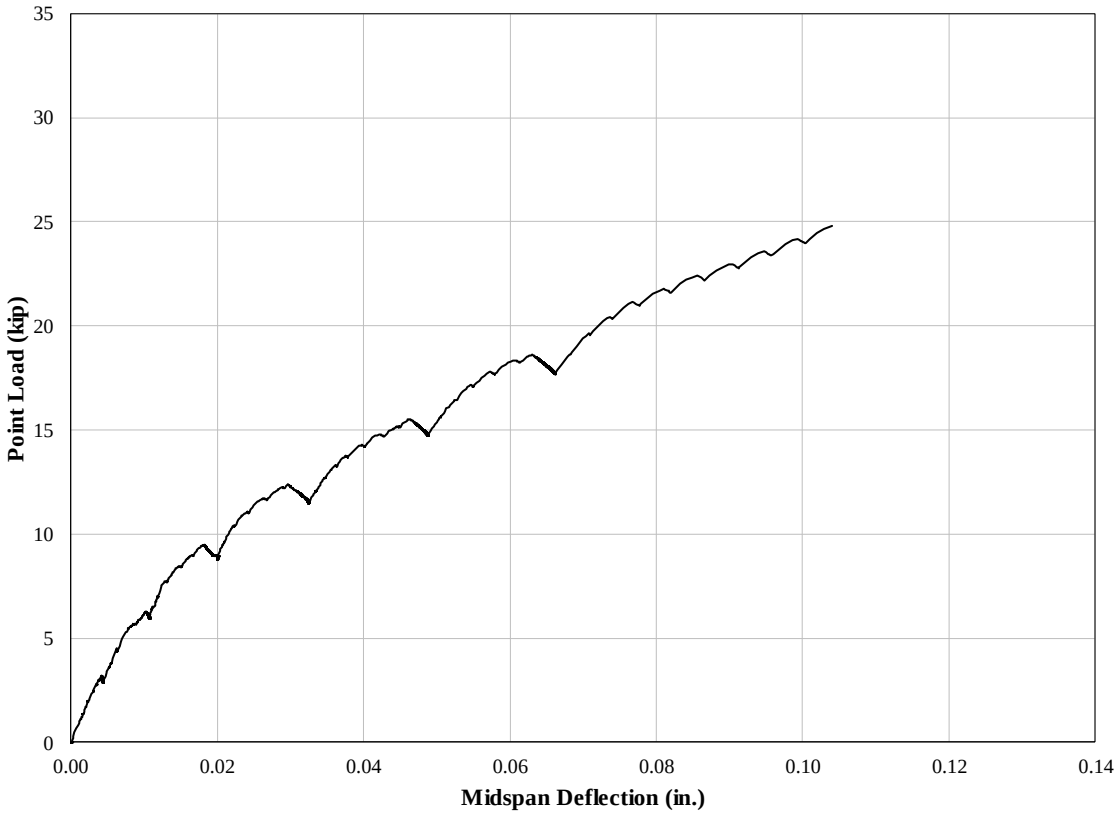

Figure 4.5 Specimen I-1 Load-Deflection Curve

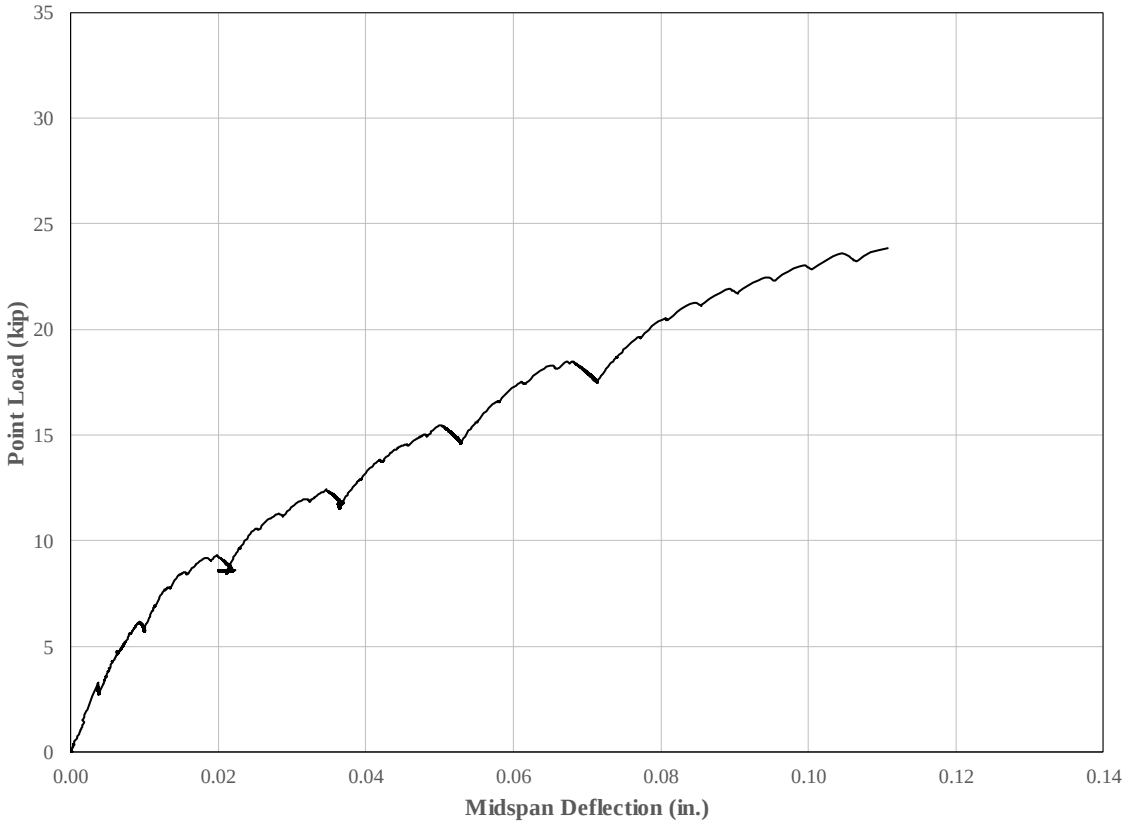

Figure 4.6 Specimen I-2 Load-Deflection Curve

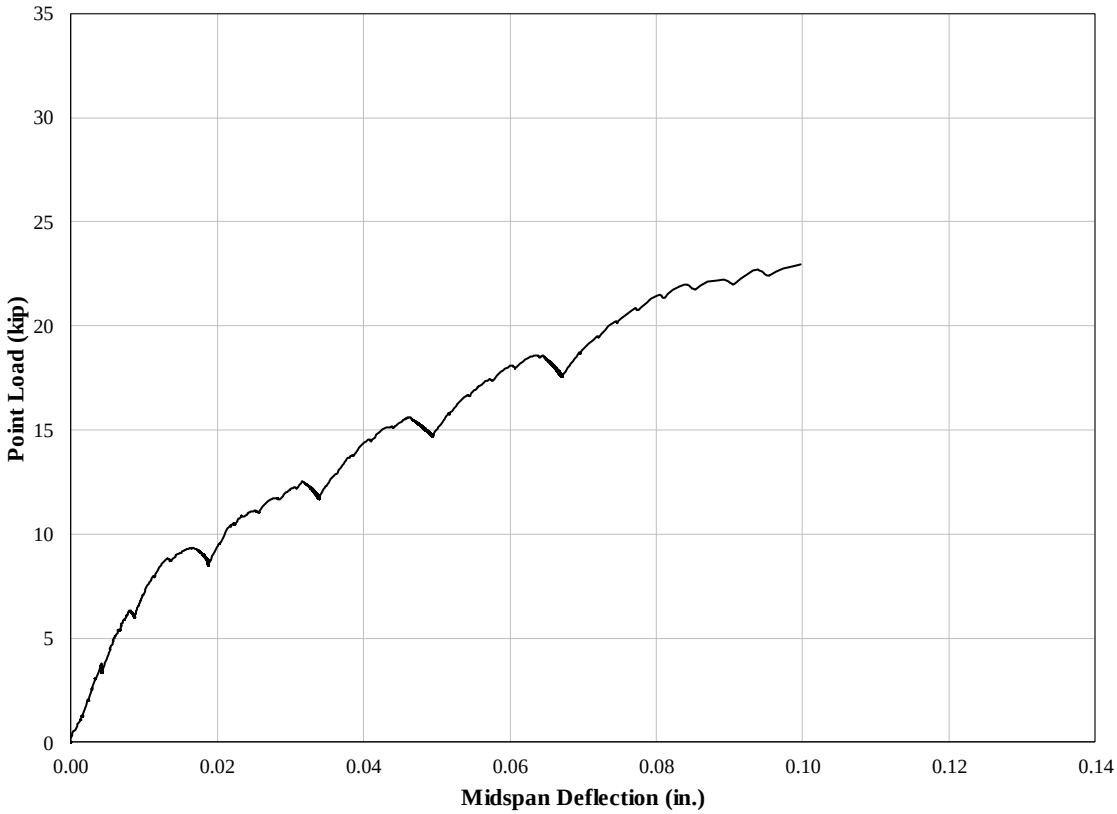

Figure 4.7 Specimen J-1 Load-Deflection Curve

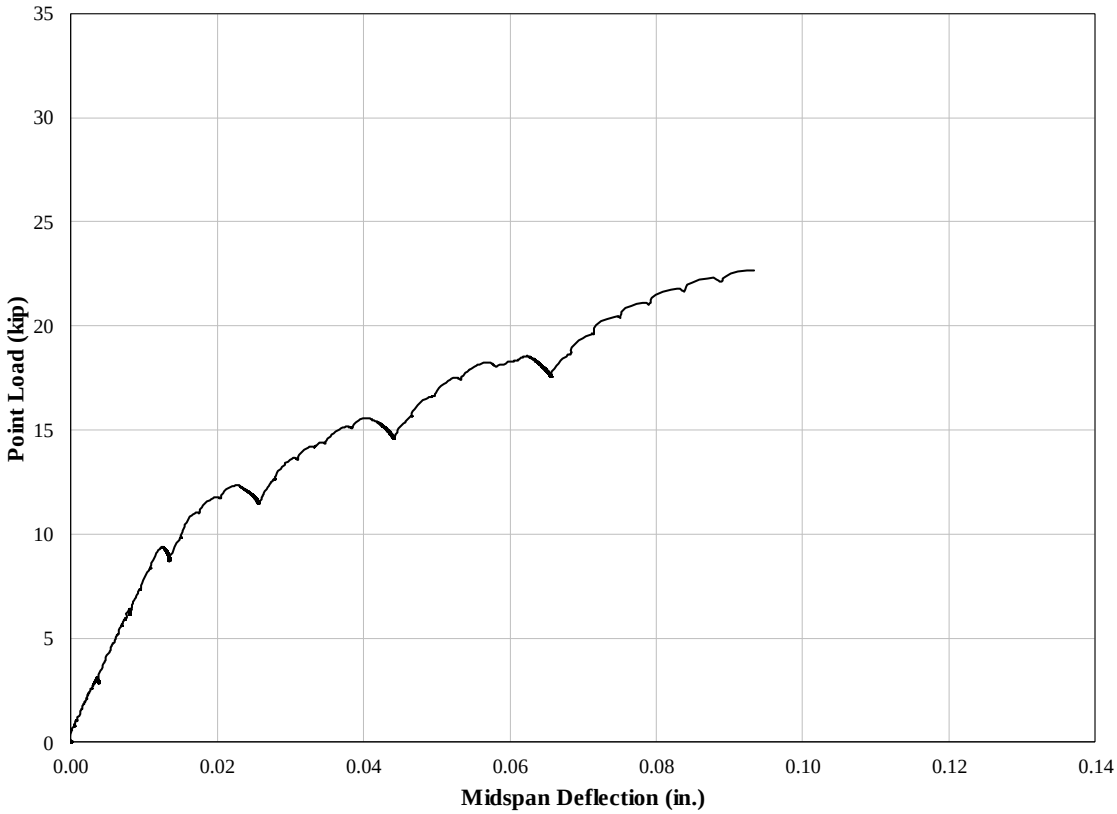

Figure 4.8 Specimen J-2 Load-Deflection Curve

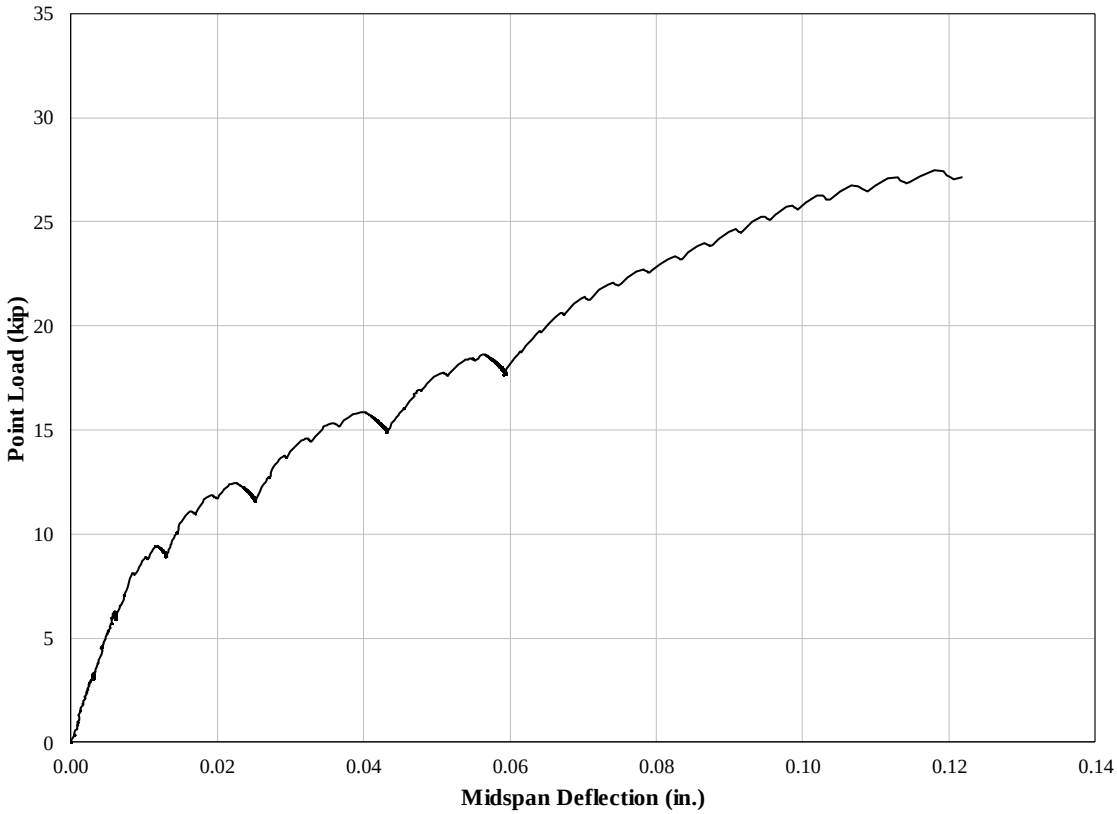

Figure 4.9 Specimen K-1 Load-Deflection Curve

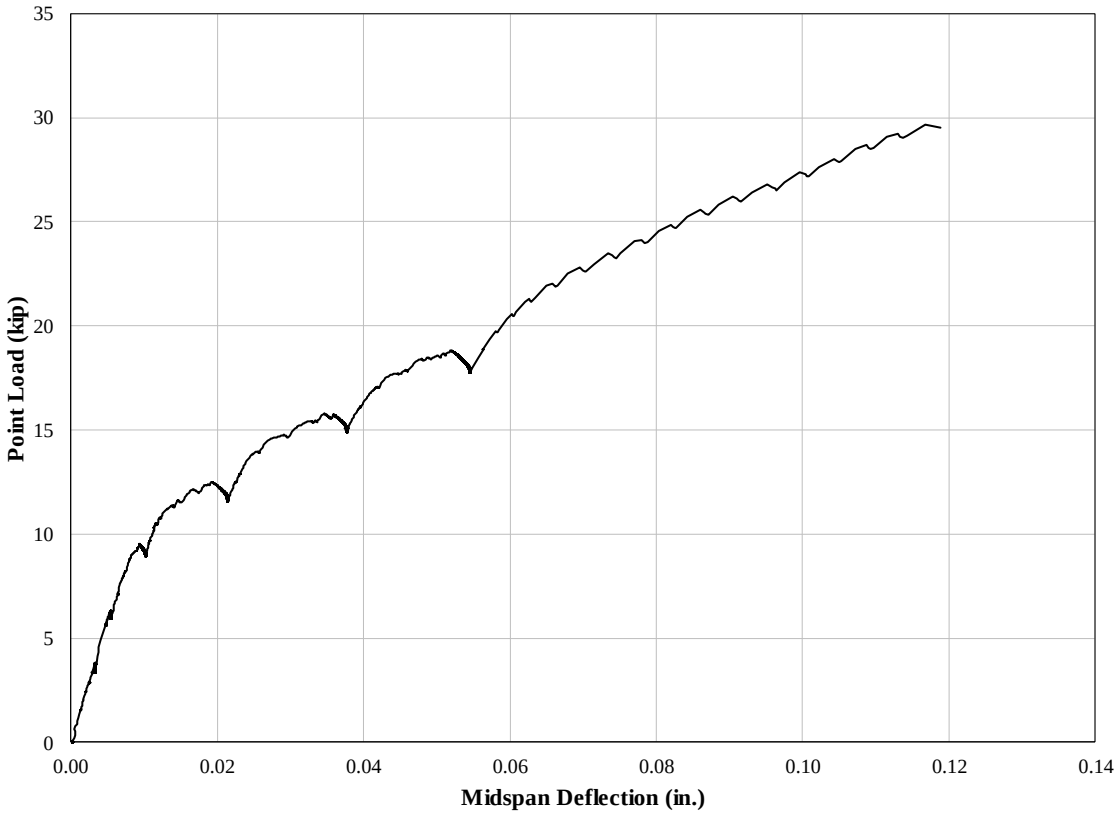

Figure 4.10 Specimen K-2 Load-Deflection Curve

(a) F-4: South Side Failure 0.00 s

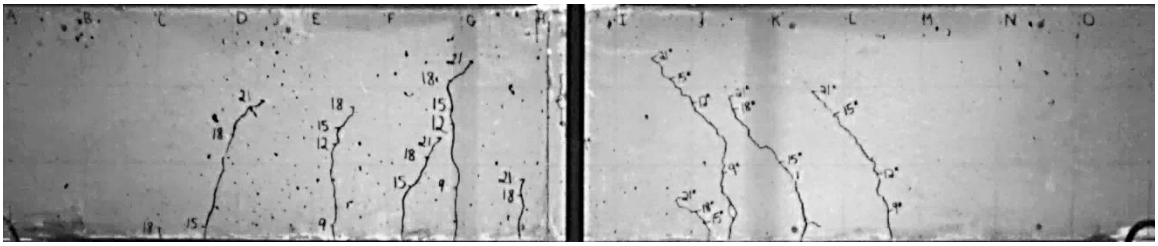

(b) F-4: South Side Failure 0.13 s

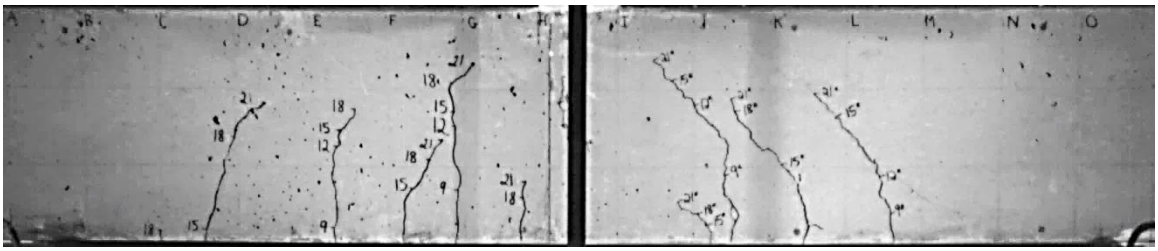

(c) F-4: South Side Failure 0.16 s

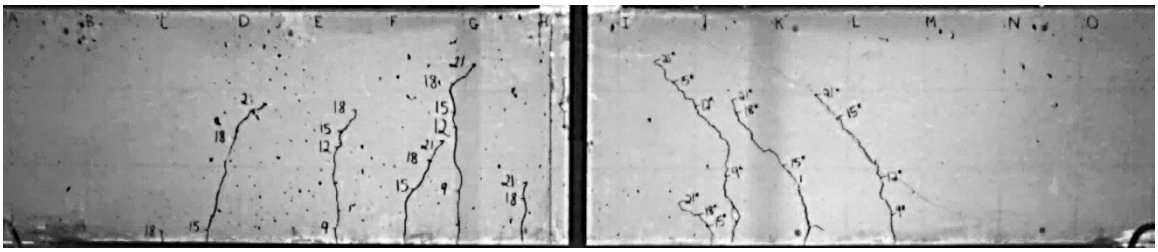

(d) F-4: South Side Failure 0.18 s

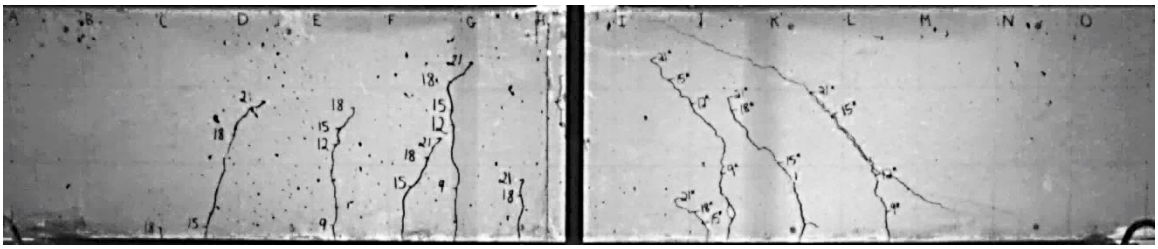

Figure 4.11 Specimen F-4 South Failure Sequence (26.6 kip)

(a) F-4: North Side Failure 0.00 s

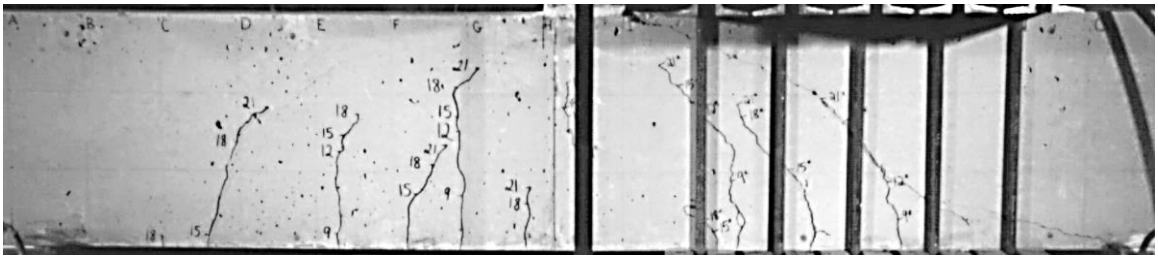

(b) F-4: North Side Failure 0.04 s

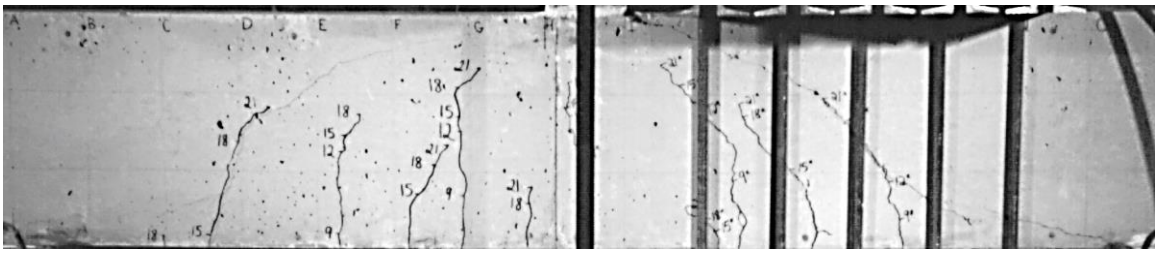

(c) F-4: North Side Failure 0.05 s

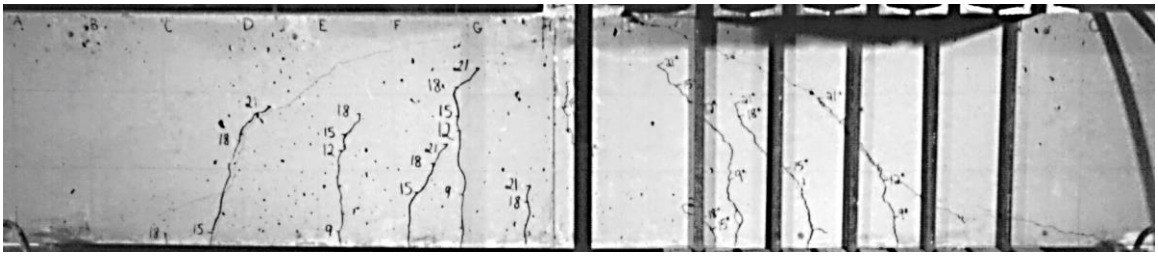

(d) F-4: North Side Failure 0.06 s

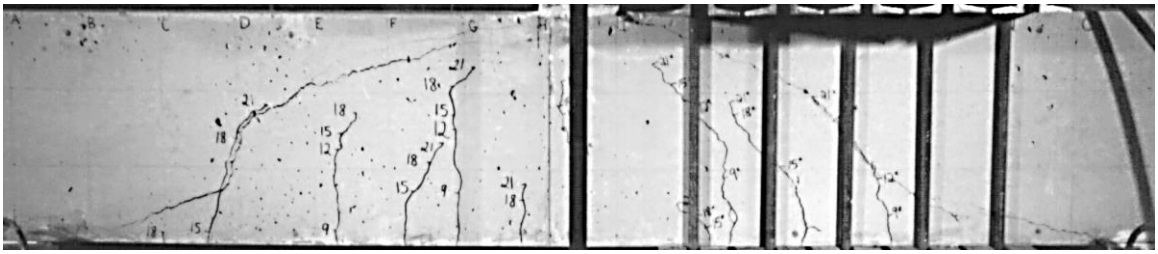

Figure 4.12 Specimen F-4: North Side Failure Sequence (31.2 kip)

(a) H-1: North Side Failure 0.00 s

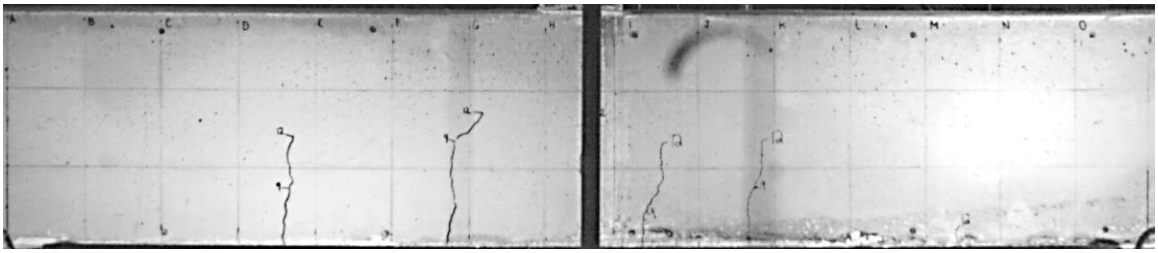

(b) H-1: North Side Failure 0.05 s

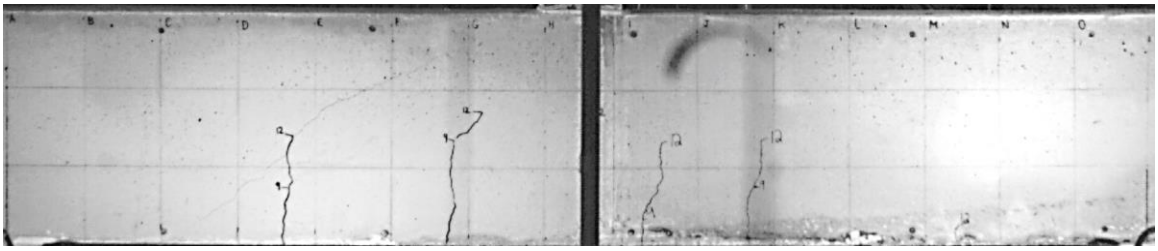

(c) H-1 North Side Failure 0.06 s

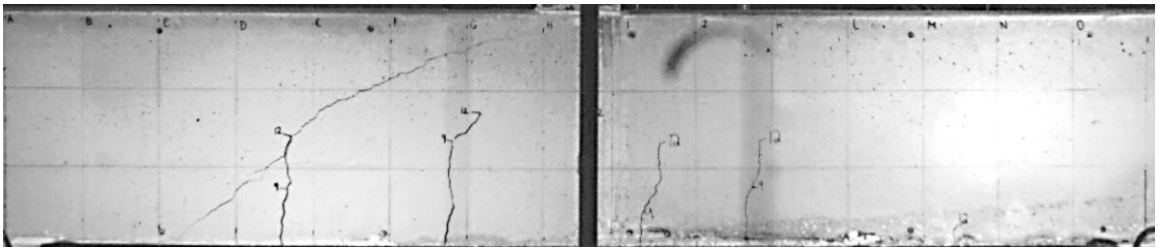

(d) H-1: North Side Failure 0.07 s

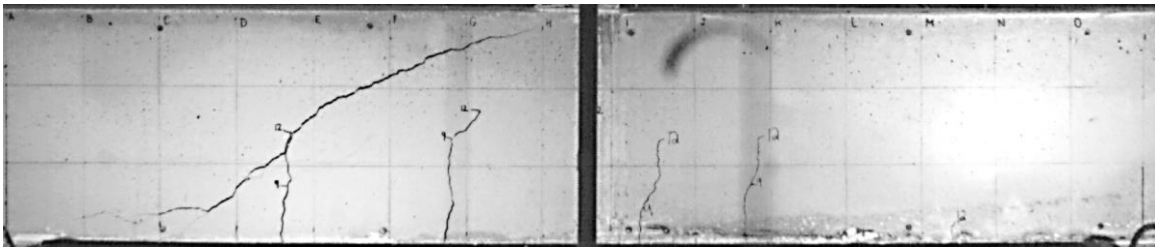

Figure 4.13 Specimen H-1: North Side Failure Sequence (19.9 kip)

(a) H-1: South Side Failure 0.00 s

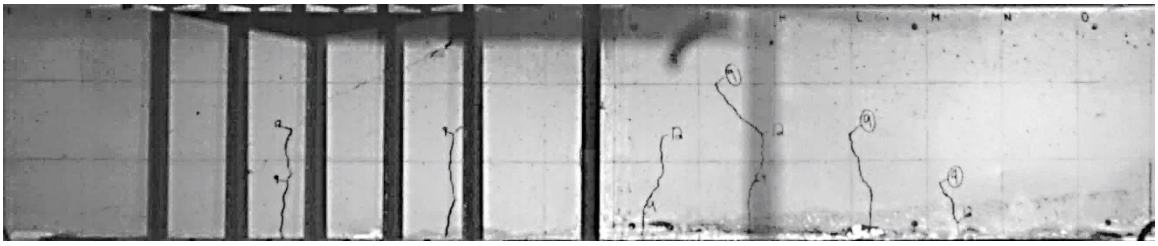

(b) H-1: South Side Failure 0.04 s

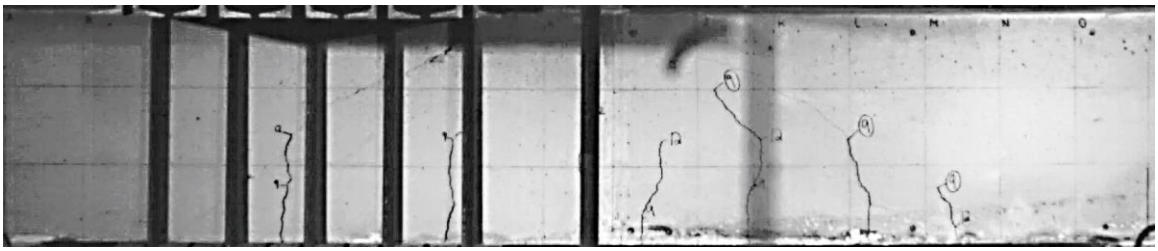

(c) H-1: South Side Failure 0.05 s

(d) H-1: South Side Failure 0.80 s

Figure 4.14 Specimen H-1: South Side Failure Sequence (24.9 kip)

(a) H-2: South Side Failure 0.00 s

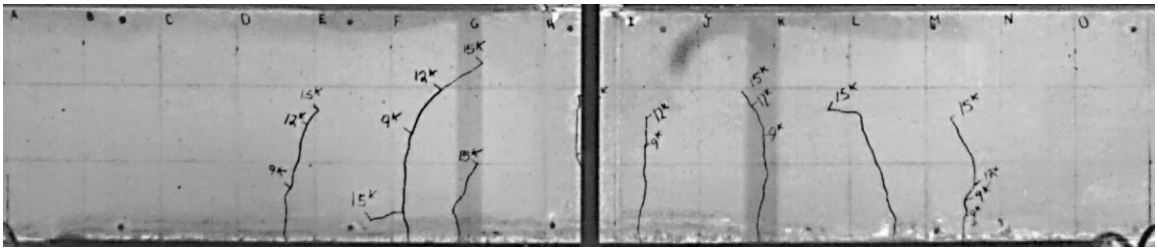

(b) H-2: South Side Failure 0.05 s

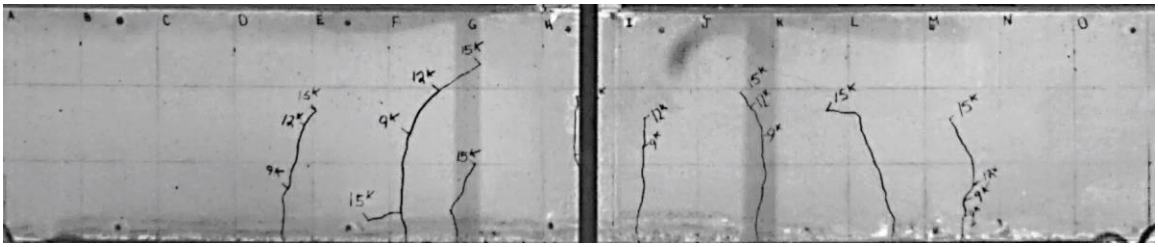

(c) H-2: South Side Failure 0.06 s

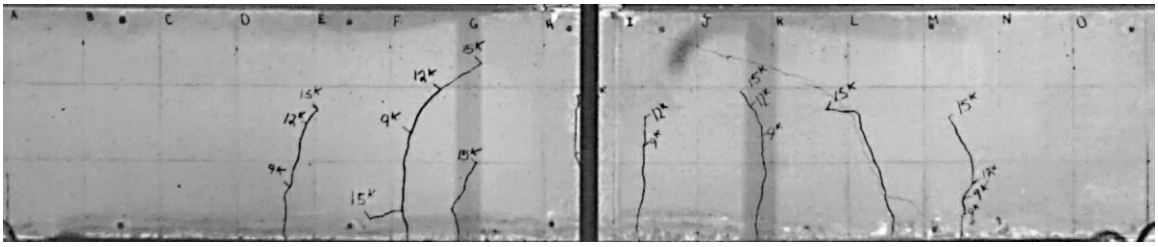

(d) H-2: South Side Failure 0.07 s

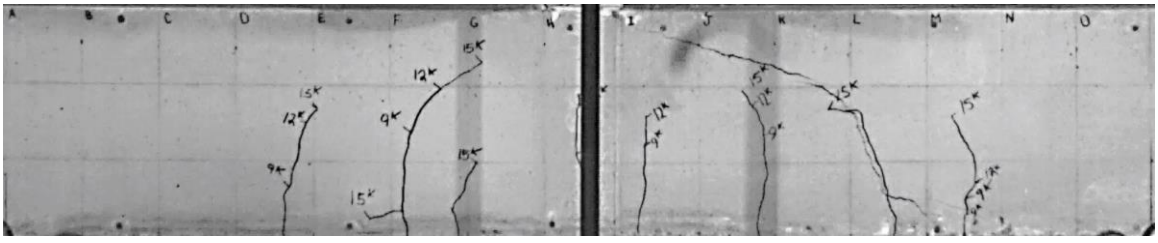

Figure 4.15 Specimen H-2: South Side Failure Sequence (21.6 kip)

(a) H-2: North Side Failure 0.00 s

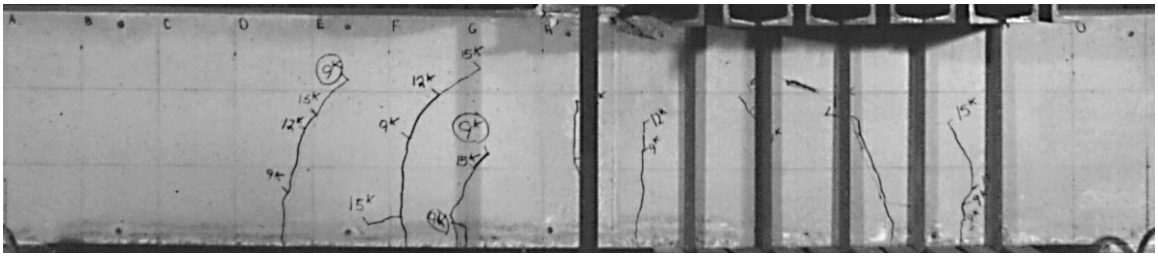

(b) H-2: North Side Failure 0.12 s

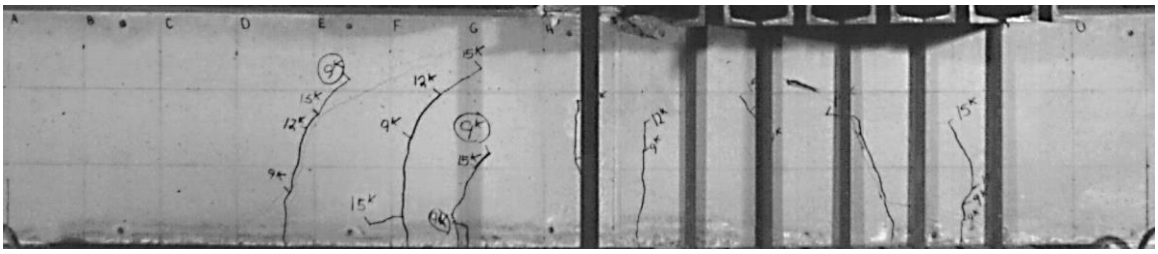

(c) H-2: North Side Failure 0.16 s

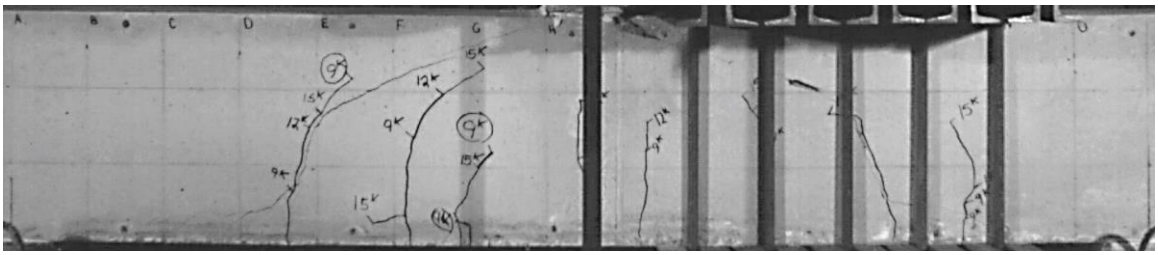

(d) H-2: North Side Failure 0.18 s

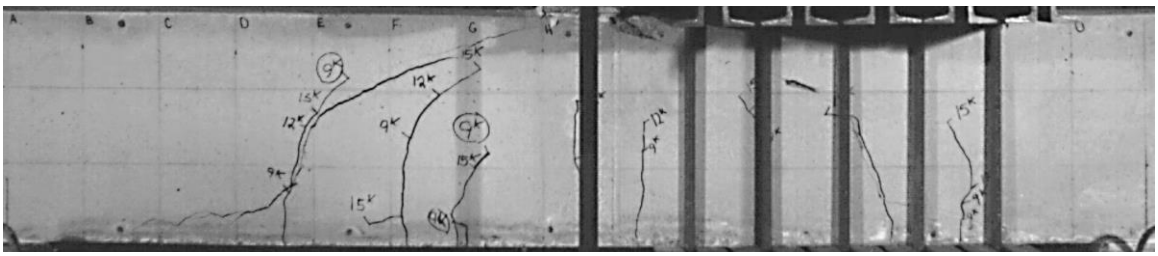

Figure 4.16 Specimen H-2: North Side Failure Sequence (23.3 kip)

(a) I-1: South Side Failure 0.00 s

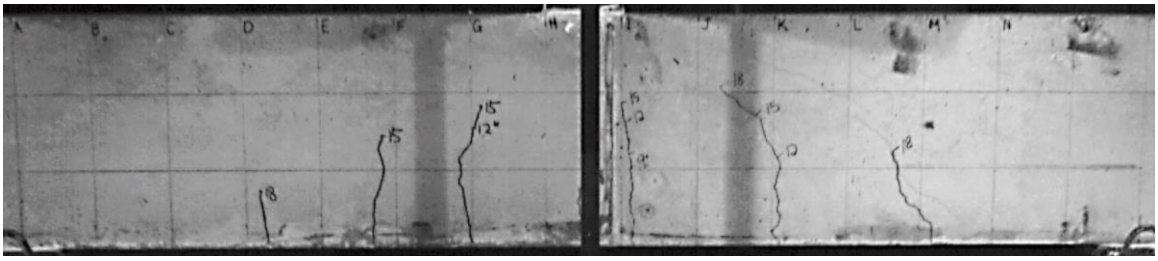

(b) I-1: South Side Failure 0.03 s

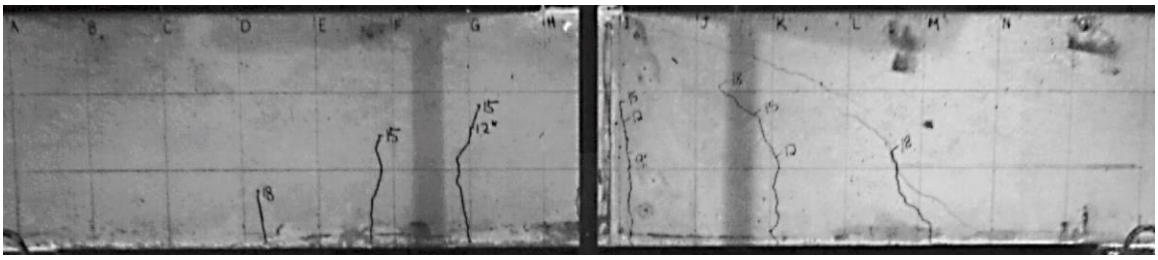

(c) I-1: South Side Failure 0.04 s

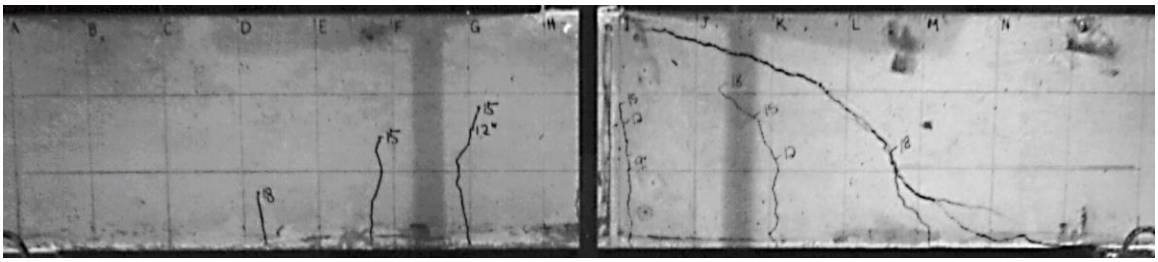

(d) I-1: South Side Failure 0.06 s

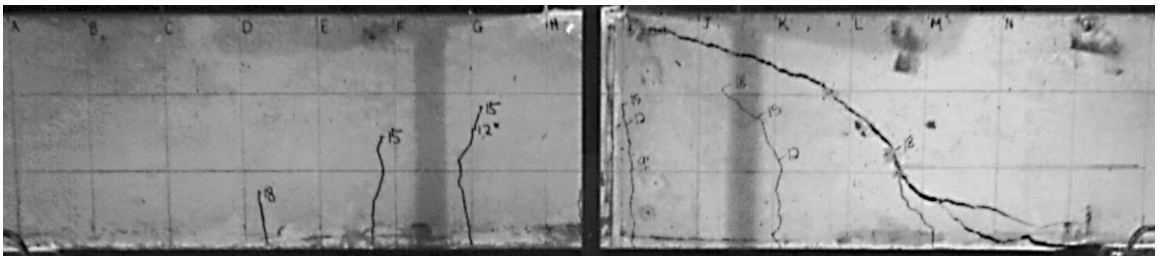

Figure 4.17 Specimen I-1: South Side Failure Sequence (24.8 kip)

(a) I-2: South Side Failure 0.00 s

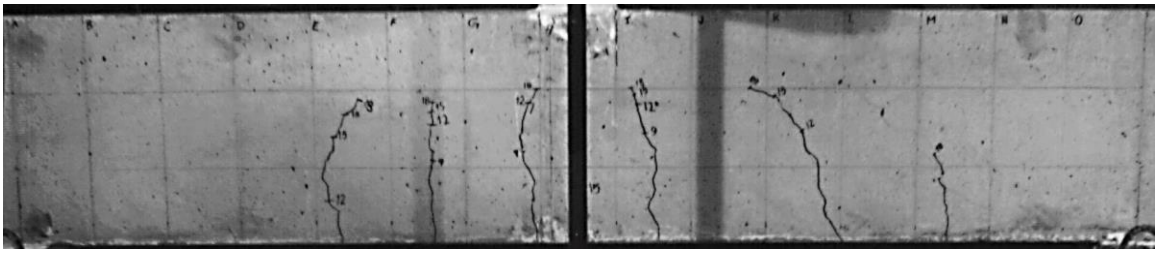

(b) I-2: South Side Failure 0.01 s

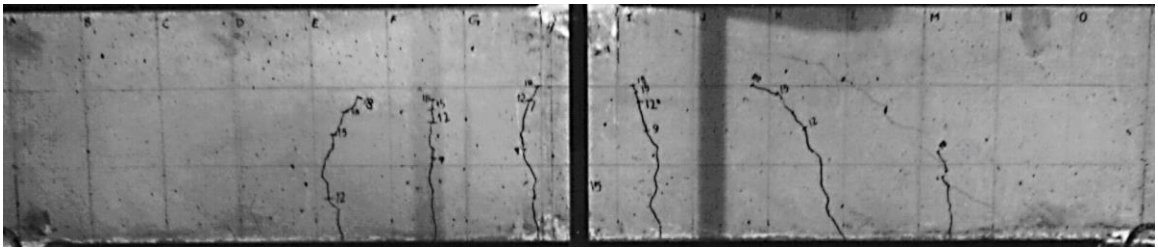

(c) I-2: South Side Failure 0.02 s

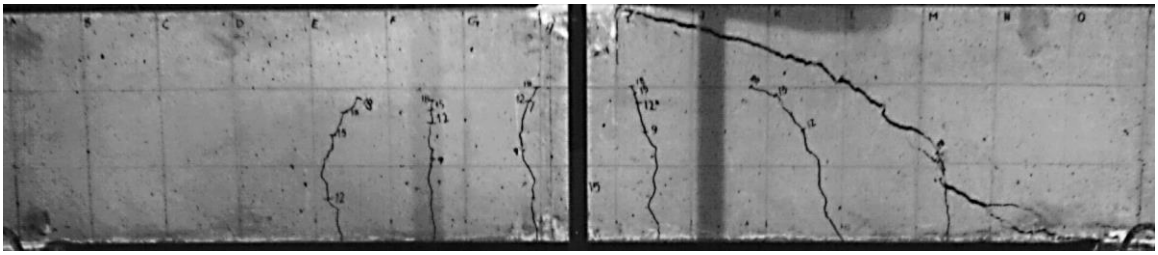

(d) I-2: South Side Failure 0.04 s

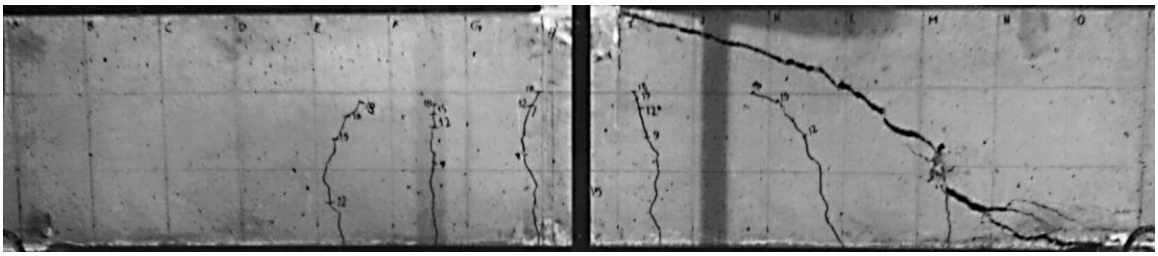

Figure 4.18 Specimen I-2: South Side Failure Sequence (23.8 kip)

(a) I-2: North Side Failure 0.00 s

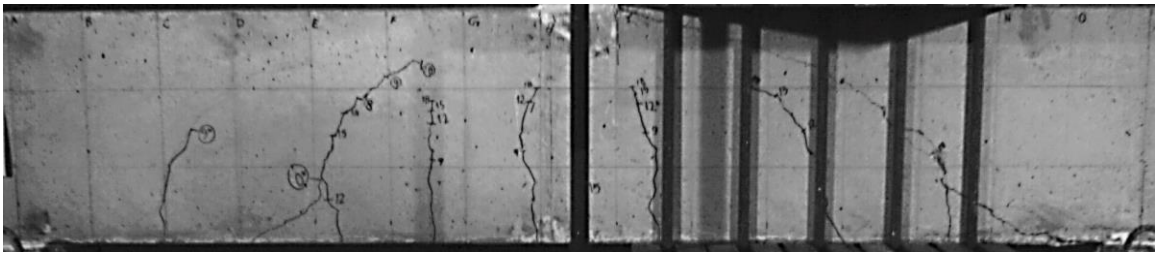

(b) I-2: North Side Failure 0.02 s

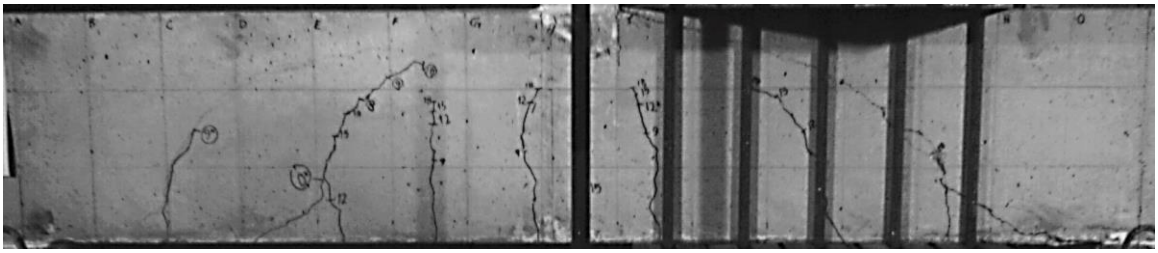

(c) I-2: North Side Failure 0.04 s

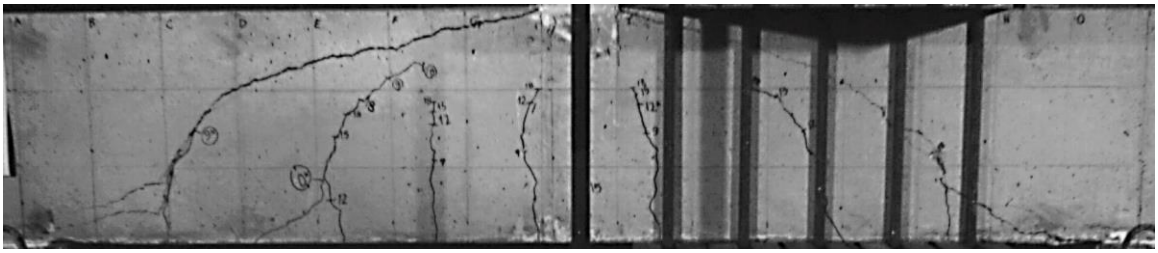

(d) I-2: North Side Failure 0.05 s

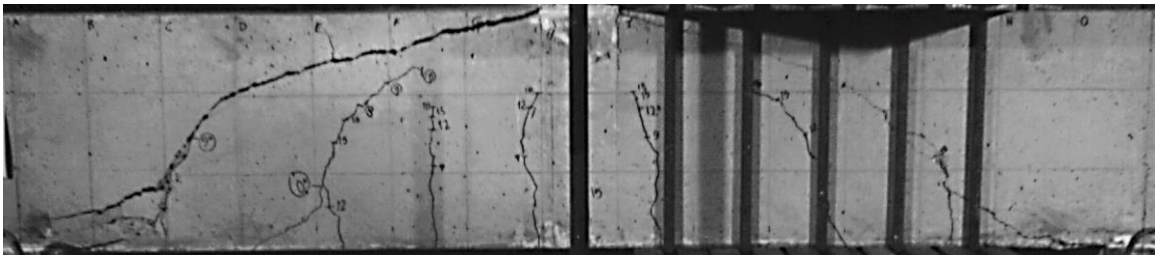

Figure 4.19 Specimen I-2: North Side Failure Sequence (27.2 kip)

(a) J-1: South Side Failure 0.00 s

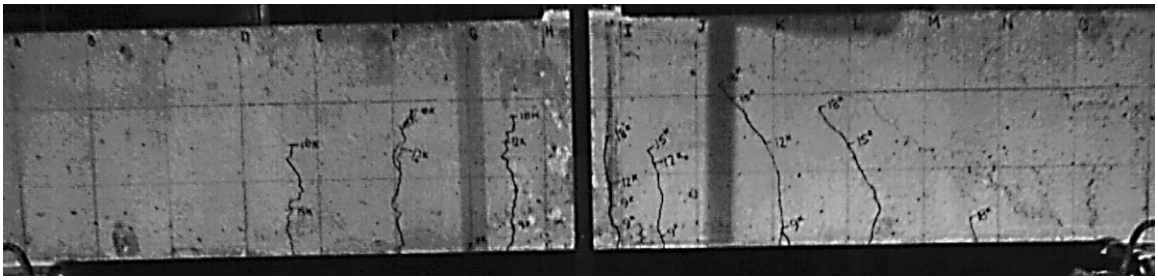

(b) J-1: South Side Failure 1.65 s

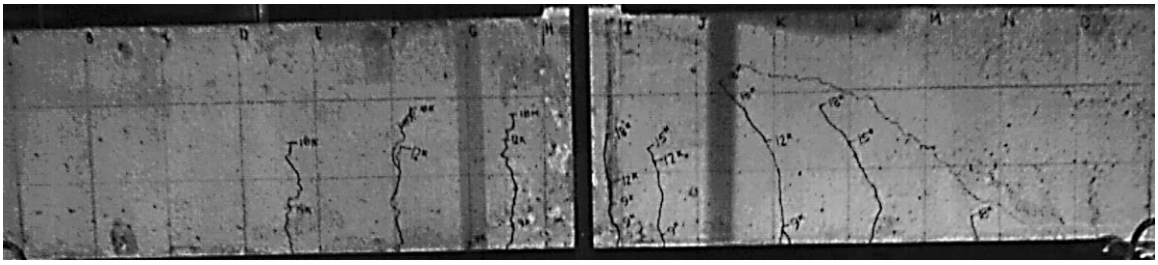

(c) J-1: South Side Failure 2.15 s

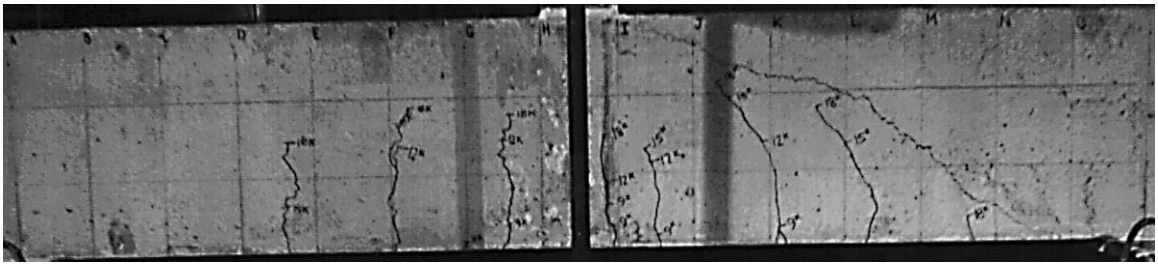

(d) J-1: South Side Failure 2.20 s

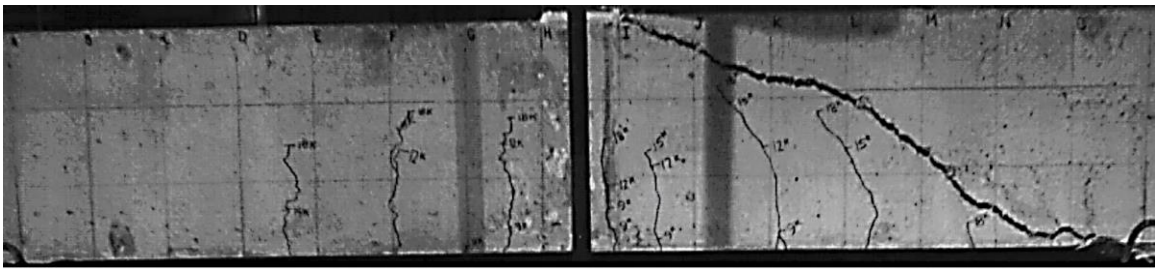

Figure 4.20 Specimen J-1: South Side Failure Sequence (22.9 kip)

(a) J-1: North Side Failure 0.00 s

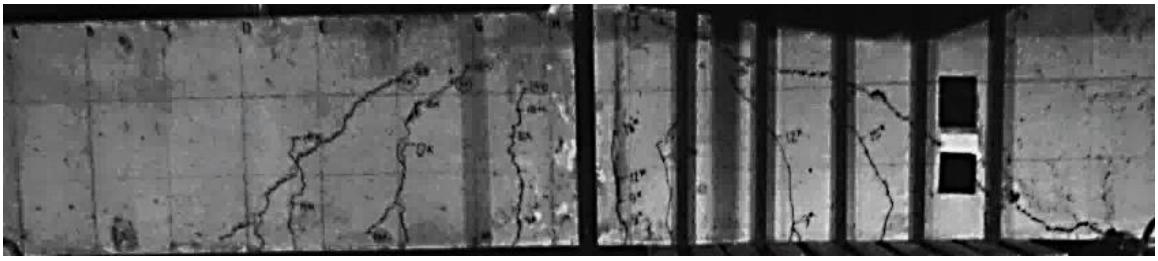

(b) J-1: North Side Failure 0.05 s

(c) J-1: North Side Failure 0.10 s

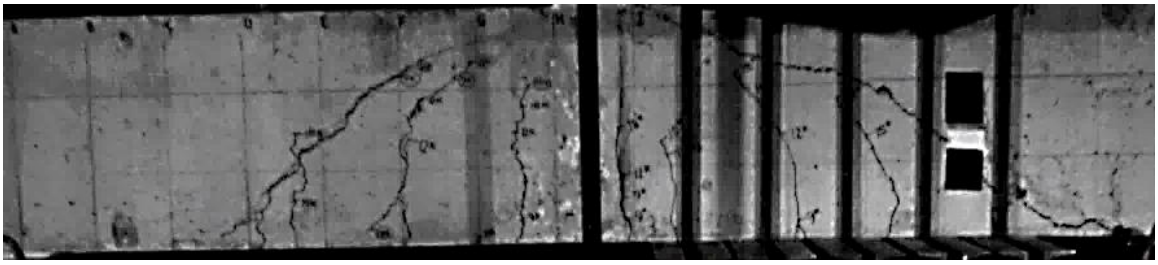

(d) J-1: North Side Failure 0.14 s

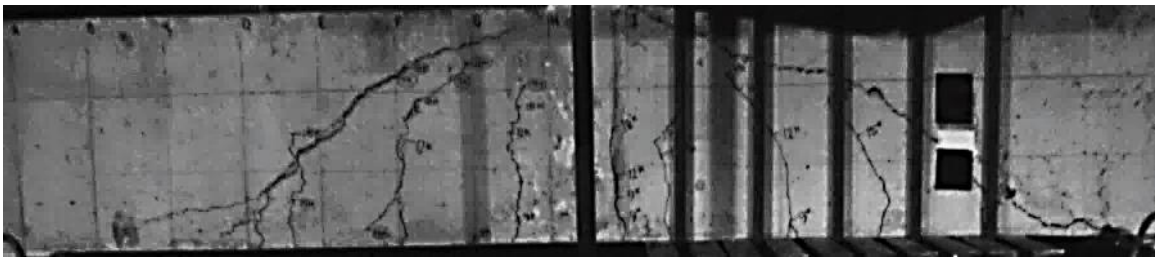

Figure 4.21 Specimen J-1: North Side Failure Sequence (23.8 kip)

(a) J-2: South Side Failure 0.00 s

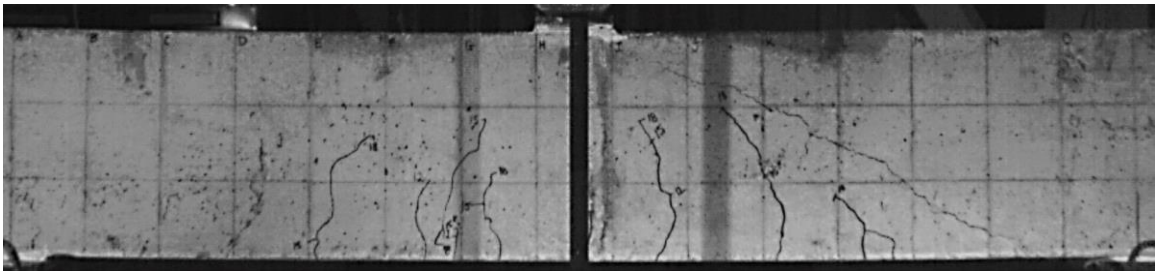

(b) J-2: South Side Failure 1.5 s

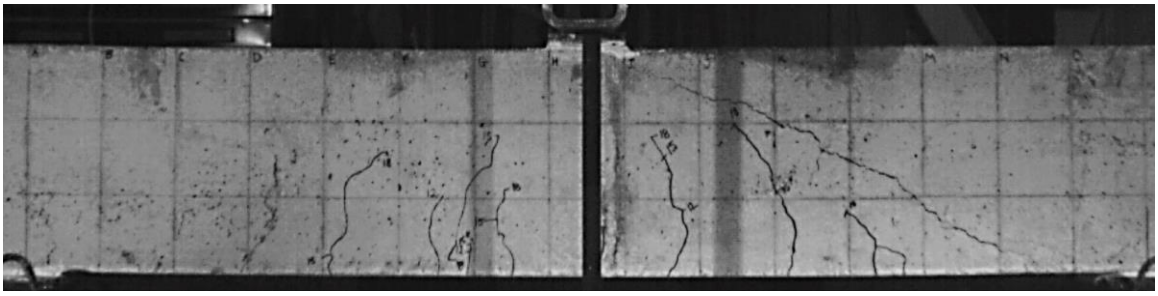

(c) J-2: South Side Failure 1.9 s

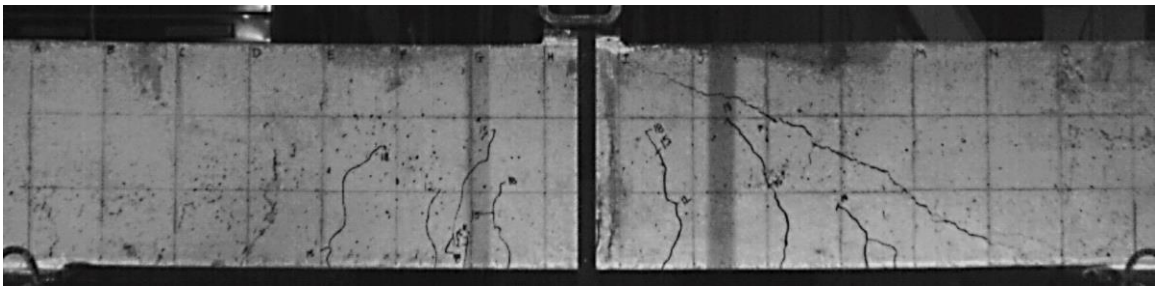

(d) J-2: South Side Failure 2.1 s

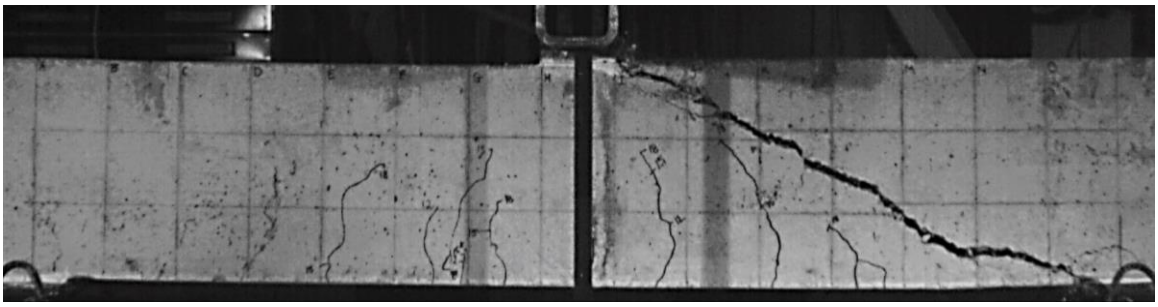

Figure 4.22 Specimen J-2: South Side Failure Sequence (22.7 kip)

(a) J-2: North Side Failure 0.00 s

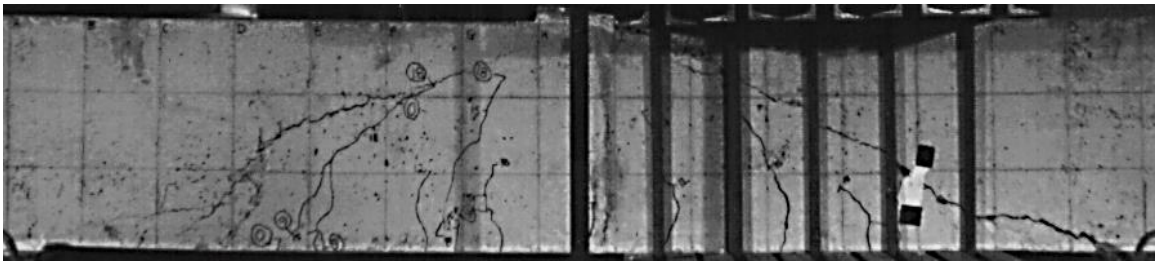

(b) J-2: North Side Failure 0.05 s

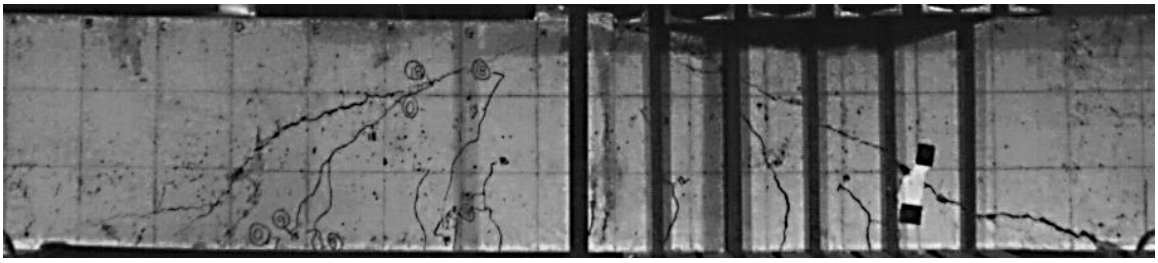

(c) J-2: North Side Failure 0.10 s

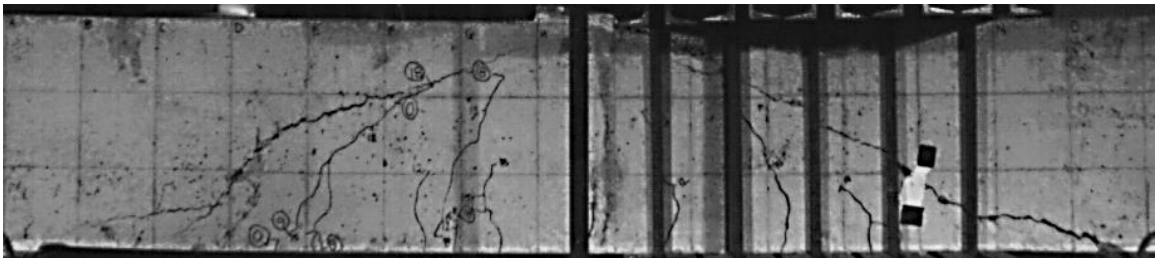

(d) J-2: North Side Failure 0.13 s

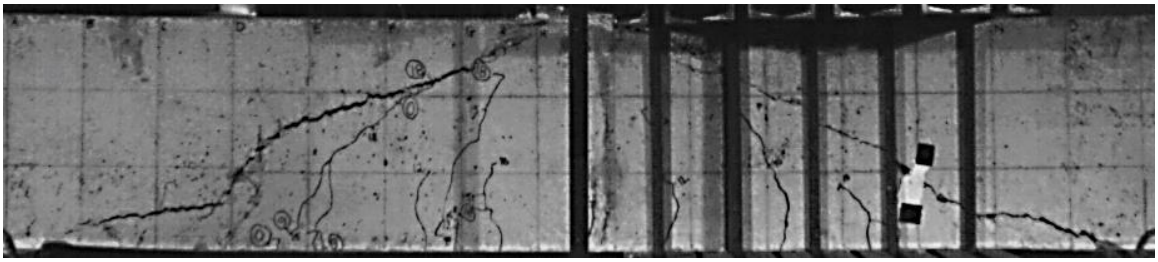

Figure 4.23 Specimen J-2: North Side Failure Sequence (26.9 kip)

(a) K-1: North Side Failure 0.00 s

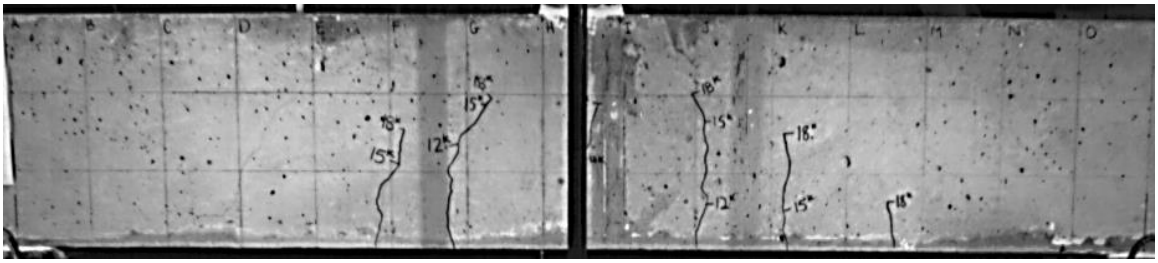

(b) K-1: North Side Failure 0.70 s

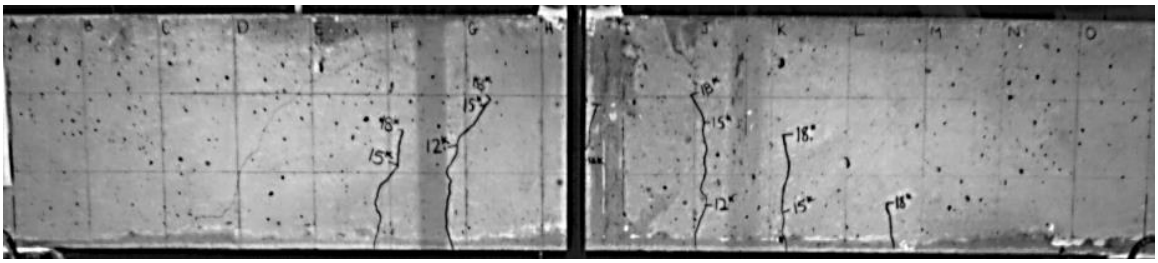

(c) K-1: North Side Failure 0.98 s

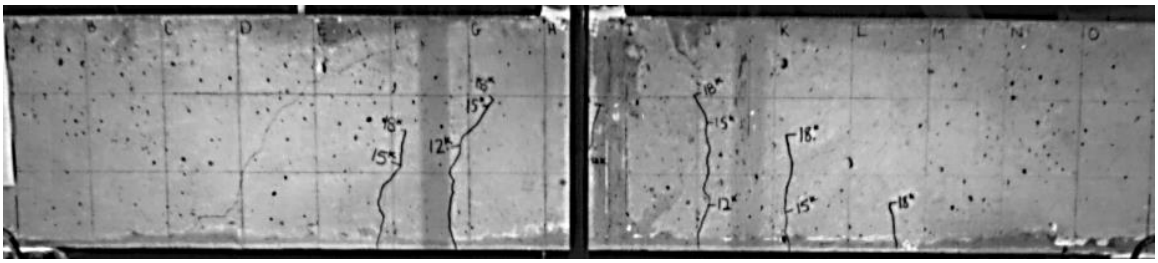

(d) K-1: North Side Failure 1.16 s

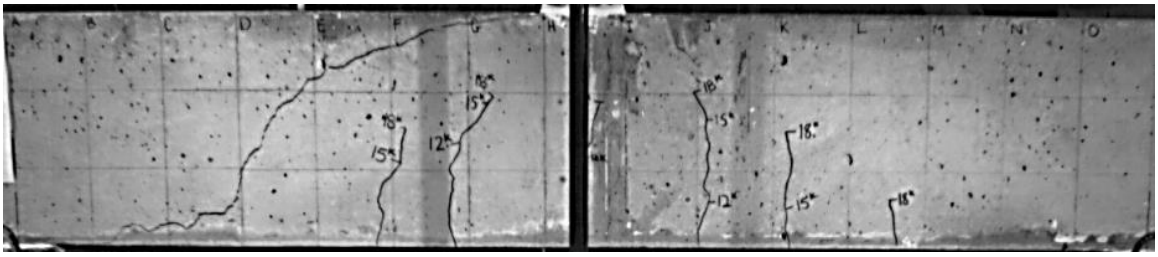

Figure 4.24 Specimen K-1: North Side Failure Sequence (27.5 kip)

(a) K-1: South Side Failure 0.00 s

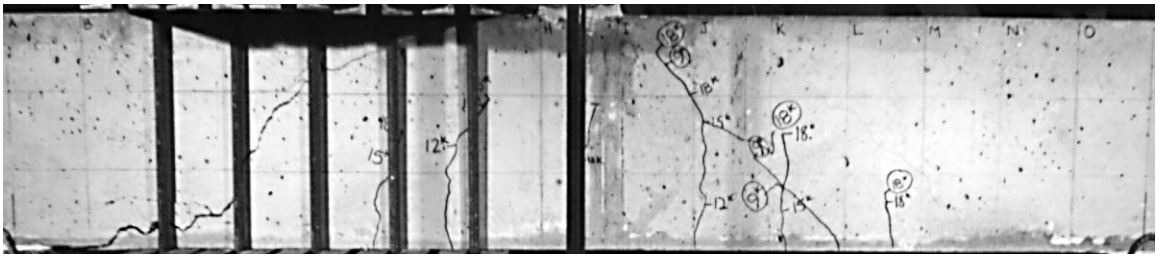

(b) K-1: South Side Failure 0.05 s

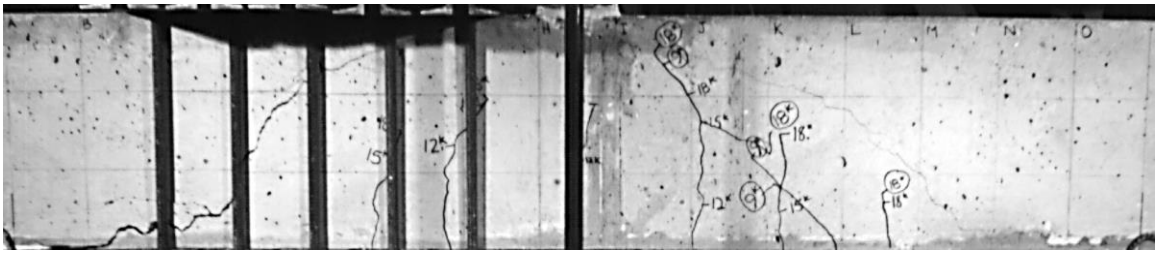

(c) K-1: South Side Failure 0.19 s

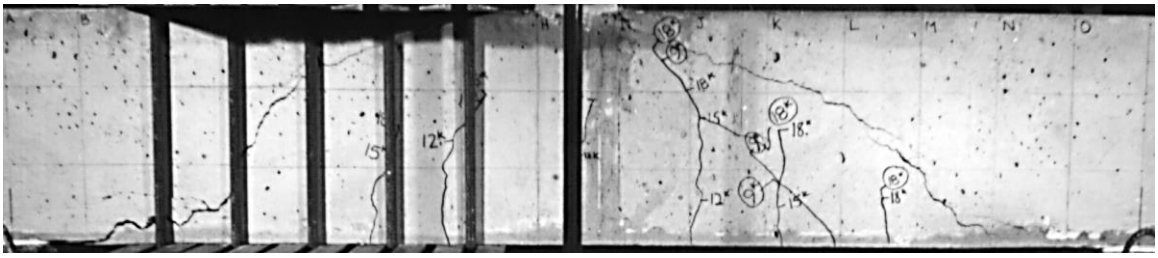

(d) K-1: South Side Failure 0.21 s

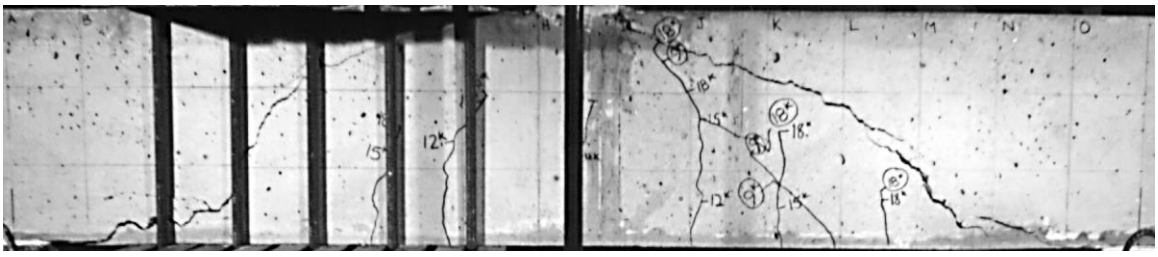

Figure 4.25 Specimen K-1: South Side Failure Sequence (28.9 kip)

(a) K-2: South Side Failure 0.00 s

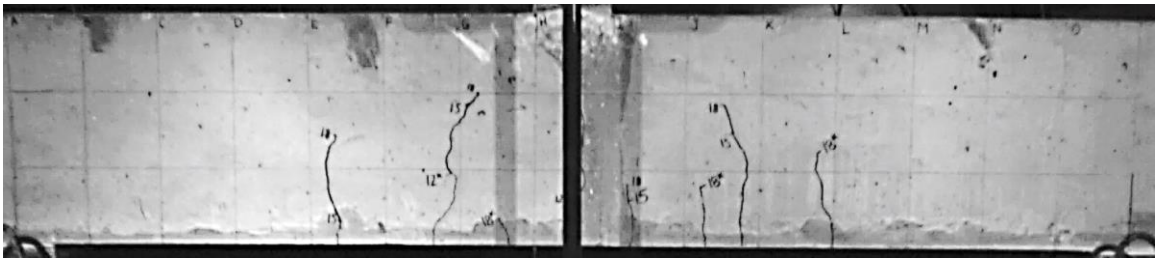

(b) K-2: South Side Failure 0.11 s

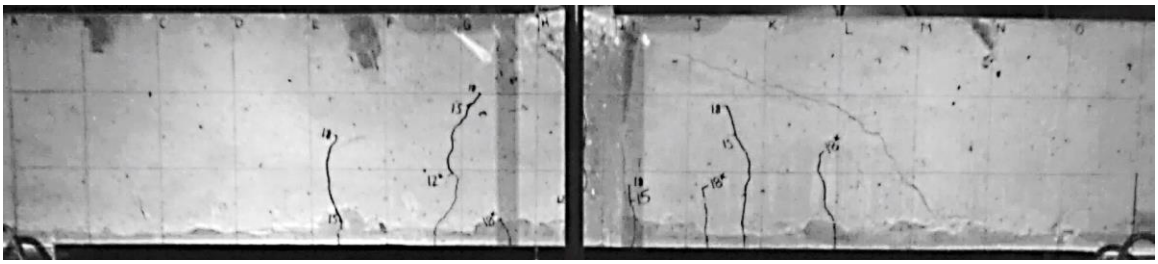

(c) K-2: South Side Failure 0.17 s

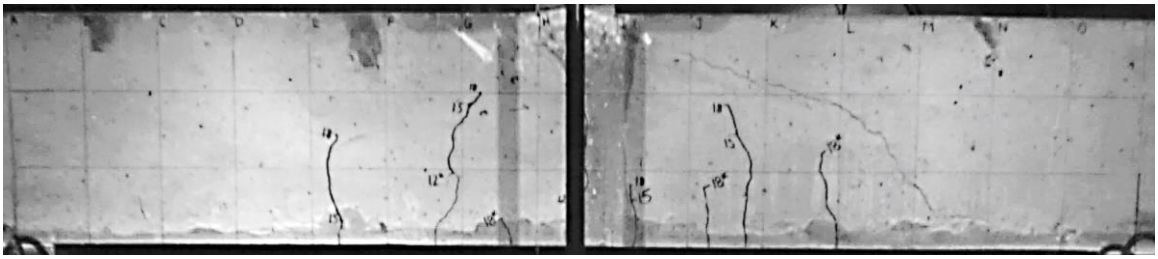

(d) K-2: South Side Failure 0.27 s

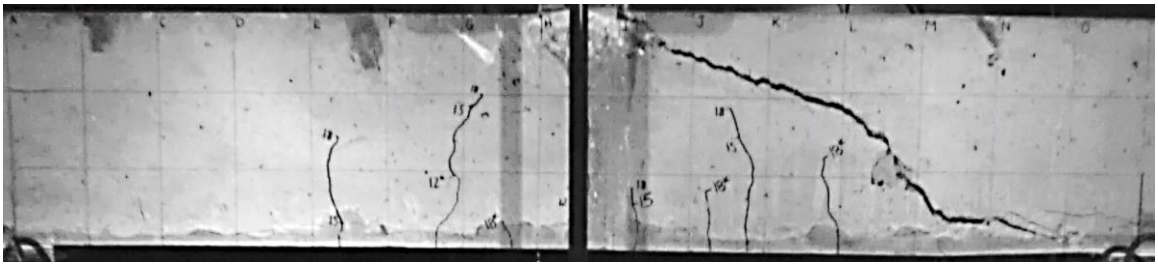

Figure 4.26 Specimen K-2: South Side Failure Sequence (29.7 kip)

(a) K-2: North Side Failure 0.00 s

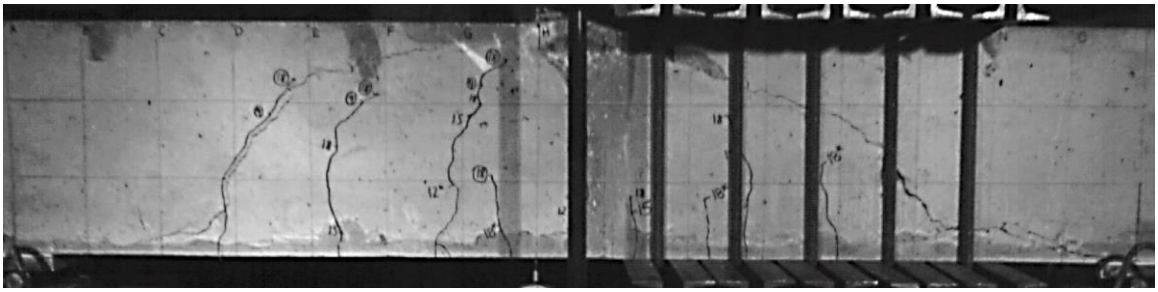

(b) K-2: North Side Failure 0.05 s

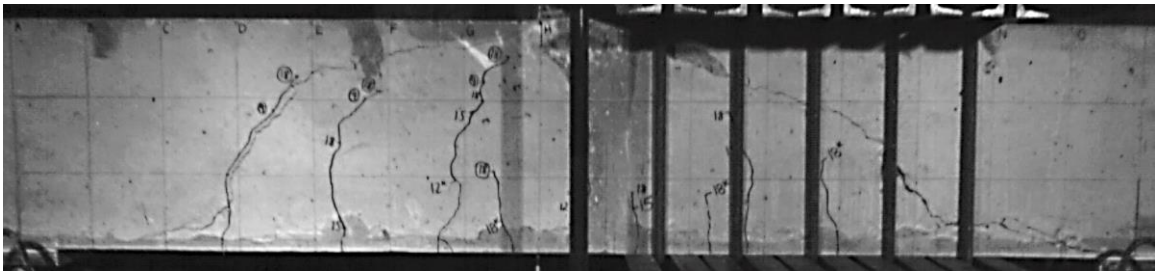

(c) K-2: North Side Failure 0.10 s

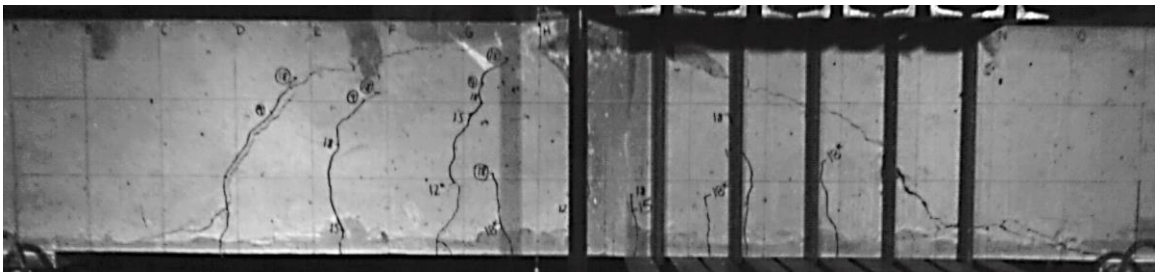

(d) K-2: North Side Failure 0.15 s

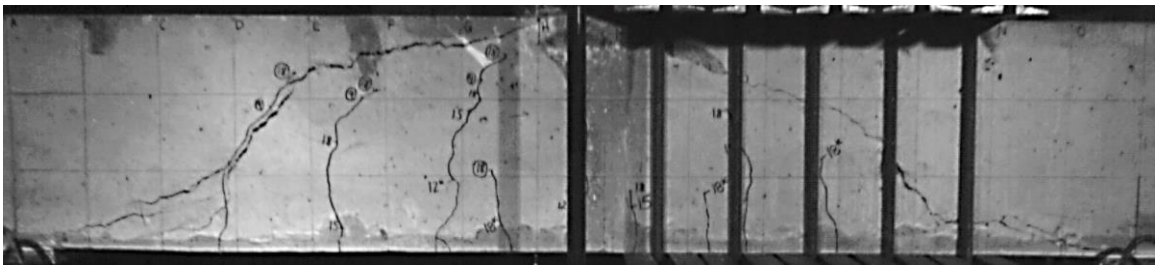

Figure 4.27 Specimen K-2: North Side Failure Sequence (32.0 kip)

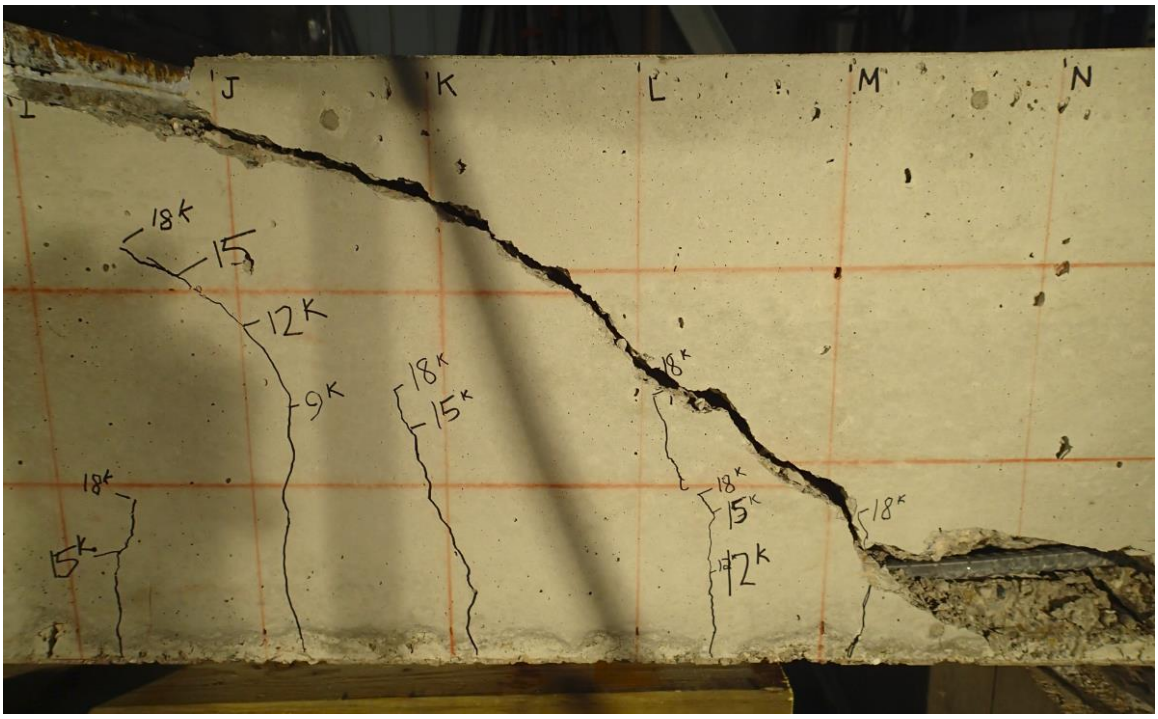

Figure 4.28 Specimen F-3: South Side Failure Inclined Crack

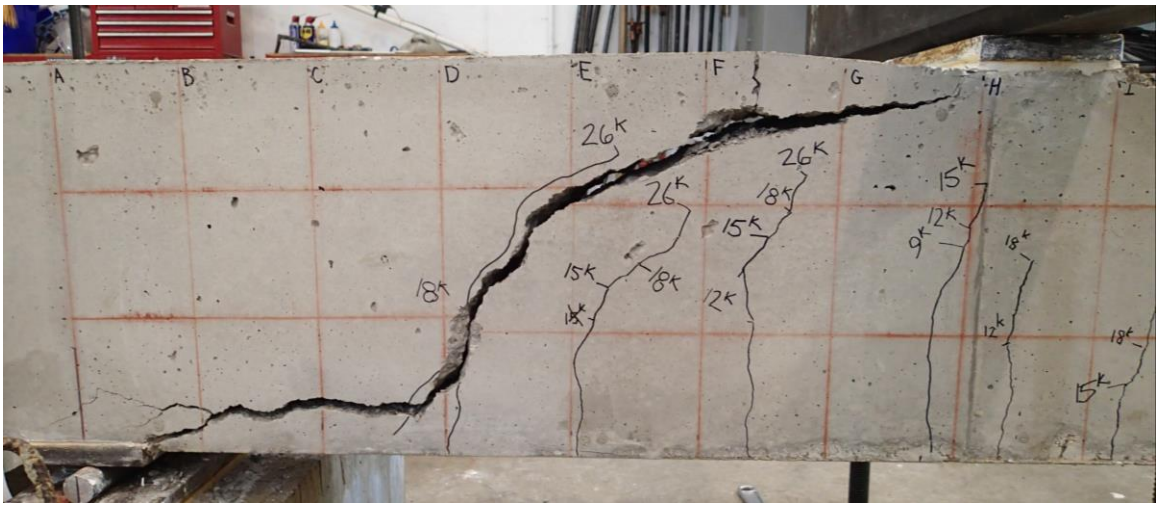

Figure 4.29 Specimen F-3: North Side Failure Inclined Crack

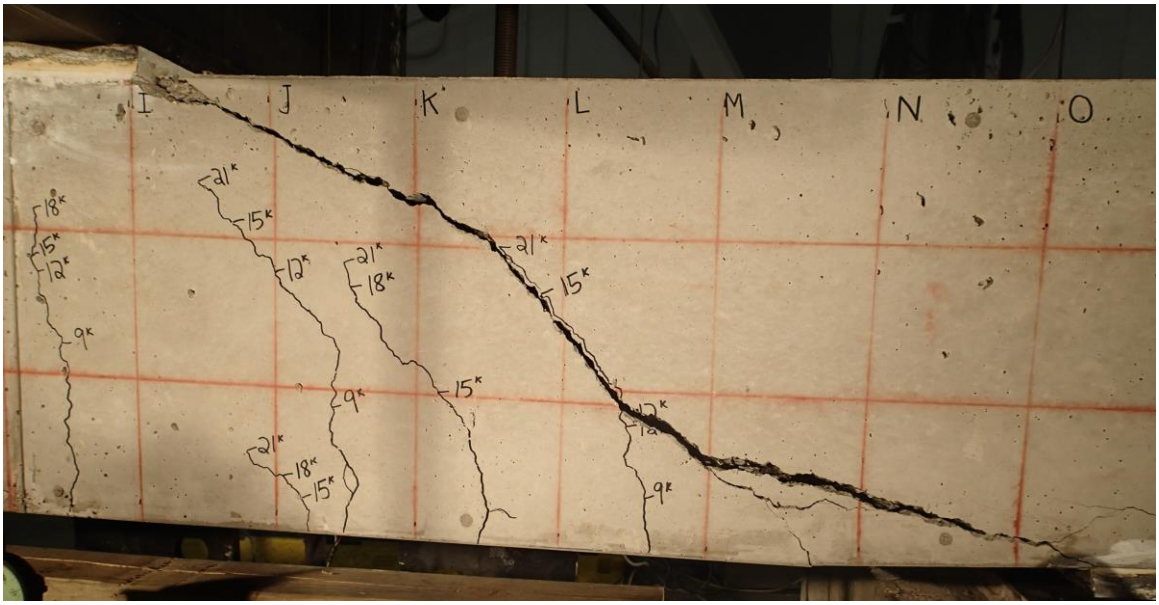

Figure 4.30 Specimen F-4: South Side Failure Inclined Crack

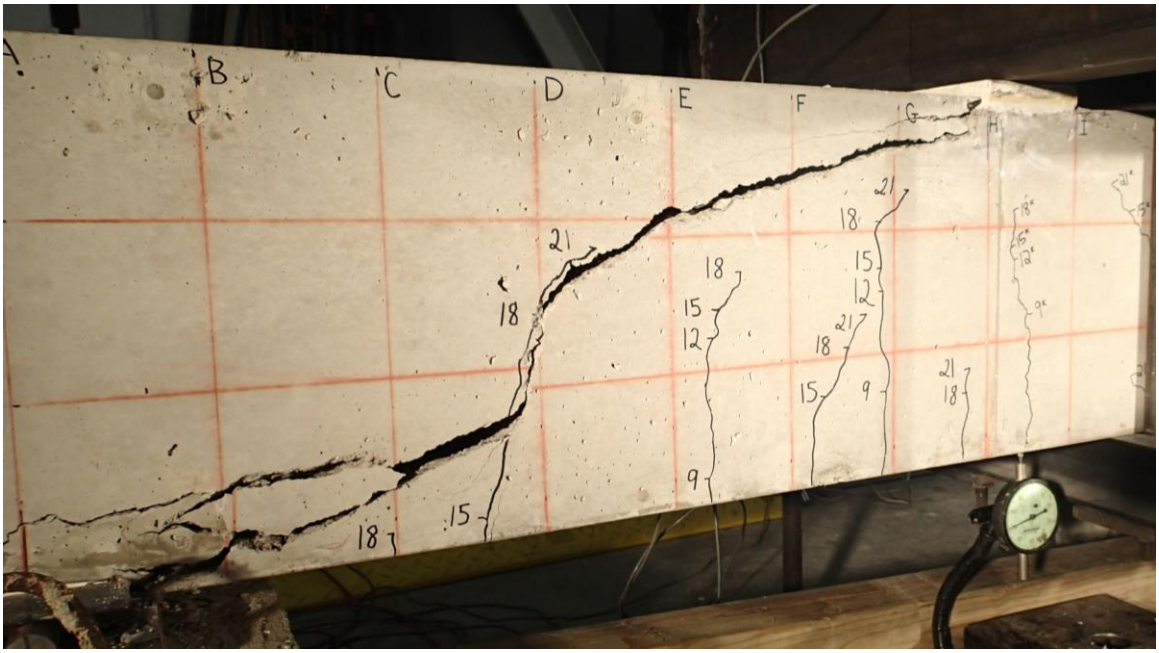

Figure 4.31 Specimen F-4: North Side Failure Inclined Crack

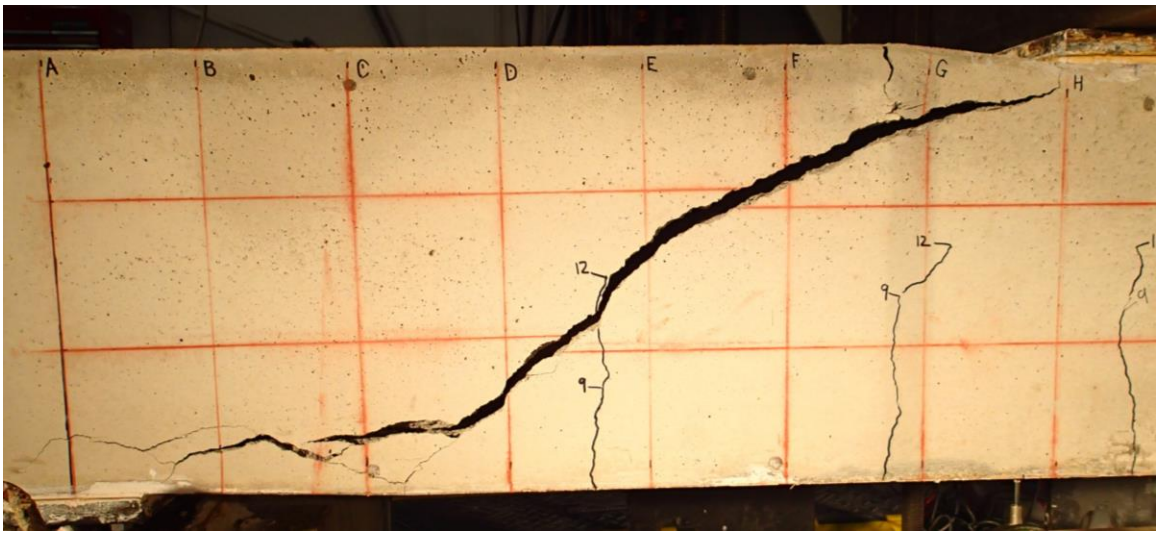

Figure 4.32 Specimen H-1: North Side Failure Inclined Crack

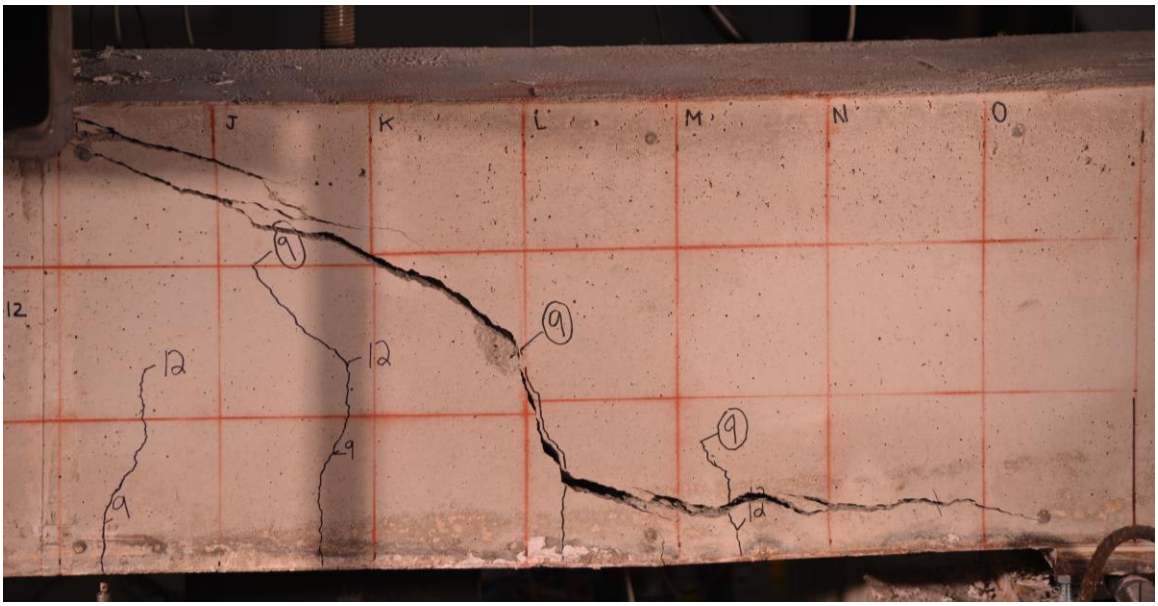

Figure 4.33 Specimen H-1: South Side Failure Inclined Crack

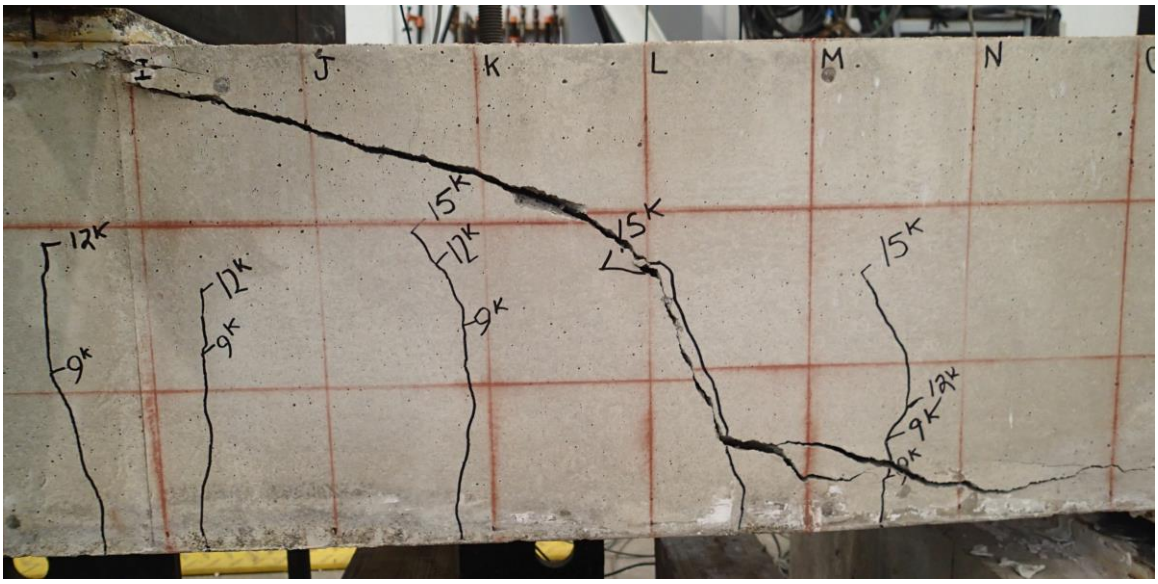

Figure 4.34 Specimen H-2: South Side Failure Inclined Crack

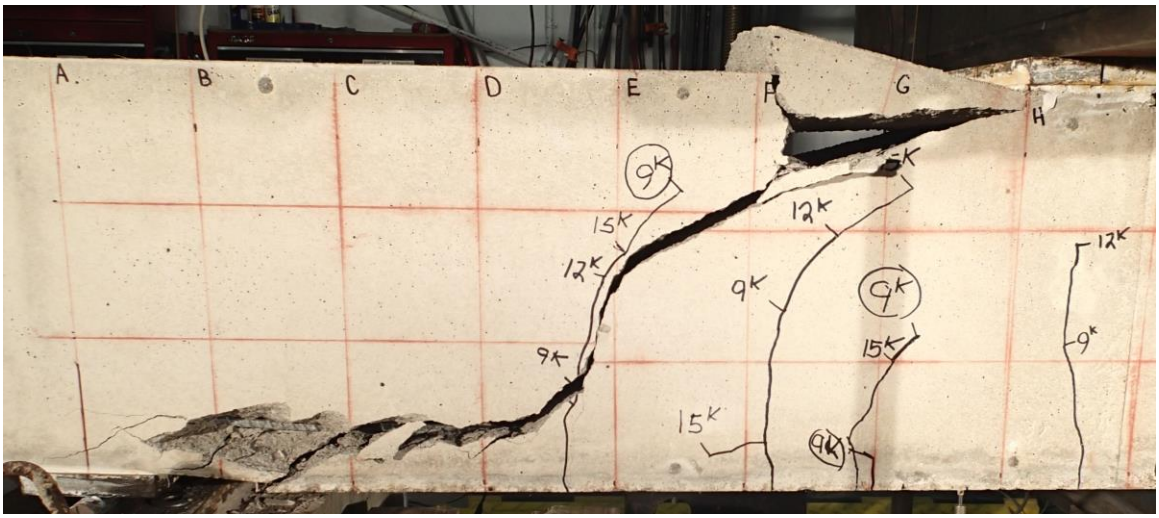

Figure 4.35 Specimen H-2: North Side Failure Inclined Crack

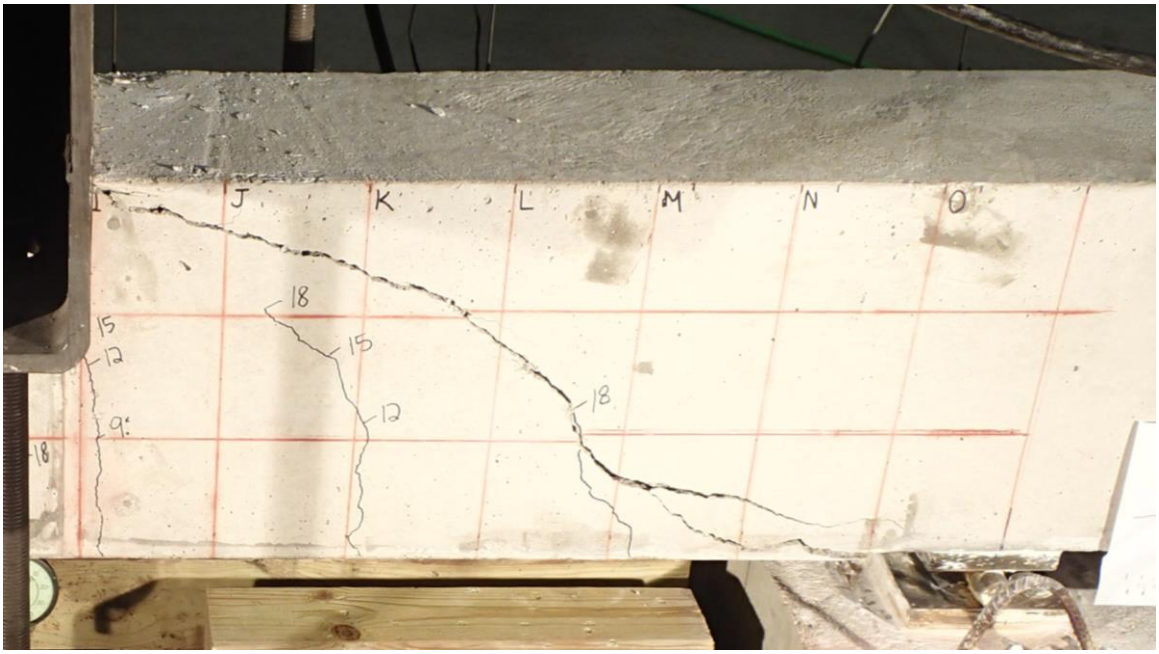

Figure 4.36 Specimen I-1: South Side Failure Inclined Crack

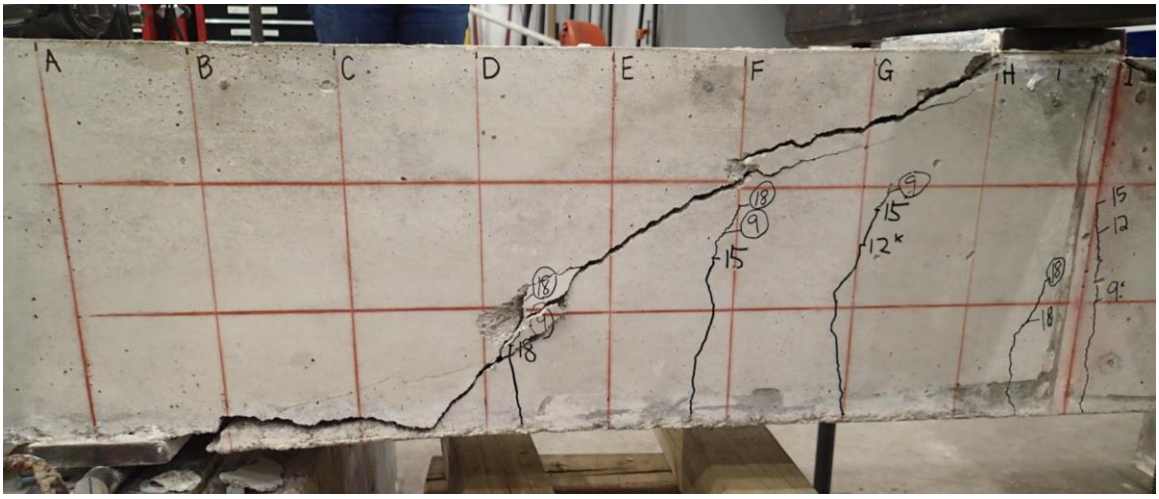

Figure 4.37 Specimen I-1: North Side Failure Inclined Crack

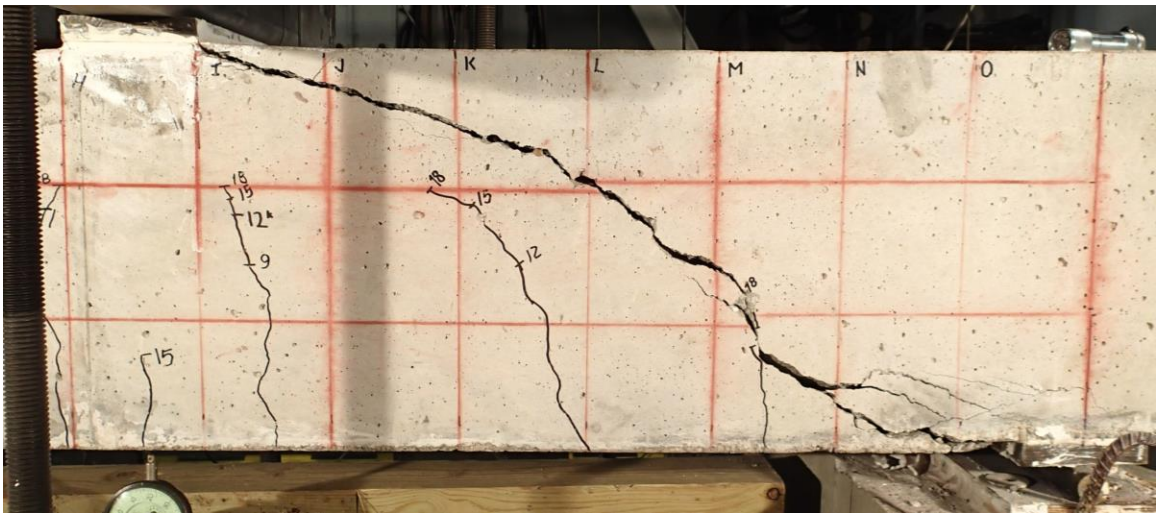

Figure 4.38 Specimen I-2: South Side Failure Inclined Crack

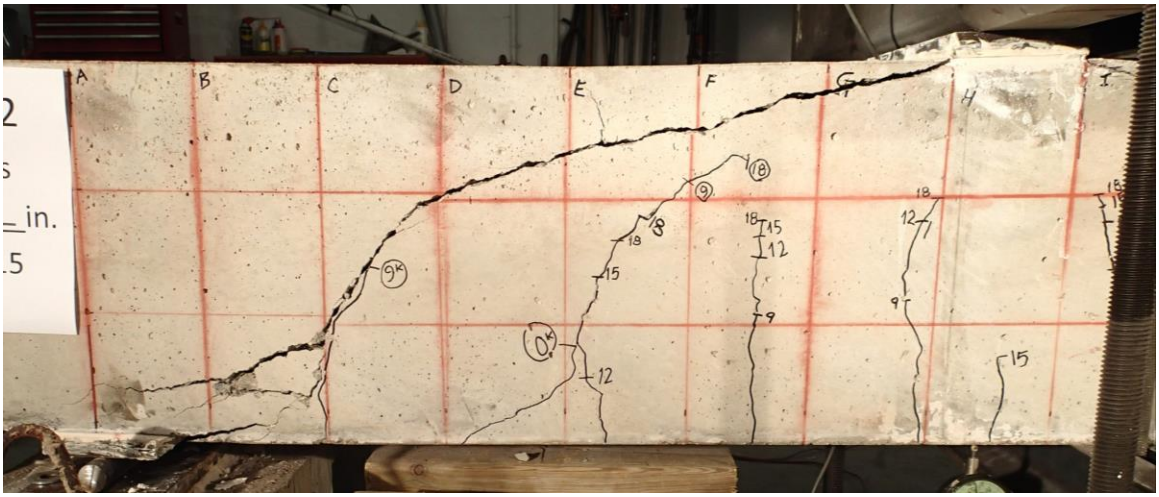

Figure 4.39 Specimen I-2: North Side Failure Inclined Crack

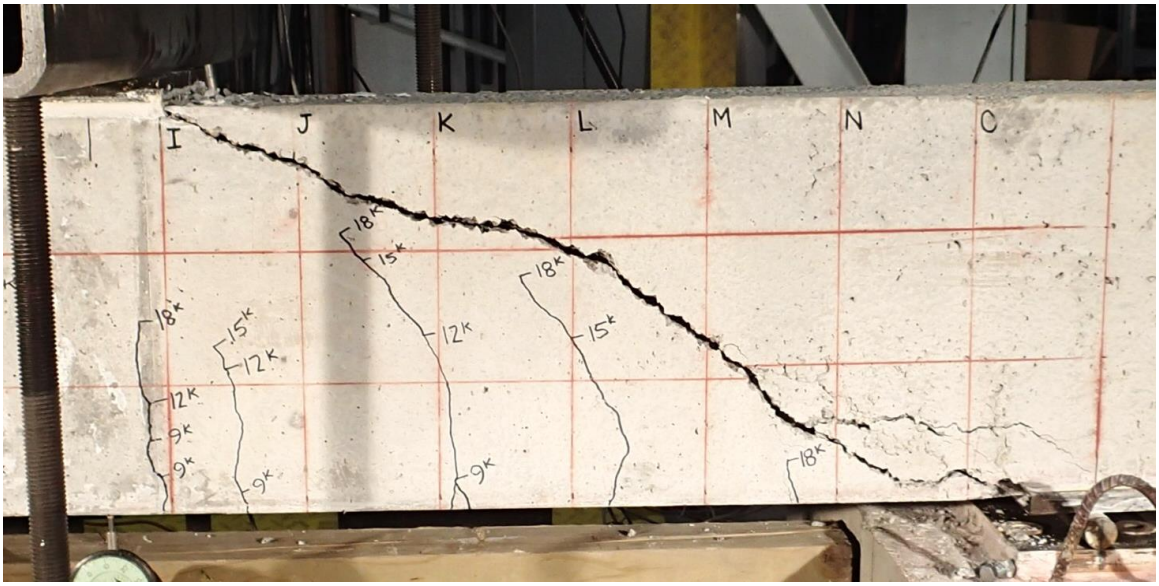

Figure 4.40 Specimen J-1: South Side Failure Inclined Crack

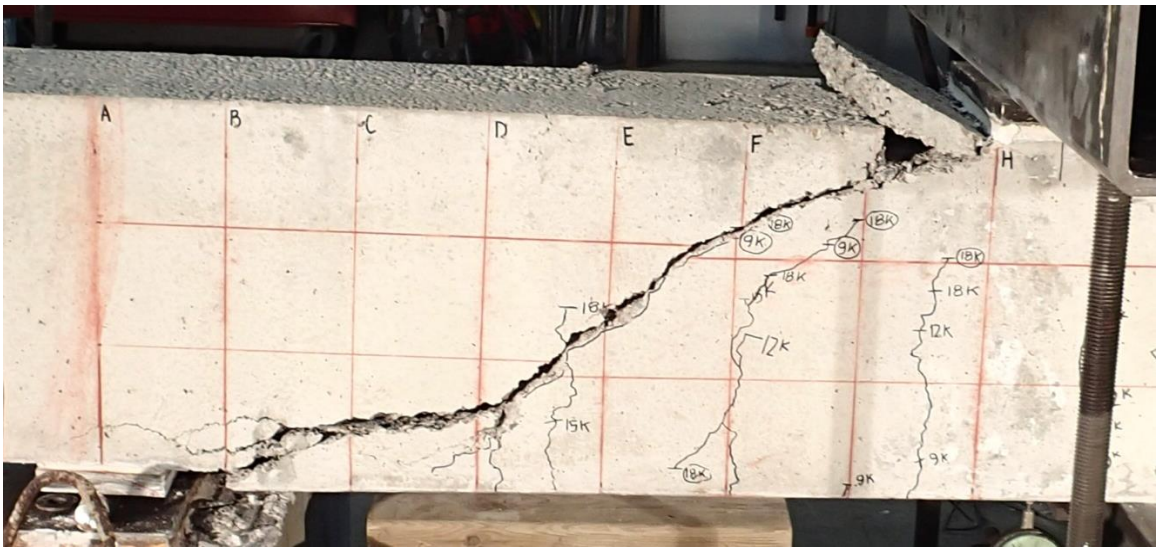

Figure 4.41 Specimen J-1: North Side Failure Inclined Crack

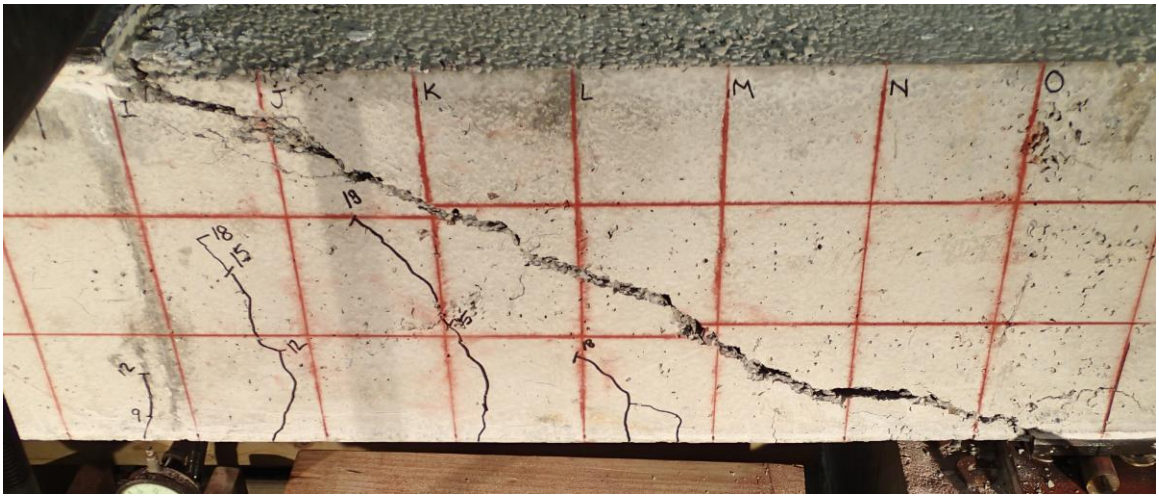

Figure 4.42 Specimen J-2: South Side Failure Inclined Crack

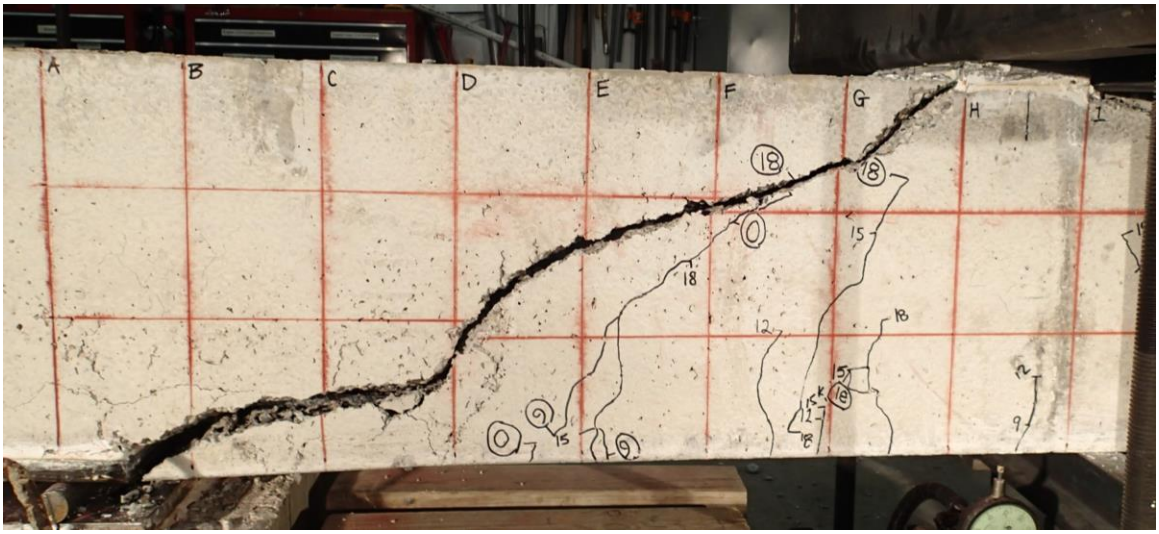

Figure 4.43 Specimen J-2: North Side Failure Inclined Crack

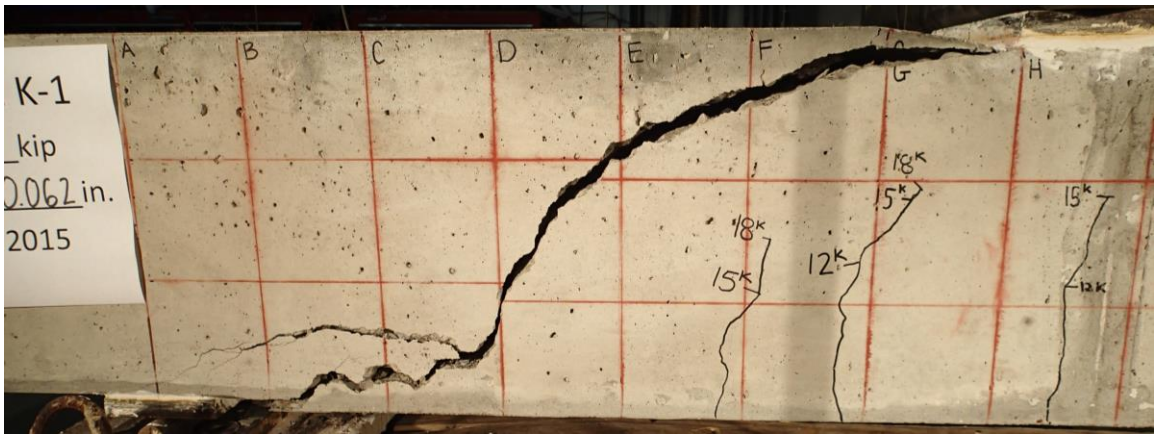

Figure 4.44 Specimen K-1: North Side Failure Inclined Crack

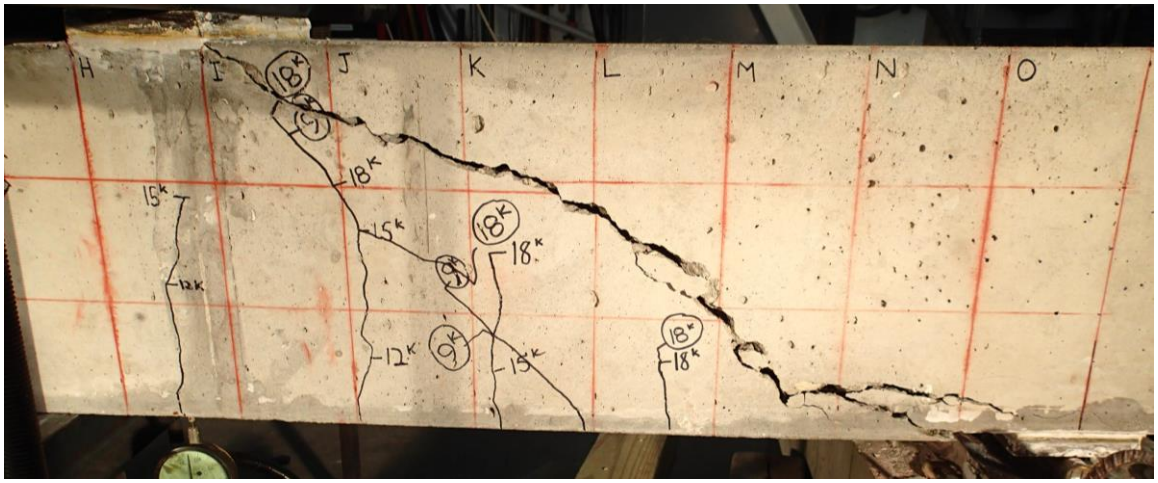

Figure 4.45 Specimen K-1: South Side Failure Inclined Crack

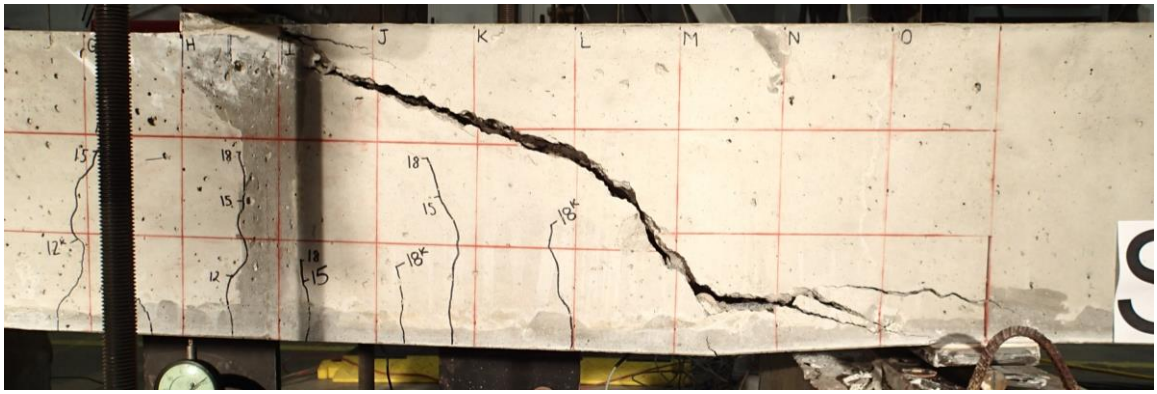

Figure 4.46 Specimen K-2: South Side Failure Inclined Crack

Figure 4.47 Specimen K-2: North Side Failure Inclined Crack

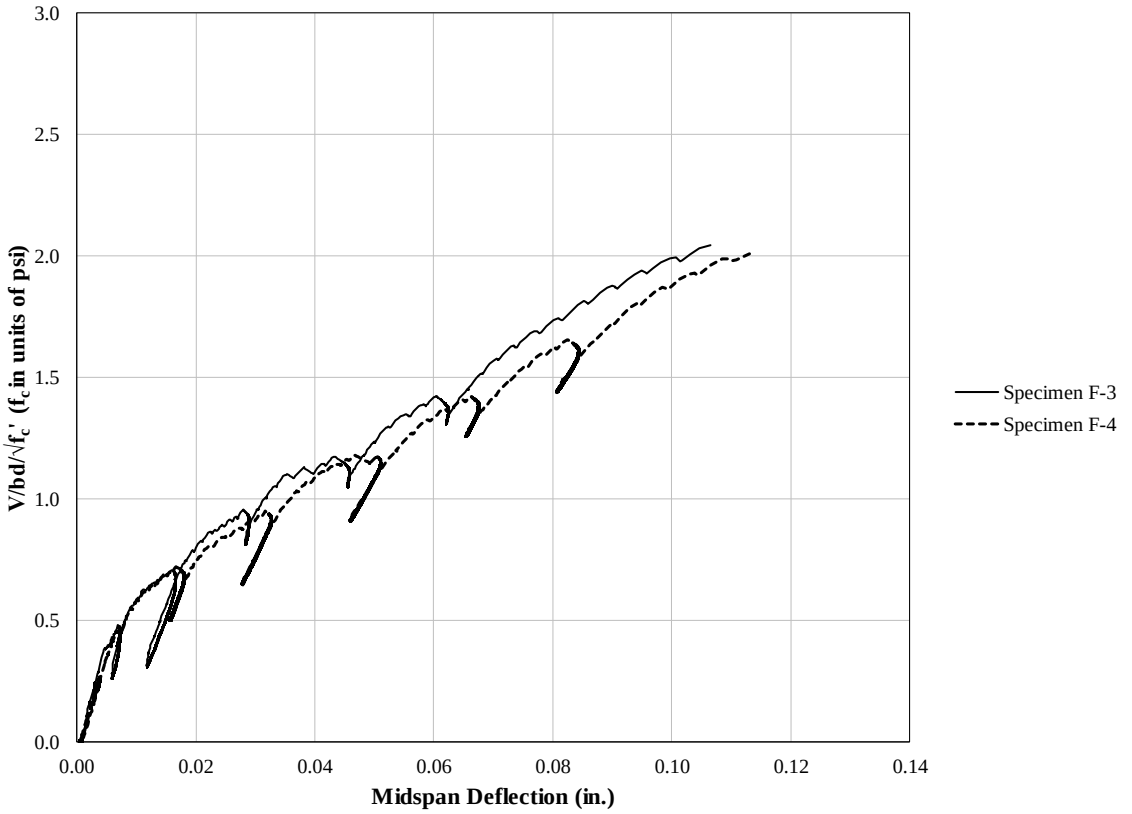

Figure 5.1 Series F Load-Deflection Curves

Note: Specimen F-1 and F-2 are not in this plot because the reinforcement ratio is not the same as Specimen F-3 and F-4.

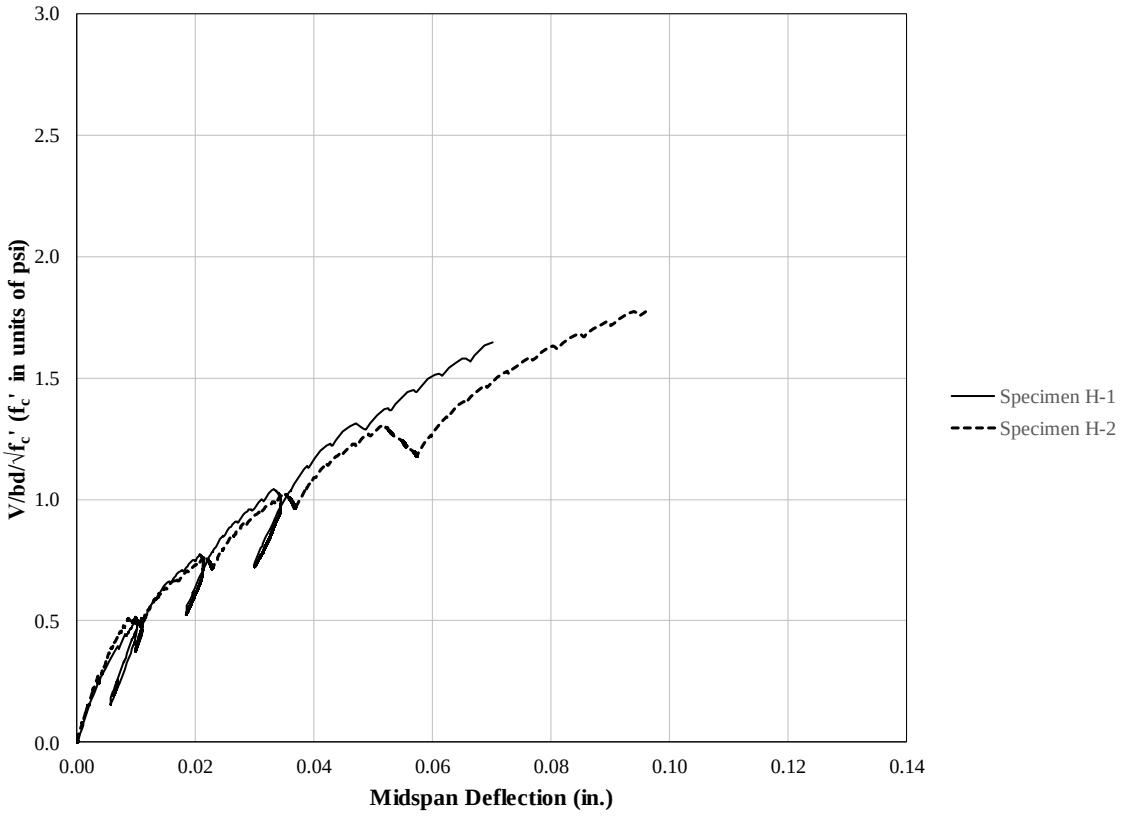

Figure 5.2 Series H Load-Deflection Curves

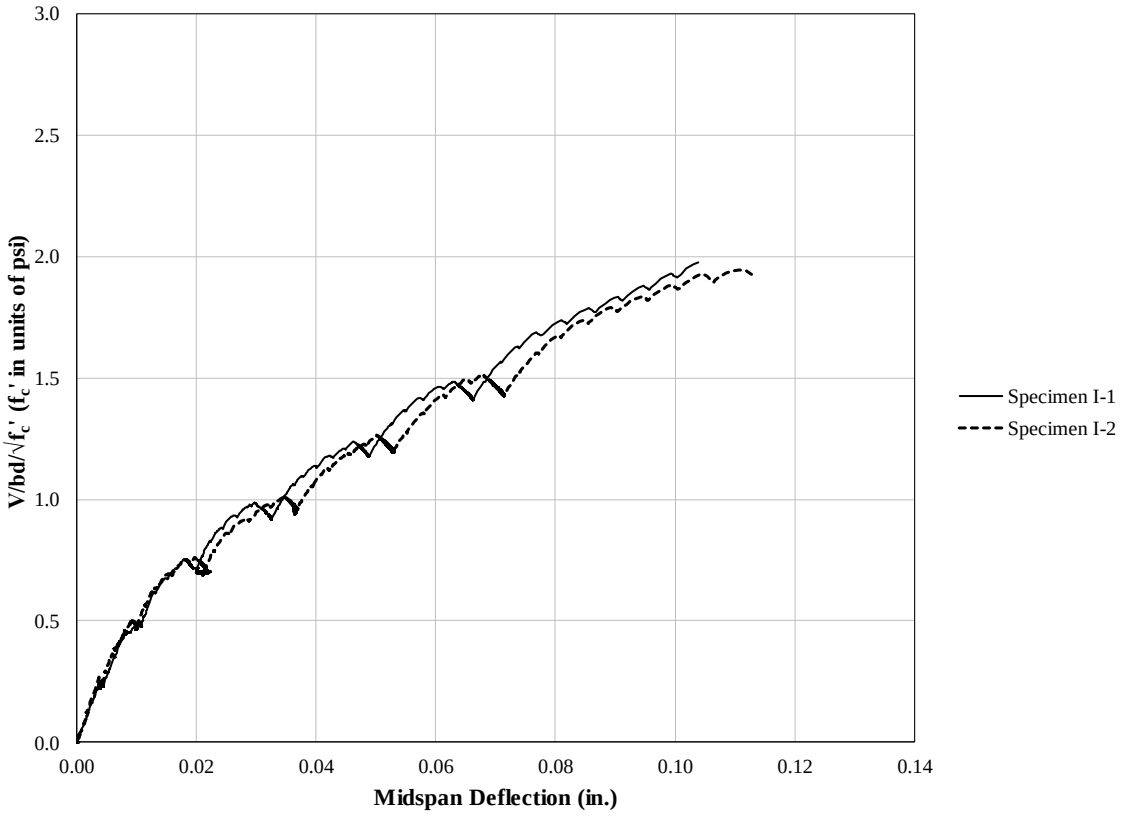

Figure 5.3 Series I Load-Deflection Curves

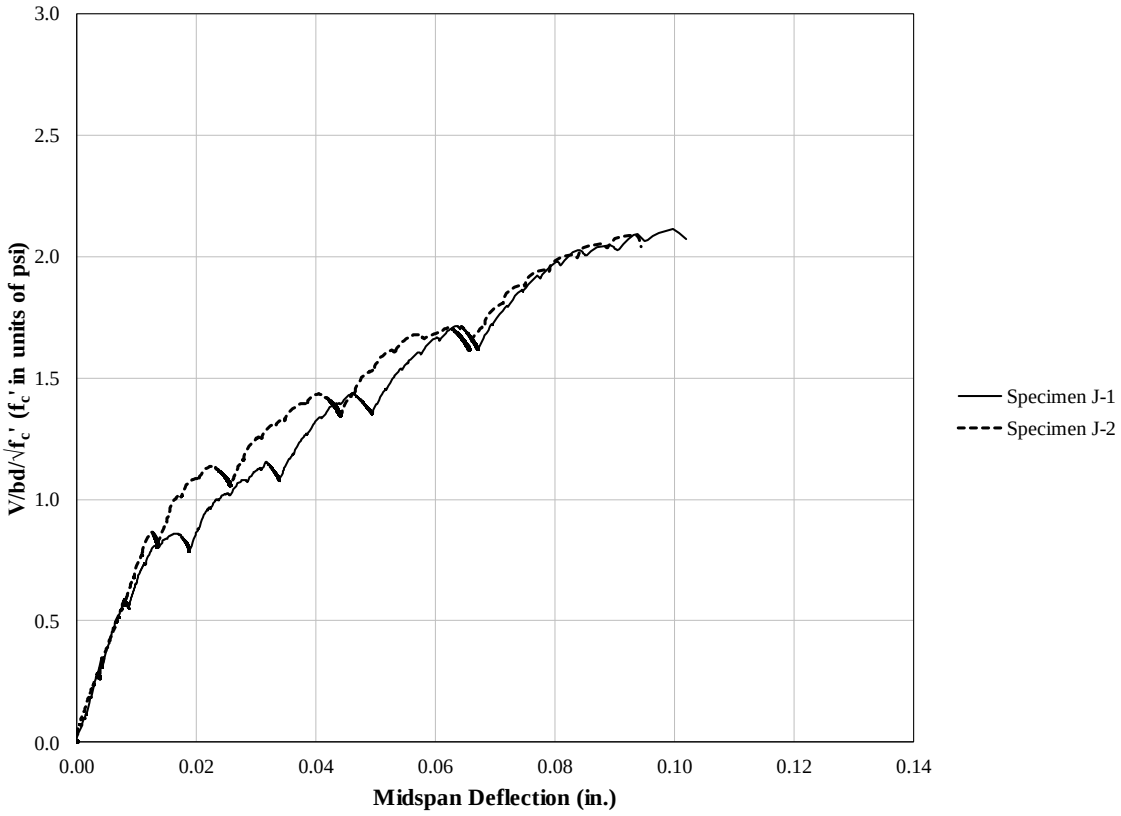

Figure 5.4 Series J Load-Deflection Curves

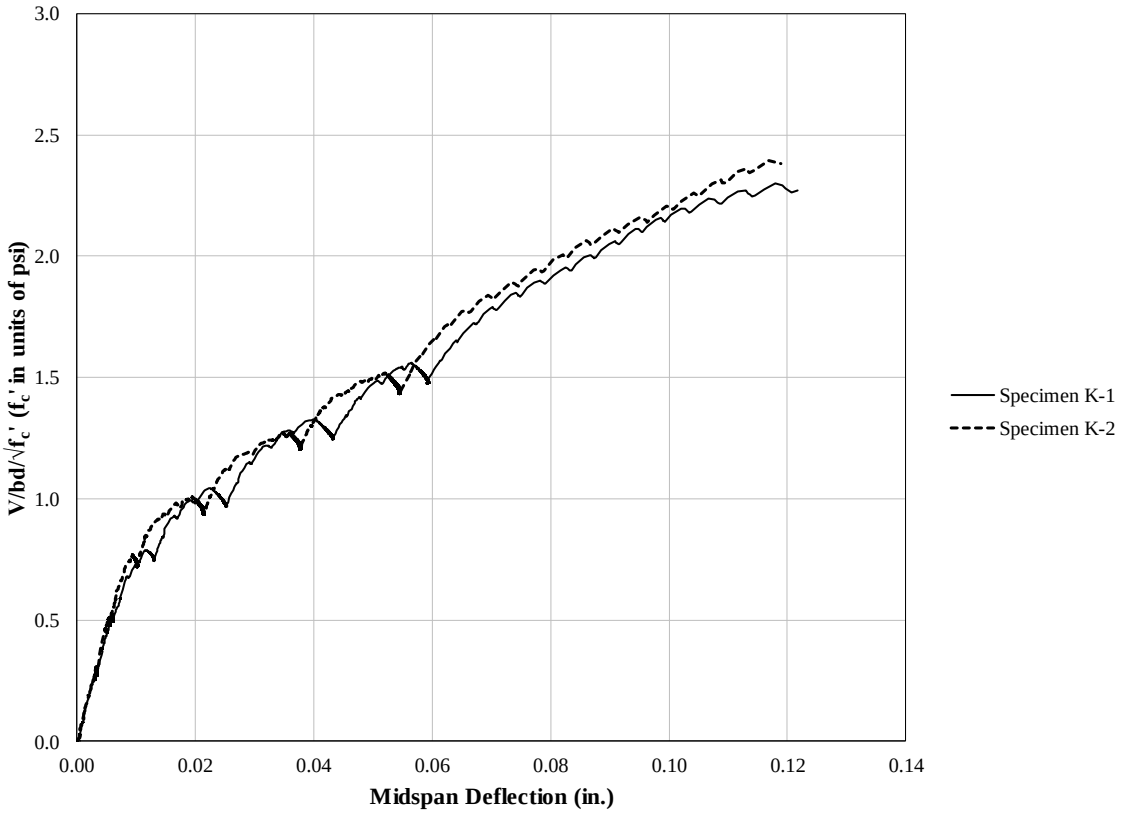

Figure 5.5 Series K Load-Deflection Curves

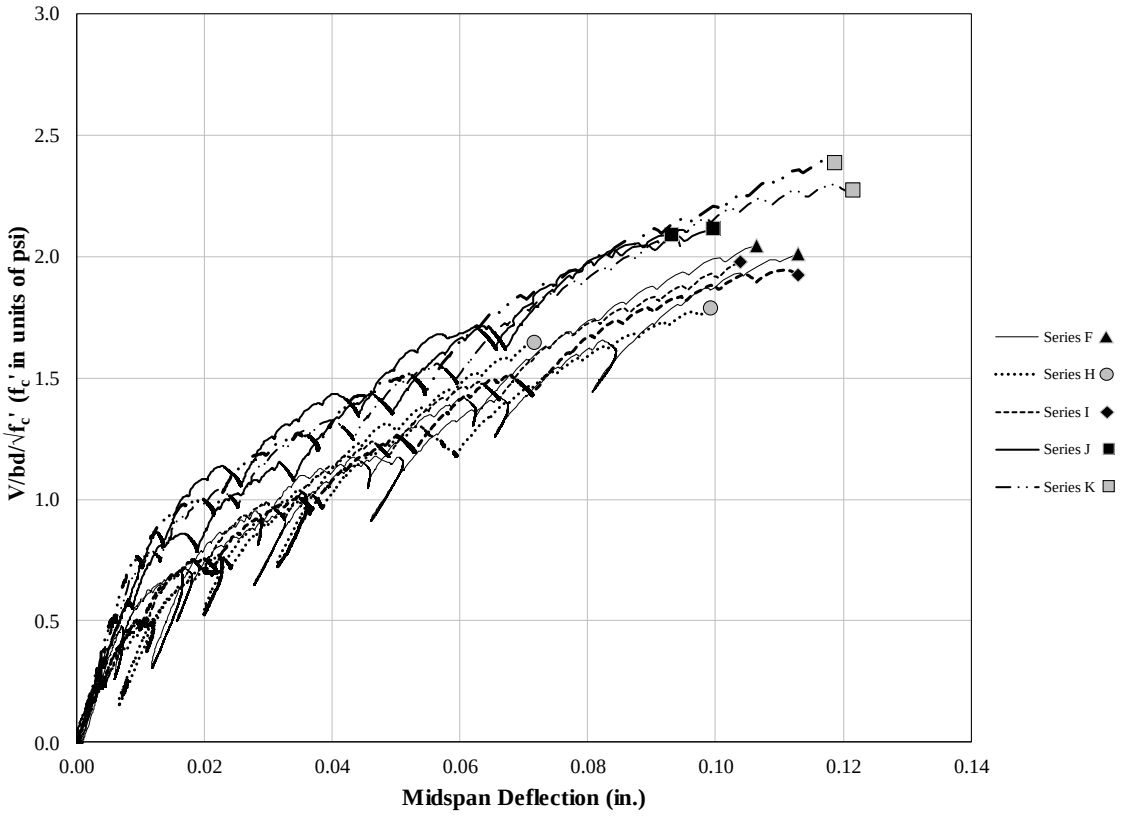

Figure 5.6 All Series Load-Deflection Curves

Note: Specimen F-1 and F-2 are not in this plot because the reinforcement ratio is not the same as other beams.

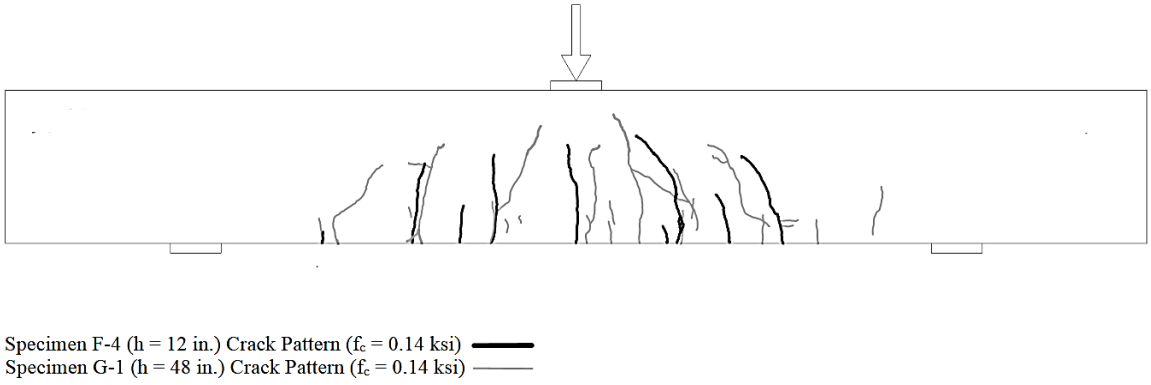

Figure 5.7 Crack Patterns

Note: Data in this figure include beams described in Section 3.1 and Appendix E. Dimensions including concrete cover, maximum aggregate size, and longitudinal reinforcement size and spacing were scaled with respect to beam depth. Crack comparisons were made at comparable loading stages (P/bd). Test beams in this figure had the following dimensions and parameters:

$$a/d = 2.9$$
$$1/2 \text{ in.} \le a_g \le 2 \text{ in.}$$
$$a_g/d = 0.05$$
$$4500 \text{ psi} \le f_c^{'} \le 4900 \text{ psi}$$
$$12 \text{ in.} \le h \le 48 \text{ in.}$$
$$P/bd = 0.14$$
$$0.63\% \le \rho \le 0.79\%$$

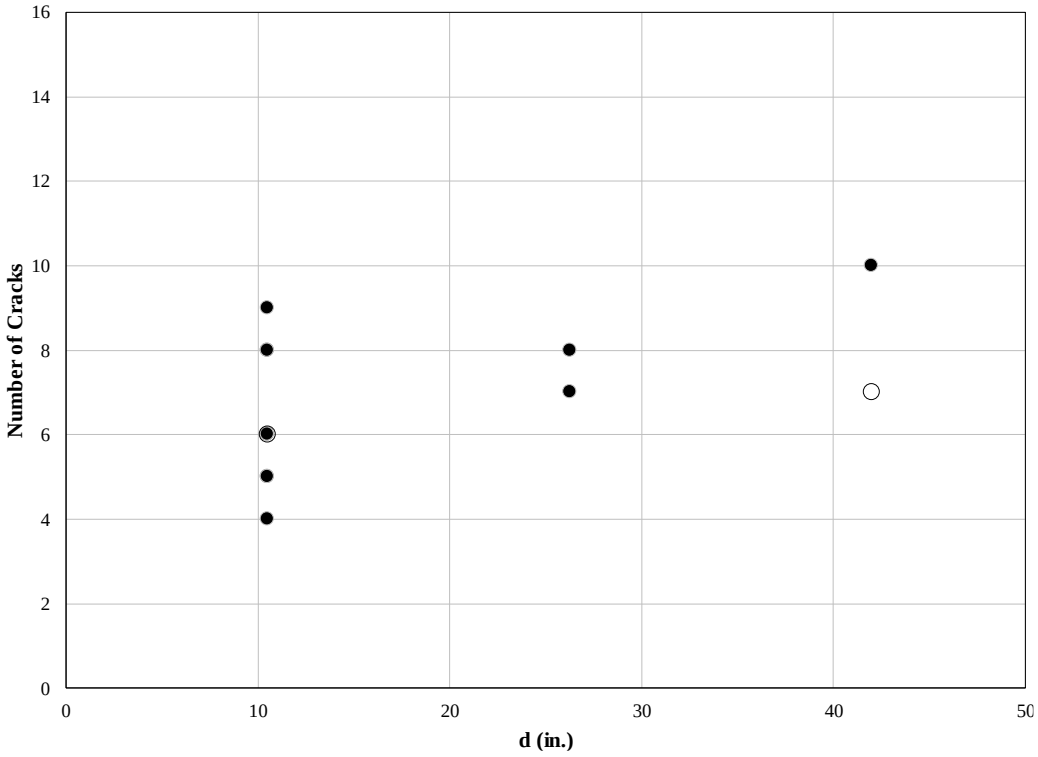

Figure 5.8 Number of Flexural Cracks Compared to Beam Depth

Note: Data in this figure include beams tested by McCain (2012) and beams described in Section 3.1 and Appendix E. Concrete cover, and longitudinal reinforcement size and spacing were scaled with respect to beam depth. Crack comparisons were made at comparable loading stages (*P/bh*). Test beams in this figure had the following dimensions and parameters:

$$a/d = 2.9$$
$$3/8 \text{ in.} \le a_g \le 2 \text{ in.}$$
$$0.04 \le a_g/d \le 0.1$$
$$3300 \text{ psi} \le f_c' \le 5000 \text{ psi}$$
$$12 \text{ in.} \le h \le 48 \text{ in.}$$
$$0.13 \le P/bh^* \le 0.14$$
$$0.63\% \le \rho \le 0.98\%$$

*Hollow points in the figure represent test beams with ($0.10 \le P/bh \le 0.11$). Crack patterns were not documented at a stress above that level.

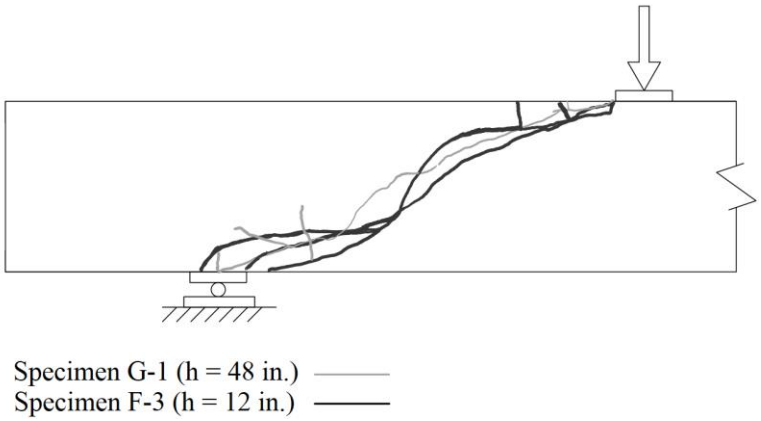

Figure 5.9 Comparison of Inclined Cracks in 12 and 48 in. deep beams

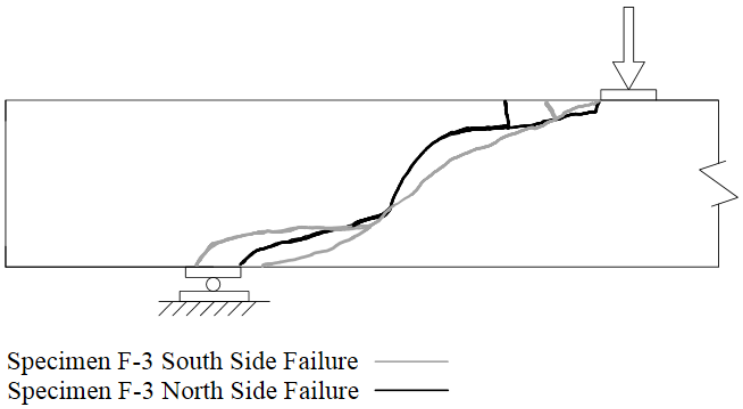

Figure 5.10 Specimen F-3 Inclined Crack Comparison

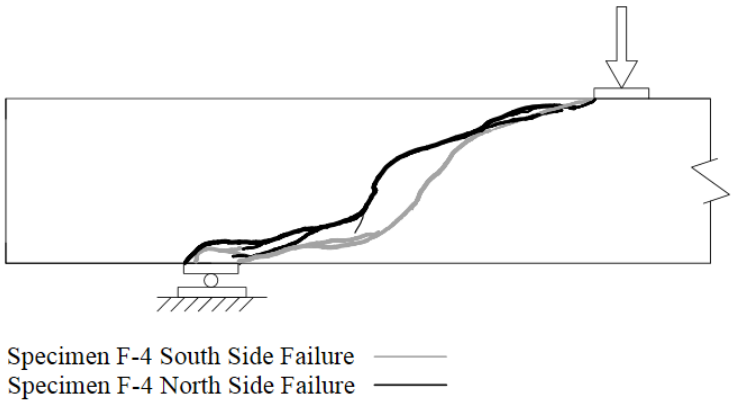

Figure 5.11 Specimen F-4 Inclined Crack Comparison

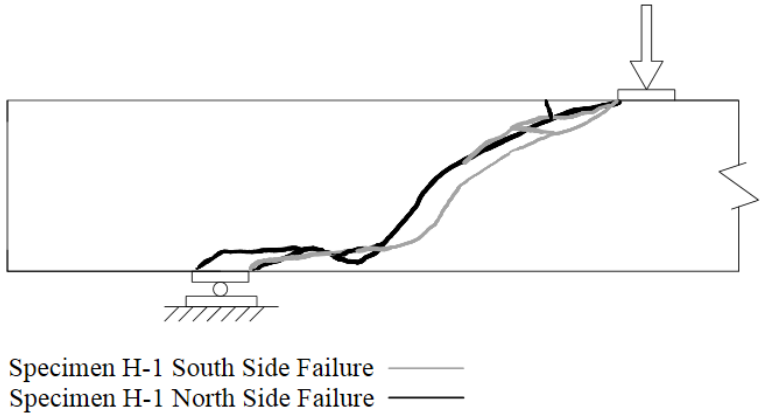

Figure 5.12 Specimen H-1 Inclined Crack Comparison

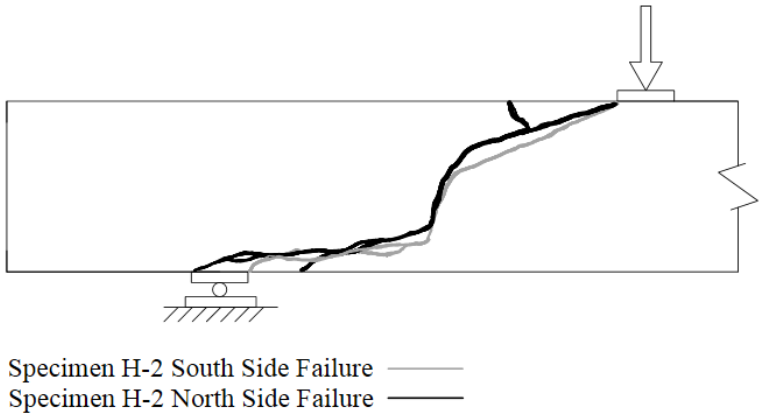

Figure 5.13 Specimen H-2 Inclined Crack Comparison

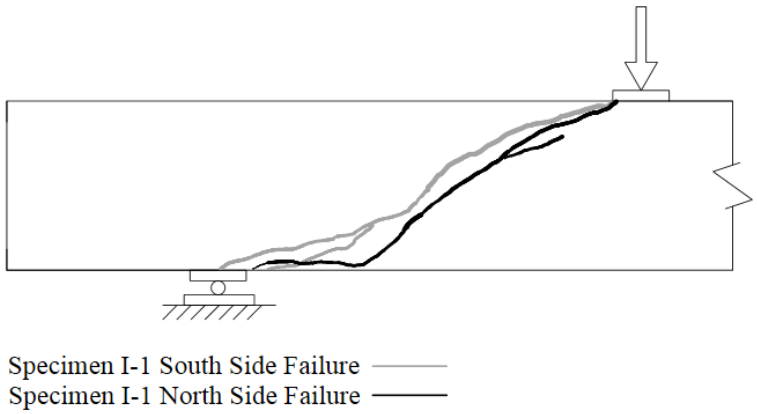

Figure 5.14 Specimen I-1 Inclined Crack Comparison

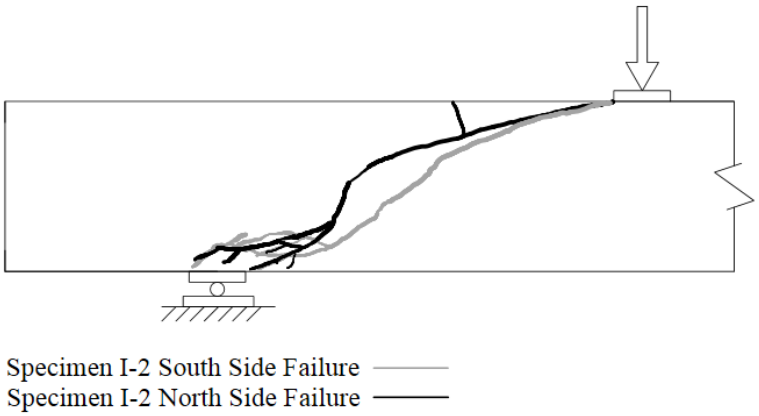

Figure 5.15 Specimen I-2 Inclined Crack Comparison

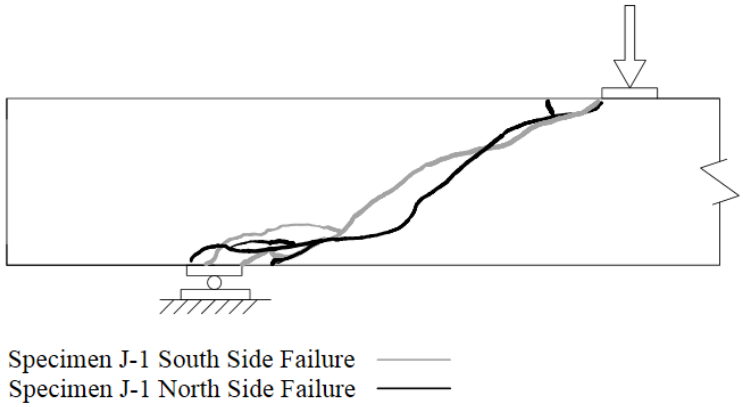

Figure 5.16 Specimen J-1 Inclined Crack Comparison

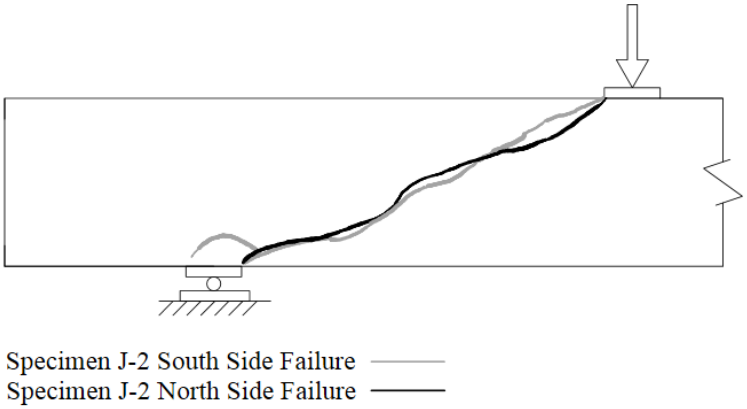

Figure 5.17 Specimen J-2 Inclined Crack Comparison

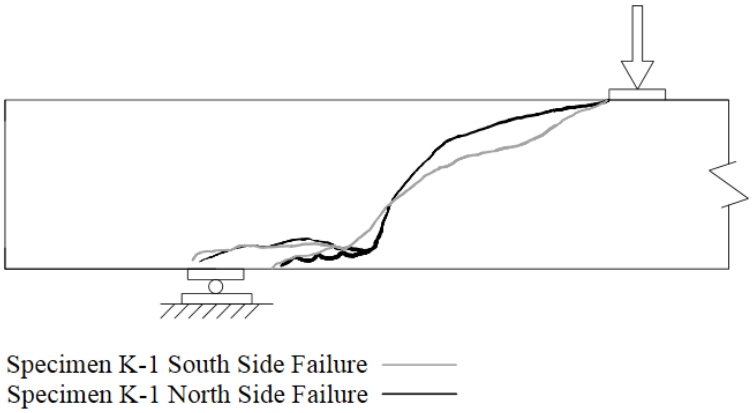

Figure 5.18 Specimen K-1 Inclined Crack Comparison

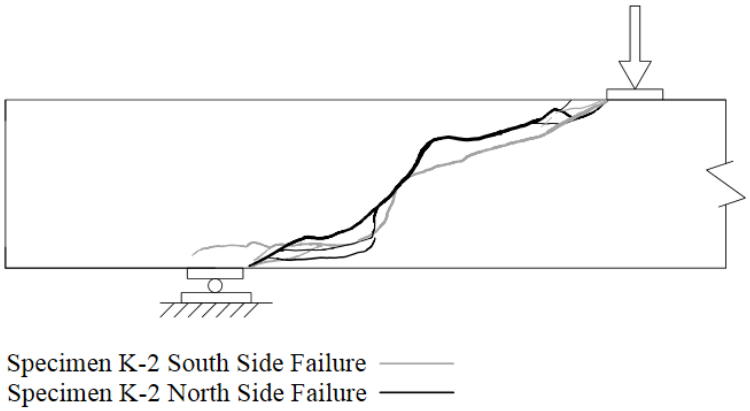

Figure 5.19 Specimen K-2 Inclined Crack Comparison

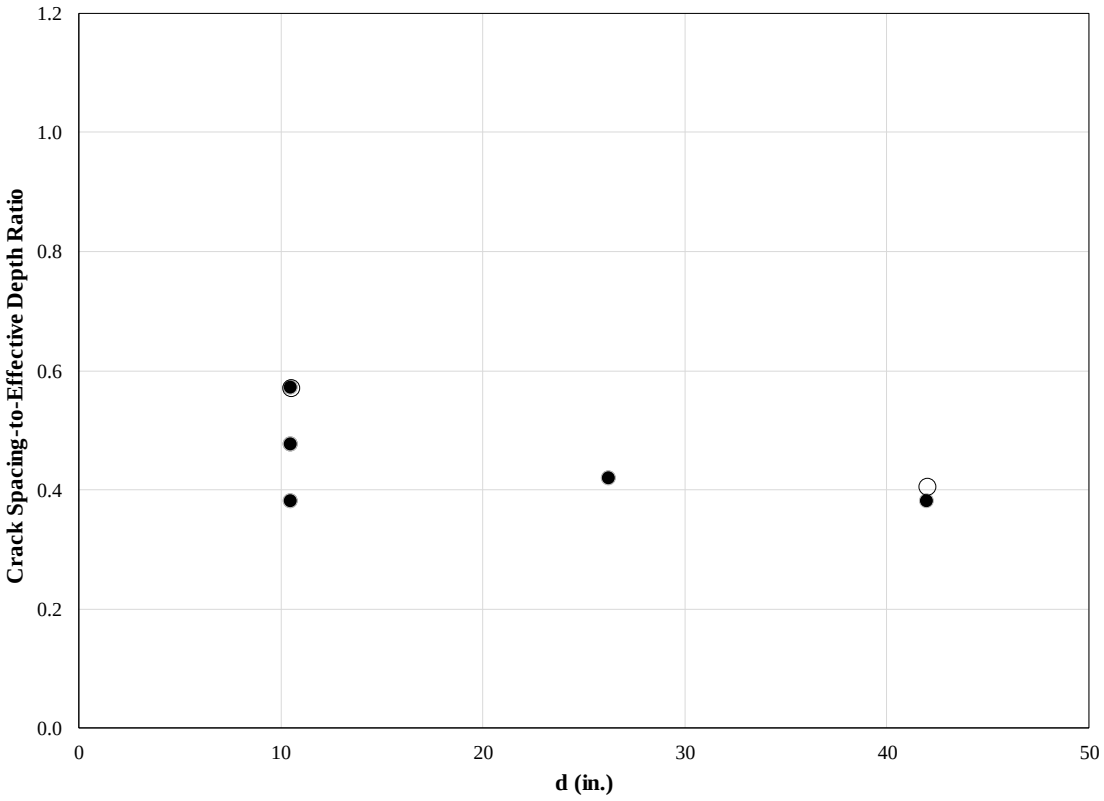

Figure 5.20 Relative Crack Spacing

Note: Data in this figure include beams tested by McCain (2012) and beams described in Section 3.1 and Appendix E. Concrete cover was scaled with respect to beam depth. Crack comparisons were made at comparable loading stages (*P/bh*). Test beams in this figure had the following dimensions and parameters:

$$a/d = 2.9$$
$$3/8 \text{ in.} \le a_g \le 2 \text{ in.}$$
$$0.04 \le a_g/d \le 0.1$$
$$3300 \text{ psi} \le f_c^{'} \le 5000 \text{ psi}$$
$$12 \text{ in.} \le h \le 48 \text{ in.}$$
$$0.13 \le P/bh^{*} \le 0.14$$
$$0.63\% \le \rho \le 0.98\%$$

*Hollow points in the figure represent test beams with ($0.10 \le P/bh \le 0.11$). Crack patterns were not documented at a stress above that level.

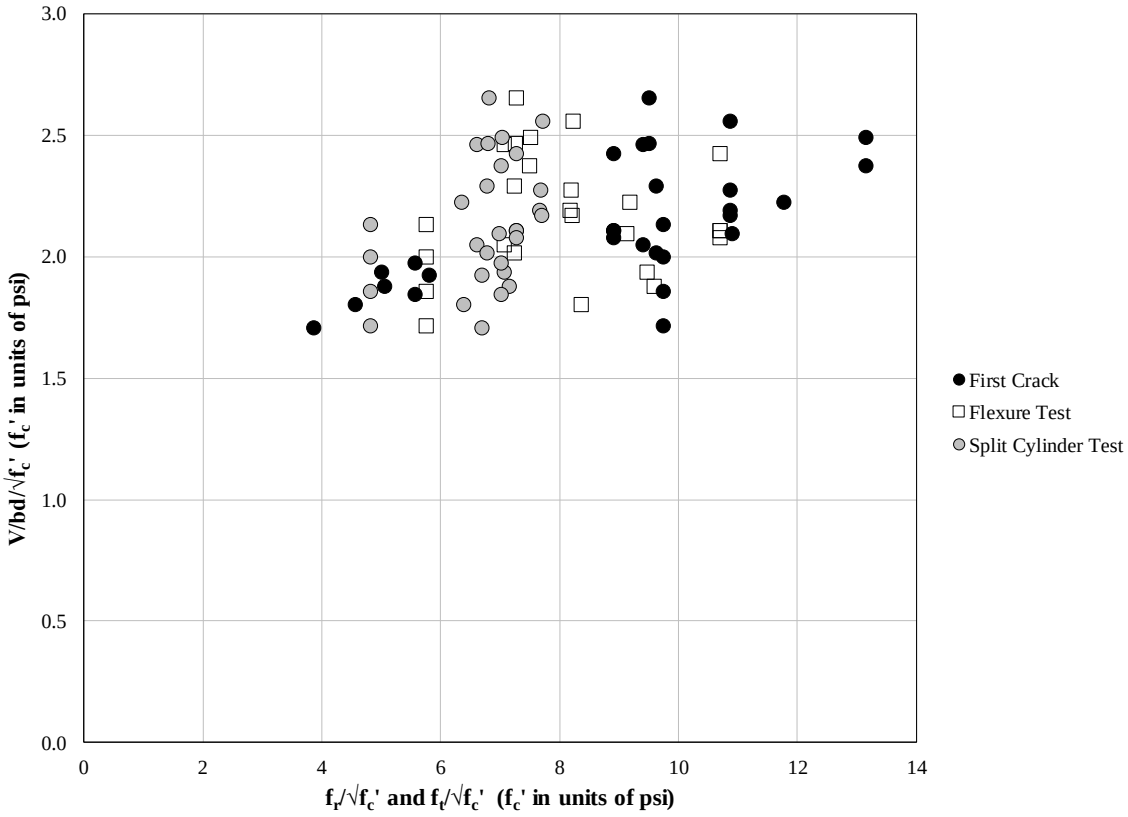

Figure 5.21 Concrete Tensile Tests versus Shear Strength

Note: Data in this figure include beams tested by McCain (2012) and beams described in Section 3.1 and Appendix E. Test beams in this figure had the following dimensions and parameters:

$$a/d = 2.9$$
$$3/8 \text{ in.} \le a_g \le 2 \text{ in.}$$
$$0.04 \le a_g/d \le 0.1$$
$$3300 \text{ psi} \le f_c^{'} \le 5000 \text{ psi}$$
$$12 \text{ in.} \le h \le 48 \text{ in.}$$
$$0.63\% \le \rho \le 0.98\%$$

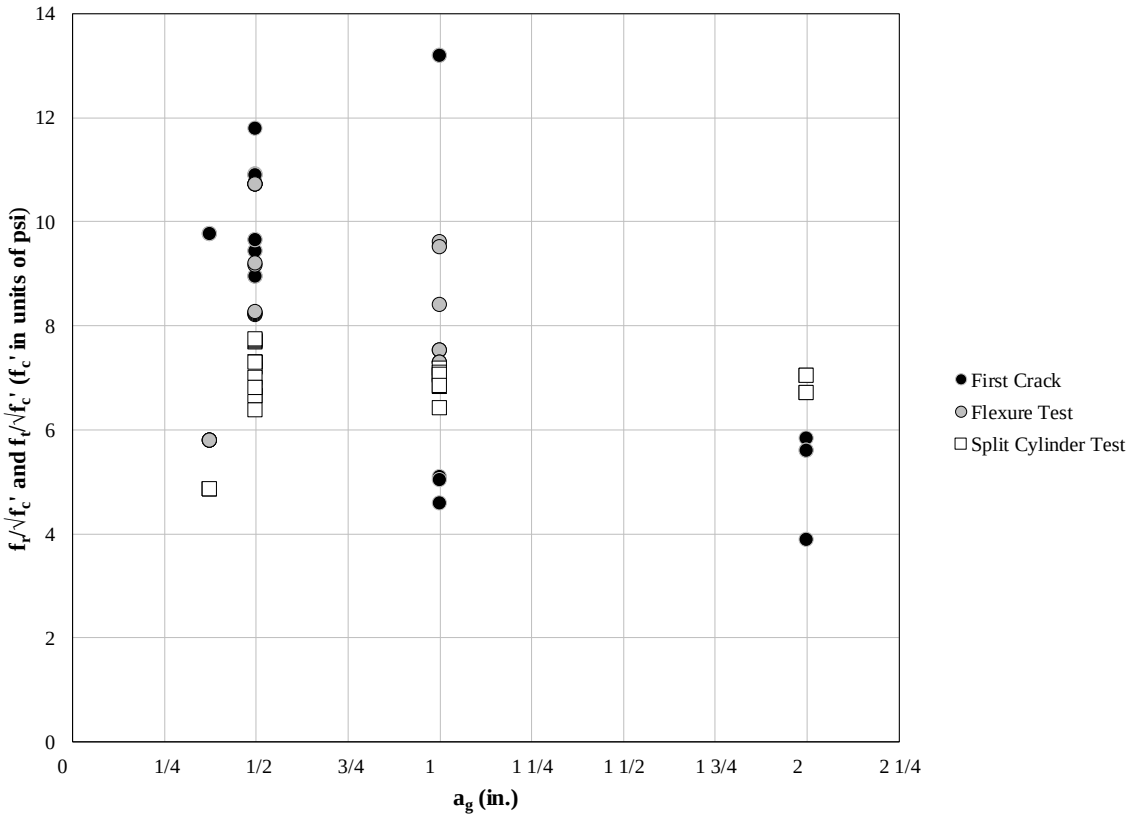

Figure 5.22 Concrete Tensile Tests versus Maximum Aggregate Size

Note: Data in this figure include beams tested by McCain (2012) and beams described in Section 3.1. Test beams in this figure had the following dimensions and parameters:

$$a/d = 2.9$$

$$3/8 \text{ in.} \le a_g \le 2 \text{ in.}$$

$$0.04 \le a_g/d \le 0.1$$

$$3300 \text{ psi} \le f_c' \le 5000 \text{ psi}$$

$$12 \text{ in.} \le h \le 48 \text{ in.}$$

$$0.63\% \le \rho \le 0.98\%$$

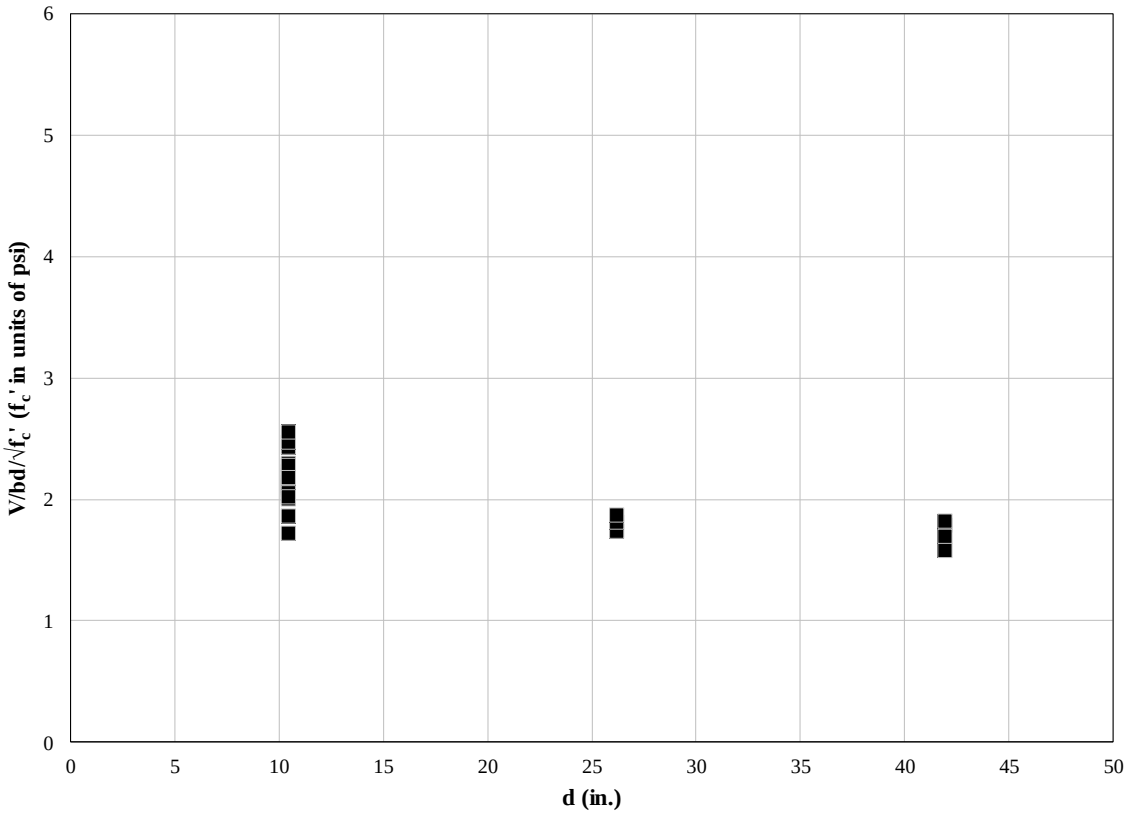

Figure 5.23 Shear Test Results: Three

Note: Data in this figure include beams tested by McCain (2012) and beams described in Section 3.1 and Appendix E. In these tests, concrete cover, and longitudinal reinforcement size and spacing were scaled with respect to beam depth. Test beams in this figure had the following dimensions and parameters:

$$a/d = 2.9$$

$$3/8 \text{ in.} \le a_g \le 2 \text{ in.}$$

$$0.04 \le a_g/d \le 0.05$$

$$3300 \text{ psi} \le f_c^{'} \le 5000 \text{ psi}$$

$$12 \text{ in.} \le h \le 48 \text{ in.}$$

$$0.63\% \le \rho \le 0.98\%$$

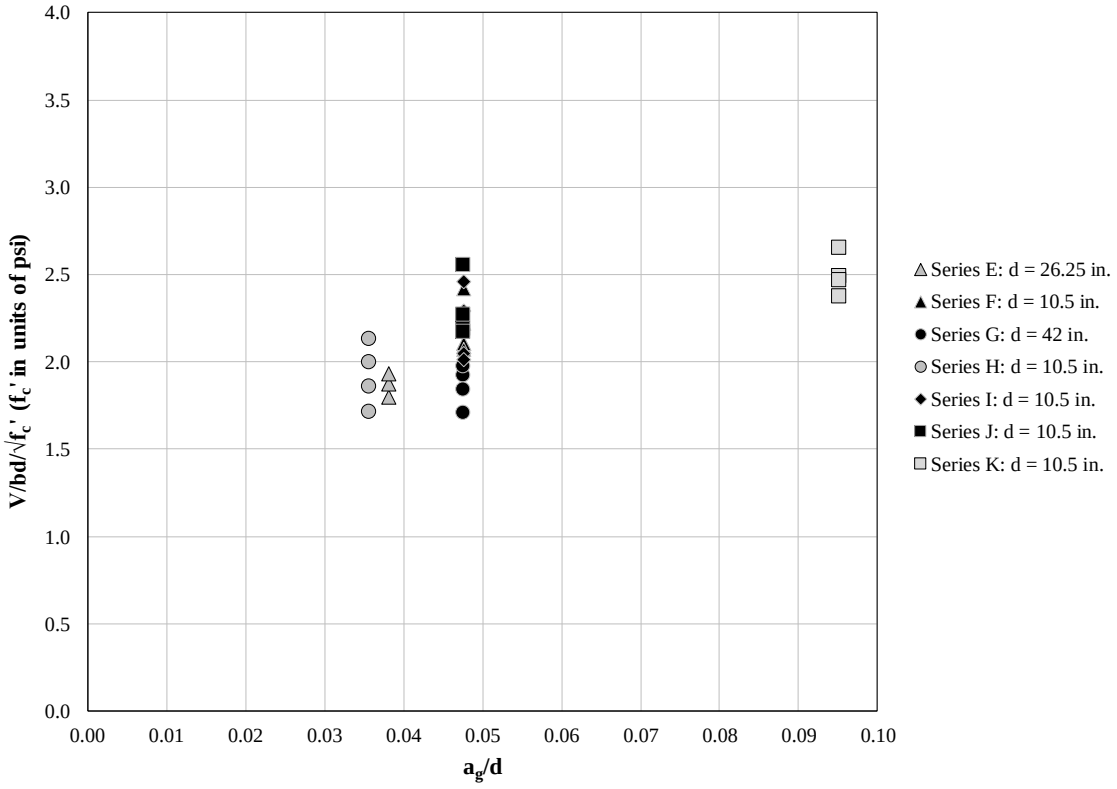

Figure 5.24 Variation of Shear Strength with Relative Aggregate Size: One

Note: Data in this figure include beams tested by McCain (2012) and beams described in Section 3.1 and Appendix E. Test beams in this figure had the following dimensions and parameters:

$$a/d = 2.9$$

$$3/8 \le a_g \le 2 \text{ in.}$$

$$0.04 \le a_g/d \le 0.1$$

$$3300 \text{ psi} \le f_c' \le 5000 \text{ psi}$$

$$12 \text{ in.} \le h \le 48 \text{ in.}$$

$$0.63\% \le \rho \le 0.98\%$$

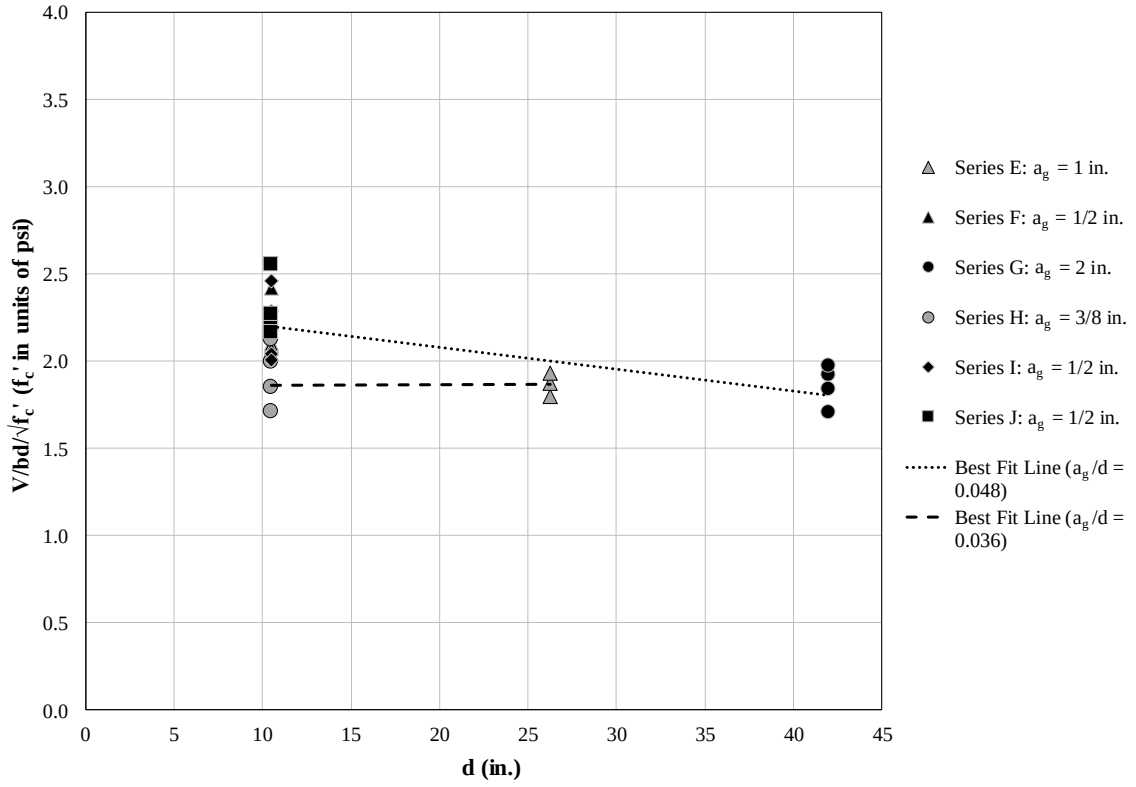

Figure 5.25 Variation of Shear Strength with Depth

Note: Data in this figure include beams tested by McCain (2012) and beams described in Section 3.1 and Appendix E. Test beams in this figure had the following dimensions and parameters:

$$a/d = 2.9$$
$$3/8 \le a_g \le 2 \text{ in.}$$
$$0.04 \le a_g/d \le 0.05$$
$$3300 \text{ psi} \le f_c^{'} \le 5000 \text{ psi}$$
$$12 \text{ in.} \le h \le 48 \text{ in.}$$
$$0.63\% \le \rho \le 0.98\%$$

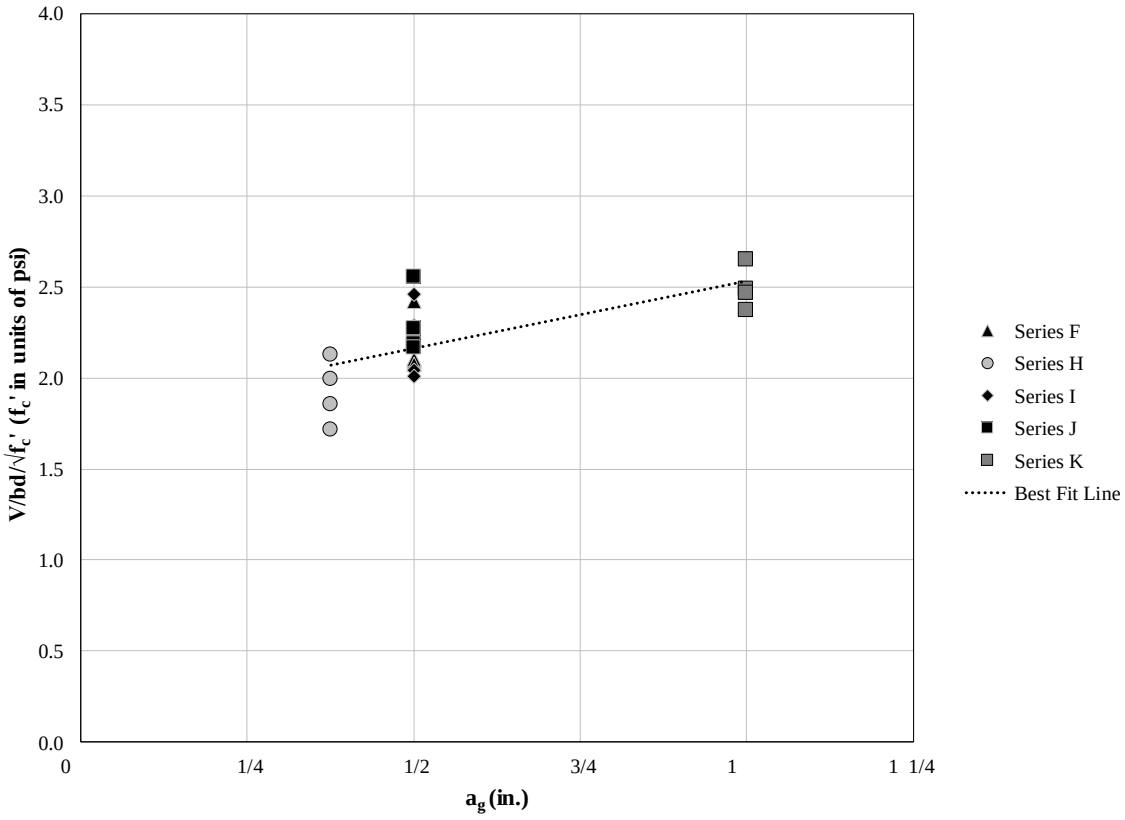

Figure 5.26 Variation of Shear Strength with Aggregate Size

Note: Data in this figure include beams tested by McCain (2012) and beams described in Section 3.1. Test beams in this figure had the following dimensions and parameters:

$$a/d = 2.9$$

$$3/8 \le a_g \le 1 \text{ in.}$$

$$0.04 \le a_g/d \le 0.1$$

$$3300 \text{ psi} \le f_c^{'} \le 5000 \text{ psi}$$

$$h = 12 \text{ in.}$$

$$0.63\% \le \rho = 0.98\%$$

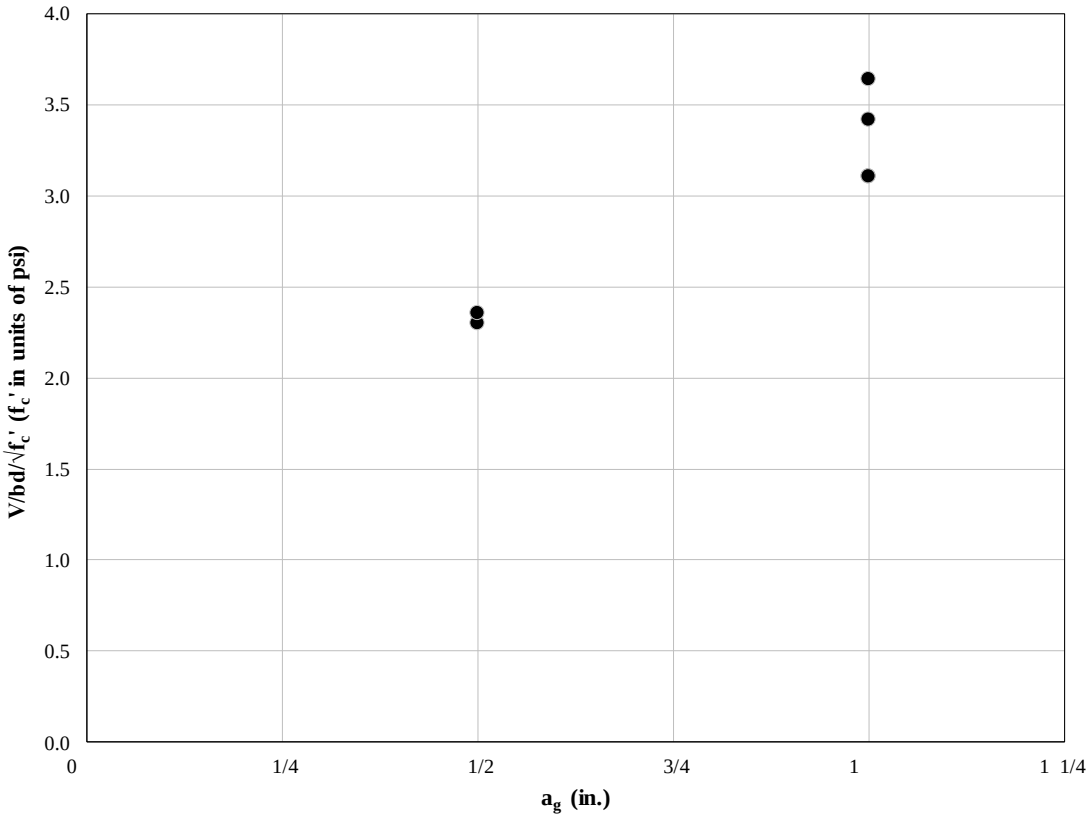

Figure 5.27 Variation of Shear Strength with Aggregate Size (Murray 2010)

Note: Test beams in this figure had the following dimensions and parameters:

$$a/d = 2.3$$

$$1/2 \le a_g \le 1 \text{ in.}$$

$$0.05 \le a_g/d \le 0.1$$

$$2700 \text{ psi} \le f_c^{'} \le 4900 \text{ psi}$$

$$h = 12 \text{ in.}$$

$$0.63\% \le \rho = 0.98\%$$

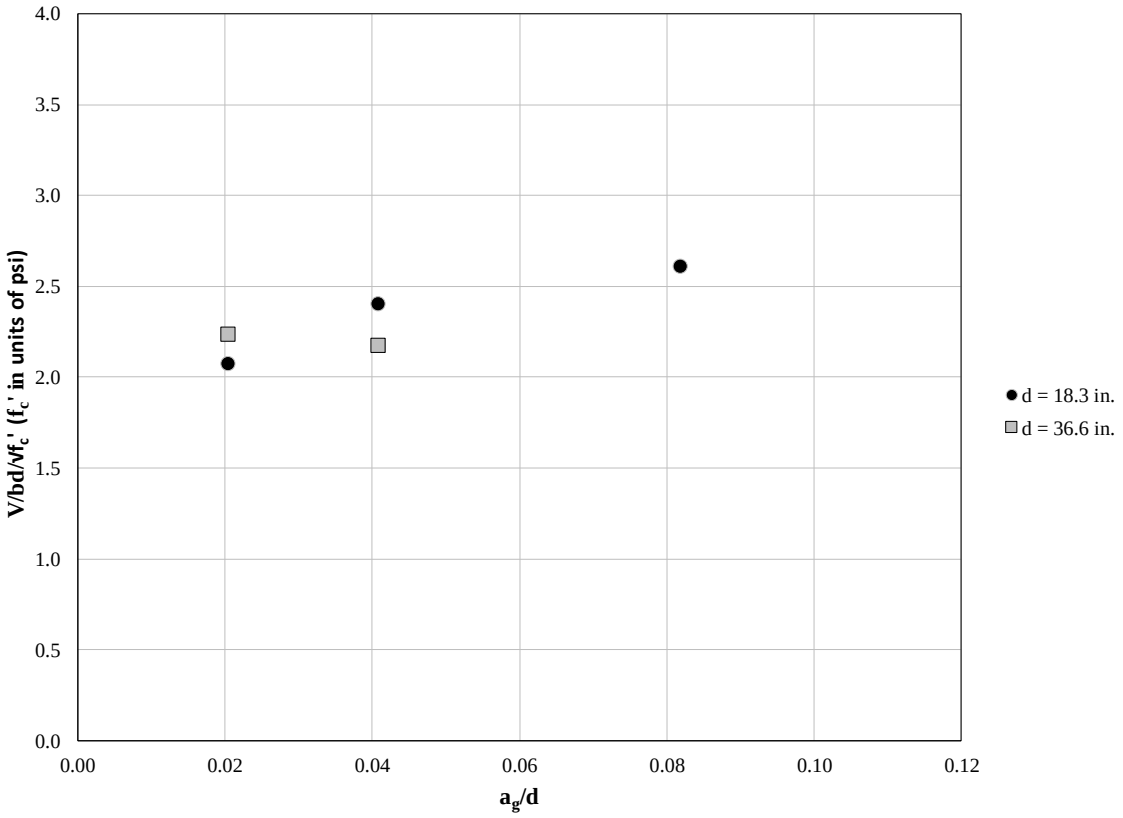

Figure 5.28 Variation of Shear Strength with Aggregate Size (Taylor 1972)

Note: Test beams in this figure had the following dimensions and parameters:

$$a/d = 3.0$$

$$3/8 \le a_g \le 1\text{-}1/4 \text{ in.}$$

$$0.04 \le a_g/d \le 0.08$$

$$2600 \text{ psi} \le f_c^{'} \le 3200 \text{ psi}$$

$$19.7 \le h \le 39.4 \text{ in.}$$

$$\rho = 1.35\%$$

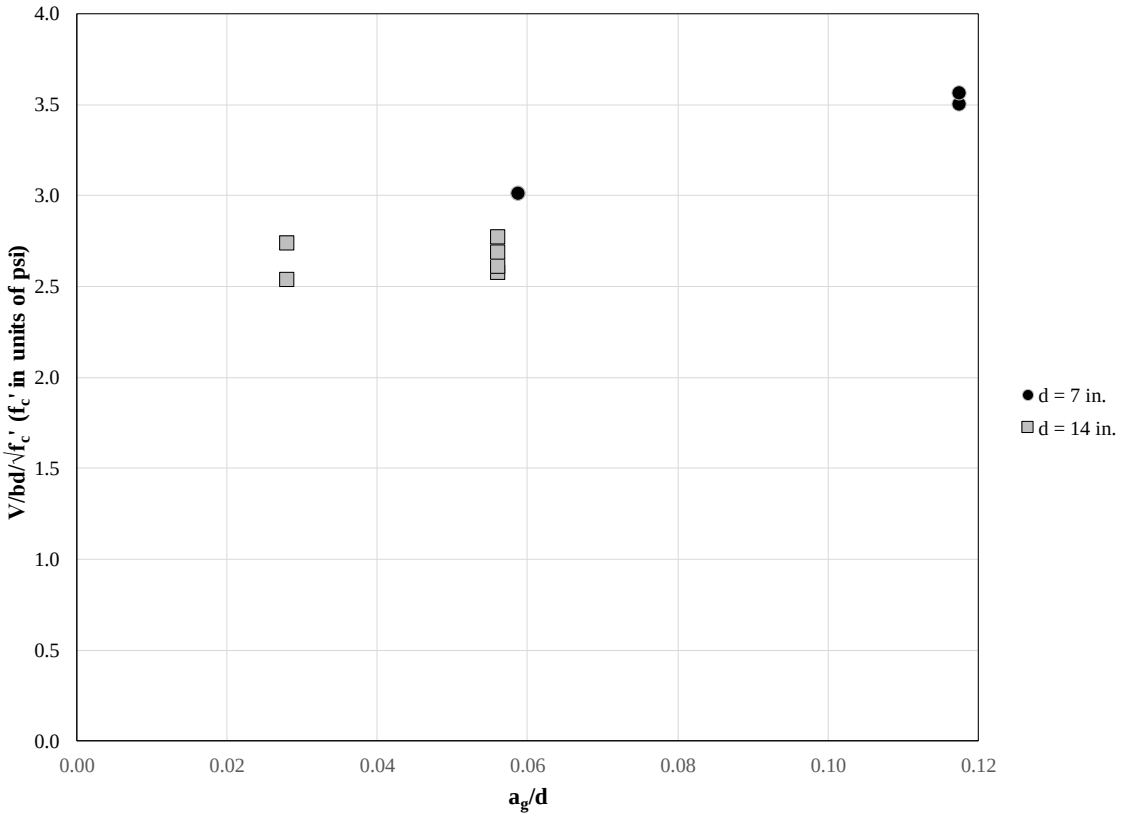

Figure 5.29 Increase of Shear Strength with Aggregate Size (Chana 1981)

Note: Test beams in this figure had the following dimensions and parameters:

$$a/d = 3.0$$

$$0.39 \le a_g \le 0.79 \text{ in.}$$

$$0.03 \le a_g/d \le 0.1$$

$$3600 \text{ psi} \le f_c^{'} \le 5600 \text{ psi}$$

$$7.9 \le h \le 16 \text{ in.}$$

$$1.69\% \le \rho = 1.74\%$$

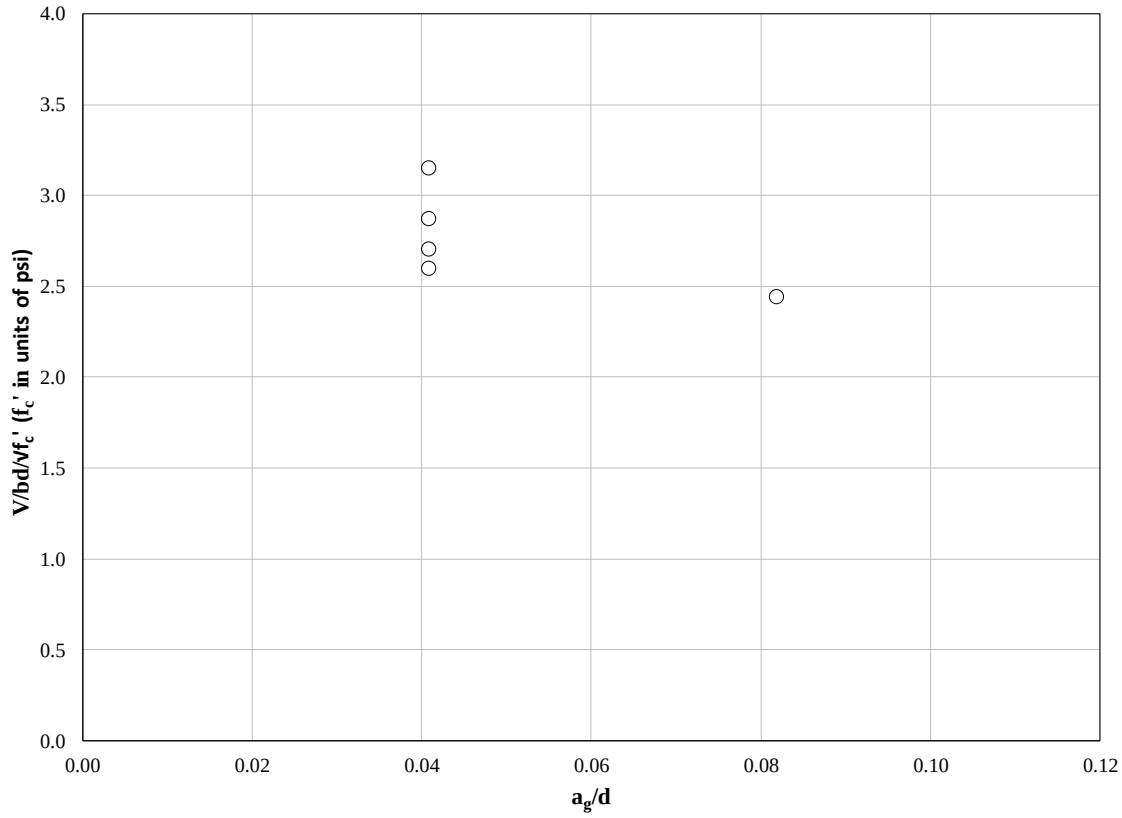

Figure 5.30 Decrease of Shear Strength with Aggregate Size (Taylor 1972)

Note: Test beams in this figure had the following dimensions and parameters:

$$a/d = 3.0$$

$$3/8 \le a_g \le 3/4 \text{ in.}$$

$$0.04 \le a_g/d \le 0.08$$

$$2600 \text{ psi} \le f_c^{'} \le 3200 \text{ psi}$$

$$h = 9.8 \text{ in.}$$

$$\rho = 1.35\%$$

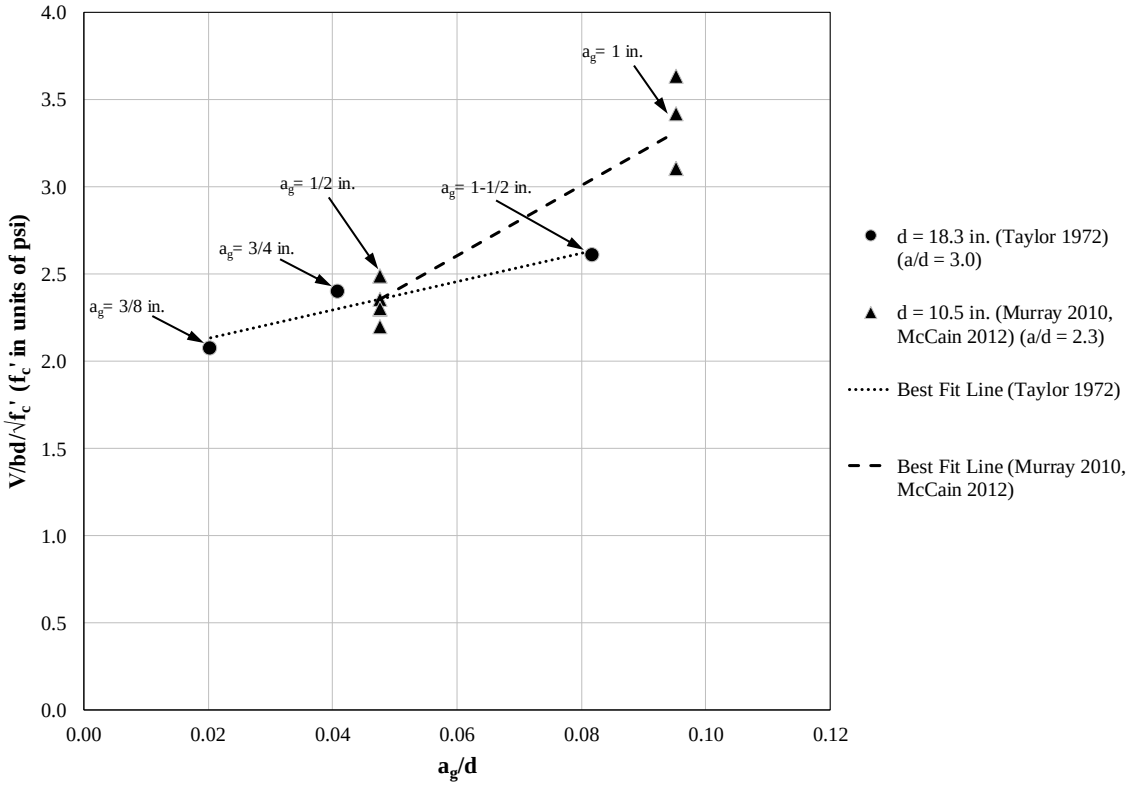

Figure 5.31 Variations in Maximum Aggregate Size with Constant Depth: One

Note: Data in this figure include beams tested by Taylor (1972), Murray (2010), and McCain (2012). Test beams in this figure had the following dimensions and parameters:

$$2.3 \le a/d \le 3.0$$

$$3/4 \le a_g \le 1\text{-}1/2 \text{ in.}$$

$$0.04 \le a_g/d \le 0.1$$

$$3100 \text{ psi} \le f_c^{'} \le 4700 \text{ psi}$$

$$12 \text{ in.} \le h \le 19.7 \text{ in.}$$

$$0.63\% \le \rho \le 1.35\%$$

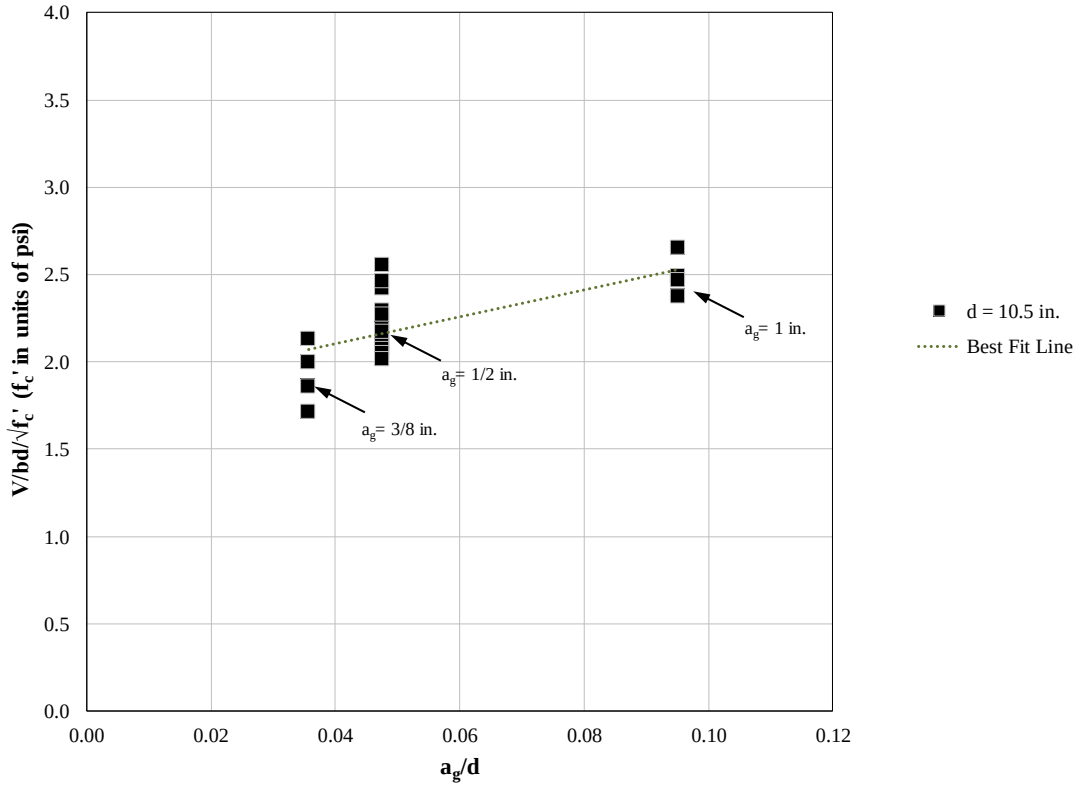

Figure 5.32 Variations in Maximum Aggregate Size with Constant Depth: Two

Note: Data in this figure include beams tested by McCain (2012) and beams described in Section 3.1. Test beams in this figure had the following dimensions and parameters:

$$a/d = 2.9$$
$$3/8 \le a_g \le 1 \text{ in.}$$
$$0.04 \le a_g/d \le 0.1$$
$$3300 \text{ psi} \le f_c' \le 5000 \text{ psi}$$
$$h = 12 \text{ in.}$$
$$0.63\% \le \rho \le 0.98\%$$

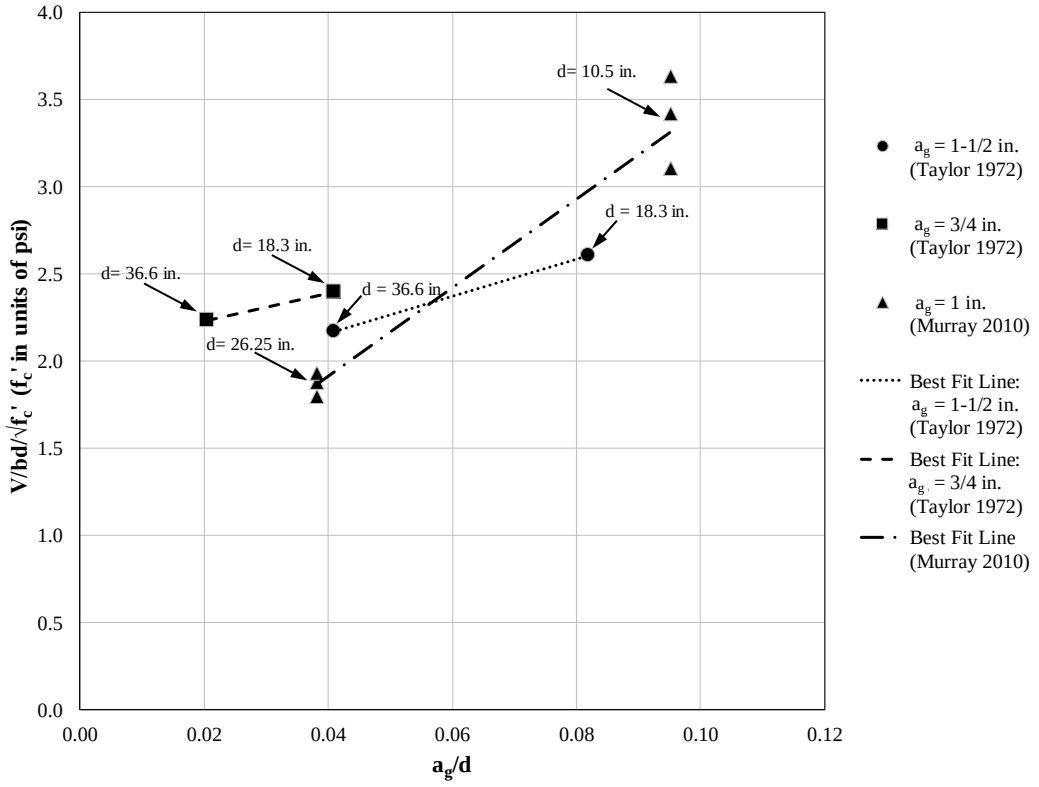

Figure 5.33 Variations in Depth with Constant Maximum Aggregate Size: One

Note: Data in this figure include beams tested by Taylor (1972) and Murray (2010). Test beams in this figure had the following dimensions and parameters:

$$2.3 \le a/d \le 3.0$$

$$3/4 \le a_g \le 1\text{-}1/2 \text{ in.}$$

$$0.04 \le a_g/d \le 0.1$$

$$3100 \text{ psi} \le f_c' \le 4700 \text{ psi}$$

$$12 \text{ in.} \le h \le 39.4 \text{ in.}$$

$$0.63\% \le \rho \le 1.35\%$$

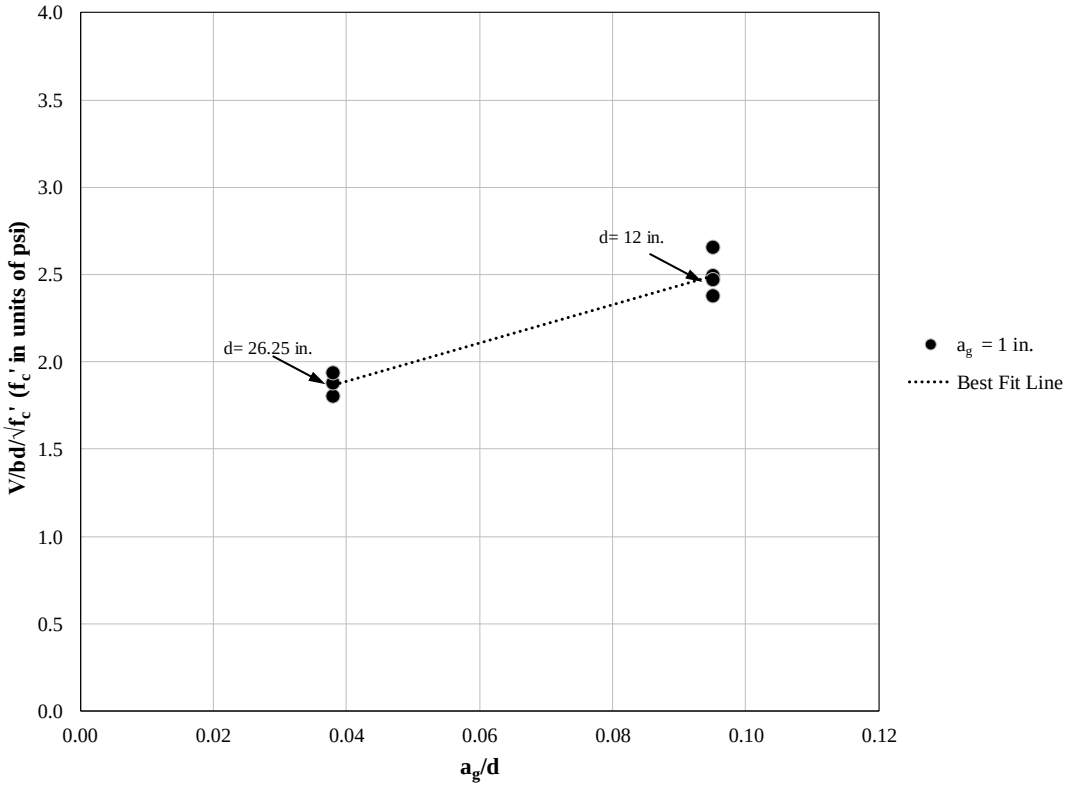

Figure 5.34 Variations in Depth with Constant Maximum Aggregate Size: Two

Note: Data in this figure include beams tested by McCain (2012) and beams described in Section 3.1. Test beams in this figure had the following dimensions and parameters:

$$a/d = 2.9$$
$$a_g = 1 \text{ in.}$$
$$0.04 \le a_g/d \le 0.1$$
$$4000 \text{ psi} \le f_c^{'} \le 4300 \text{ psi}$$
$$12 \text{ in.} \le h \le 30 \text{ in.}$$
$$0.63\% \le \rho \le 0.79\%$$

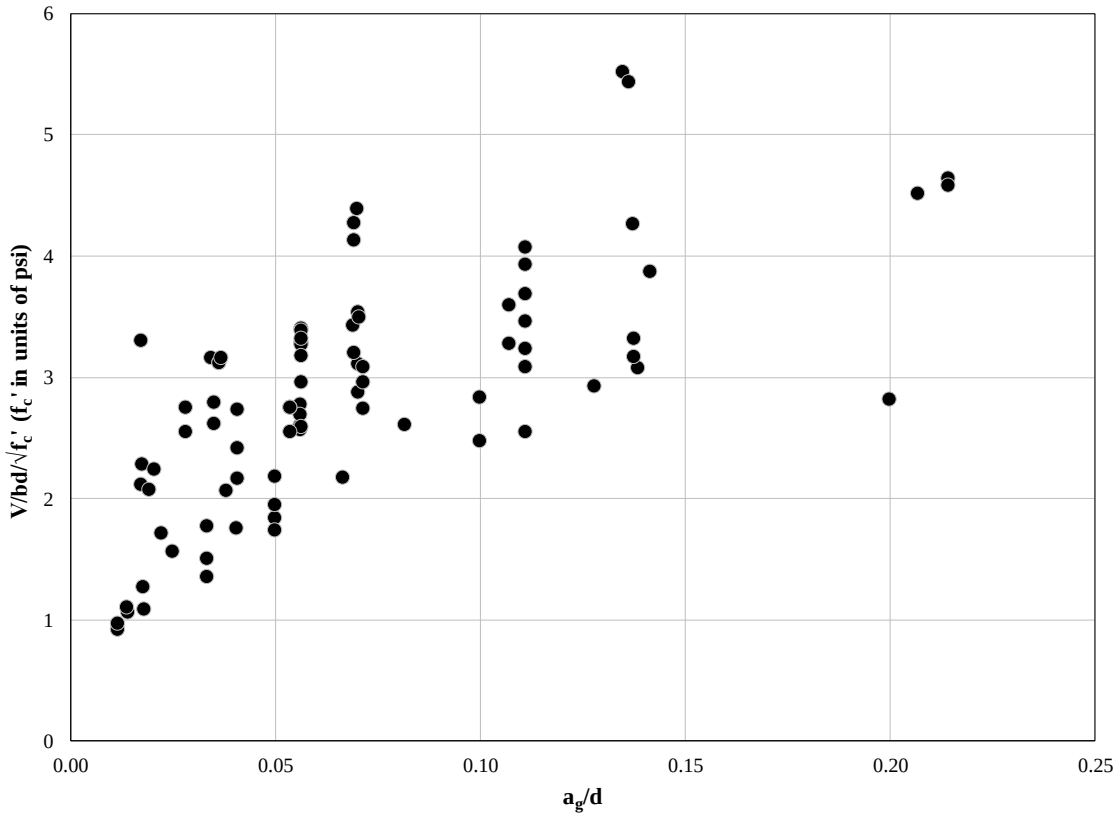

Figure 5.35 Variation of Shear Strength with Relative Aggregate Size: Two

Note: The vertical axis on this scale is different than other plots in Chapter 5 because of the wide range in unit shear strength. Data in this figure were collected by Reineck et al. (2003) and include beams tested by Leonhardt and Walther (1962), Kani (1967), Bhal (1968), Taylor (1972), Walraven (1981), and Sneed (2007). In these tests concrete cover, maximum aggregate size, and longitudinal reinforcement size and spacing were not all scaled with respect to beam depth. Test beams in this figure had dimensions and parameters within the following ranges:

$$2.3 \le a/d \le 4.0$$

$$3/8 \text{ in.} \le a_g \le 1\text{-}1/2 \text{ in.}$$

$$0.01 \le a_g/d \le 0.2$$

$$1900 \text{ psi} \le f_c^{'} \le 10{,}800 \text{ psi}$$

$$6 \text{ in.} \le h \le 49 \text{ in.}$$

$$0.59\% \le \rho \le 2.9\%$$

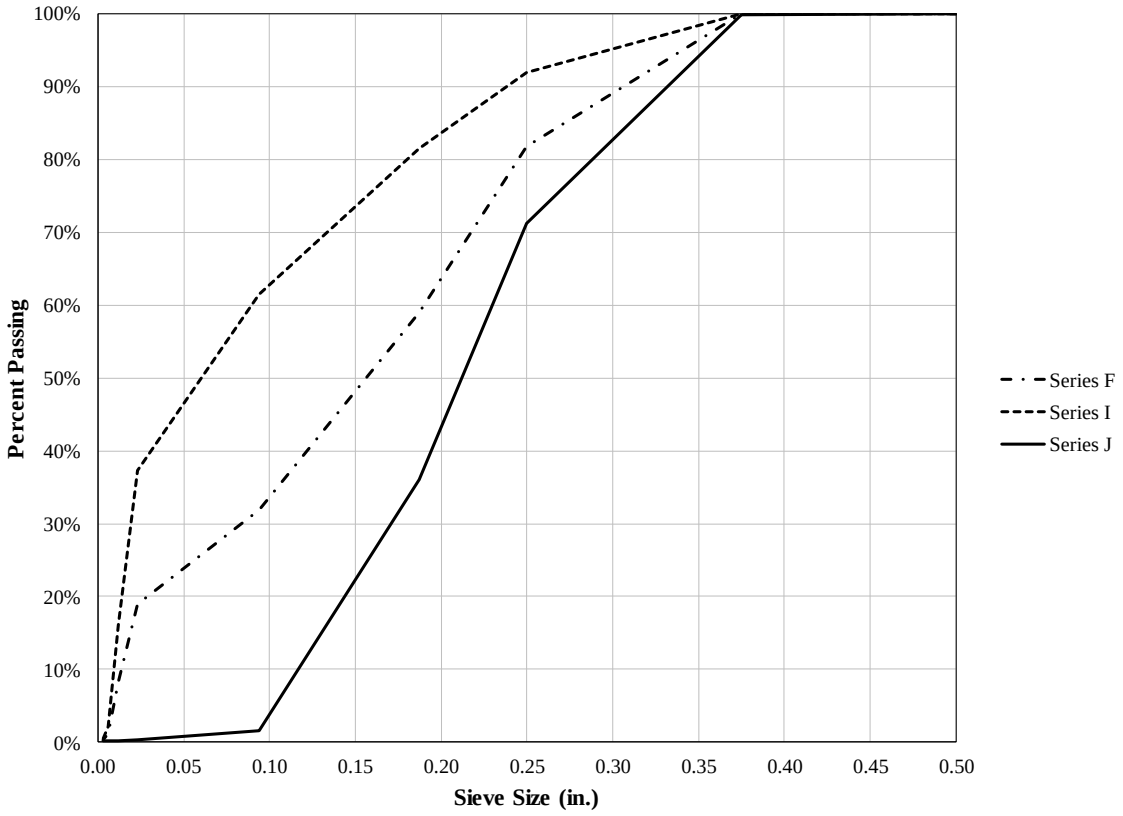

Figure 5.36 Particle Distributions for Mixture F, I, and J

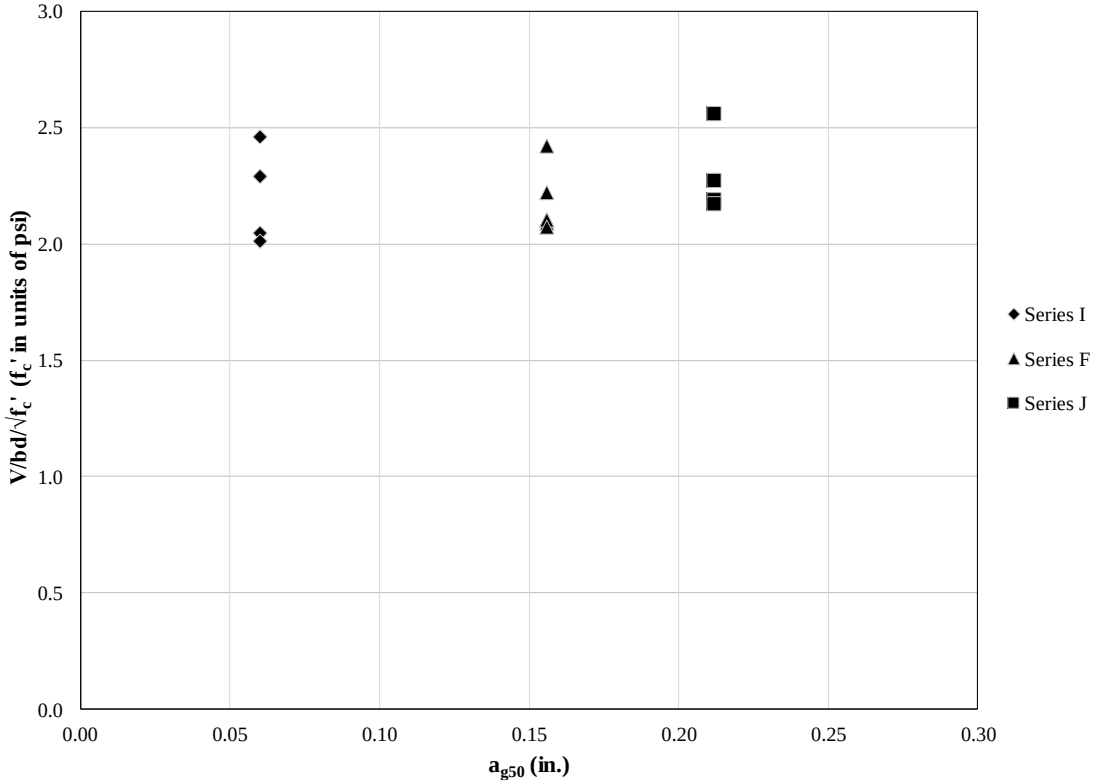

Figure 5.37 Variation of Shear Strength with Gradation

Note: The term a_{g50} is defined here as the size of the sieve catching 50% of the particles. Test beams in this figure had the following dimensions and parameters:

$$a/d = 2.9$$
$$a_g = 1/2 \text{ in.}$$
$$a_g/d = 0.05$$
$$3300 \text{ psi} \le f_c^{'} \le 4900 \text{ psi}$$
$$h = 12 \text{ in.}$$
$$\rho = 0.63\%$$

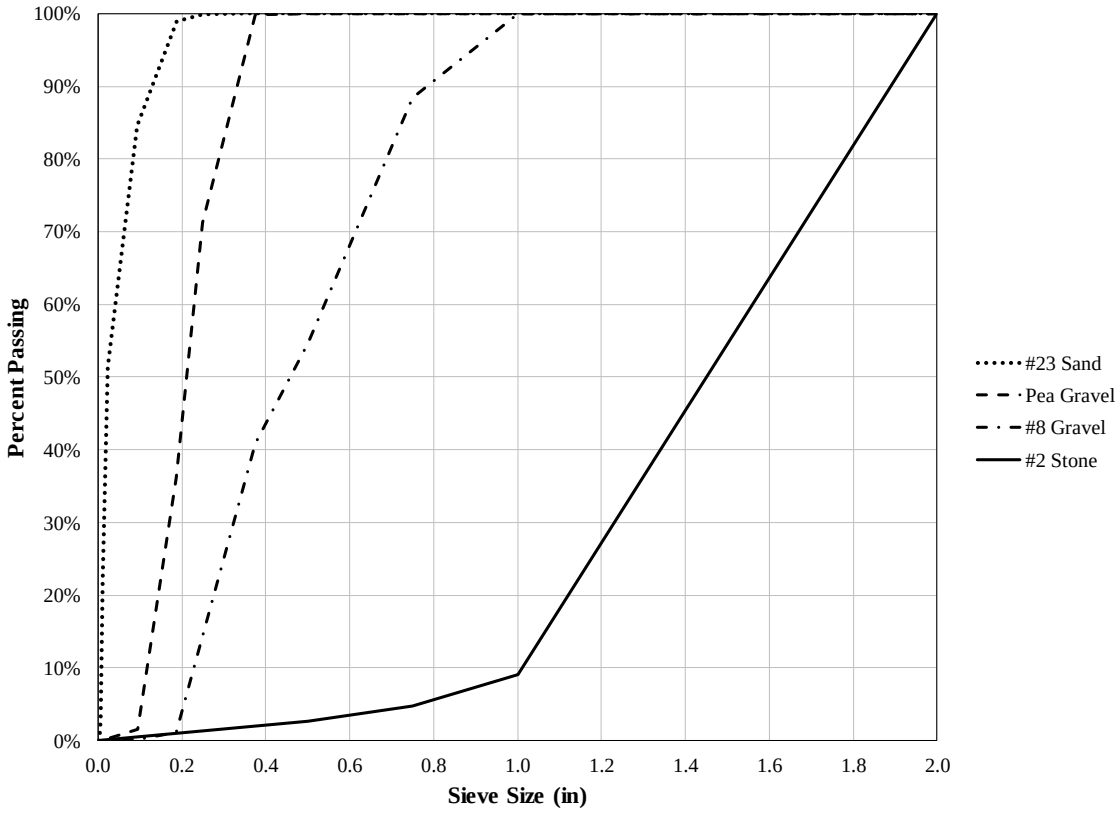

Figure A.1 Particle Distributions for Aggregates

Figure A.2 Concrete Compressive Strength Test Setup

Figure A.3 Split Cylinder Test Setup

Figure A.4 Modulus of Elasticity Test Setup

Figure A.5 Flexure Beam Test Setup

Figure B.1 Specimen Formwork

Figure B.2 Transverse Reinforcement Layout

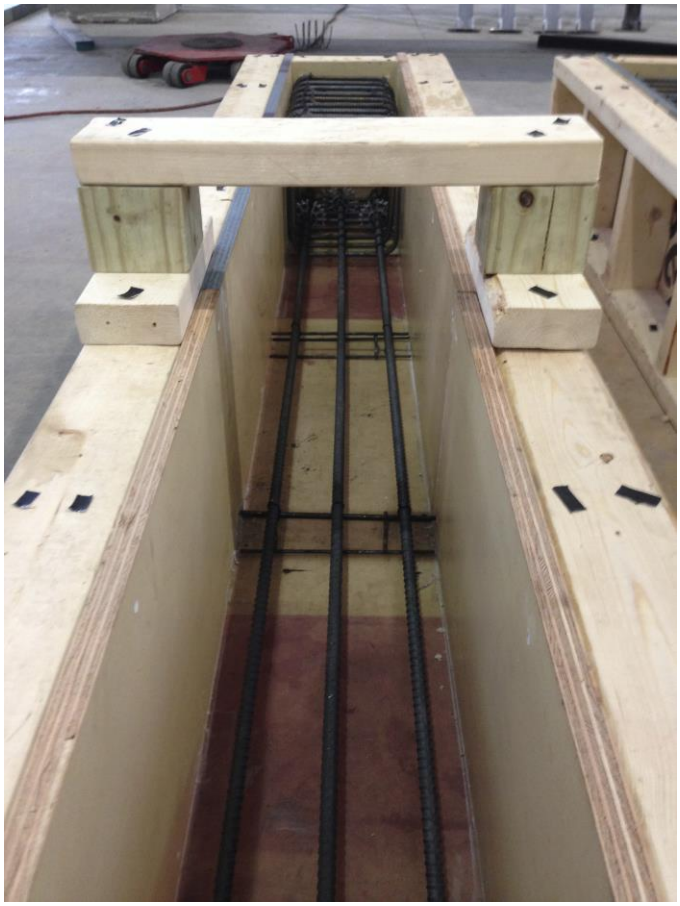

Figure B.3 Reinforcement Chairs in Shear Span

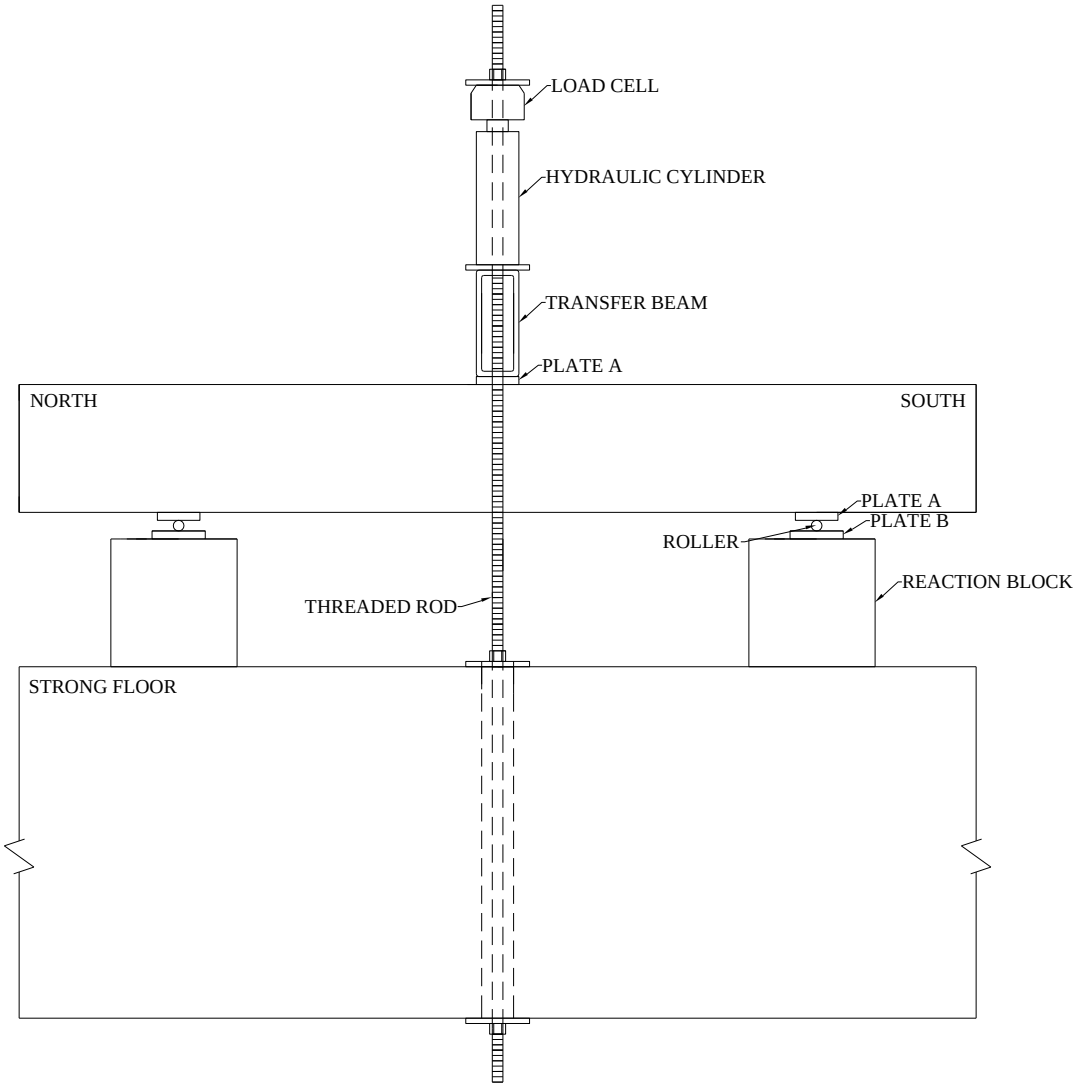

Figure C.1 Elevation View of Test Setup

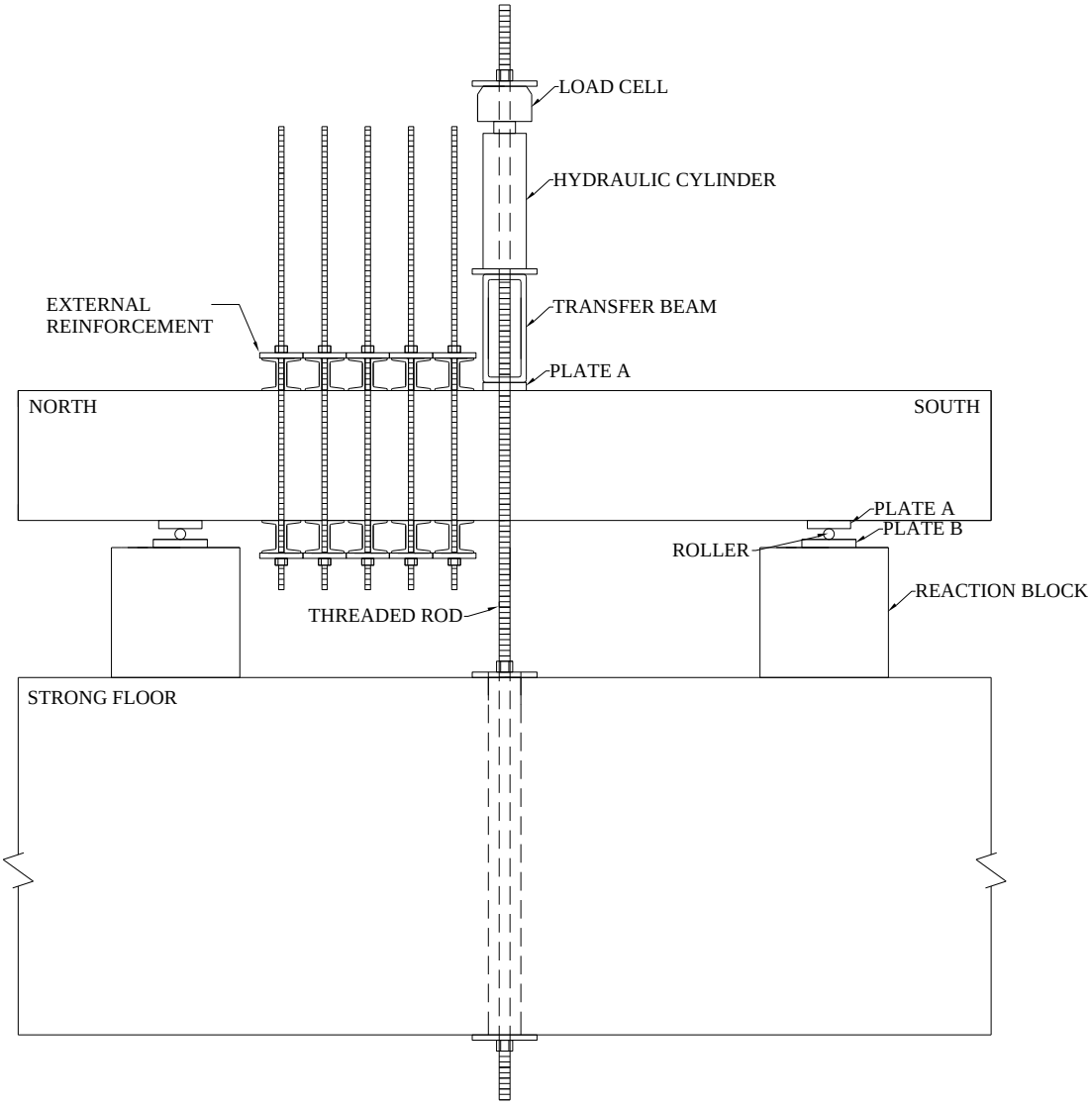

Figure C.2 Elevation View of Test Setup with External Reinforcement

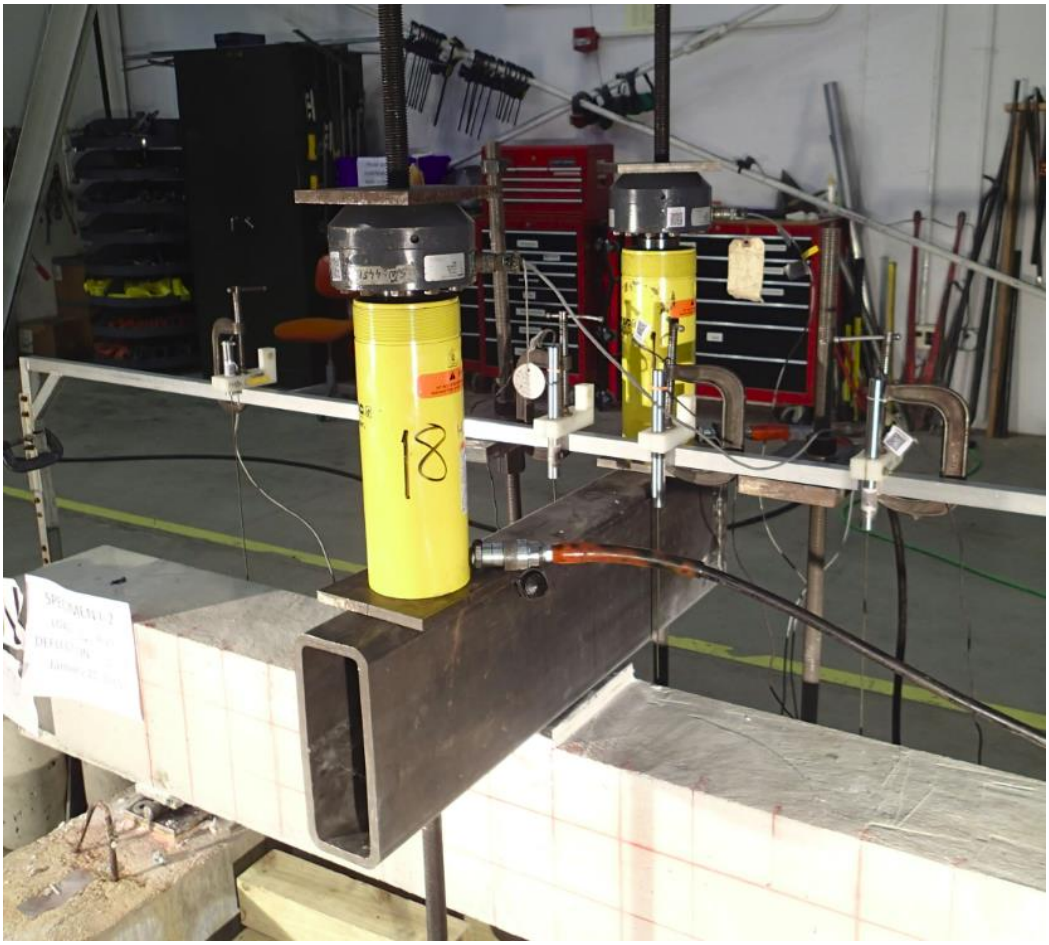

Figure C.3 Loading Setup

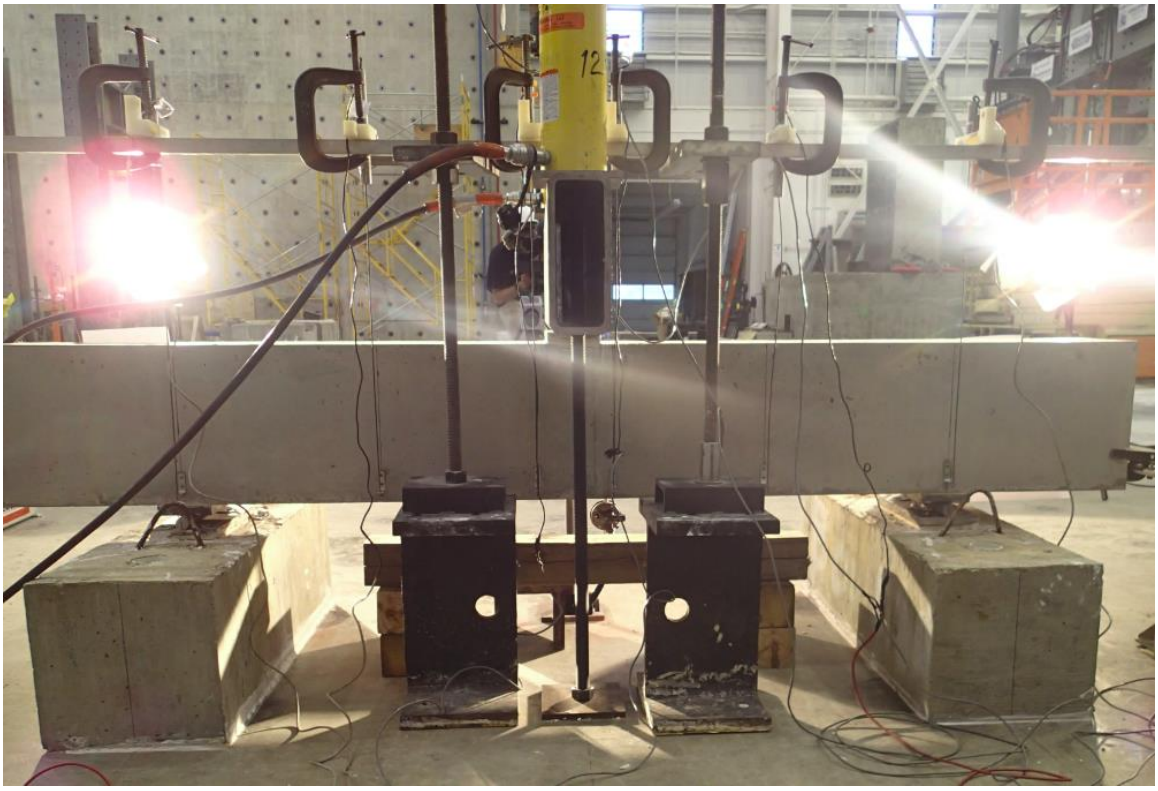

Figure C.4 LVDT Experimental Setup

Figure C.5 Midspan Dial Gage

Figure C.6 Bar Slip Dial Gage

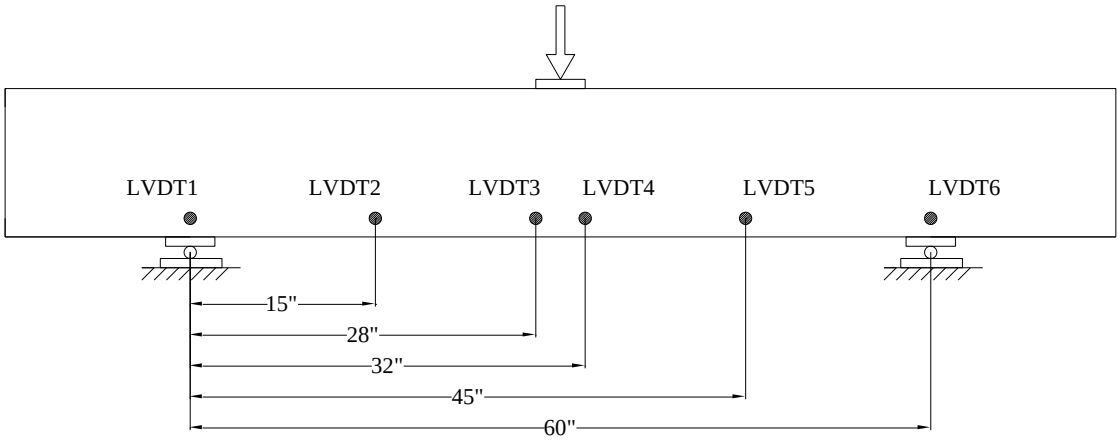

Figure D.1 LVDT Locations

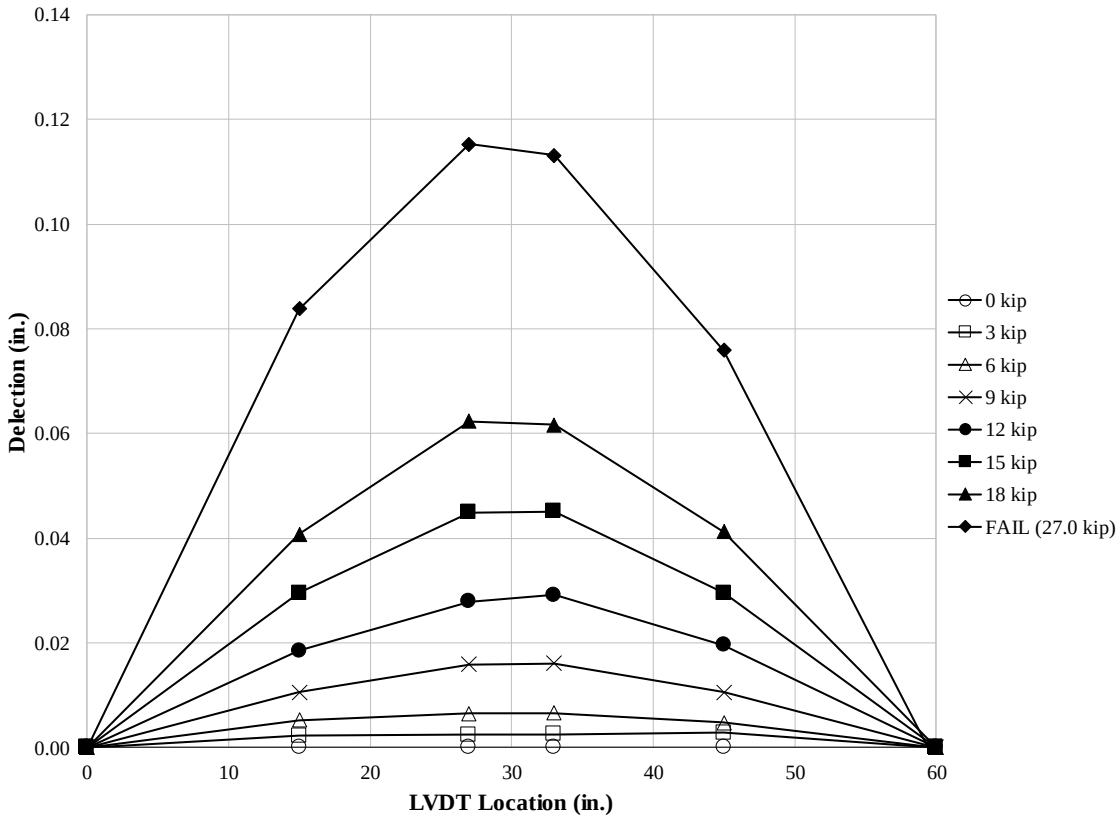

Figure D.2 Specimen F-3 Deflection Profile

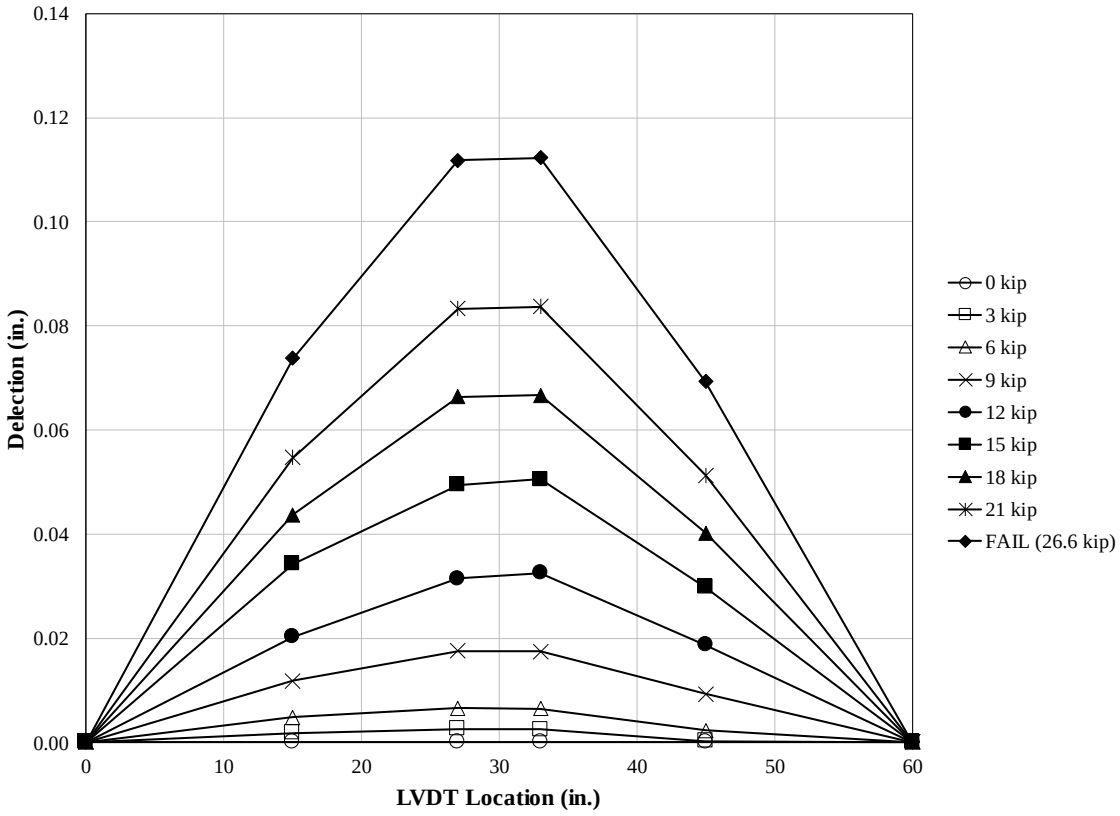

Figure D.3 Specimen F-4 Deflection Profile

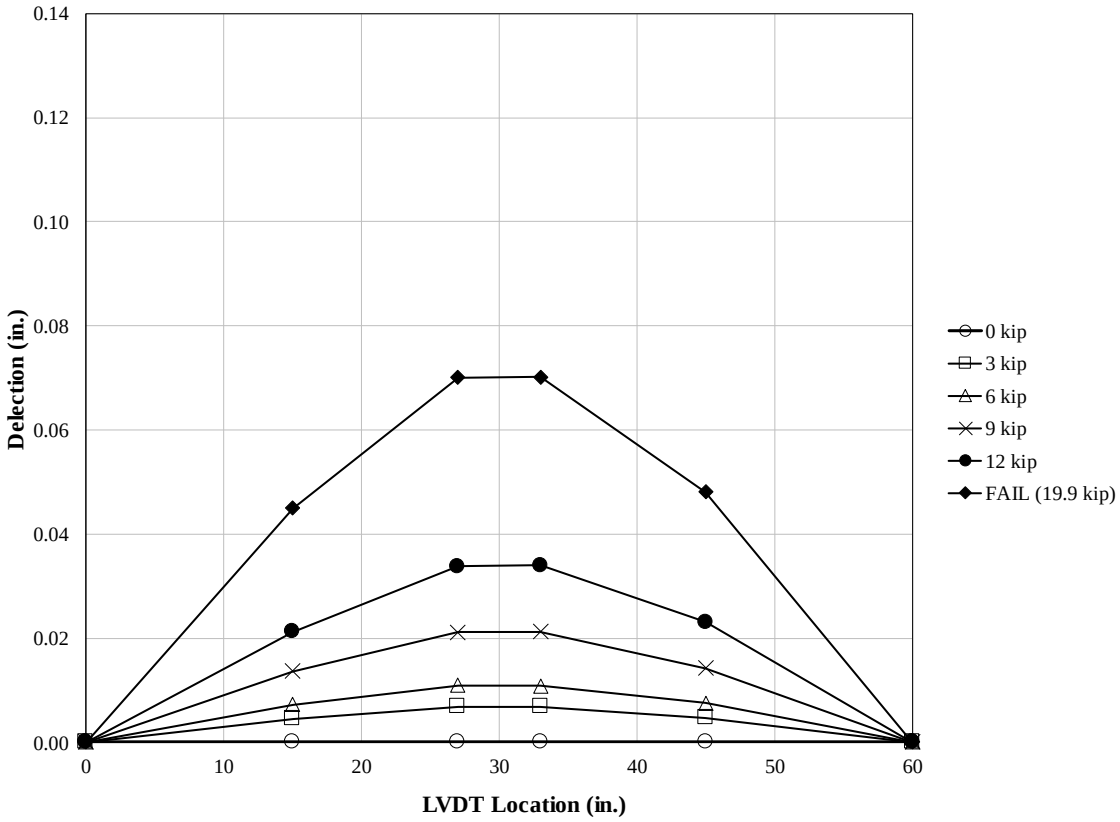

Figure D.4 Specimen H-1 Deflection Profile

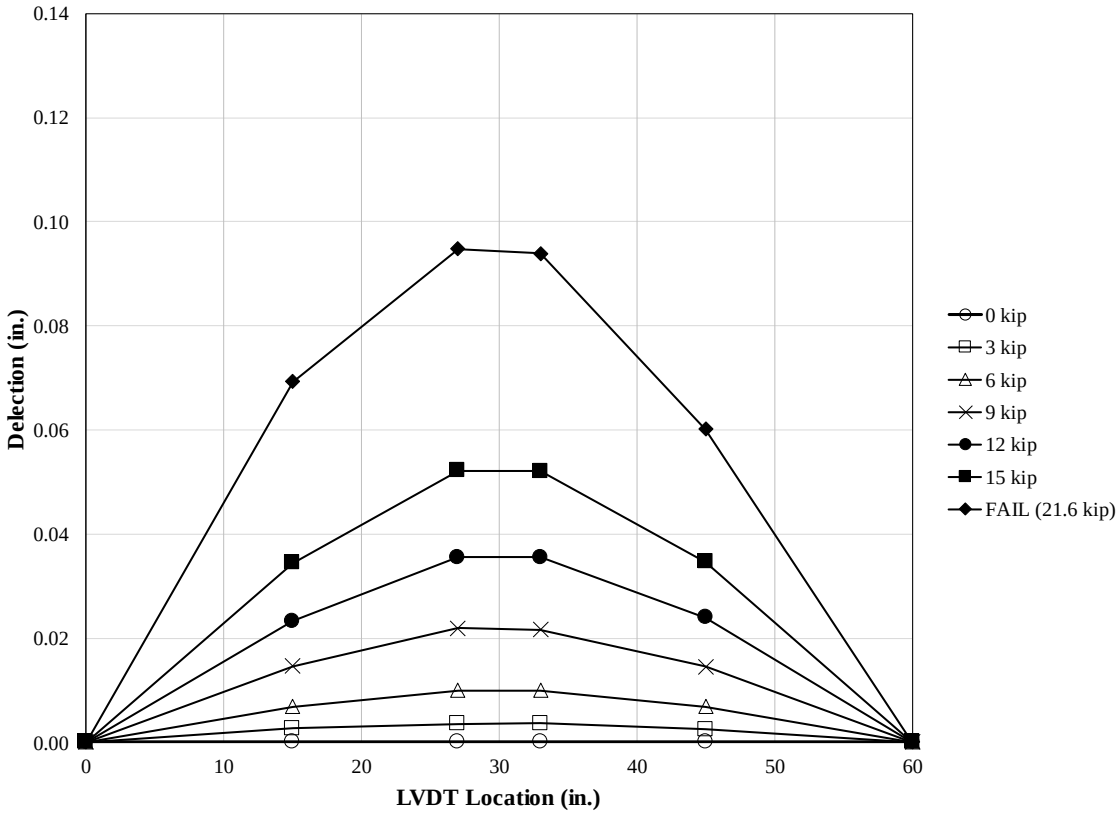

Figure D.5 Specimen H-2 Deflection Profile

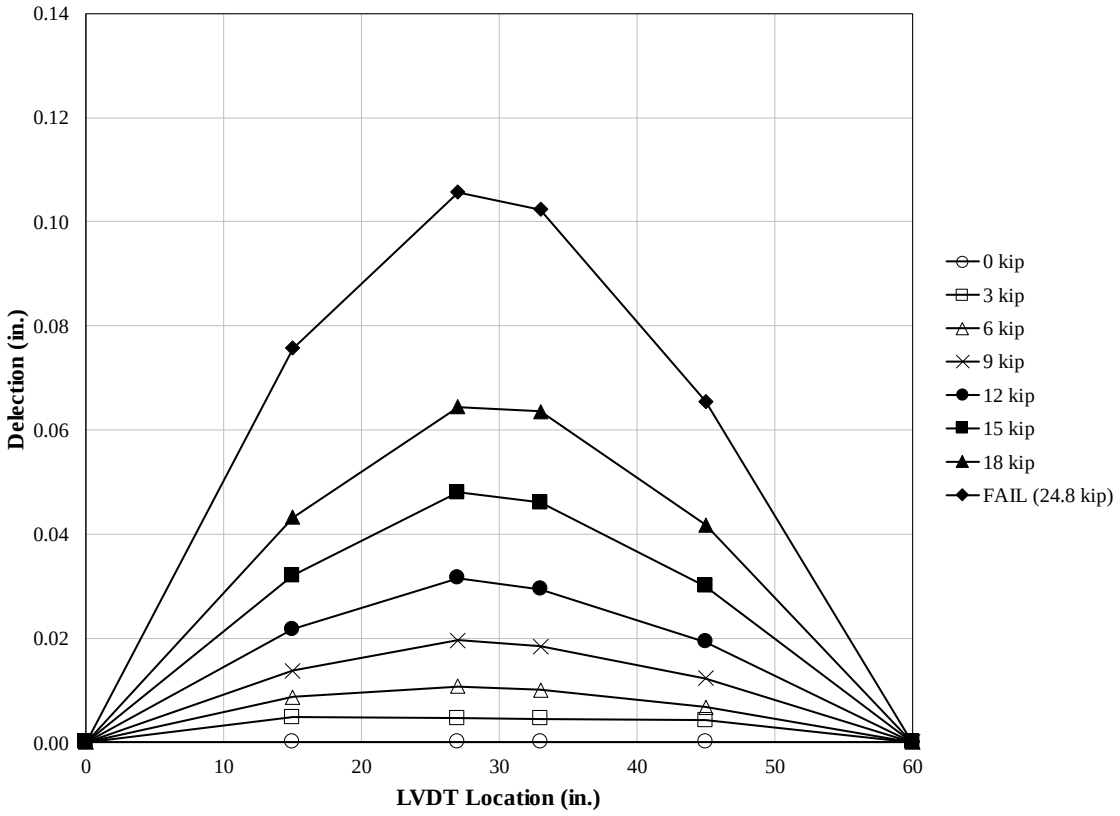

Figure D.6 Specimen I-1 Deflection Profile

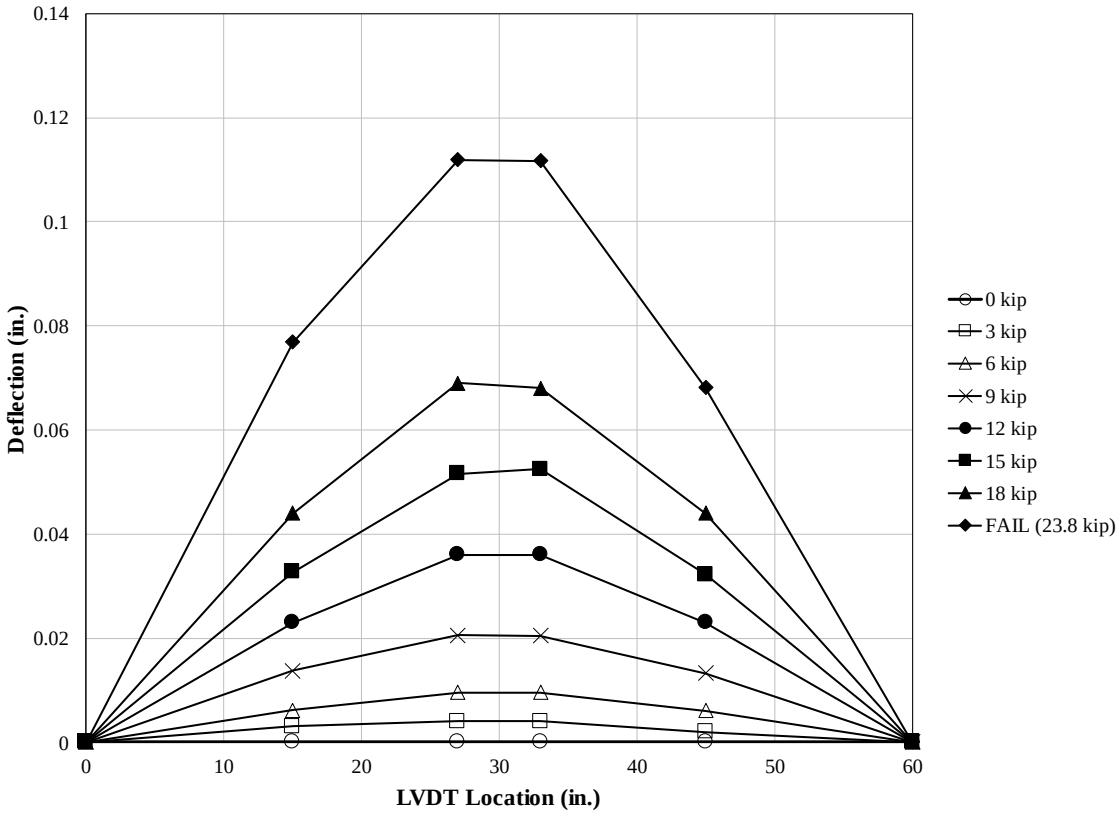

Figure D.7 Specimen I-2 Deflection Profile

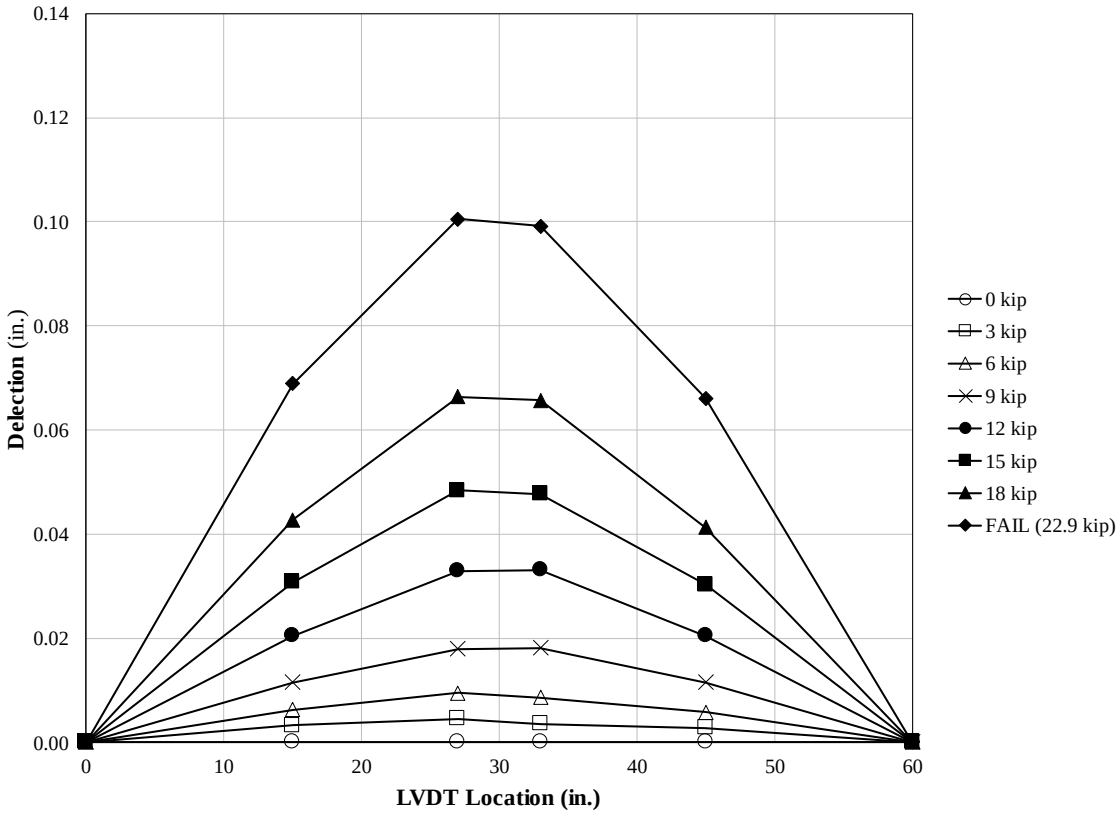

Figure D.8 Specimen J-1 Deflection Profile

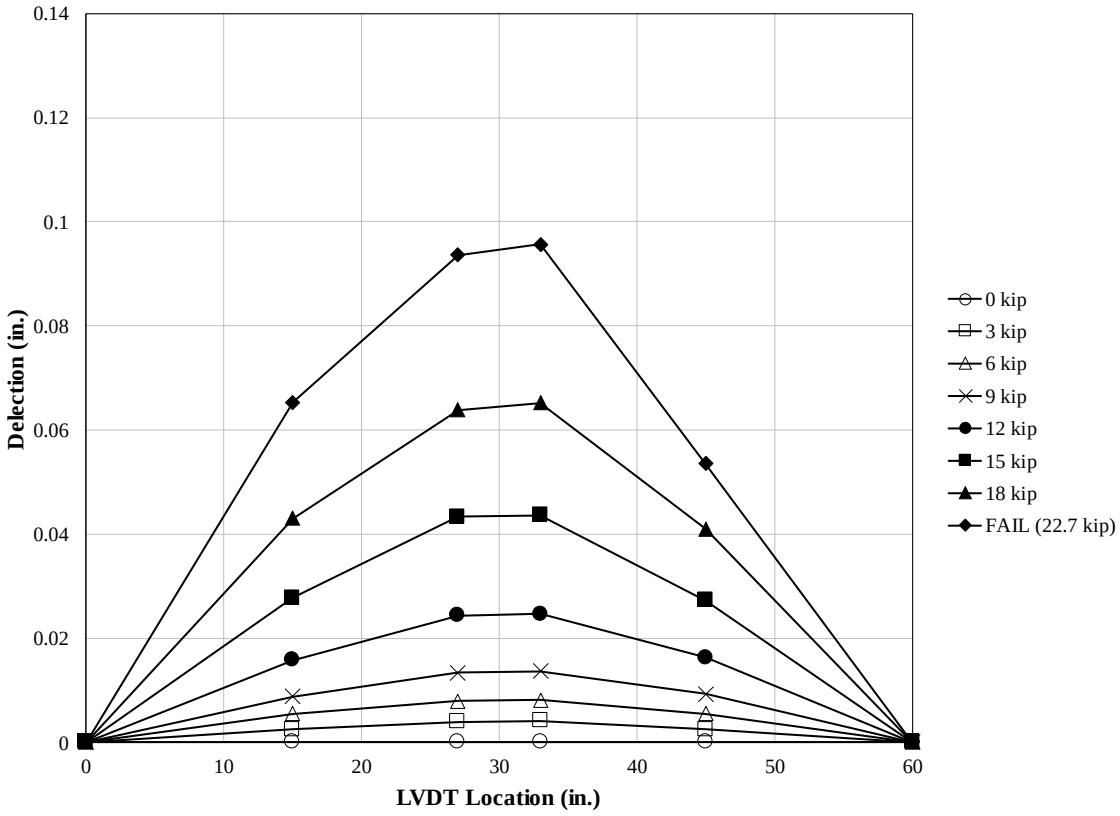

Figure D.9 Specimen J-2 Deflection Profile

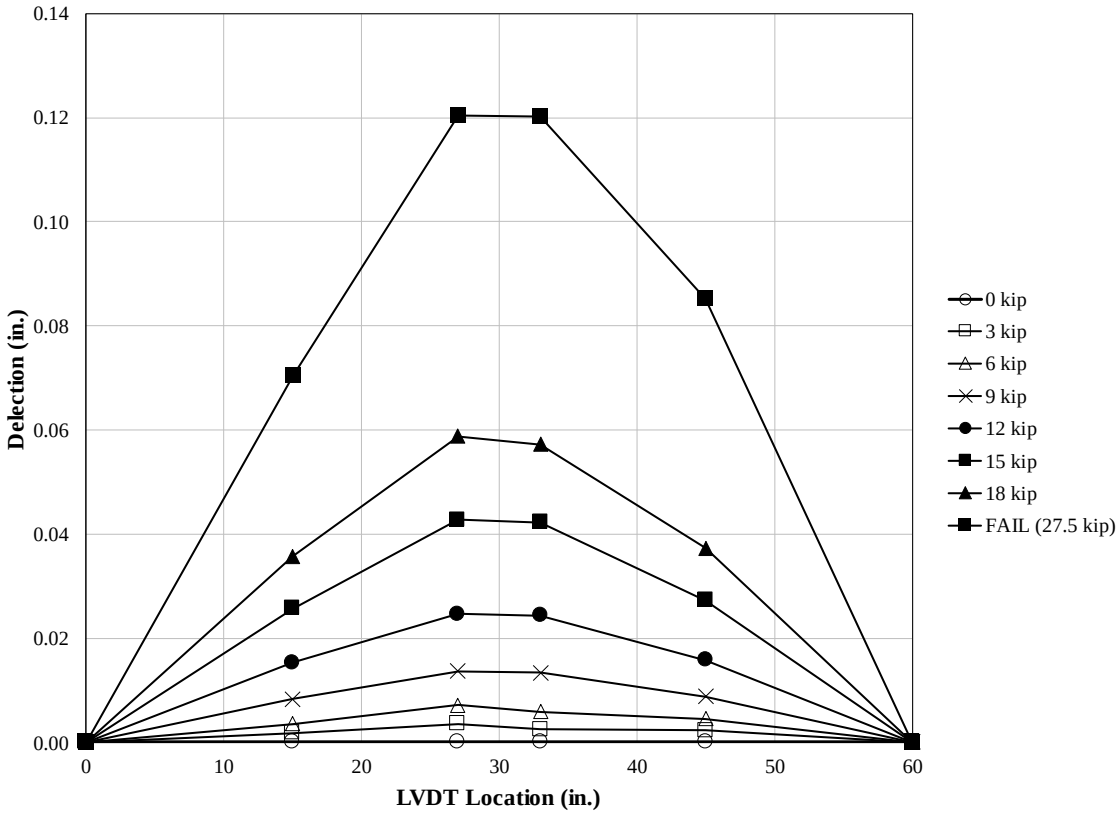

Figure D.10 Specimen K-1 Deflection Profile

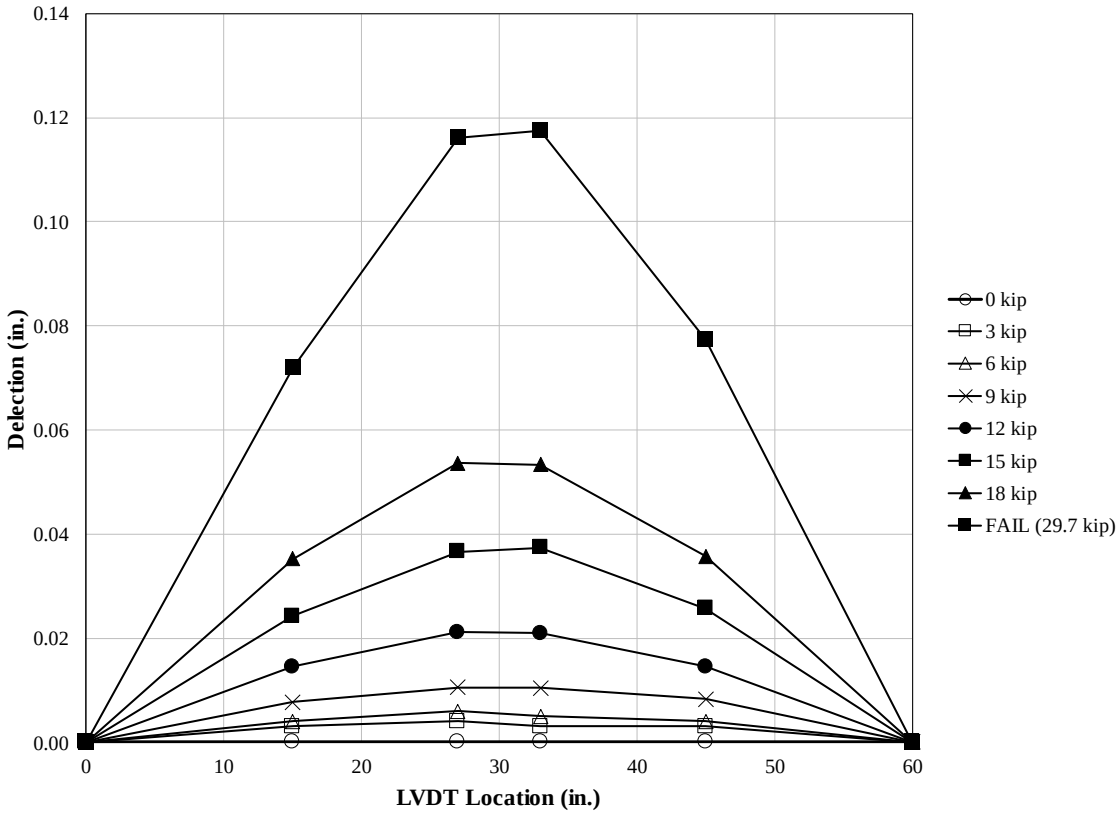

Figure D.11 Specimen K-2 Deflection Profile

(a) F-3: 9 kip

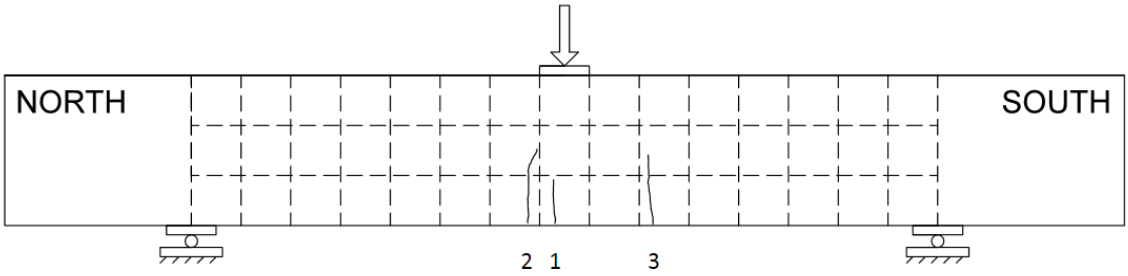

(b) F-3: 12 kip

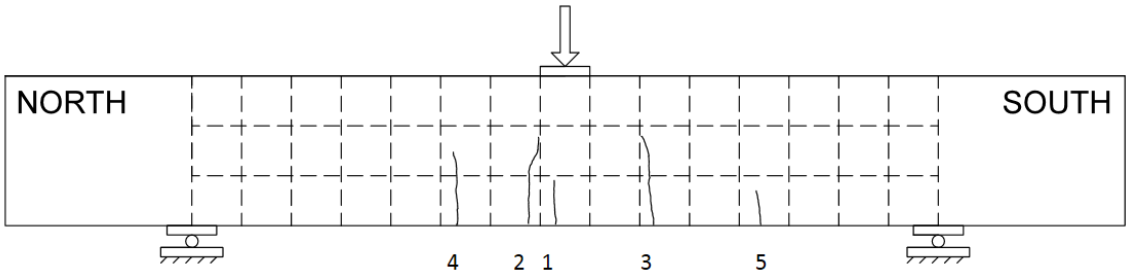

(c) F-3: 15 kip

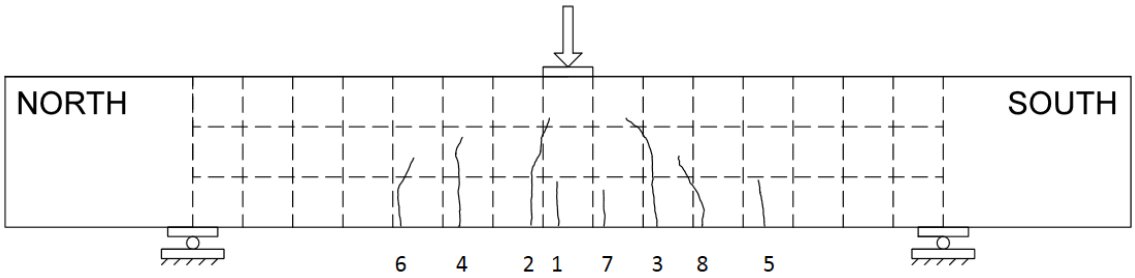

(d) F-3: 18 kip

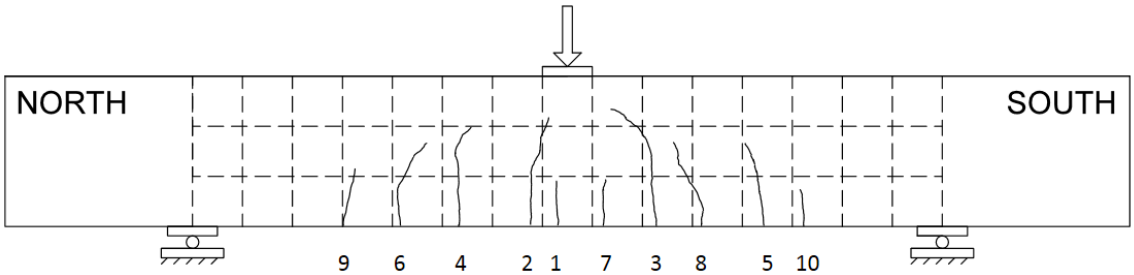

Figure D.12 Specimen F-3 Crack Maps

(e) F-3: South Side Failure: 27.0 kip

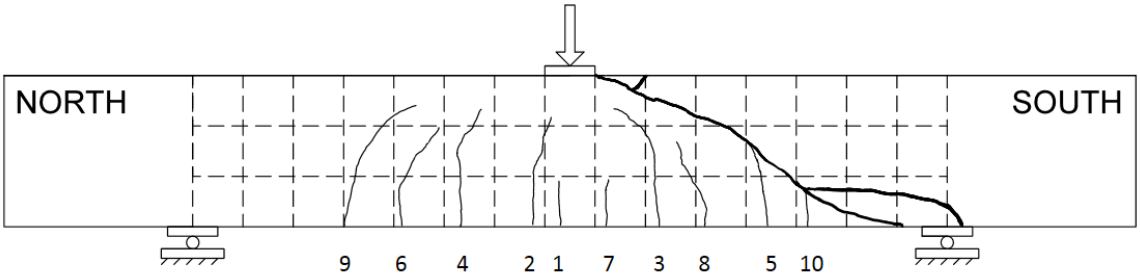

(f) F-3: North Side Failure 27.0 kip

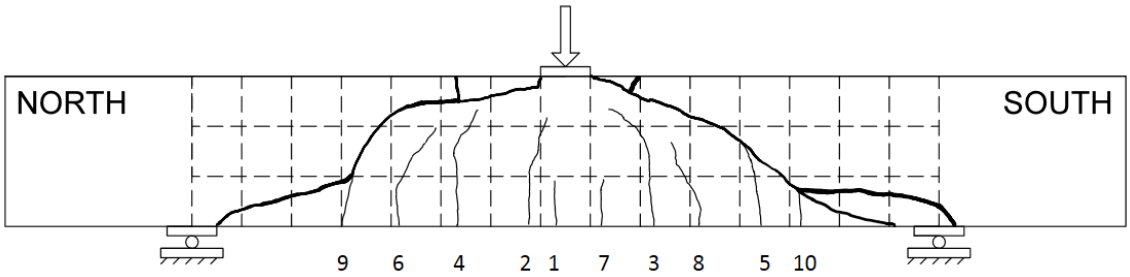

Figure D.12 Specimen F-3 Crack Maps Continued

(a) F-4: 9 kip

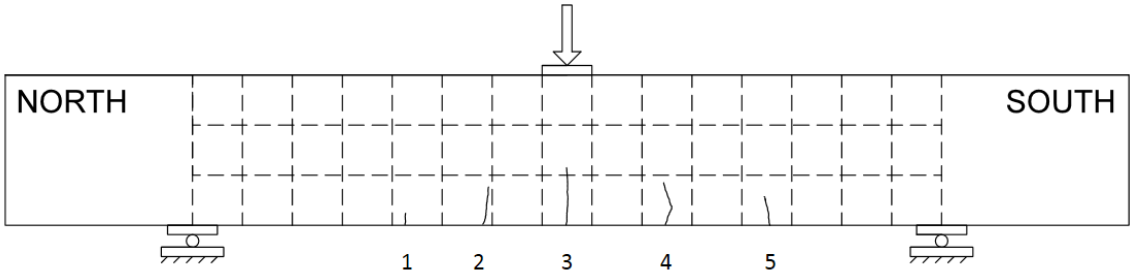

(b) F-4: 12 kip

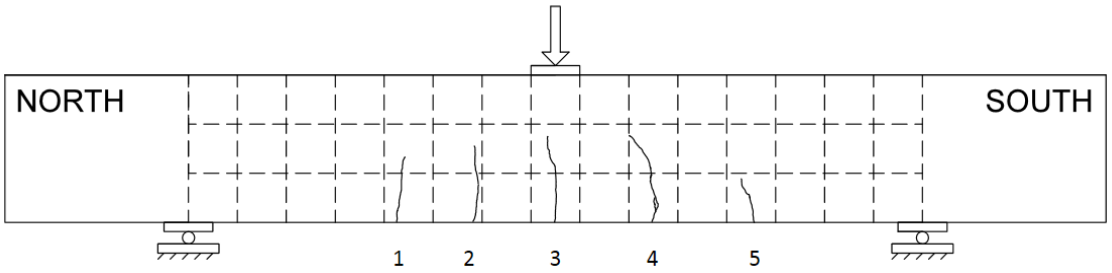

(c) F-4: 15 kip

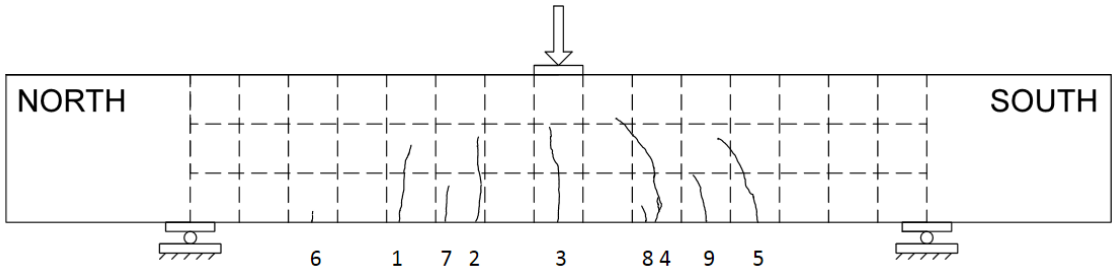

(d) F-4: 18 kip

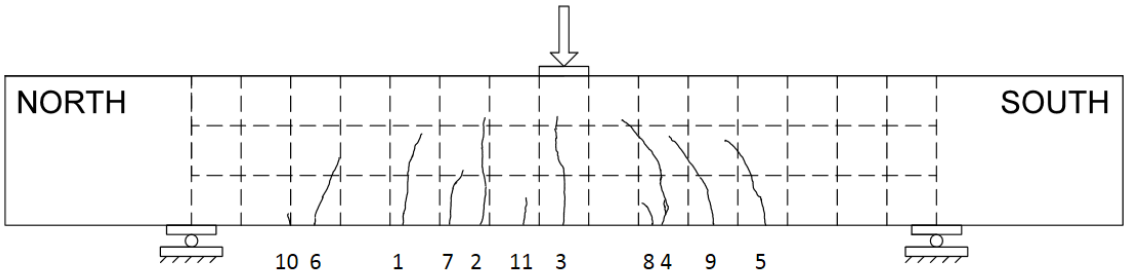

Figure D.13 Specimen F-4 Crack Maps

(e) F-4: 21 kip

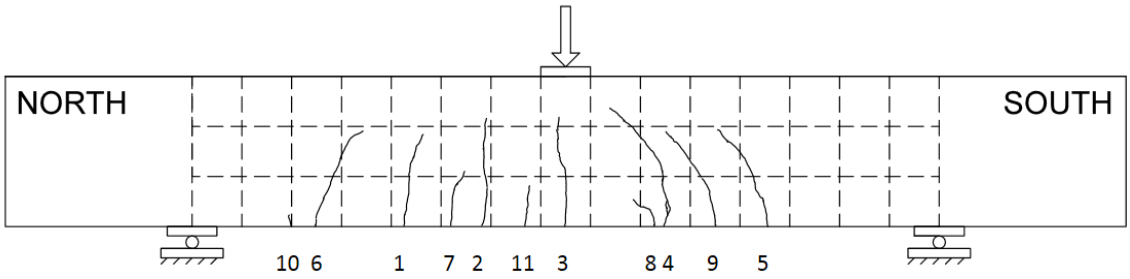

(f) F-4: South Side Failure: 26.6 kip

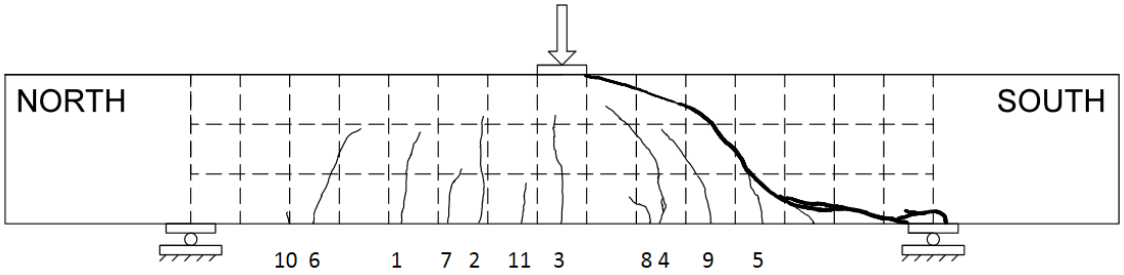

(g) F-4: North Side Failure 31.2 kip

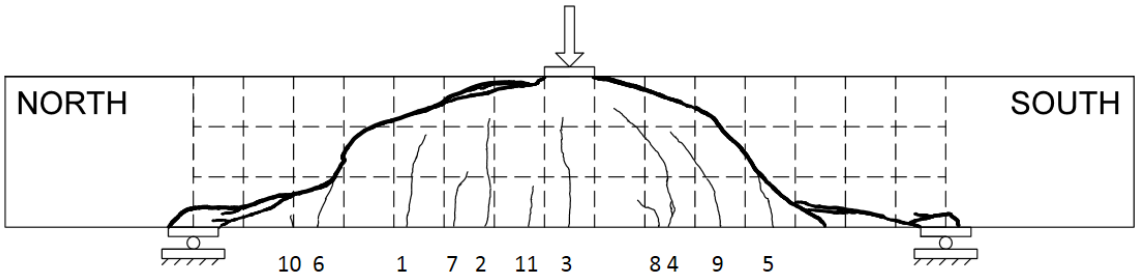

Figure D.13 Specimen F-4 Crack Maps Continued

(a) H-1: 9 kip

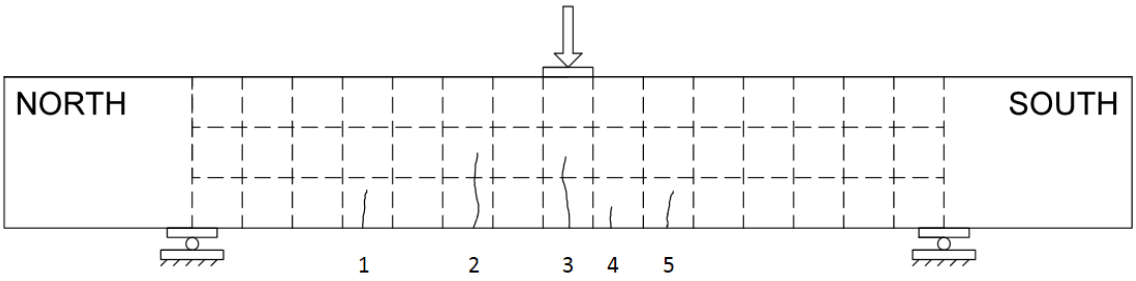

(b) H-1: 12 kip

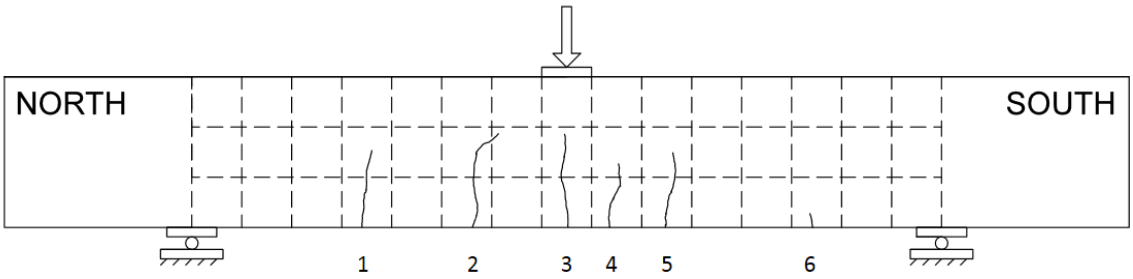

(c) H-1: North Side Failure 19.9 kip

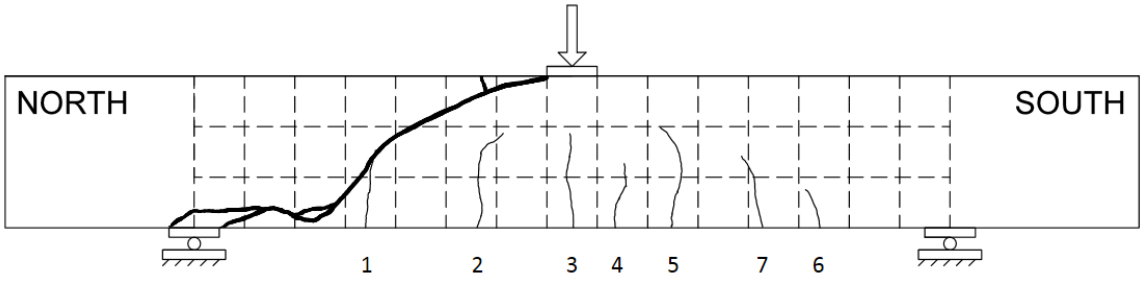

(d) H-1: South Side Failure 24.9 kip

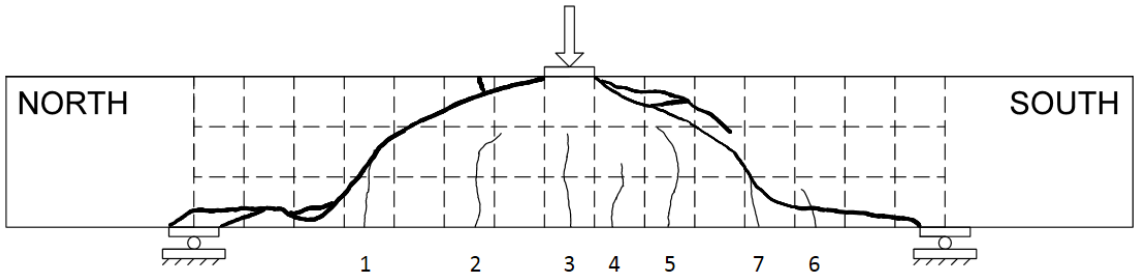

Figure D.14 Specimen H-1 Crack Maps

(a) H-2: 9 kip

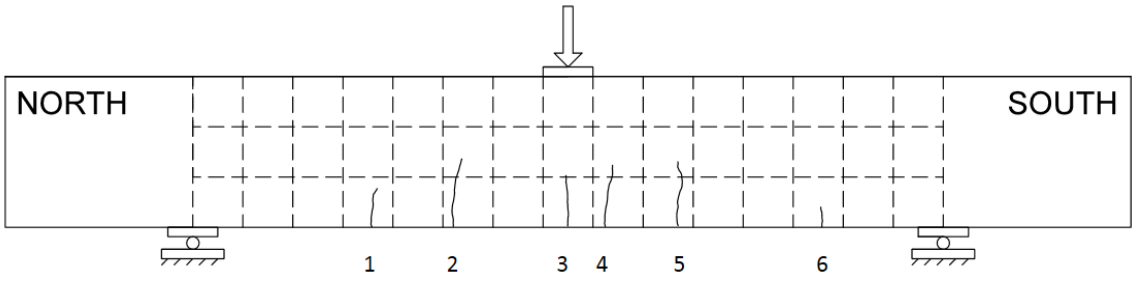

(b) H-2: 12 kip

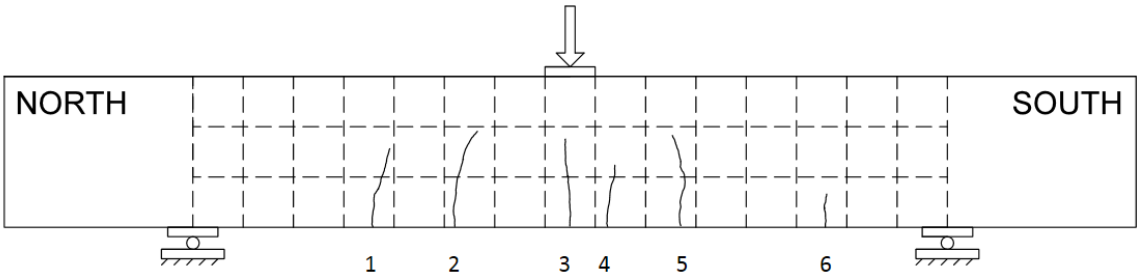

(c) H-2: 15 kip

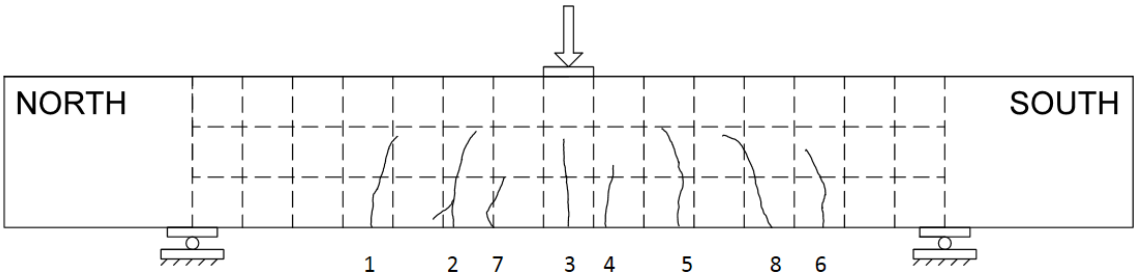

(d) H-2: South Side Failure 21.6 kip

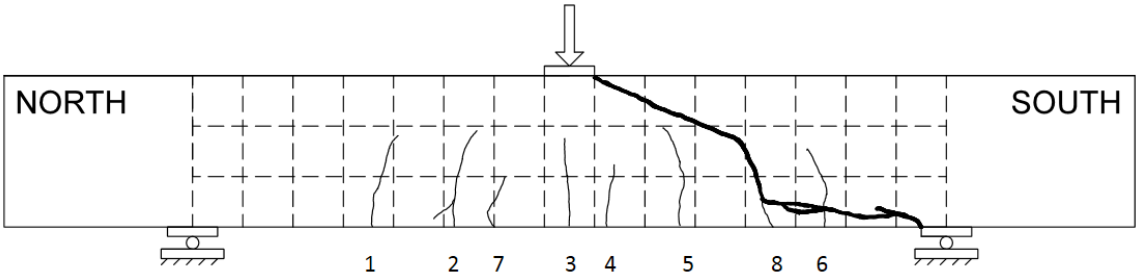

Figure D.15 Specimen H-2 Crack Maps

(e) H-2: North Side Failure: 23.3 kip

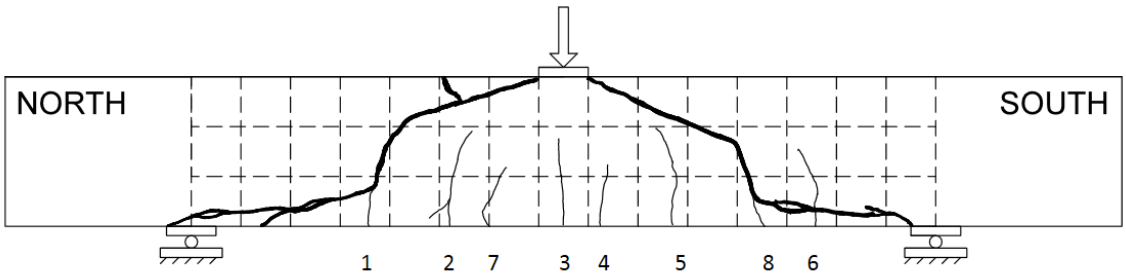

Figure D.15 Specimen H-2 Crack Maps Continued

(a) I-1: 9 kip

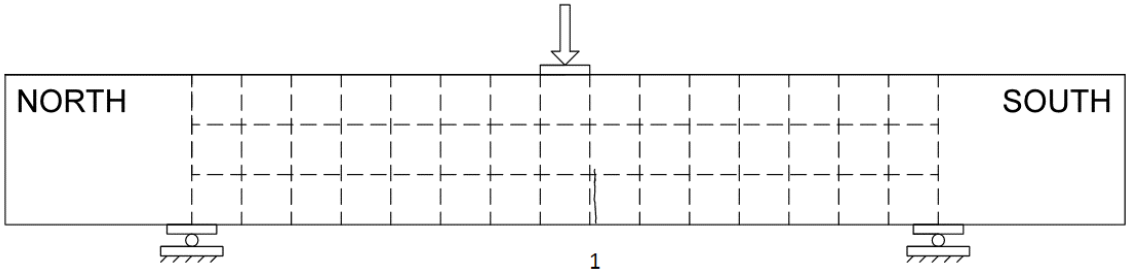

(b) I-1: 12 kip

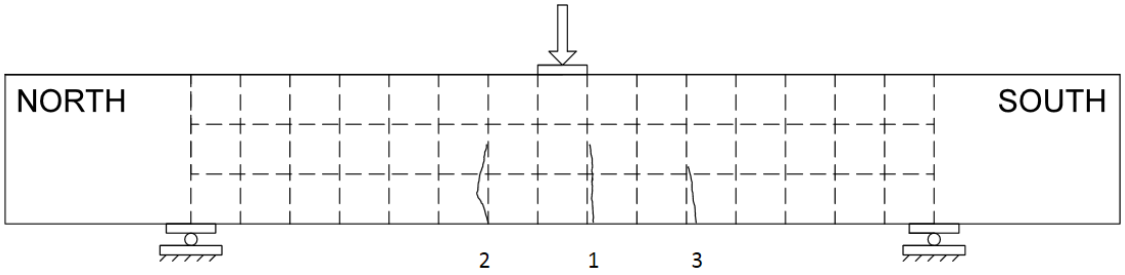

(c) I-1: 15 kip

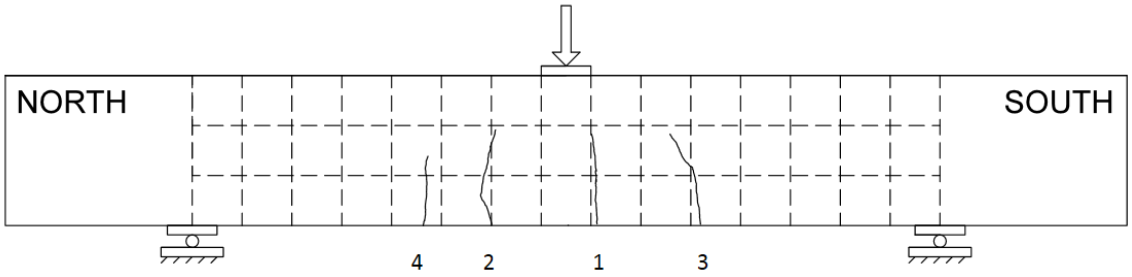

(d) I-1: 18 kip

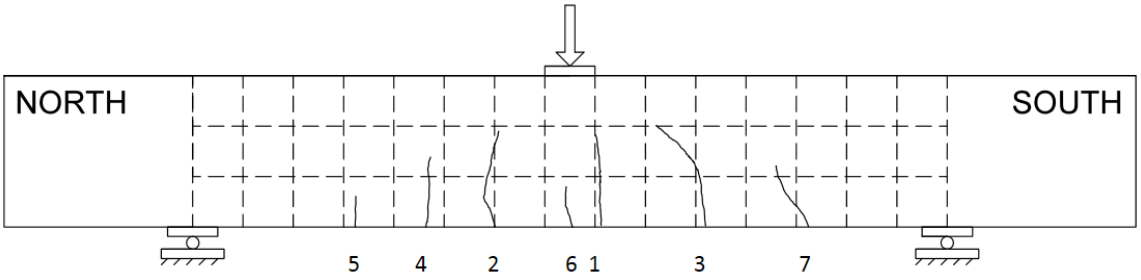

Figure D.16 Specimen I-1 Crack Maps

(e) I-1: South Side Failure: 24.8 kip

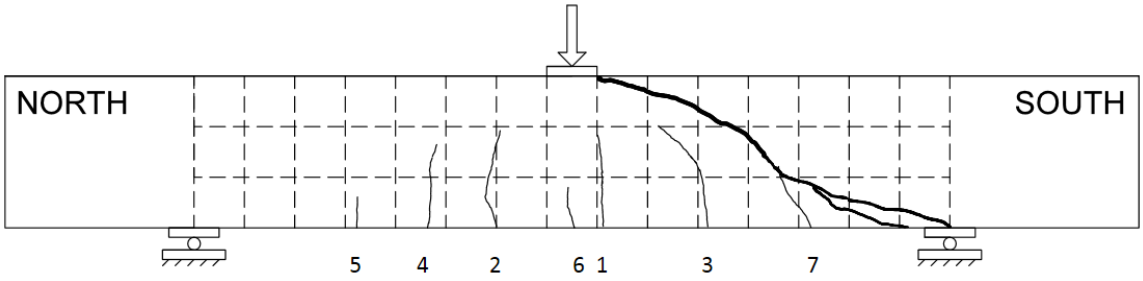

(f) I-1: North Side Failure 30.0 kip

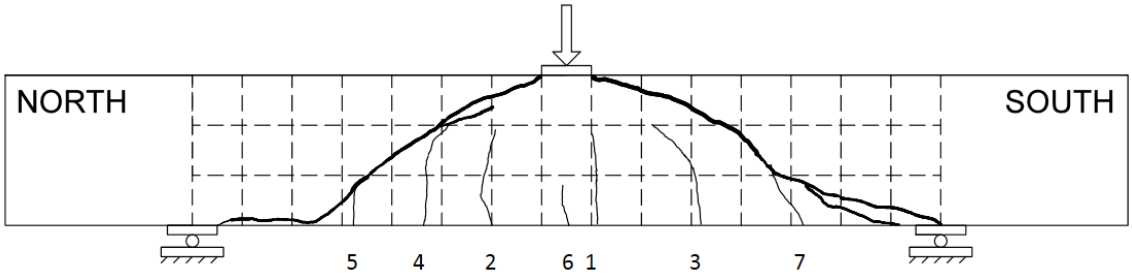

Figure D.16 Specimen I-1 Crack Maps Continued

(a) I-2: 9 kip

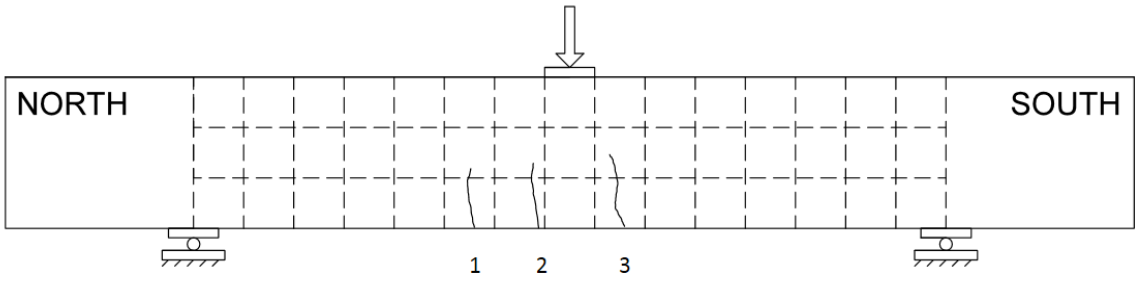

(b) I-2: 12 kip

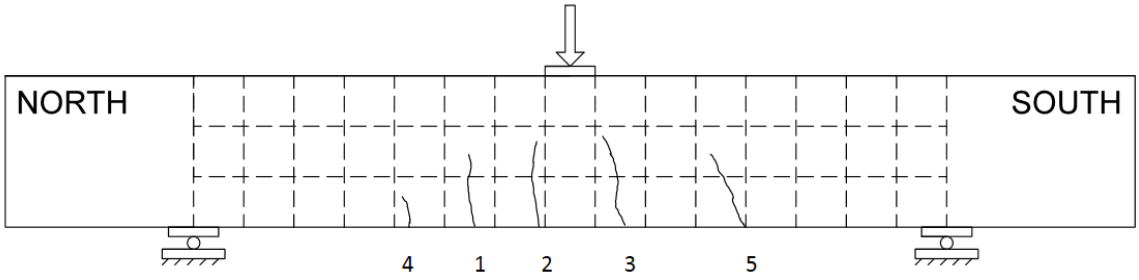

(c) I-2: 15 kip

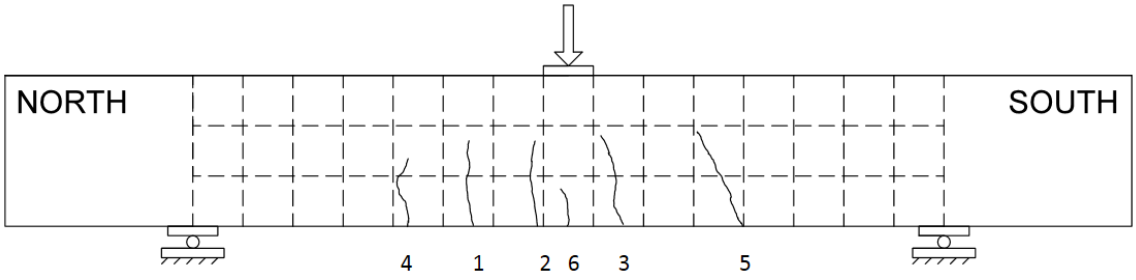

(d) I-2: 18 kip

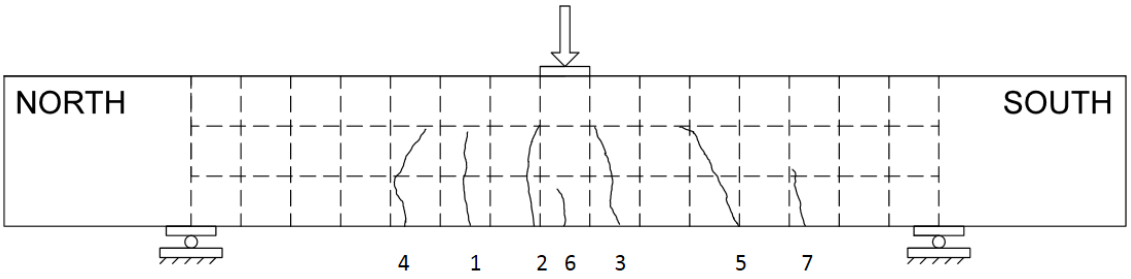

Figure D.17 Specimen I-2 Crack Maps

(e) I-2: South Side Failure: 23.8 kip

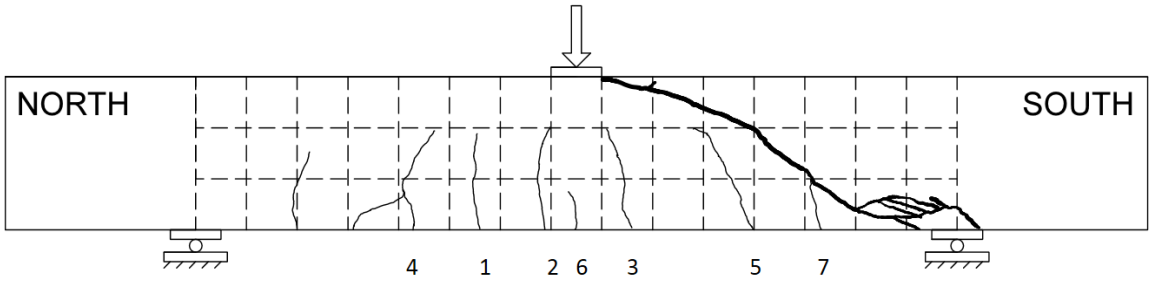

(f) I-2: North Side Failure 27.2 kip

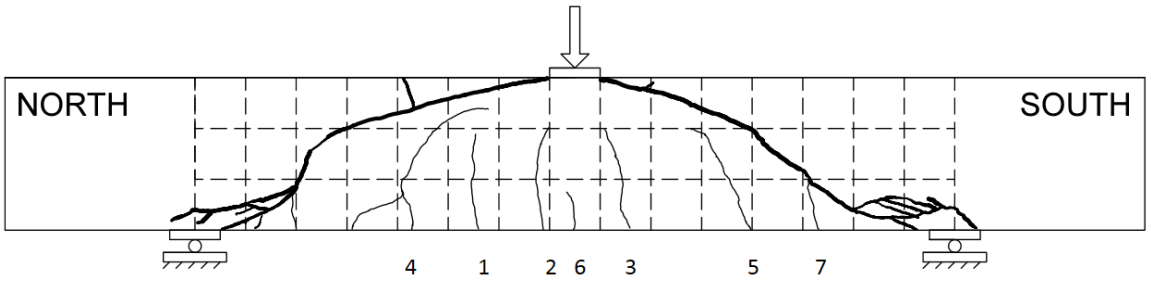

Figure D.17 Specimen I-2 Crack Maps Continued

(a) J-1: 9 kip

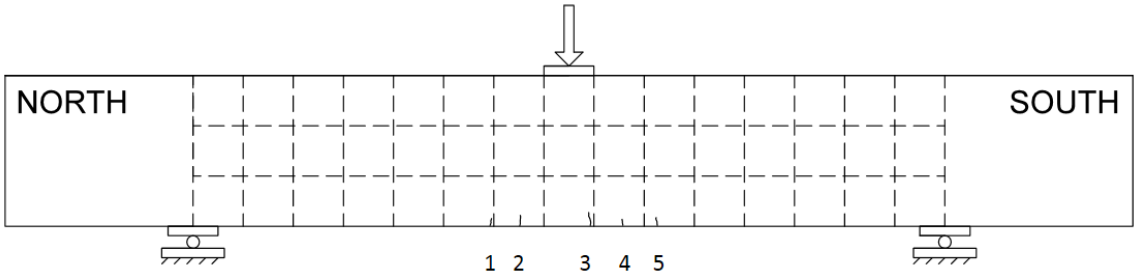

(b) J-1: 12 kip

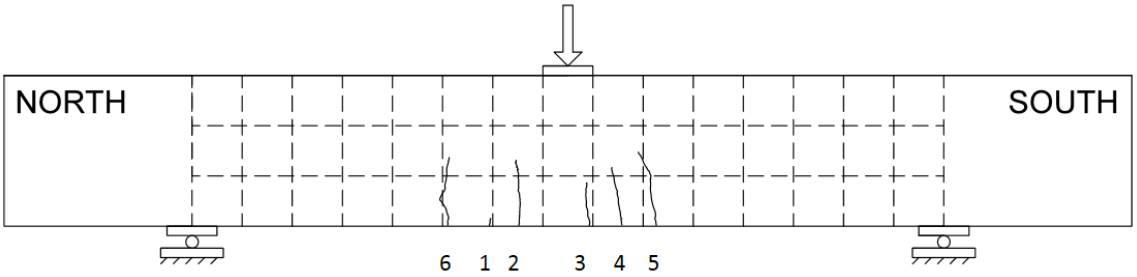

(c) J-1: 15 kip

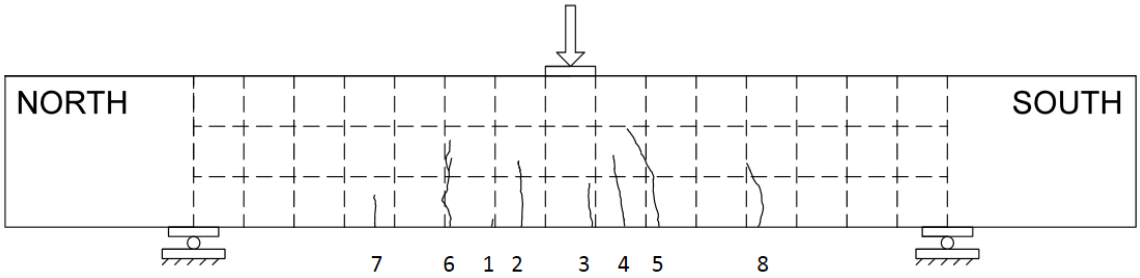

(d) J-1: 18 kip

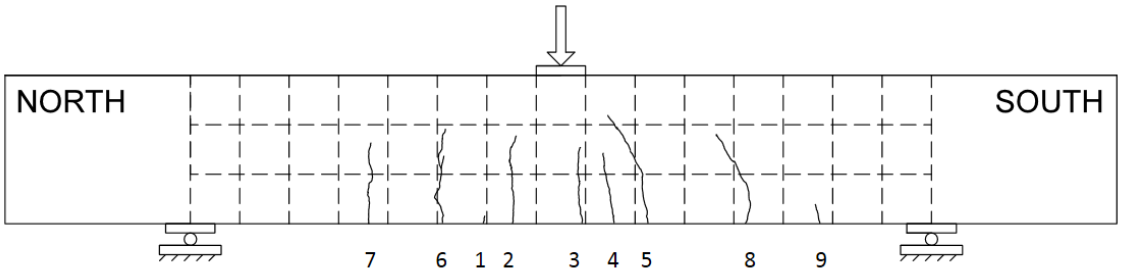

Figure D.18 Specimen J-1 Crack Maps

(e) J-1: South Side Failure 22.9 kip

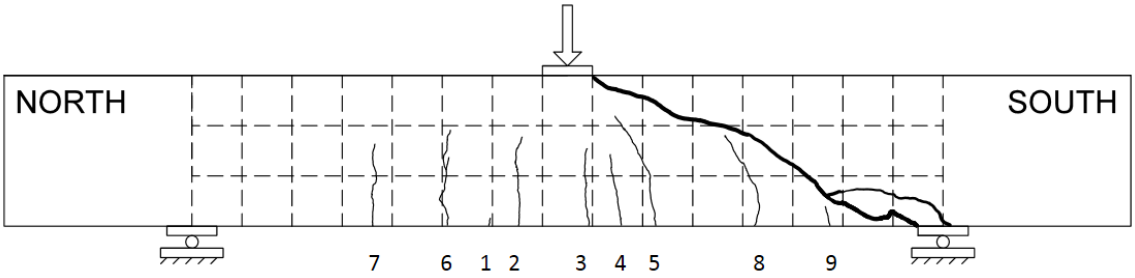

(f) J-1: North Side Failure 23.8 kip

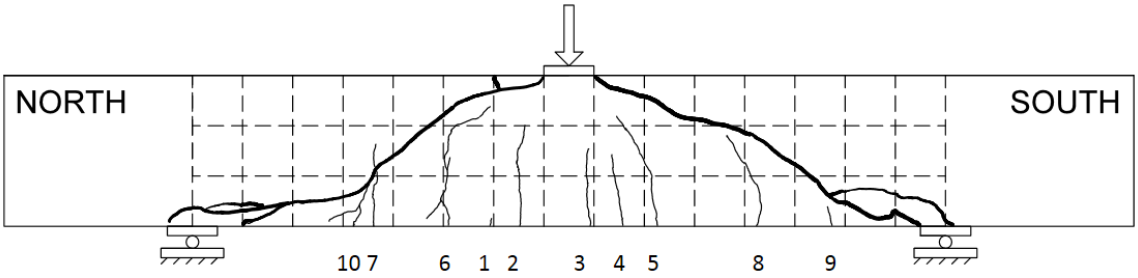

Figure D.18 Specimen F-3 Crack Maps Continued

(a) J-2: 9 kip

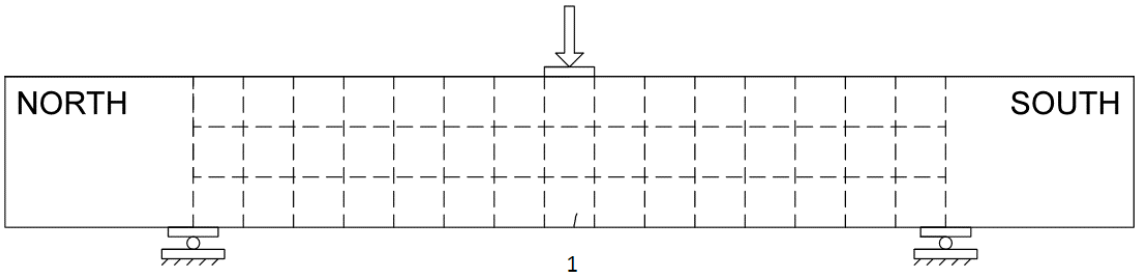

(b) J-2: 12 kip

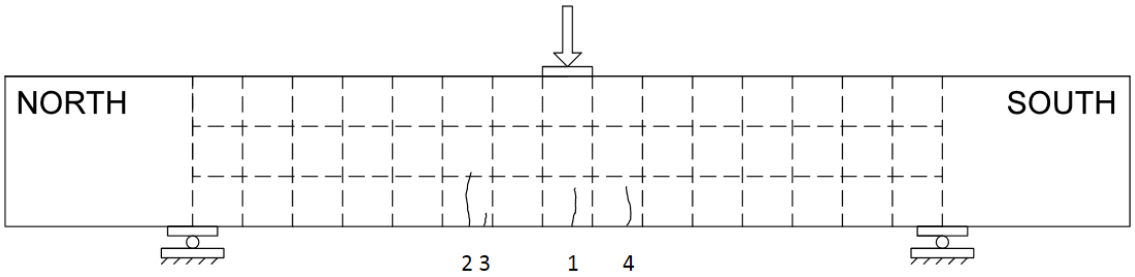

(c) J-2: 15 kip

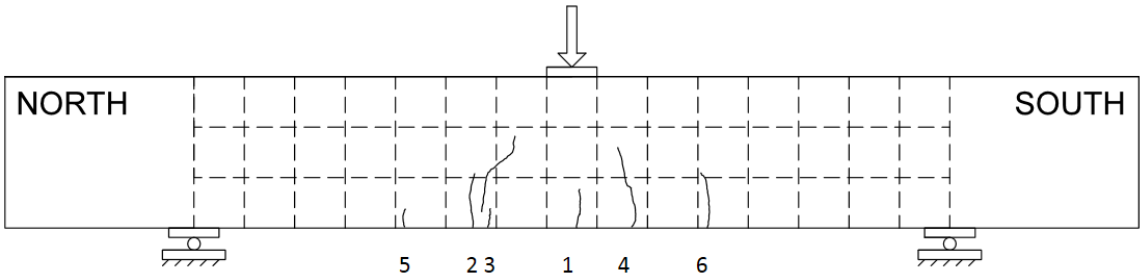

(d) J-2: 18 kip

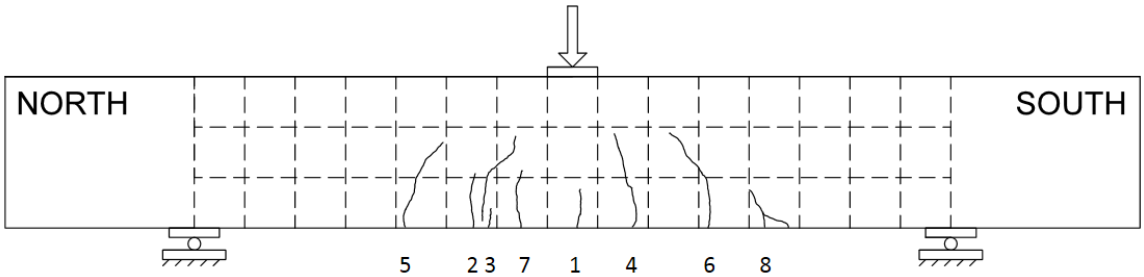

Figure D.19 Specimen J-2 Crack Maps

(e) J-2: South Side Failure: 22.7 kip

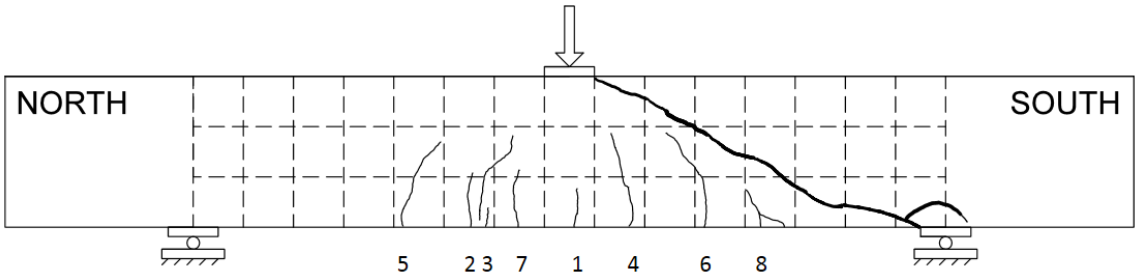

(f) J-2: North Side Failure 26.9 kip

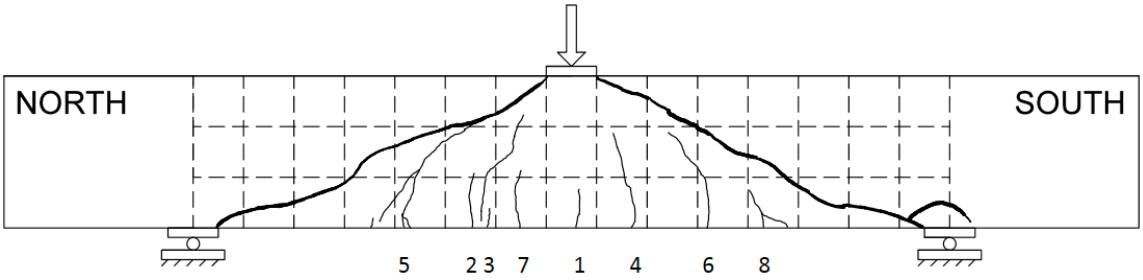

Figure D.19 Specimen J-2 Crack Maps Continued

(a) K-1: 12 kip

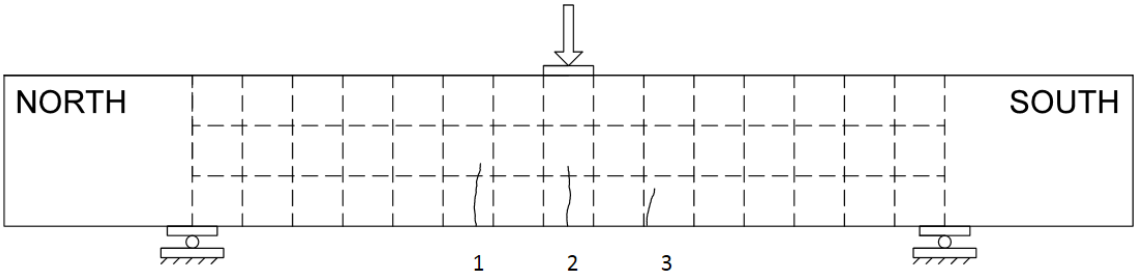

(b) K-1: 15 kip

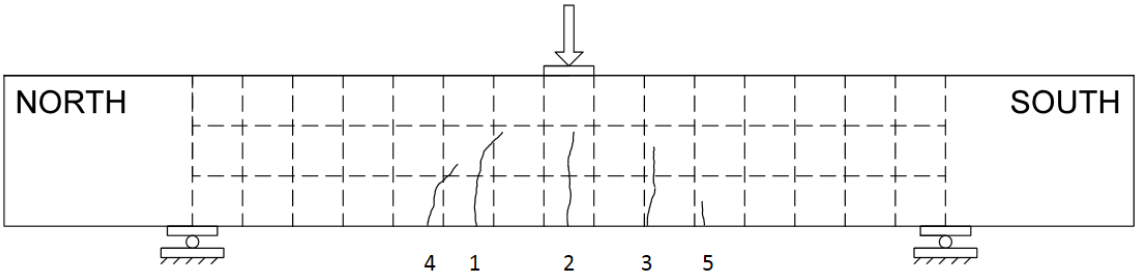

(c) K-1: 18 kip

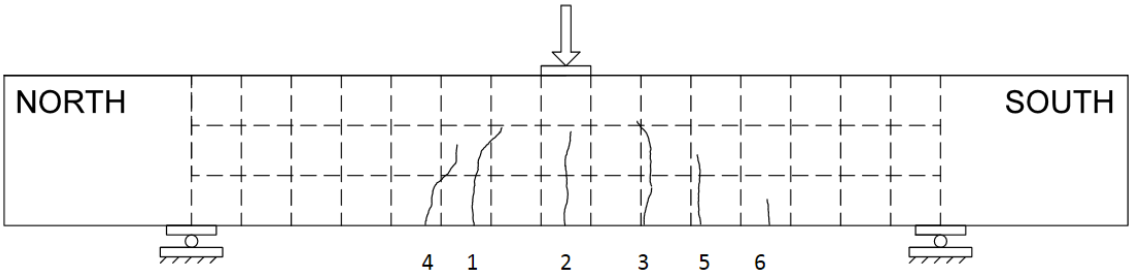

(d) K-1: North Side Failure: 27.5

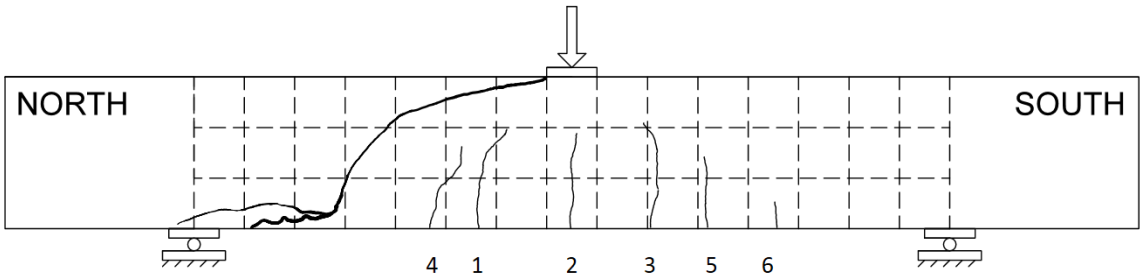

Figure D.20 Specimen K-1 Crack Maps

(e) K-1: North Side Failure 28.9 kip

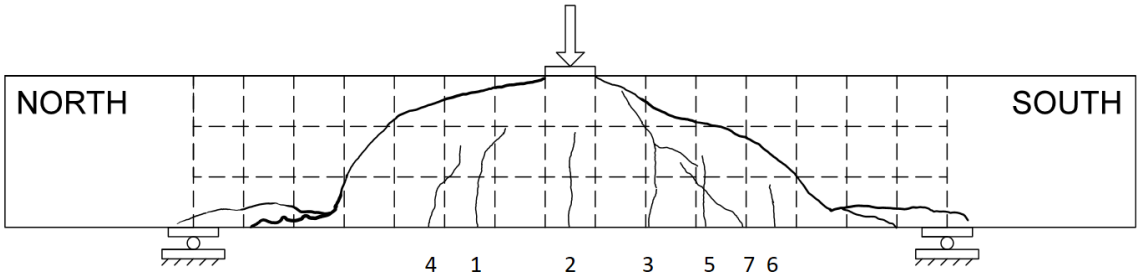

Figure D.20 Specimen K-1 Crack Maps Continued

(a) K-2: 12 kip

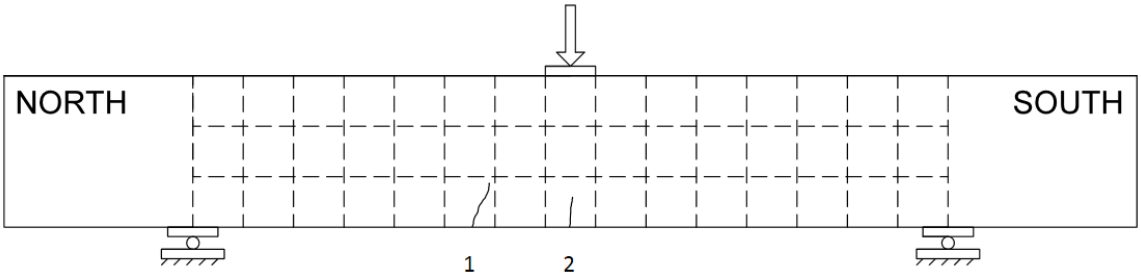

(b) K-2: 15 kip

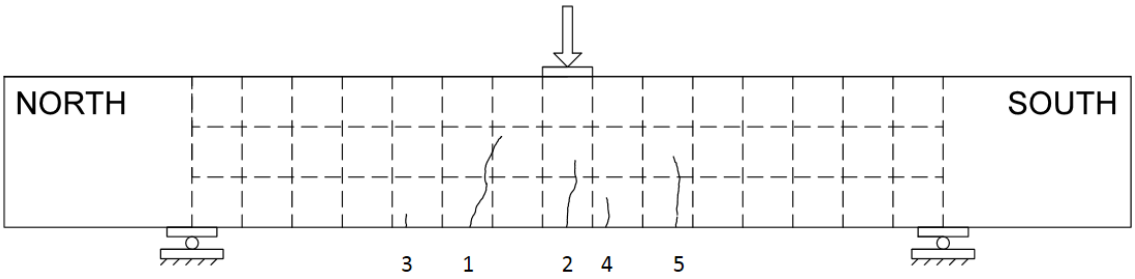

(c) K-2: 18 kip

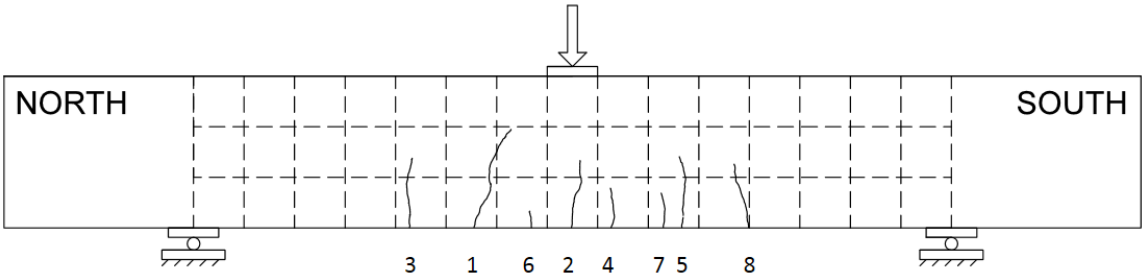

(d) K-2: South Side Failure: 29.7 kip

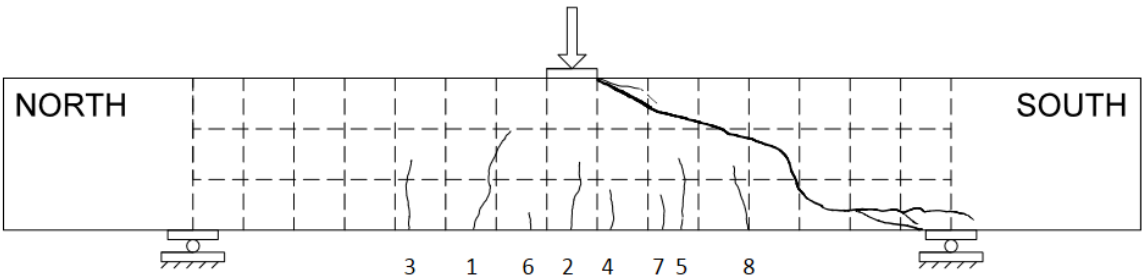

Figure D.21 Specimen K-2 Crack Maps

(e) K-2: North Side Failure 32.0 kip

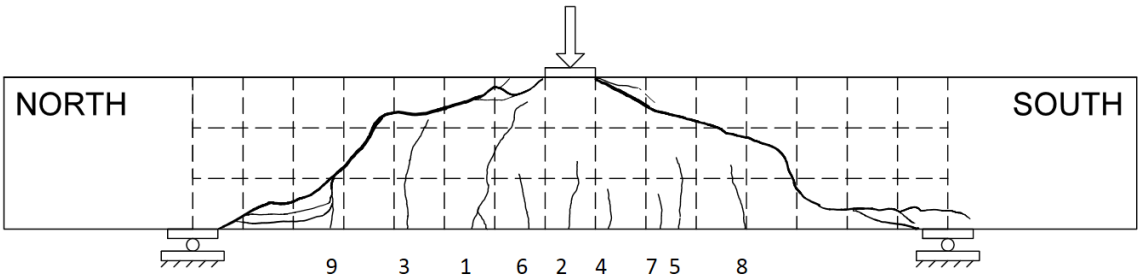

Figure D.21 Specimen K-2 Crack Maps Continued

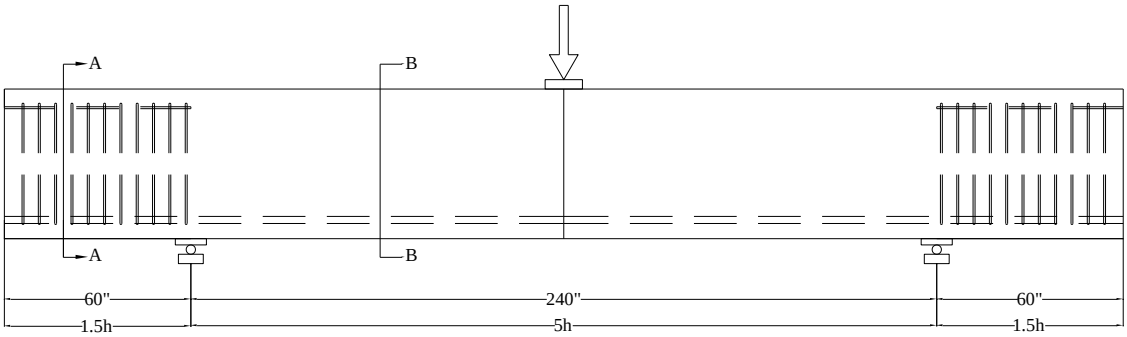

Figure E.1 Series G Elevation View of Beam

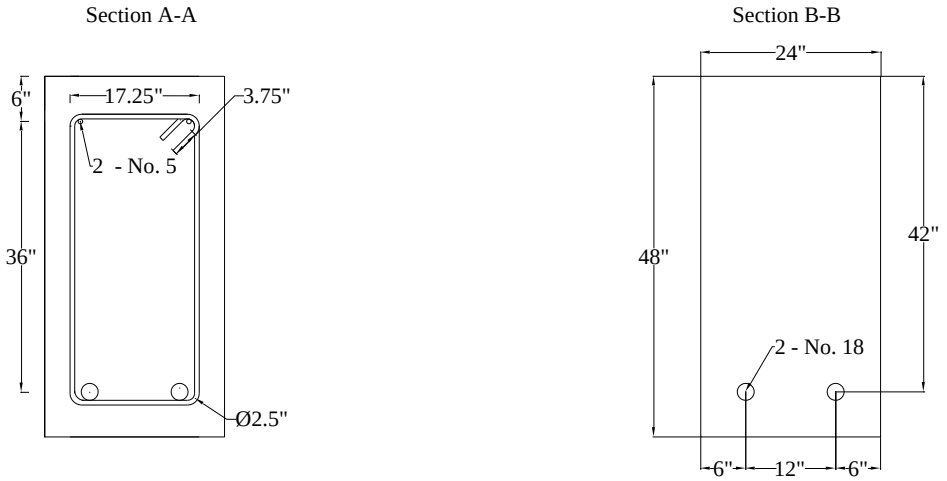

Figure E.2 Series G Cross Section View of 48 in. Deep Beam

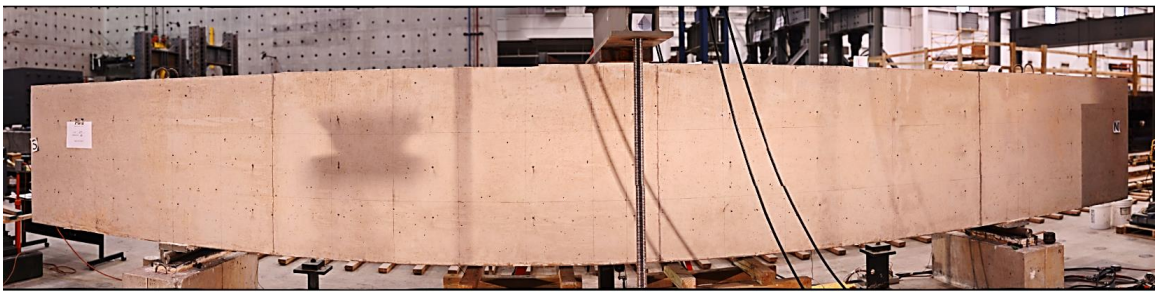

Figure E.3 Series G Experimental Test Setup

Figure E.4 Series G Experimental Test Setup with External Stirrups

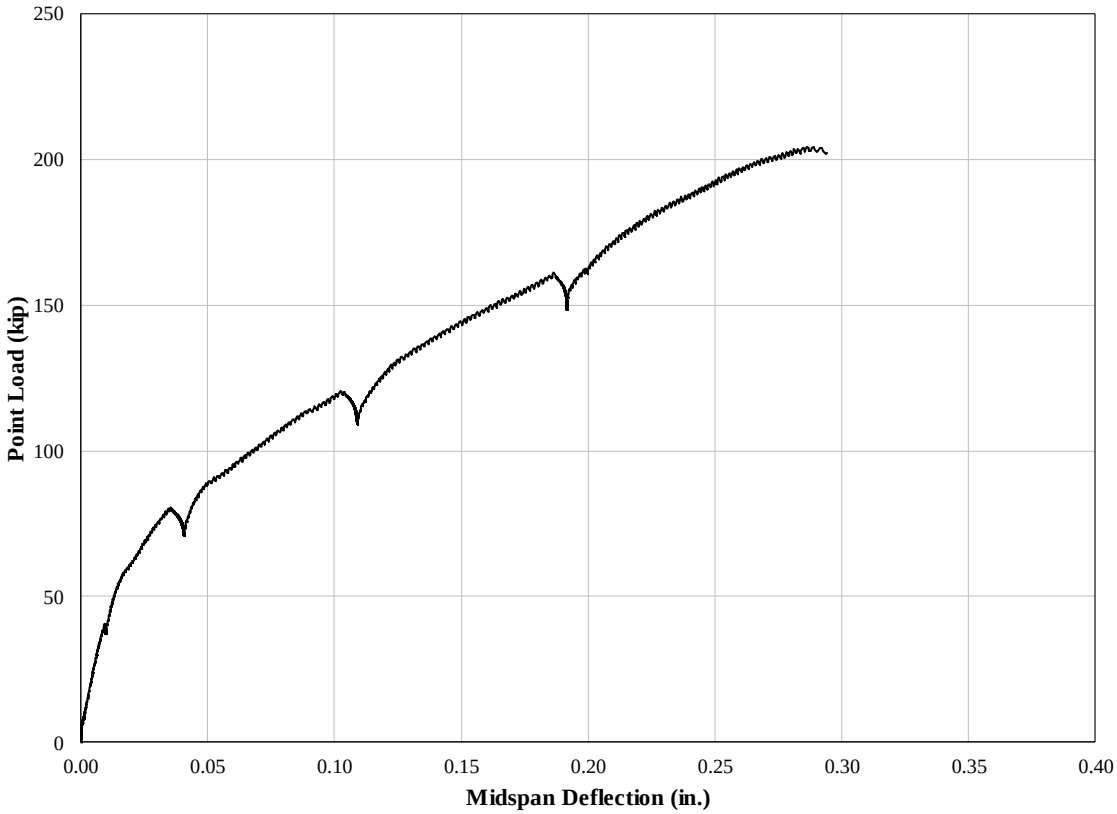

Figure E.5 Specimen G-1 Load-Deflection Curve

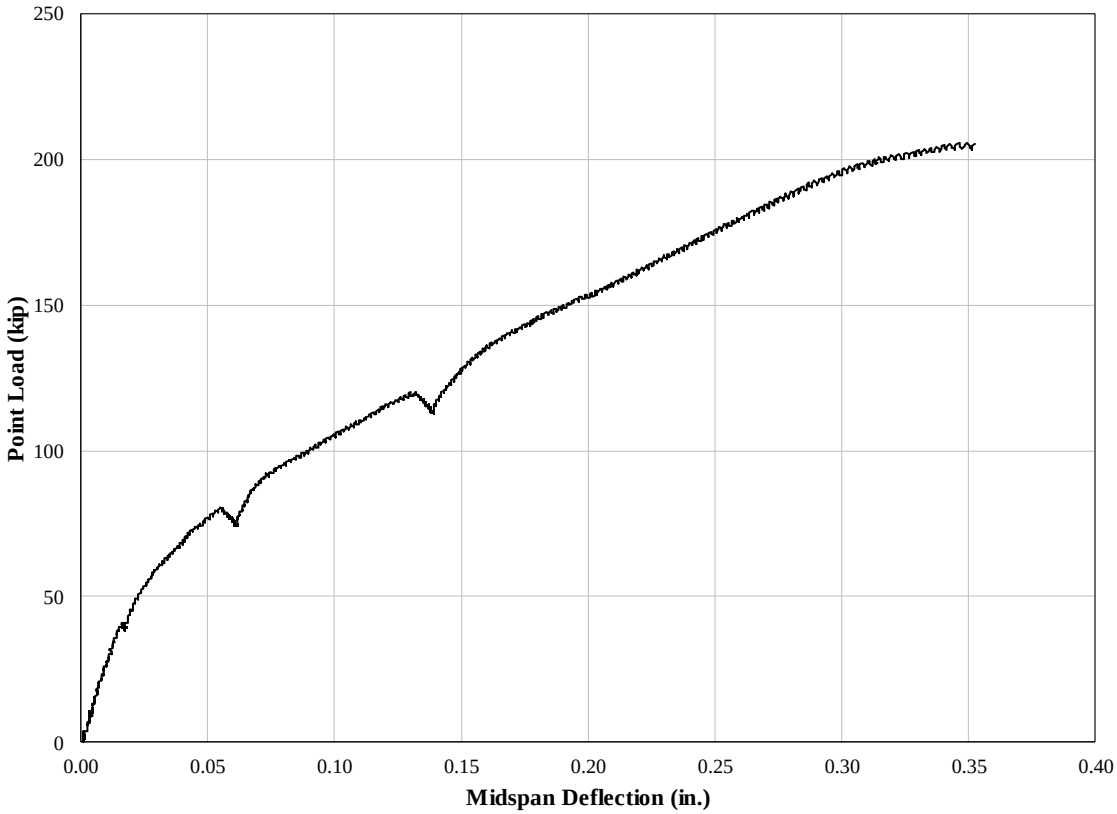

Figure E.6 Specimen G-2 Load-Deflection Curve

Figure E.7 Specimen G-2: South Side Failure Inclined Crack

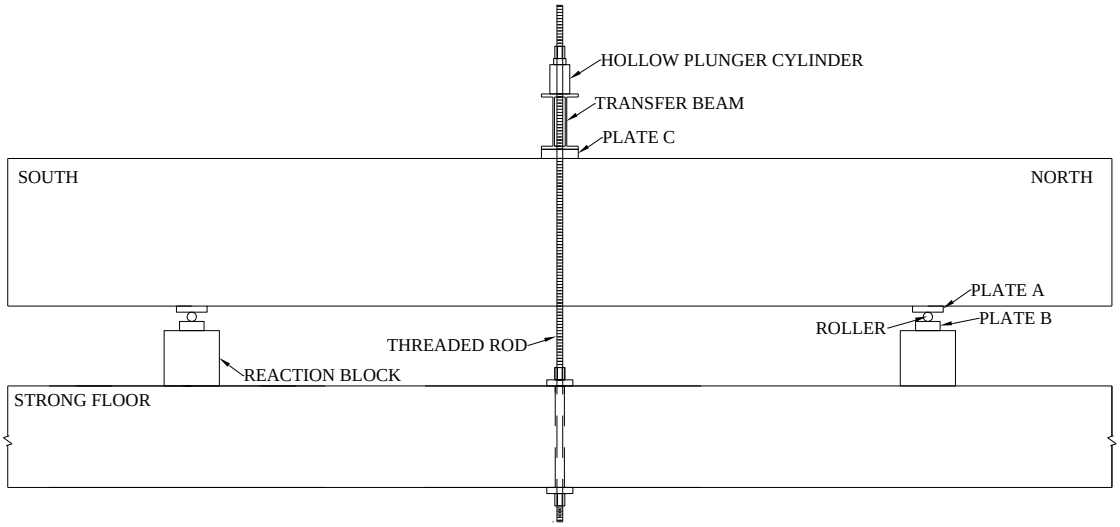

Figure E.8 Elevation View of Series G Test Setup

Figure E.9 Series G Loading Setup

Figure E.10 Series G LVDT Experimental Setup

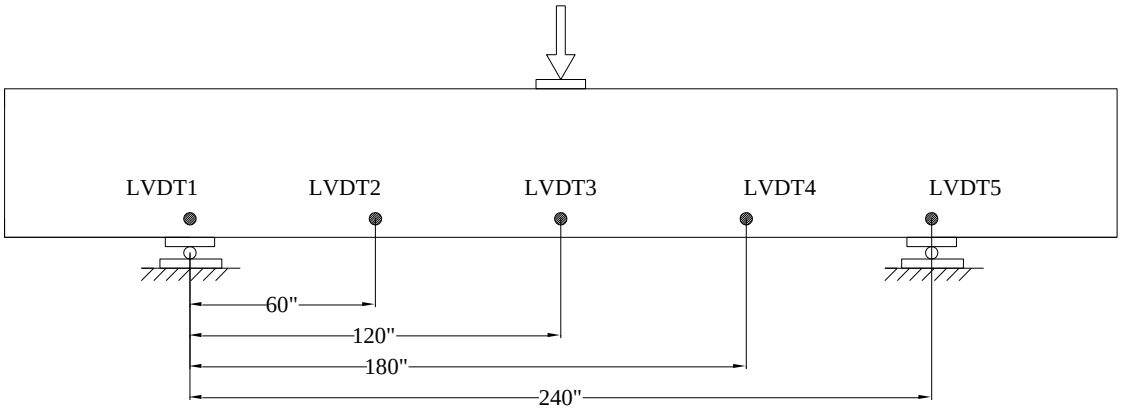

Figure E.11 Series G LVDT Locations

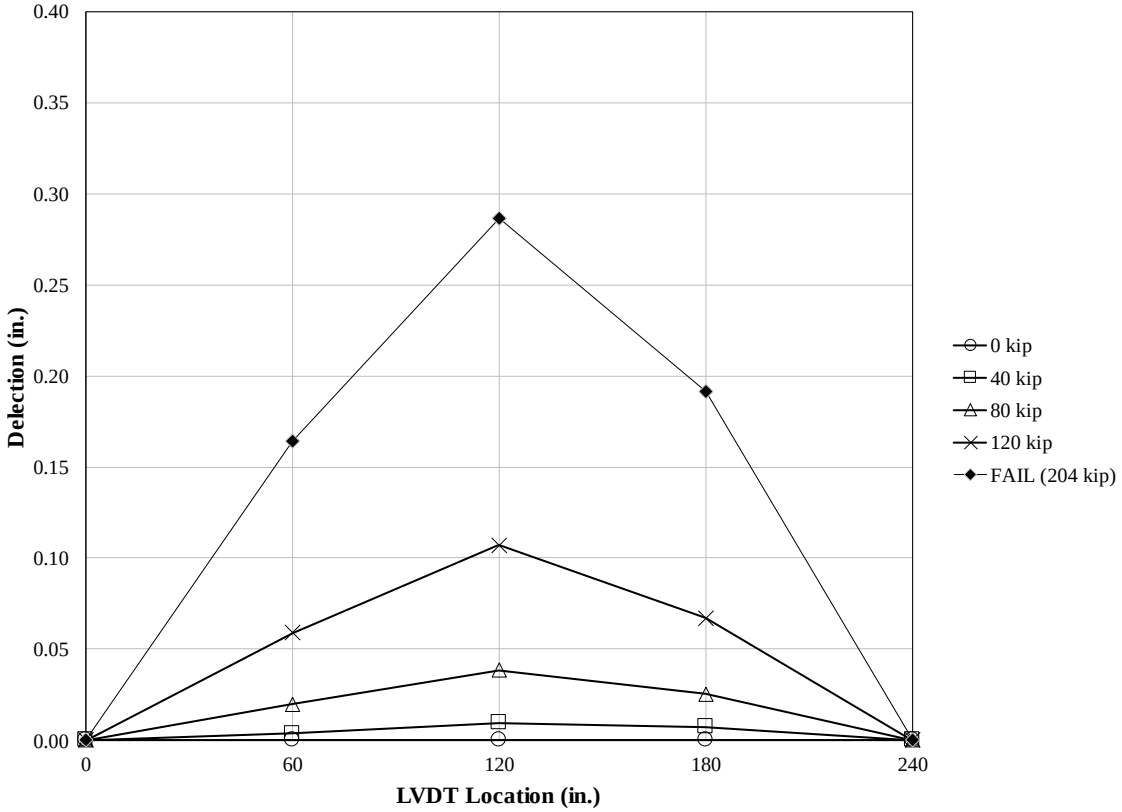

Figure E.12 Specimen G-1 Deflection Profile

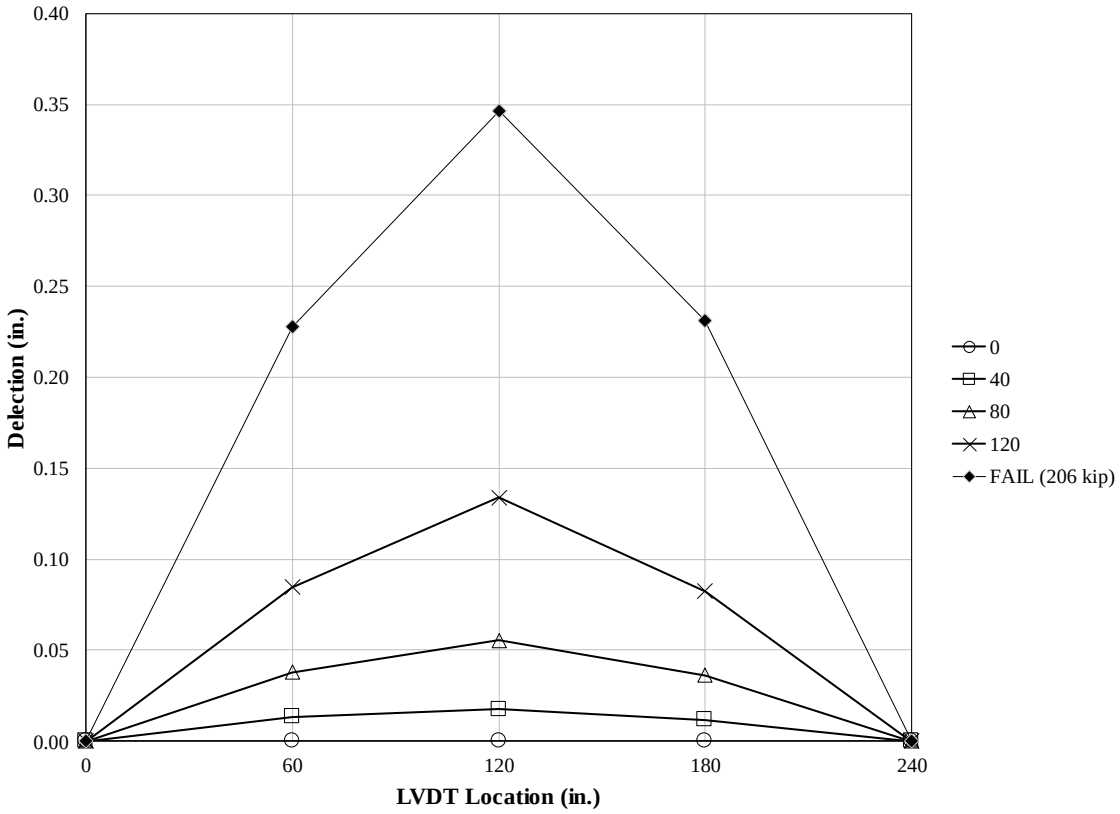

Figure E.13 Specimen G-2 Deflection Profile

(a) G-1: 40 kip

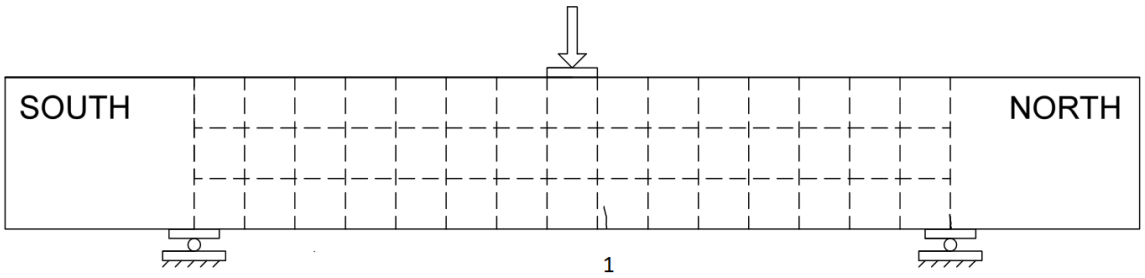

(b) G-1: 80 kip

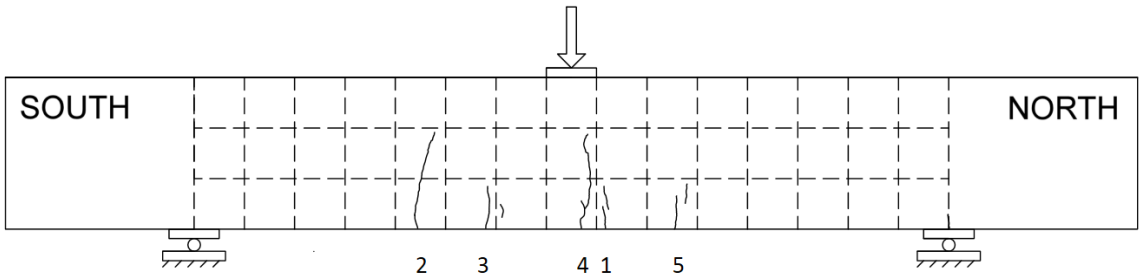

(c) G-1: 120 kip

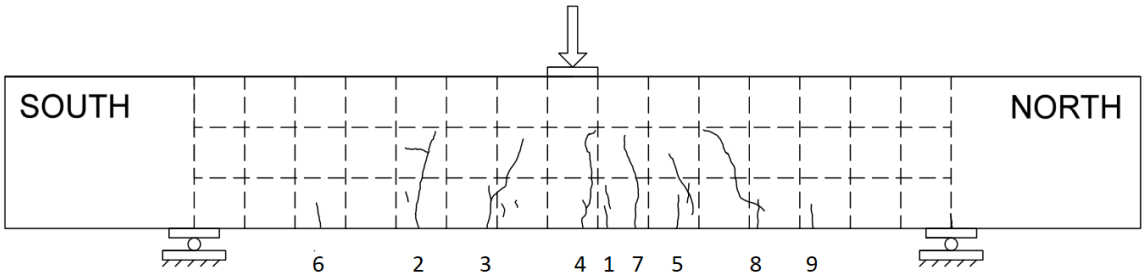

(d) G-1: 160 kip

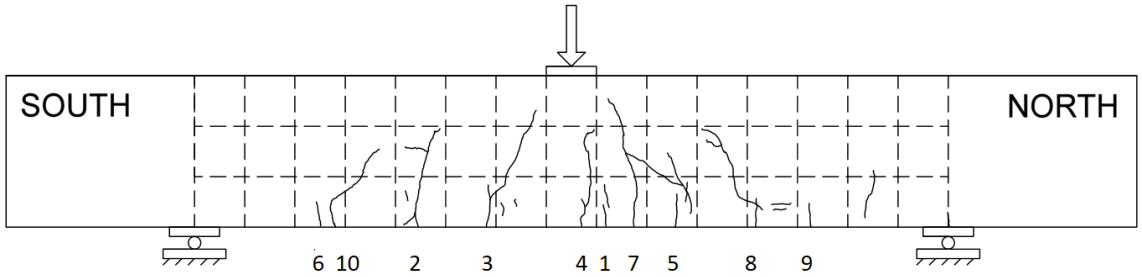

Figure E.14 Specimen G-1 Crack Maps

(e) G-1: North Side Failure: 204.4 kip

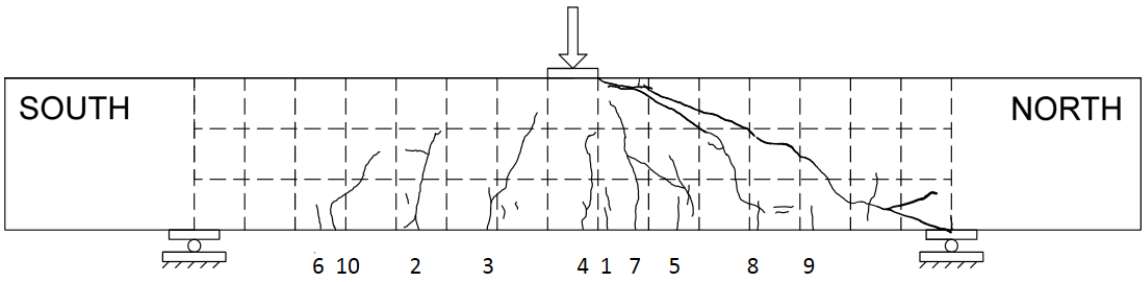

(a) G-1: South Side Failure: 233.4 kip

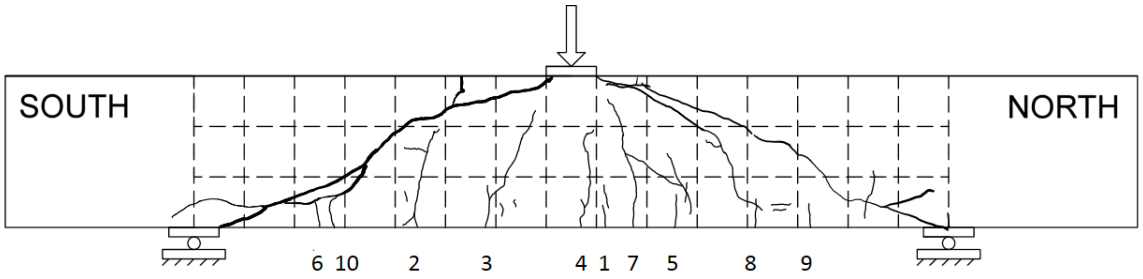

Figure E.14 Specimen G-1 Crack Maps Continued

(a) G-2: 80 kip

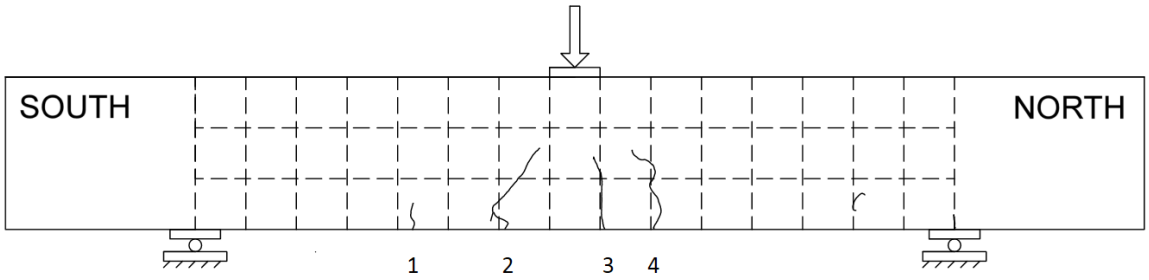

(b) G-2: 160 kip

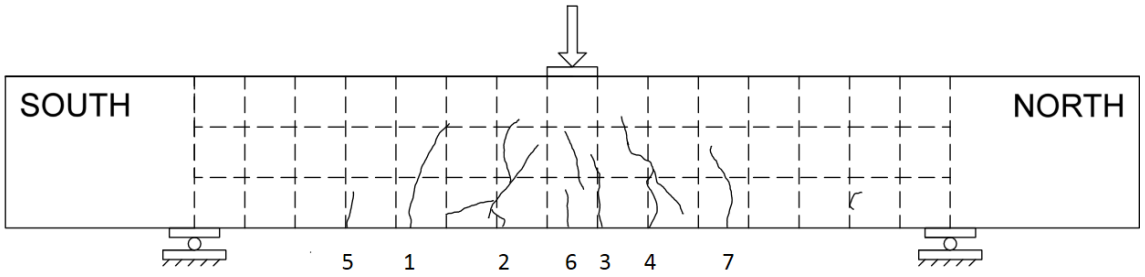

(c) G-2: South Side Failure: 205.7 kip

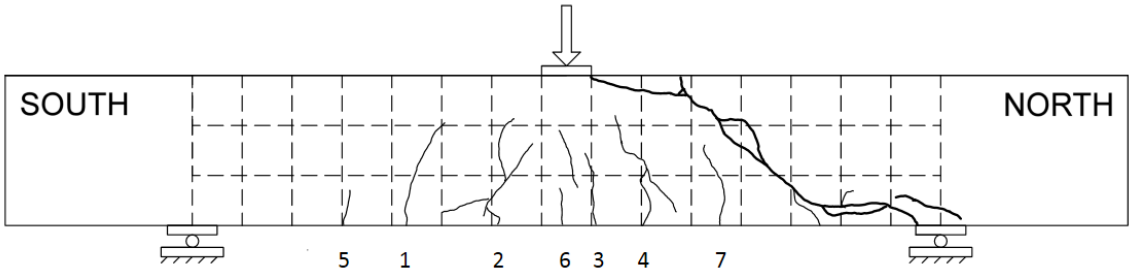

(d) G-2: North Side Failure 190.2 kip

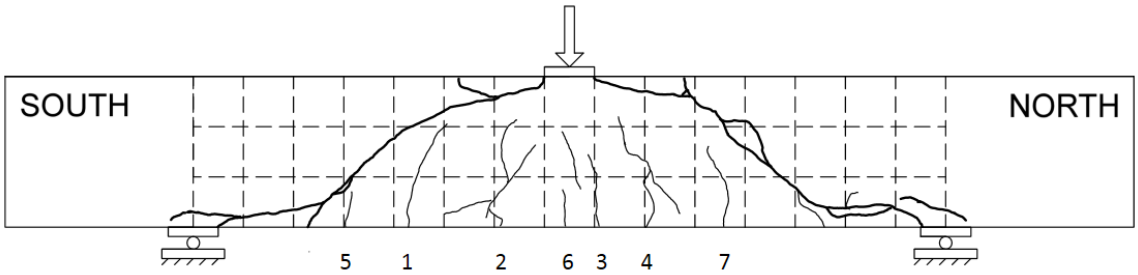

Figure E.15 Specimen G-2 Crack Map